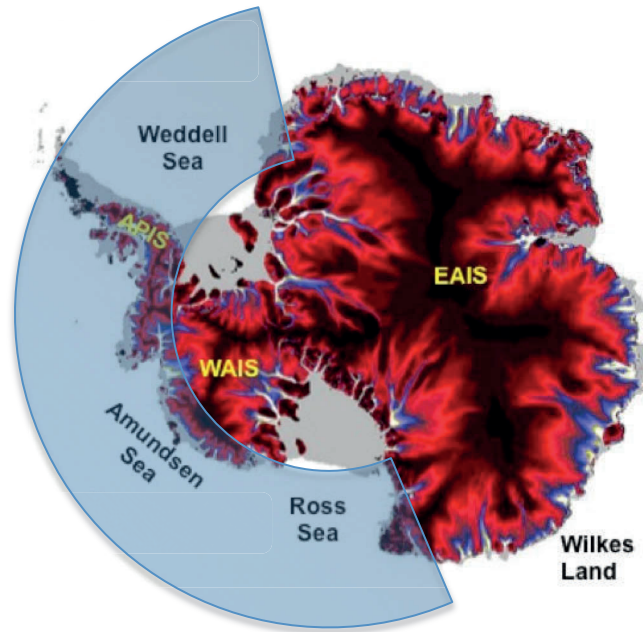


Palaeoenvironment of the Weddell Sea and  
Amundsen Sea – eastern Ross Sea basins, Antarctica:  
Insights from comprehensive seismostratigraphic analysis



**DISSERTATION**

submitted to the Department of Geosciences at the University of Bremen, Germany,  
in fulfilment of the Dr. rer. nat degree, by

*zur Erlangung des Grades Dr. rer. nat. vorgelegt  
dem Fachbereich Geowissenschaften der Universität Bremen von*

**ANSA LINDEQUE**

Alfred Wegener Institute, Helmholtz Centre for Polar and Marine Research (AWI)  
Bremerhaven, Germany

London, 26 January 2014





*First examiner /* Erstgutachter:

Prof. Dr. Heinrich Miller

*Second examiner /* Zweitgutachterin:

Prof. Dr. Cornelia Spiegel

*Date of the Defense /* Datum des Kolloquiums:

19. Mai 2014



Name: Ansa Phoenix Titania Sapphire Garnet Snow Datum: 26.01.2014

Nachname: LINDEQUE

Anschrift: Flat 5 Derwent House  
May Bate Avenue  
Kingston Upon Thames  
Greater London, Surrey  
KT2 5UN, United Kingdom

#### ERKLÄRUNG / *Declaration*

---

Hiermit versichere ich, dass ich

*I hereby declare that I*

1. die Arbeit ohne unerlaubte fremde Hilfe angefertigt habe,  
*/ completed this Dissertation without unauthorized external assistance,*
2. keine anderen als die von mir angegebenen Quellen und Hilfsmittel benutzt habe  
und */ used no other sources, references or material other than those cited and*
3. die den benutzten Werken wörtlich oder inhaltlich entnommenen Stellen als  
solche kenntlich gemacht habe. */ cited sources in all cases, whether the contents were  
used verbatim or in part.*

London, den 26.01.2014

Ansa Phoenix T.S.G.S. Lindeque

---





I dedicate this thesis to my long-standing  
mentor Prof. Dr. Maarten de Wit,  
the giant on whose shoulders I was allowed to stand.

**“PIGMAEI GIGANTUM HUMERIS IMPOSITI  
PLUSQUAM IPSI GIGANTES VIDENT”**

“If I have been able to see further,  
it was only because I stood on the shoulders of giants.”

— Sir Isaac Newton, *Principia: Vol. I: The Motion of Bodies*

“Bernard of Chartres used to say  
that we are like dwarfs on the shoulders of giants,  
so that we can see more than they and things at a greater distance,  
not by virtue of any sharpness on sight on our part,  
or any physical distinction,  
but because we are carried high  
and raised up by their giant size.”

— Sir John of Salisbury, *Metalogicon*, 1159AC



## SUMMARY

---

The marine sediment record on the Pacific margin of West Antarctica spans the Weddell Sea, Bellingshausen Sea, Amundsen Sea and Ross Sea, and encapsulate at least 90 million years of Antarctica's climate, tectonic, ice sheet, ocean-circulation and topographic evolution. Analyses of the sedimentary sequences and the structural elements within this record reveal changes in the sediment transport processes that can be tied back to this history. These changes are imaged in multichannel seismic reflection data as variations in seismic reflectivity characteristics and altered geometry of sediment deposits.

This work focuses on identifying the seismic sequence and structural geometry changes that represent the pre-glacial (PG, pre-ice sheet), transitional (T, first arrival of the ice sheets on the shelf) and full glacial (FG, grounding of the ice sheets on the shelf) processes, in order to understand the sediment distribution, bottom current development and ice sheet growth on this margin since the Cretaceous. The results are especially relevant for reconstructing more robust palaeotopography surfaces of the Eocene–Oligocene boundary (34 Ma) and mid-Miocene (15.5 Ma), which is associated with abrupt changes in climate proxies ( $p\text{CO}_2$ ,  $\delta^{18}\text{O}_2$ , sea surface temperature and sea level). These palaeotopography surfaces are essential for modelling past and near-future climate and ice sheet scenarios.

This research is rooted in the seismic horizon stratigraphy analyses of two deep-sea basins: (i) the Weddell Sea basin and (ii) the previously unexplored central Amundsen Sea basin (120° W to 175° W). The key findings are subsequently expanded to include the Pacific margin of West Antarctica. As a result it is possible to present the margin's first collective total sediment thickness, pre-glacial, transitional and full-glacial sediment thickness grids, as well as volume estimates and residual basement depth – all needed for the palaeotopography reconstructions.

A ~3300 km long Weddell Sea to Scotia Sea transect was constructed through the central part of the Weddell Sea basin using published and unpublished pre-existing seismic data. ODP Leg 113 and SHALDRIL borehole data constrain the upper ages, and seafloor spreading magnetic anomalies compiled from literature, constrain the basement ages in the constructed age model. A basin-wide seismic horizon stratigraphy was defined as follows: The Cretaceous–Palaeocene pre-glacial sequence (>27 Ma) comprises units WS-S1 to WS-S3; The Eocene–Oligocene transitional sequence (27 to 11 Ma) is WS-S4; and the Miocene–Pleistocene full glacial climate regime (11 to 0 Ma) consists of units WS-S5 to WS-S7. A Cretaceous proto-Weddell Gyre bottom current is proposed based on a mound and eroded flank geometry observed in the pre-glacial sequence.

The seismic data and interpretation suggest evidence for Eocene East Antarctic Ice Sheet expansion, Oligocene grounding of the West Antarctic Ice Sheet and Early Miocene grounding of the Antarctic Peninsula Ice Sheet, which are all earlier than other studies suggest. The total sediment thickness range between 1756 to 3136 m, and the total sediment volume of the deep-sea part of the Weddell Sea basin is estimated at 3.3 to 3.9 x 10<sup>6</sup> km<sup>3</sup>.





In the central Amundsen Sea basin, seismic data acquired during the 2010 ANT-26/3 and the 2006 TAN0602 expeditions enabled the construction of a ~2000 km long Amundsen Sea – Ross Sea transect across a large underexplored sector. Borehole information from IODP Leg 318 site U1356, and DSDP Leg 28 Sites 270–272 constrain the constructed age model, and recently published magnetic seafloor spreading anomaly data provide basement age control. A first basin-wide seismic horizon stratigraphy is proposed: The Cretaceous to Eocene pre-glacial sequence (70–38 Ma) comprises units AS-1 to AS-3; the Eocene to mid-Miocene transitional sequence (38–15.5 Ma) consists of units AS-4 to AS-6; and the mid-Miocene to Pleistocene full glacial climate sequence (15.5–1 Ma) includes units AS-7 to AS-11. The 71 Ma old basin accumulated up to ~3.9 km of sediment (3 s TWT; interval velocities from new sonobuoy and refraction data). Seismic facies geometry analysis suggests an eastward flowing Paleogene–Eocene bottom current and an Eocene grounding of the West Antarctic ice sheet, which is consistent with the latest climate ice sheet model.

This seismic interpretation was expanded via (i) a shelf-slope link between the Ross Sea shelf seismic data and the central Amundsen Sea basin seismic data, and (ii) correlation with previous work in the eastern Amundsen Sea, Bellingshausen Sea and Antarctic Peninsula. Horizons were used as published except in the Bellingshausen Sea where the transitional boundary was interpreted. The collective margin-wide interpretation was correlated to the IODP Leg 318 site U1356 in Wilkes Land, using a visual correlation of seismic reflectivity characteristics and facies changes.

The derived total sediment thickness grid for the Pacific margin of West Antarctica extends the NGDC grid further south and indicates total sediment thickness up to 4 km. The PG, T and FG sediment grids depict an even distribution of sediment along the margin in the pre-glacial regime. The depocentres shift to the East during the Eocene–Oligocene transition, as the ice sheets arrive on the shelf. The eastward shift is continued into mid-Miocene. A new depocentre formed North of the Amundsen Sea Embayment, possibly related to ice sheet advancement that changed previous drainage patterns and a ~4.6 km (~10.2 x 10<sup>6</sup> km<sup>3</sup>) reduction in West Antarctic margin topography. Hypothetical estimates indicate that a sediment pile of ~2.7 km thick (~6 x 10<sup>6</sup> km<sup>3</sup>) should be placed back onto land in the 34 Ma Eocene–Oligocene palaeotopography reconstruction, and a pile of ~3.6 km thick (~8 x 10<sup>6</sup> km<sup>3</sup>) for the 15.5 Ma mid-Miocene palaeotopography reconstruction. The revised residual basement topography of the South Pacific shows an asymmetric trend over the Pacific–Antarctic Ridge. Values are anomalously high in the Ross Sea area, possibly due to persistent mantle processes. The elevated basement topography offshore Marie Byrd Land is therefore rather attributed to crustal thickening due to intra-plate volcanism. This revised basement topography of the South Pacific contradicts present-day dynamic topography models, and subsequent palaeotopography reconstructions would remain fairly uncertain.

Collectively this work presents initial impressions of the basin geometry and sediment distribution and transport processes, which were previously unknown for the central Amundsen Sea basin and the entire Pacific Margin of West Antarctica. These findings set the framework for planning future drilling and seismic data acquisition surveys, and for refining ice sheet models, palaeo-ocean current and palaeotopography studies.



---

SUMMARY.....	i
<b>1. Introduction.....</b>	<b>1</b>
1.1. Motivation.....	1
1.2. Open questions.....	4
1.3. Structure of the thesis.....	6
<b>2. Sediment transport processes.....</b>	<b>8</b>
2.1. Ice sheet advance and mass sediment transport processes.....	8
2.2. Inland to the outer shelf.....	9
2.3. Down-slope processes.....	10
2.4. Along-slope processes.....	11
2.4.1. Depositional features in the seismic reflection data images.....	15
2.4.2. Seismic characteristics of bed forms from down-/along slope processes.....	15
2.4.3. Seismic characteristics of pre-glacial, transitional and full glacial units.....	17
<b>3. Background.....</b>	<b>18</b>
3.1. Selected pre-glacial to glacial seismic stratigraphy studies.....	18
3.1.1. Weddell Sea.....	20
3.1.2. Bellingshausen Sea.....	21
3.1.3. Amundsen Sea.....	22
3.1.4. Wilkes Land.....	22
3.2. Study area.....	24
<b>4. Seismic reflection database and methods.....</b>	<b>26</b>
4.1. Acquisition.....	26
4.1.1. Method.....	27
4.1.2. Source.....	28
4.1.3. Receiver.....	28
4.2. Processing.....	29
4.2.1. Demultiplexing, geometry and sorting.....	29
4.2.2. Filtering.....	30
4.2.3. Editing.....	30
4.2.4. Static correction.....	30
4.2.5. Multiple removal.....	32
4.2.6. Deconvolution.....	32
4.2.7. Migration.....	32

<b>5. Other datasets and methods.....</b>	<b>34</b>
5.1. Borehole data.....	34
5.2. Magnetic seafloor spreading anomaly data.....	34
5.3. Refraction data analysis.....	35
5.4. Sonobuoy velocity data for the Amundsen Sea.....	37
<b>6. Contributions to Scientific Publications.....</b>	<b>39</b>
6.1. Deep-sea pre-glacial to glacial sedimentation in the Weddell Sea and southern Scotia Sea from a cross-basin transect.....	39
6.2. Pre-glacial to glacial stratigraphy in the unexplored Amundsen Sea deep-sea basin: A first cross regional correlation of deep-sea seismic reflection data .....	39
6.3. Anomalous South Pacific lithosphere dynamics derived from new total sediment thickness estimates off the West Antarctic margin.....	40
6.4. Pre-glacial to glacial sediment thickness grids for the Pacific margin of West Antarctica .....	41
<b>7. First paper: Weddell Sea – Scotia Sea transect.....</b>	<b>42</b>
7.1. Abstract.....	42
7.2. Introduction.....	43
7.3. Tectonic, palaeoceanographic and palaeoclimate setting.....	45
7.4. Datasets and methods.....	49
7.4.1. Magnetic anomaly isochron compilation.....	49
7.4.2. Borehole stratigraphy.....	50
7.4.3. Seismic characterization.....	52
7.4.4. Sediment thickness estimates.....	57
7.4.5. Age model and sedimentation rates.....	59
7.5. Observations, results and interpretation.....	60
7.5.1. Basement ages.....	60
7.5.2. Borehole correlation.....	60
7.5.3. Seismic characterization and horizon stratigraphy.....	60
7.5.4. Sediment thickness.....	62
7.5.5. Age model.....	63
7.5.6. Sedimentation rates.....	64
7.6. Discussion.....	65
7.6.1. Pre-glacial (PG) regime.....	66
7.6.2. Transitional (T) regime.....	69
7.6.3. Full glacial (FG) regime.....	72
7.7. Conclusions.....	74
7.8. Acknowledgements.....	76
7.9. References.....	76

<b>8. Second paper: Amundsen Sea – Ross Sea transect.....</b>	<b>83</b>
8.1. Abstract.....	83
8.2. Introduction.....	84
8.3. Tectonic and palaeoclimate setting.....	86
8.3.1. Rifting and basin development.....	86
8.3.2. Palaeoclimate development.....	88
8.4. Database and methods.....	91
8.4.1. Seismic reflection data.....	91
8.4.2. Interpretations approach.....	95
8.4.3. Integrating pre-existing data.....	98
8.4.4. Age model and sedimentation rate estimates.....	100
8.5. Results.....	100
8.5.1. Seismic interpretation and horizon characteristics.....	100
8.5.2. Seismic stratigraphic links.....	108
8.5.3. Sediment thickness.....	111
8.5.4. Sedimentation rates.....	113
8.6. Discussion.....	113
8.6.1. Pre-glacial (PG) sequence.....	114
8.6.2. The uPG-T boundary process: arrival of WAIS to the margin.....	116
8.6.3. Transitional (T) sequence.....	117
8.6.4. The uT-FG boundary process: permanent grounding.....	119
8.6.5. Full glacial (FG) sequence.....	119
8.6.6. Basement geometry.....	120
8.7. Conclusions.....	122
8.8. Acknowledgements.....	124
8.9. References.....	124
<b>9. Third paper: Anomalous South Pacific lithosphere and total sediment thickness.....</b>	<b>131</b>
9.1. Abstract.....	131
9.2. Introduction.....	132
9.3. Sediment thickness grids of the West Antarctic margin.....	133
9.3.1. Sediment thickness calculations.....	133
9.3.2. Data merging and gridding.....	134
9.3.3. Comparison to previous work and uncertainties.....	136
9.4. Age result of the oceanic lithosphere and basement depth.....	139
9.4.1. Residual basement depth anomalies.....	140
9.4.2. Residual basement depth vs. seafloor roughness.....	141
9.4.3. Residual basement depth vs. Shear wave velocity.....	143
9.5. Discussion.....	145
9.6. Conclusions.....	146

9.7.	Acknowledgements.....	148
9.8.	References.....	148
<b>10.</b>	<b>Fourth paper: Pre-glacial to glacial sediment thickness grids for the Pacific margin of West Antarctica.....</b>	<b>153</b>
10.1.	Abstract.....	153
10.2.	Introduction.....	154
10.3.	Database and methods.....	156
10.3.1.	Stratigraphic correlation.....	156
10.3.2.	Sediment thickness calculation.....	158
10.3.3.	Data merging and gridding.....	158
10.4.	Results and discussion.....	160
10.4.1.	The Pre-glacial sediment thickness grid.....	160
10.4.2.	The transition to ice sheets sediment thickness grid.....	162
10.4.3.	The full glacial sediment thickness grid.....	164
10.5.	Conclusions.....	164
10.6.	Acknowledgements.....	165
<b>11.</b>	<b>Conclusions and Outlook.....</b>	<b>170</b>
<b>12.</b>	<b>References for Chapters 1 to 5.....</b>	<b>176</b>
<b>13.</b>	<b>Acknowledgements.....</b>	<b>182</b>
<b>14.</b>	<b>Curriculum Vitae.....</b>	<b>183</b>

## Appendices

### A: Weddell Sea and Scotia Sea

A-1. Fold-out plot of the WS–SS transect

### B: Amundsen Sea and Ross Sea

B-1. A0 fold-out plot of the AS–RS transect

B-2. Velocity model from seismic reflection data

### C: South Pacific Lithosphere dynamics

C-1. Present-day dynamic topography models

C-2. List of seismic reflection profiles used for grids

# Chapter 1

## INTRODUCTION

Key aspects:

- Project motivation
  - Working hypotheses
  - Structure of the thesis
- 

### 1.1 Motivation

The deep-sea sedimentary record represents an archive of the pre-glacial to glacial development of Antarctica and can be used to reconstruct past dynamic ice sheet behaviour and palaeo bottom current development. Since initial glaciation in the greenhouse to icehouse climate transition, multiple episodes of ice sheet advance and retreat intertwined with past changes in world climate (Fig. 1-1; Zachos et al., 2001; Haq and Schutter, 2008; Tripathi et al., 2009, 2011), topographic uplift/subsidence (Fig. 1-2), plate tectonic reorganisation and ocean circulation (Ch. 3). These events change sediment erosion, transport and deposition.

Continental scale ice sheets increase erosion and rapidly transport massive amounts of sediments from inland to the coast, and as ice sheet growth continues, also onto the shelf edge, slope and deep-sea. Such events of ice sheet related increased sediment supply and deposition can be observed in seismic reflection images around Antarctica and are distinguished from other sequences through evaluating the varying internal structure, reflectivity characteristics and geometry of sedimentary bodies (e.g. Nitsche et al., 1997, 2000; De Santis et al., 2003; Rogenhagen et al., 2004; Maldonado et al., 2006; Scheuer et al., 2006a, b; Leitchenkov et al., 2007; Escutia et al., 2005, 2011; Uenzelmann-Neben and Gohl, 2012).

The interplay of ice sheet expansion, sediment erosion, transport and deposition processes that operated in the past are still poorly understood. Open questions such as the exhumation history and the mass balancing of offshore sediment deposits back onto land, for palaeotopography and palaeobathymetry reconstructions, are unresolved. To address parts of these aspects, quantification of the volume, thickness and distribution of

the pre-glacial to glacial components in the offshore sedimentary record on a circum-Antarctic scale are necessary. Past topography and bathymetry surface reconstructions provide boundary conditions for palaeoclimate models, which help to predict future ice sheet behaviour and the impact on sea level in case of partial or total ice sheet collapse (e.g. Pollard and DeConto, 2009; Fig. 1-3).

Current coupled ice-sheet climate models typically use the present day BEDMAP topography (Lythe et al., 2001; Fig. 1-2c) or ALBMAP (Le Brocq et al., 2010). However, the topography changed due to tectonics, palaeoclimate subsidence/uplift and erosion. For example, compared to the BEDMAP reconstruction (Fig. 1-2c), half of Antarctica was above sea level in the Cretaceous (Fig. 1-2a) and in the Eocene–Oligocene (Wilson et al., 2011; Fig. 1-2b), the latter time period marking the onset of glaciation in Antarctica (Barker et al., 2007).

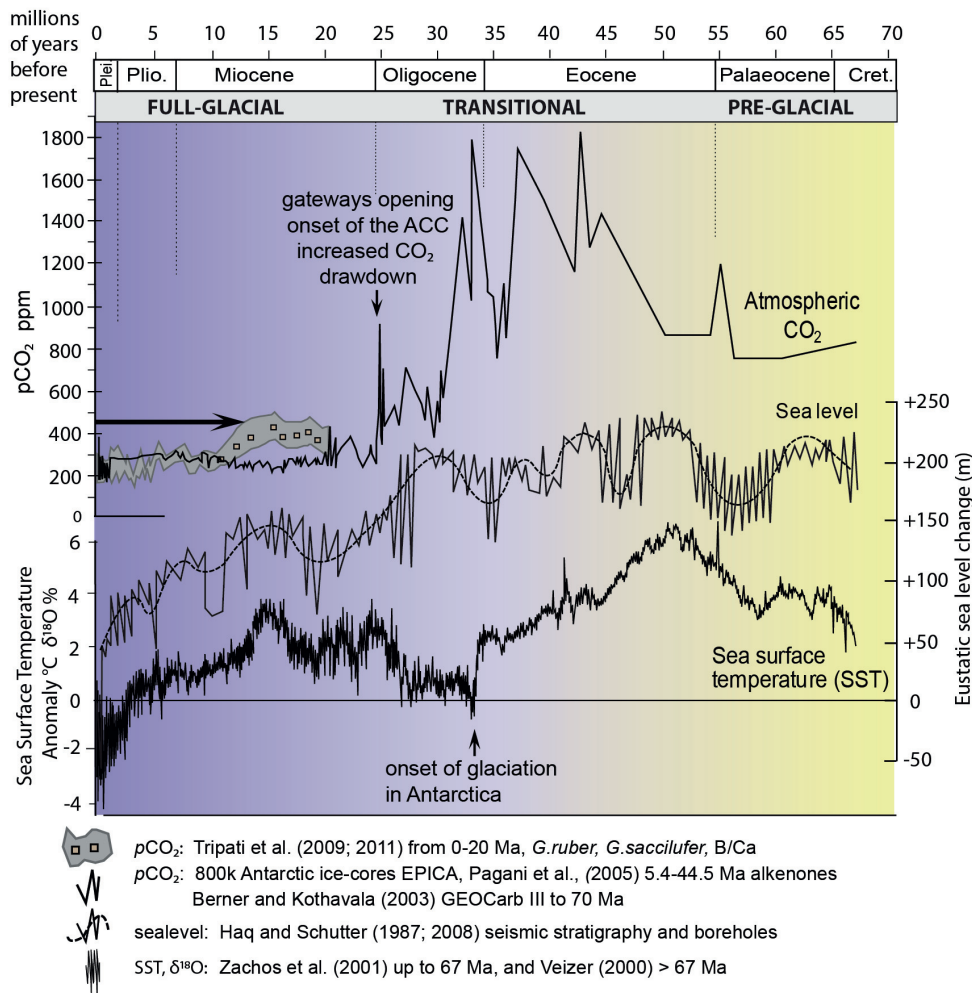


**Fig. 1-1.** Diagram of the changes in atmospheric CO<sub>2</sub>, sea level and sea surface temperatures (SST), from the Cretaceous (70 million years ago, Ma) to present. Atmospheric CO<sub>2</sub> for 0–20 Ma compiled from Triпати et al. (2009; 2011, shaded grey area with blocks) agree with the Antarctic ice core data up to 800k (Petit et al., 1999; Siegenthaler et al., 2005), but contradicts Pagani (2005, black line up to 44.5 Ma). The remainder of the CO<sub>2</sub> curve was taken from Berner and Kothavala (2001). Sea level curve was compiled from Haq et al. (1987) and Haq and Schutter (2008). Sea surface temperature (SST) δ<sup>18</sup>O curve taken from Zachos et al. (2001) for 0–67 Ma and from Veizer et al. (2000) after 67 Ma.



Modelling will therefore produce a very different scenario of past and future ice sheet behaviour and volume, depending on which palaeosurface was used in the model calculation. We thus need input parameters from the past geological record with similar or higher CO<sub>2</sub> levels than today such as the Mid-Miocene, Miocene–Oligocene and Eocene–Oligocene (Fig. 1-1) to test likely scenarios adequately. To derive more accurate data-constrained palaeosurface reconstructions, we first need to quantify the pre-glacial to glacial sediment thickness and volumes, which are some of the parameters for forcing the reconstructions that indirectly constrain the palaeoclimate models (Fig. 1-3).

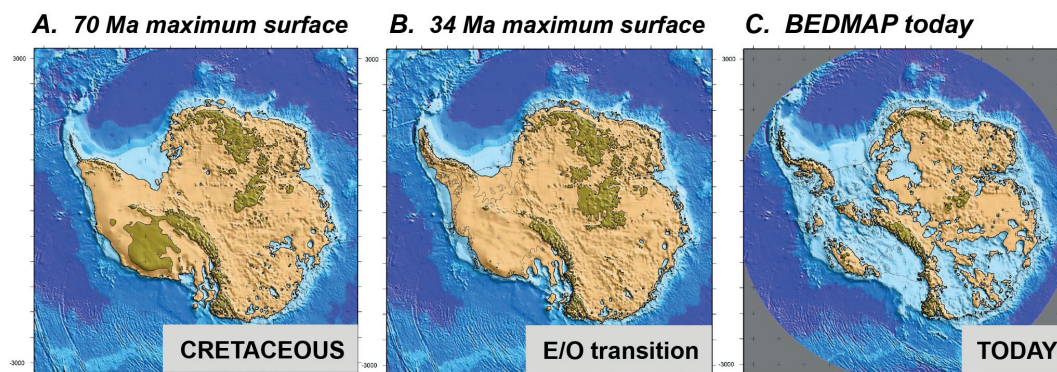


**Fig. 1-2.** Examples of palaeotopography models for Antarctica. **A.** The Cretaceous residual sediment grid model from the ANTScape group (pers. comm). **B.** The Eocene–Oligocene transition palaeosurface with sediment load corrected for the Ross Sea (Wilson et al., 2011). **C.** The present day BEDMAP topography (Lythe et al., 2001), and used in current palaeoclimate models, not isostatically corrected. Note the variation in heights between the models, light blue = 250 m below sea level and olive brown = 3000 m above sea level. Ma = million years.

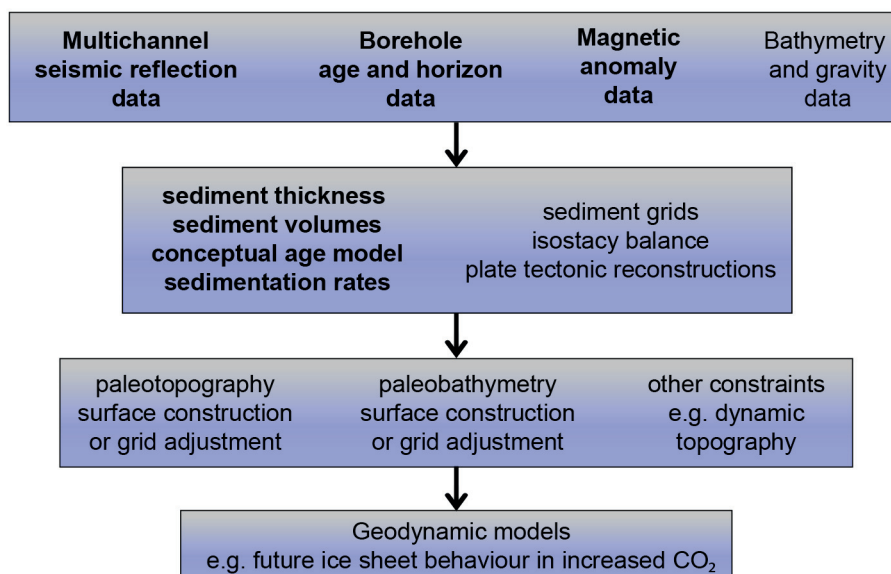


**Fig. 1-3.** Flow diagram illustrating the relationships between measured geophysical data and first order derived parameters such as sediment thickness and volume that feed into the mass balance palaeotopography and palaeobathymetry surface reconstructions. The latter subsequently provide boundary constraints for palaeoclimate models. Items in bold pertain to datasets and results in this thesis. Borehole and magnetic data were used for age control, see references in Chapters 5 to 9.

The continuously increasing seismic reflection data network around Antarctica (SDLD in Wardell et al., 2007; Ch. 2) now make it possible to image and identify the pre-glacial to glacial components in the sedimentary record over large regions e.g. the Weddell Sea and Bellingshausen to Amundsen Sea (Fig. 1-4), and enable initial cross-regional comparisons.

The research presented in this dissertation centres on identifying the pre-glacial, transitional and glacial components in the deep-sea sedimentary record of Antarctica in two large cross-regional scale case studies in the Weddell Sea and Amundsen Sea (Fig. 1-4). The goals are to gain insight into past ice sheet and bottom current development, and to provide measured constraints for mass balance reconstructions in palaeotopography and palaeobathymetry reconstructions (Fig. 1-2). Existing and recently acquired seismic reflection data form the basis for identifying these components and for developing a new cross-basin seismic horizon stratigraphy.

Preliminary age models are constructed from the horizon stratigraphy, seafloor spreading magnetic anomalies and borehole data, and used to estimate previously unknown sediment thickness, -volume and sedimentation rates. Periods associated with marked changes in sea level, atmospheric carbon dioxide budget and sea surface temperature proxies (Fig. 1-1) such as the Eocene–Oligocene (33 million years ago, Ma), Mid-Miocene (14 Ma), Miocene–Pliocene (5 Ma), are of particular interest for understanding the past ice sheet dynamics.

### 1.2 Open questions

Some of the unresolved aspects to consider for understanding initial Antarctic ice sheet development and past ocean bottom water circulation are encapsulated in the following questions, illustrated in Fig. 1-4:

#### **Q1 Does sediment thickness, volume and geometry of the pre-glacial to glacial sequences vary within a regional basin and between regions?**

- How do these parameters vary between the southeastern and northwestern Weddell Sea basin, and across the eastern Ross Sea to the eastern Amundsen Sea (Fig. 1-4)?
- Would the larger drainage areas (yellow dashed lines in Fig. 1-4) supply more sediment to the deep-sea basin and result in thicker units offshore (blue clouds in Fig. 1-4)?
- What do these variations imply for past bottom current activity?
- Do the basement geometry and topography reveal clues of the tectonic development?

**Q2 Was ice sheet advancement and initial grounding on the outer continental shelf relatively synchronous on a regional and cross-regional scale?**

- Higher sediment supply and mass sediment transport changes are captured as facies and internal geometry changes in the seismic images. The latter can be used to deduce the onset of the full glacial regime. In separating the pre-glacial, transitional and glacial components, can the initial advance of the ice sheet to the outer shelf be identified?
- Is it possible to determine when the ice sheets in each region initially advanced to the outer shelf from the hypothesized age models?
- Were glaciation onset in the Weddell Sea, Amundsen Sea, Ross Sea, Prydz Bay, and Wilkes Land synchronous and were similar amounts of sediment transported into the deep-sea (Fig. 1-4, blue clouds), or are there differences?

**Q3 Quantification of offshore sediments helps to constrain palaeotopography and palaeobathymetry surface reconstructions (Figs. 1-2 and 1-3).**

- What proportion of the deep-sea sediments can be assigned to pre-glacial (PG), transitional (T) and fully glacial (FG) conditions for mass balancing?
- What are the implications for mass balancing (white clouds in Fig. 1-4b) and the palaeosurface reconstructions, e.g. the 70 Ma palaeotopography surface model (Fig. 1-2a)?

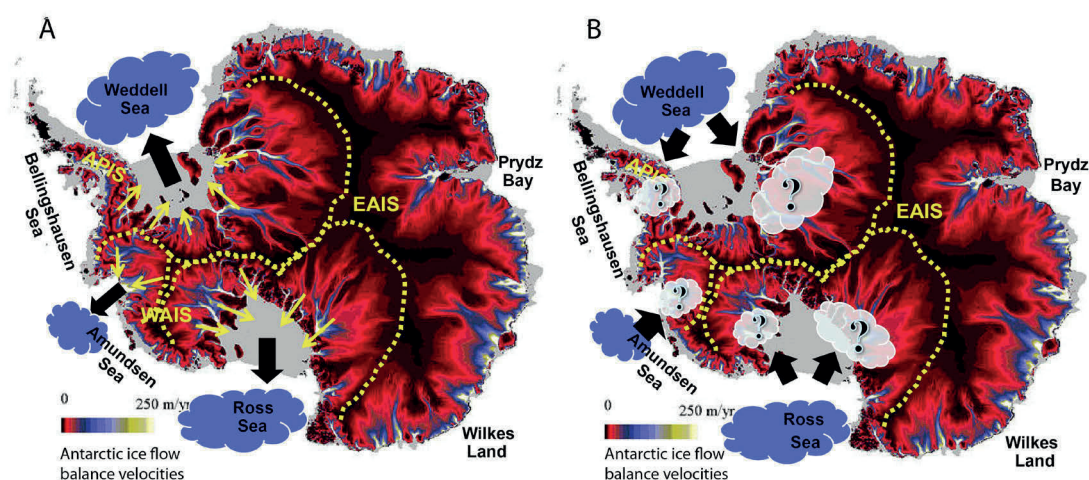


**Fig. 1-4.** Ice flow map of Antarctica, modified from Bamber et al. (2009). Yellow dashed lines demarcate major drainage areas for the Antarctic Peninsula Ice Sheet (APIS), the West Antarctic Ice Sheet (WAIS) and the East Antarctic Ice Sheet (EAIS). Black = regions with very low velocity drainage, blues to yellows = regions with high ice stream flow velocities (100–250 metres per year). Blue clouds in the Weddell Sea, Amundsen Sea and Ross Sea = hypothesized relative sediment thicknesses and volumes expected in the deep-sea sediments. Large cloud = high volume/thickness, small cloud = lower volume/thickness. Arrows and question marks represent the hypotheses of balancing eroded sediments for pre-glacial, transitional and glacial periods, back on to land in palaeotopography reconstructions.

### 1.3 Structure of the thesis

**Chapter 2** describes the down-slope sediment erosion and transport processes from inland to the coast, shelf and slope, and along-slope processes from the lower slope to the abyssal plane. These processes form distinct sedimentary bodies that can be identified in the seismic reflection data images, which could provide clues in separating the pre-glacial, transitional and full glacial components so as to understand the initial grounding of the ice sheets and palaeo bottom current development.

**Chapter 3** summarizes the tectonic and palaeocean circulation development of Antarctica from the Cretaceous to present, and provides a timeframe for this research. Selected deep-sea seismic stratigraphy studies that identified pre-glacial, transitional and full glacial components in the deep-sea basins around Antarctica are presented, and set the platform for two large case studies in the Weddell Sea and Amundsen Sea – Ross Sea basins, with a margin wide comparison.

**Chapter 4** explains the acquisition and processing of the recently acquired multichannel seismic reflection data in the Amundsen Sea and eastern Ross Sea during the ANT-26/3 expedition.

**Chapter 5** outlines the borehole data and magnetic seafloor spreading anomalies used for age control and estimation of the basement age range, and, the refraction and sonobuoy velocity datasets used for the sediment thickness estimates and the calculation of sedimentation rates.

**Chapter 6** lists the breakdown of contributions made to four scientific publications.

**Chapter 7** is the first published paper regarding the ~3300 km long cross-basin Weddell Sea – Scotia Sea (WS–SS) transect case study. The WS–SS transect consists of continuous multichannel seismic reflection (MCS) data, and a new compilation of the magnetic seafloor spreading anomalies across the Weddell Sea basin. Most of the pre-existing lines used were unpublished and uninterpreted. Consequently, a new seismic stratigraphy age model presented, with key horizons linked to those of localised studies in the Scotia Sea, northwestern Weddell Sea and southeastern Weddell Sea.

**Chapter 8** presents the second paper, which centres on the ~2000 km long Amundsen Sea – Ross Sea (AS–RS) seismic reflection transect. The AS–RS transect consists entirely of newly acquired seismic reflection data from the AWI Ant-26/3 survey and the GNS New Zealand Tan0602 survey. Both datasets have not been published before and is located across a large historically unsurveyed sector. A first seismic horizon stratigraphy model and age framework is presented, which may contribute to planning future survey and drilling operations.

**Chapter 9** is the third paper and presents the first total sediment thickness grid for the Pacific margin of West Antarctica, which extends the NGDC grid. The residual basement topography was derived from the total sediment thickness grid and explores whether palaeobathymetry reconstructions would be feasible.

**Chapter 10** encapsulates the fourth paper, where a correlation of key seismic horizons across the Pacific margin of West Antarctica is done. The two main horizons followed, represent processes related to the first ice sheet advance to the shelf, and the subsequent grounding on the shelf with advance/retreat cycles to the shelf edge. Sediment thickness, volumes and hypothetical mass-balancing values are derived for input into palaeotopography reconstructions, and the first margin wide pre-glacial, transitional and full glacial grids are presented. The Cretaceous development and trends of the depocentres expands our knowledge of the palaeocean circulation, and timing of the initial grounding of the Antarctic ice sheets on the outer shelf.

**Chapter 11** summarizes all the major conclusions of this research with respect to the questions presented in Chapter 1 and gives a short outlook for on-going and future work.





## Chapter 2

# SEDIMENT TRANSPORT PROCESSES

Key aspects:

- Sediment transport from inland, to the outer shelf and abyssal plain
- Down-slope processes: slumps, slides, turbidites, channel-levee systems
- Along-slope processes: bottom currents, sediment drifts/contourites
- Recognising some of these deposits in seismic reflection data

---

### 2.1 Ice sheet advance and mass sediment transport processes

The long tectonic time scale climate change periods of the pre-glacial to glacial transition of Antarctica over the last 70 million years is the time frame for this project. The past climates spanning the Cretaceous to present are broadly defined as the Pre-Glacial (PG), Transitional (T) and Full-Glacial (FG) regimes (Figs. 1-2 and 2-1). The PG-regime is outlined as a relatively warm, tundra/alpine-like climate that was predominantly ice sheet free, with river systems, smaller glaciers on high altitudes and open ocean conditions (Fig. 2-1a), but no continental scale ice sheets with wide ice streams as we see in Antarctica today.

The T-regime depicts a colder climate during the Eocene–Oligocene climate transition (Warny and Askin, 2011; Fig. 1-1). Sea-ice developed and larger ice sheets began to transport sediments to the outer shelf through ice-streams, and multiple retreat and re-advance cycles (Fig. 2-1b). The FG-regime designates a cold polar climate in which continental scale ice sheets expanded to the coast and permanently grounded on the outer shelf; similar than Antarctica today (Fig. 2-1c). The shorter time-scale interglacial cycles are considered as being part of the FG sequence. Details of the full-glacial period such as the last glacial maxima, or consideration of the reverse pre-Cretaceous snowball earth events (Hoffmann 1999) are beyond the project scale.

Within the T to FG time, repeated growth/demise cycles of continental scale ice sheets increased the onshore erosion and acted as an effective mass transport mechanism, which supplied higher volumes of sediment to the continental shelf over a relatively short period of time.

## 2. Sedimentary processes

---

The slope to deep-sea transport, and deposition into various sediment bodies, were mostly controlled by a combination of down-slope gravitational- and along-slope bottom current driven processes. Collectively, these processes resulted in complex structures in the sedimentary record that can today be used to enhance our understanding of past ice sheet and bottom ocean current development.

Before describing and interpreting the features observed in the seismic data of the Weddell Sea and Amundsen Sea case studies (Ch. 7 and 8), it is necessary to clarify the terminology used, and to understand three aspects around mass sediment transport processes: (i) which past climate regimes were involved and what may the landscapes have looked like during each regime, (ii) which transport processes produce particular sedimentary features and (iii), what would these features look like when imaged in seismic reflection data.

Sediments deposited in the PG, T and FG regimes are typically distinguished from another in seismic reflection imaging through variation in reflectivity characteristics, seismic facies and the geometry of the sediment body. A few seismic stratigraphy models around Antarctica already associated certain components of the sedimentary record with the PG, T and FG regimes respectively, and some of these have been verified by drilling (e.g. Escutia et al., 2011; Ch. 3). To understand which sediment transport processes produce particular sedimentary deposits we compare the depositional domains. The comparison starts inland and moved towards the deep-sea, across the continental shelf, slope and abyssal plane.



**Fig. 2-1.** Modern day climate analogues illustrate the possible pre-glacial to glacial landscape development of Antarctica. **A.** Pre-glacial (PG) tundra/alpine-like landscape with glaciers, broad U-shaped valleys and river systems. **B.** Transitional (T) climate regime with ephemeral ice sheets and ice-streams or glaciers expanding down to the coast. **C.** Full-glacial (FG) landscape with sea-ice conditions, ice shelves and continental scale ice sheets to the coastline, grounded on the outer continental shelf. Source: [www.garycook.co.uk](http://www.garycook.co.uk)

### 2.2 Inland to the outer shelf

During the PG-climate, inland to coast sediment erosion and transport predominantly occurred through river systems and smaller glaciers (Fig. 2-1a). Poorly sorted riverbank and moraine deposits would have been carried to the sea by the fast flowing rivers and eventually be deposited on the floodplain or in the delta fan. Such river and glacier driven erosion could have increased due to higher relief and mountain building from



tectonic uplift. Consequently, these processes would have led to high PG-regime sedimentation rates on the shelf and abyssal plane.

In the T-climate, ice streams and sub-glacial rivers would presumably have been the dominating sediment erosion and transport mechanisms as ephemeral ice sheets reached the coastline (Fig. 2-1b). Typical glacial morphologic bed forms would include large cross-shelf troughs, mega-scale glacial lineations (MSGSL), drumlins, iceberg scours, and melt water channel systems (Fig. 2-2; Dowdeswell and Siegert, 1999; Graham et al., 2009, 2010; Livingstone et al., 2012).

The highest inland-to-outer shelf sediment transport rates would have probably occurred in the FG-climate regime as initial grounding cycles of the advancing ice sheet pushed sediments in front of it with a bulldozing effect, combining high erosion and high sediment transport via the ice streams (Ó Cofaigh et al., 2005; Domack et al., 2006; Evans et al., 2006; Wellner et al., 2006; Bell et al., 2007). Typical FG-geomorphic submarine landforms would include grooved and gouged bedrock, grounding zone wedges, cross-cutting MSGSL if the ice streams changed direction, larger channels and drumlins (Fig. 2-2; Graham et al., 2009, 2010; Livingstone et al., 2012), and inter ice-stream ridges (Klages et al., 2012). These processes are illustrated in Fig. 2-2.

### 2.3 Down-slope processes

Once the sediments reach the outer edge of the continental shelf through glacial and/or fluvial transport, gravity driven mass sediment transport down-slope processes such as slides, slumps, debris flows and turbidity flows displace the accumulated sediment load from the shelf edge to the upper slope, lower slope and finally onto the abyssal plane (Fig. 2-2). The basic down-slope transport motion is a combination of sliding and suspension and continues until movement ends due to friction (Niedorada et al., 2003).

Slumps and slides move the lowest amount of sediment over the shortest distance, whereas debris flows and turbidite flows travel faster and farther, and have the highest erosion capacity (Shanmugam, 2008). Turbidites typically move in V-shape channels or submarine canyons and subsequent bed forms such as asymmetrical channel-levee systems and turbidite fans form through suspension settling (Fig. 2-2; Wynn and Stow, 2003; Dowdeswell et al., 2004a, b; Shanmugam, 2000, 2008).

Channel-levee systems deposits and channel fill deposits often show preferential asymmetrical deposition on the left flank due to the Coriolis force effect (Uenzelmann-Neben and Gohl, 2012). These gravitational down-slope mass sediment transport processes and the melt water erosion of ice streams typically leave a network of gullies on the upper slope that lies perpendicular to the margin (Fig. 2-2; Evans et al., 2006; Wellner et al., 2006; Dowdeswell et al., 2004a, b; Noormets et al., 2009).

In the T- and FG-climates, ice sheet advances would bulldoze most of the sediment deposits off the shelf and thereby rapidly increase sediment supply to the outer shelf and upper-slope, and amplify the gravitational down-slope sediment movements. This results in thicker progradational sequences and more complex depositional patterns at the foot of the slope, which have been observed in reflection seismic images around Antarctica and used to separate decipher multiple ice sheet advance and retreat cycles (e.g. De Santis et al., 1999, 2003; Rogenhagen et al., 2004; Escutia et al., 2005; Maldonado et al., 2006; Scheuer et al., 2006a, b; Leitchenkov et al., 2007; Graham et al., 2009; Smith and Anderson, 2011). Some of these studies are discussed in more detail in the next chapter. In contrast, the PG sequences would show fewer of these mass sediment transport deposits in the seismic reflection images, which could indicate a comparatively lower sediment supply.

### 2.4 Along-slope processes

Along-slope processes occur typically parallel to the continental margin, concentrated at the foot of the slope and on the abyssal plane. Bottom currents predominantly control the distribution of the down-slope sediment supply and reworking of existing deposits through traction, saltation, sliding, rolling and suspension (Allen 1984; Shanmugam 2008). In along-slope processes, sediment composition can be fine to coarse grained and have mixed origins (glacial, pelagic, terrigenous and volcanoclastic).

The term “bottom current” is used in a general sense and refers to long period, semi-permanent thermohaline-induced geostrophic (contour) currents and wind-driven currents as defined in Rahmstorf (2006). It is recognised that sub-processes such as deep-water tidal bottom currents, canyon currents, up/down-welling, internal waves, benthic storms, large eddies and vortices also contribute sediment to nepheloid layer (i.e. the bottom 200–1000 m of the seawater column that is also in direct contact with the seafloor at its base). However, little is still known about the dynamics and contributions of these periodic sub-processes. Therefore, within the context of the cross-regional scale and scope of this study, the more permanent thermohaline and wind-driven bottom current generating components are being referred to.

Bottom currents are thought to primarily form when heat loss at the sea surface, accelerated by cold winds, leads to an increase of the surface layer density. Sea ice forms and increases the surface layer salinity further. Consequently, the layer becomes unstable and convective mixing is initiated as the layer sinks to form bottom water (Van Aken, 2007). This typically occurs on the continental shelf where the water mass pools until it finally spills down the slope and onto the abyssal plane where it forms an along-slope bottom current and joins the global thermohaline deep-water circulation (Rahmstorf, 2006).

Bottom currents may flow parallel, perpendicular or up/down the slope at intermediate speeds of 10-30 cm/s and higher, which is considered fast enough to entrain and transport coarse grains from the down-slope turbiditic fans (Stow et al., 2008).

The mixed down-slope and along-slope sediment load are re-deposited parallel to the margin in bed forms called contourite drifts, also referred to as drifts or sediment drifts (Fig. 2-2; Shanmugam, 2008; Stow et al., 2008). The accumulation rates and geometry of the drifts are controlled by the flow direction, velocity and entrainment capacity of the bottom current, sediment supply, winnowing and deposition (e.g. Koenitz et al., 2008; Rebesco and Camerlenghi, 2008). In addition, the Coriolis force also influences the geometry of these features, causing an asymmetrical and preferred deposition to the left of the current flow direction in the southern hemisphere.

Based on the shape and position with respect to the slope, these contourites are subdivided into five principal types: sheeted drifts, asymmetrical elongated mounded drifts, channel-related drifts, confined/plastered/patched drifts and a mixed drift/turbidite system (Fig. 2-2; Faugères et al., 1999; Rebesco and Stow, 2001; Stow et al., 2002; Rebesco 2005; Faugères and Stow, 2008; Shanmugam, 2000, 2008; Nielsen et al., 2008).

Sheeted drifts, separated mounded drifts, patched drifts and mixed systems are most relevant to this work and are most common on the abyssal plane around Antarctica (e.g. Maldonado et al., 2006; Uenzelmann-Neben and Gohl, 2012; Fig. 2-2). Sheeted drifts accumulate over a broad area on the abyssal plain ( $1 \times 10^6 \text{ km}^2$ ), are laterally extensive, have a fairly uniform thickness and show low relief (Fig. 2-2). Typical sedimentation rates for sheeted drifts are 3–10 cm/ka and 5–30 cm/ka for mounded drifts (Stow et al., 2008).

Mounded drifts mostly occur near the foot of the slope and are more elongate over a narrow region ( $> 0.1 \times 10^6 \text{ km}^2$ ). They can be up to 1000 km long, 10-100 km or more wide and display a relief or thickness of up to 2 km (Faugères and Stow, 2008). A steep and less inclined flank and discontinuities at their bases are often diagnostic.

Patched drifts occur at the foot of the slope and have a mostly symmetrical convex shape. Mixed systems often show along-slope and down-slope depositional geometry, e.g. stacked channel-levee and drift deposits that are often difficult to identify separately (Faugères and Stow, 2008).

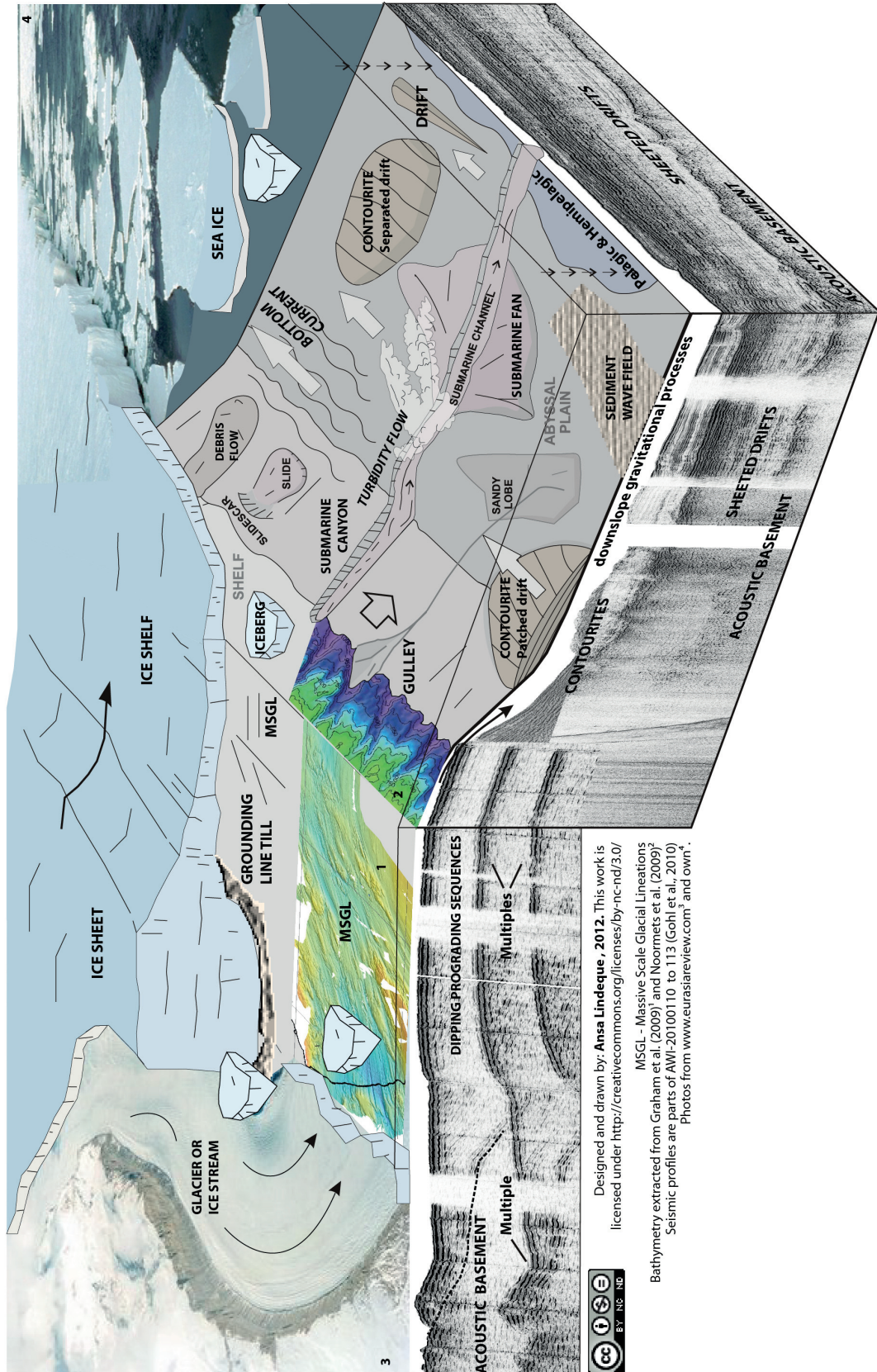


**Fig. 2-2.** Schematic 3D-diagram showing the main large scale simplified sedimentary transport environments and depositional features on the slope, shelf and abyssal plane. Tides, waves, moving ice streams, ice shelves and glaciers dominate the shelf. The slope is characterised by mass volume movements under gravity (slides, slumps, turbidity flows) and tidal bottom currents in the canyons. Typically thermohaline-induced slope parallel bottom currents, contourite deposits and sediment drifts mark the abyssal plane. However, these can be cross cut perpendicularly by down-slope gravity-induced turbidity flow bottom currents.



Though sediment drifts bed forms indicate bottom current activity, their absence does not unequivocally imply that no bottom current existed. Non-deposition can occur if the sediment supply is lower than the erosion rate, or if the contourite has been completely eroded and reworked (Stow et al., 2008). Hence, the regional and cross regional tectonic and palaeocean circulation context should also be considered during interpretation of seismic reflection and borehole log data.

Bottom currents have an enormous influence on the along-slope geometry and thickness of the sedimentary sequences. The development of bottom currents around Antarctica within plate tectonic changes should also be considered when looking at the sedimentary record in the seismic images. The tectonic history of the study area will be discussed in Ch. 3 and is only briefly introduced here to tie the sedimentary processes, PG, F and T climate regime changes, and tectonic and bottom current development into a reference framework.

The pre-glacial (PG) climate regime falls in the Cretaceous time (Fig. 1-1) when the Tasmanian gateway (Stickley et al., 2004) and Drake Passage (Barker and Thomas, 2004) were still closed to deep water circulation and the Antarctic Circumpolar Current (ACC) system undeveloped (Livermore, 2005; Barker et al., 2007; Ch. 3). During the PG-regime, even if ice sheets were absent or short lived, mountain building due to plate tectonics and strong river systems of a warm climate may have caused high erosion and increased sediment supply to the outer shelf.

Precursor gyres and localised bottom currents (e.g. Stickley et al., 2004) could have eroded, transported and re-deposited sediments. Hence, one could still expect contourites as along-slope bed forms, but smaller and sparsely distributed compared to the transitional to full glacial regimes.

In the Transitional (T) to full-glacial (FG) climate regimes (Eocene to Pliocene, Fig. 1-1) it is generally assumed that alpine-style glaciers, polar ice streams and grounding ice-sheets increased sediment input to the outer shelf exponentially and triggered significant down-slope sediment movement.

Similarly, the opening of gateways and formation/intensification of the ACC would increase bottom current volume and velocity. In response to ice-sheet induced increased sediment supply and stronger bottom currents, the occurrence, size and lateral extent of the contourite bed forms would increase (Ó Cofaigh et al., 2003, 2004, 2005).

In seismic images, these dynamic ice sheet and tectonically induced bottom current/sediment supply changes correspond to a marked difference in the reflection pattern in the seismic image. Proceeding “up-sequence” (from acoustic basement to seafloor, Fig. 2-3) modifications or burial of older drift morphologies, a marked increase in “new” drifts and channel-levee systems, and high amplitude discontinuities can usually be observed.

Analyses of these sediment drift modifications have been used to extract information towards constraining past ice sheet dynamics, bottom current pathways and palaeocean circulation reconstructions (e.g. Maldonado et al., 2003, 2005; Rebesco et al., 2002, 2007; Uenzelmann-Neben and Gohl, 2012), which I elaborate on in the next section and chapter.

### 2.5 Depositional features in the seismic reflection data images

We now look at an overview of the main seismic reflection characteristics useful for (i) identifying principle, large-scale, down-/along-slope deposit geometries on the abyssal plain, and (ii) for mapping the pre-glacial to glacial (PG, T and FG) units observed in seismic reflection images. The examples were taken from the same region as the case studies for more relevant comparison when interpreting the seismic images in the Weddell Sea and Amundsen Sea study areas (Ch. 7 to 10).

Sedimentary processes are often complexly intertwined. Down-slope mass transport deposits (e.g. turbidites or debris-flows) may be indistinguishable from along-slope deposits (e.g. contourite drifts) if solely based on geometry, elongation trend or reflection patterns (Faugères and Stow, 2008). The bed form geometry seen in the seismic images also depends on the profile orientation. The features should ideally be crossed perpendicular and parallel to the margin, but this is often not the case due to sea-ice and survey constraints. The following examples are therefore, only a guideline for interpreting the system end-members and by no means extensive. For additional examples of contourites in seismic images around Antarctica, the reader is referred to Hernández-Molina (2008a,b).

#### 2.5.1 Seismic characteristics of bed forms from down-/along-slope processes

**Mass sediment transport deposits** appear transparent to opaque, with chaotic or discontinuous internal reflection pattern (Fig. 2-3a). The lenses contain coarser material and are relatively homogeneous or poorly sorted – resulting in a scattered seismic signal without noticeable internal structure.

**Contourite drifts** are usually elongated with a lens-shaped convex upwards geometry (Fig. 2-3a,c,d), except in the case of large regional sheeted drifts (Fig. 2-3b). The internal seismic reflections are distinct and continuous, forming a parallel lamination that follows the overall drift geomorphology. Some sheeted drifts can have low-amplitude and discontinuous reflectors up to transparent reflectors and contain large sediment wave fields (Figs. 2-2 and 2-3a; Faugères and Stow, 2008). Elongated-mounded or separated drifts can show low angle-downlap or termination of internal reflections onto the basal unconformity. Variations include the patched drift (Fig. 2-3a), sheeted drift (Fig. 2-3b),

an asymmetrical separated drift with moat (Fig. 2-3c) and an elongated mounded drift (Fig. 2-3d).

**Channel levee systems** have a diagnostic current-scoured channel and associated asymmetrical levee (Fig. 2-3b). Similar to drifts, the internal reflections are continuous and follow the overall geometry. If buried, the upper boundary is characterised by a continuous high amplitude reflection and draped post-drift sediments fill the palaeochannel (Fig. 2-3c).

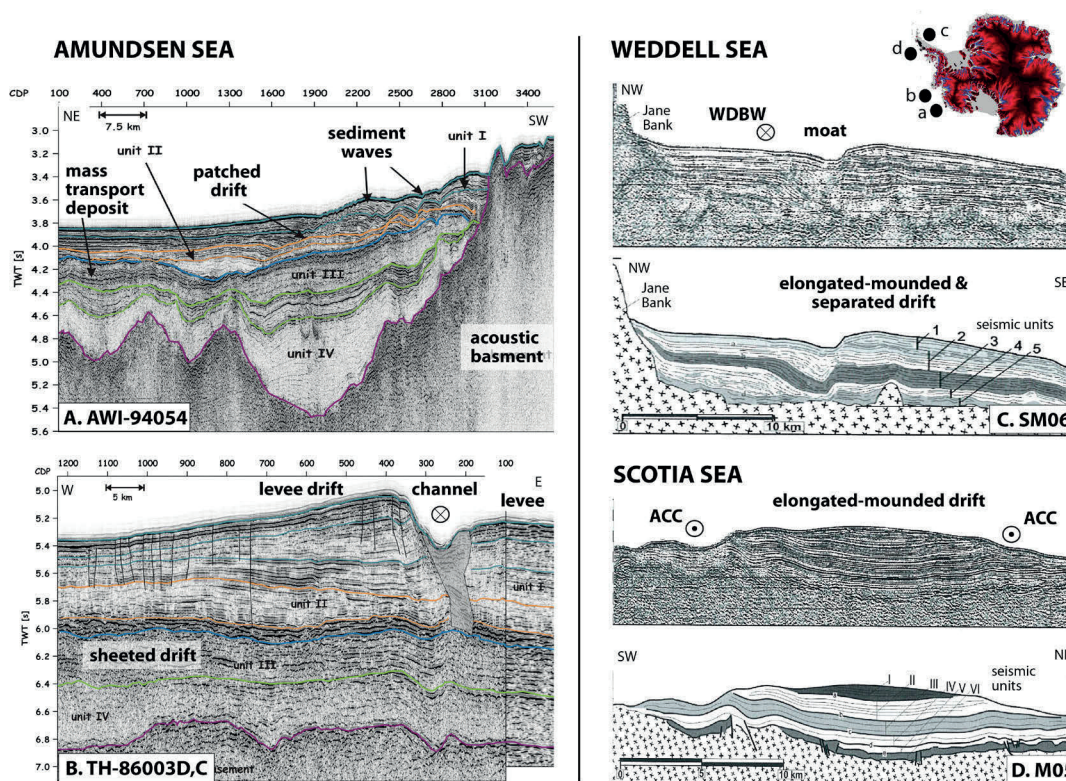


**Fig. 2-3.** Selected multichannel seismic reflection profiles and line drawing interpretations in the Amundsen-, Weddell- and Scotia Seas to illustrate the basic characteristics of large-scale contourite bed forms on the abyssal plain, formed by down-slope and along-slope processes (Fig. 2-2 and section 2.4). Diagrams a and b are modified after Uenzelmann-Neben and Gohl (2012) and c and d after Maldonado et al. (2006a,b)

**A.** Profile AWI-94054 with an interpreted down-slope mass transport deposit (debris flow in unit I), patched drift (unit III, IV) and sediment waveforms (unit V).

**B.** Profile TH-86003 parts D and C in the eastern Amundsen Sea depict a channel-levee system with preferential coriolis-forced deposition on the left, and sheeted drifts in unit III. Grey shaded area – filled channel, vertical black lines – small faults.

**C.** Profile SCAN97-SM06 near the Jane Bank in the northwestern Weddell Sea shows an along-slope process separated drift and moat. WSBW – Weddell Sea Bottom Water, circle with cross – bottom current flow direction away from the viewpoint, circle with dot – bottom current flow towards the viewpoint.

**D.** Profile SCAN2001-Sm05 in the central Scotia Sea illustrates an elongated-mounded drift formed by the bottom component of the Antarctic Circumpolar Current (ACC).



### 2.5.2 Seismic characteristics of Pre-glacial, Transitional and Full-glacial units

The sediment depositional style changes from a non-current to current dominated regime, or from a pre-glacial to glacial climate change regime. These changes result in regional extent unconformities or strong high-amplitude boundary reflectors (Nielsen et al., 2008). A type section after the descriptions of Escutia et al. (1997, 2000, 2011) and De Santis et al. (2003) represents typical characteristics of the pre-glacial to glacial seismic units (Fig. 2-4a,b). This section was chosen because it was recently drilled in IODP leg 318 (Fig. 2-4c) and is near the Amundsen Sea study area.

Pre-Glacial units show low amplitudes, an almost transparent image, and a few discontinuous internal reflections that are predominantly parallel to each other and the basement topography. The Transitional units have higher amplitude, lateral continuous reflectors, and show internal structure or discontinuities. Buried drifts and cut-and-fill geometries can occur infrequently. The Full-Glacial units have the highest amplitude reflections with strong lateral continuity. Contourite drifts, channel-levees systems and high relief are widespread within this sequence. The bed forms geometries are mostly well developed, which indicates high sediment supply and stronger bottom current activity.

These interpretations are geometric information on the bed forms as seen in the profiles. When available, borehole information provides a time-scale to the seismic unit and in combination; this is the only method to determine which units can be assigned to the PG, T and FG climates.

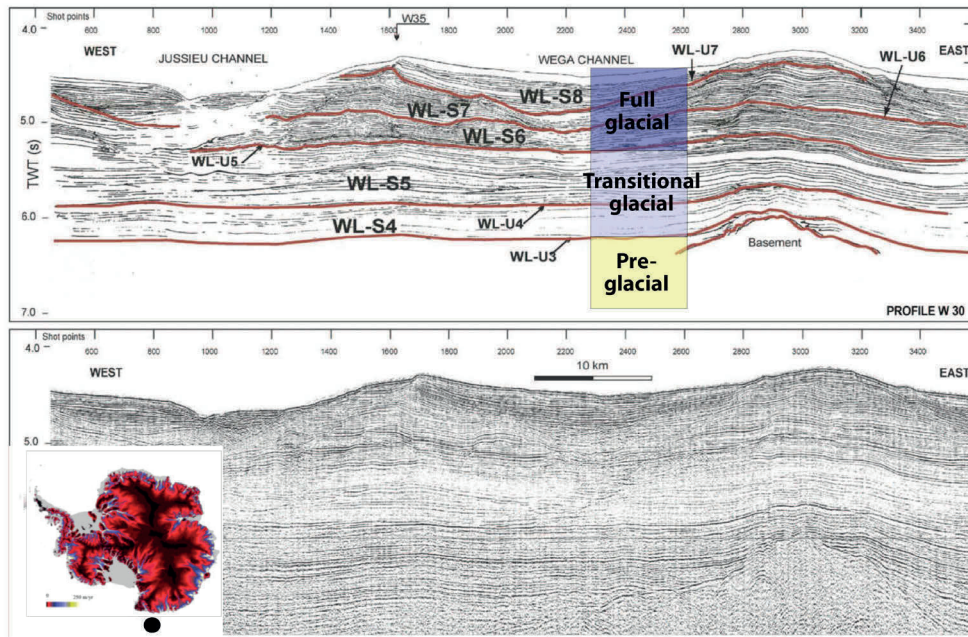


**Fig. 2-4.** Deep sea multichannel seismic reflection line WEGA30 in Wilkes Land (insert map), interpreted by Escutia et al. (2005; 2011) and De Santis et al. (2003), and modified to highlight the relevant sequences that they interpreted to represent the pre-glacial, transitional and full glacial periods, based on borehole data from IODP leg 318, sites U1355-1362 (Escutia et al., 2011). WEGA30 is one of the most relevant lines for this work, because it lies between two boreholes (U1359, U1361 with coincident seismic tie lines), runs coast parallel and is located on the continental rise. The stratigraphy is thus well defined, dated and least influenced by shelf processes.



## Chapter 3

# BACKGROUND

Key aspects:

- Selected pre-glacial to glacial studies
  - Study areas: Weddell Sea, Amundsen Sea, Pacific margin of West Antarctica
- 

Several studies around the Antarctic margin identified pre-glacial to glacial components in the offshore sedimentary record using drilling and seismic reflection imaging data (e.g. De Santis et al., 1999, 2003; Rogenhagen et al., 2004; Escutia et al., 2005; Maldonado et al., 2006; Scheuer et al., 2006a,b; Leitchenkov et al., 2007). These findings have been related back to changes in sediment distribution, associated with ice sheet advances or ocean bottom current development.

### 3.1 Selected deep sea seismic stratigraphy studies

Sediment thickness and volumes are among the key parameters for forcing palaeotopography and palaeobathymetry models (Fig. 1-3 in Ch. 1) but these are often excluded (e.g. Brown et al., 2006) or, if considered, based on out-of-date information from the 1970's (Hayes and LaBrecque, 1991; Hayes et al., 2009) and few data points (Laske and Masters, 1997), which distort the grids in sparsely surveyed regions.

One of the main reasons why palaeo-models omit offshore sediment thickness lies therein that current seismic stratigraphy studies around Antarctica are local scaled, stratigraphically disconnected from each other, and often limited by sparse borehole age control or data availability (e.g. Larter and Barker, 1989; Nitsche et al., 1997, 2000; De Santis et al., 1999, 2003; Cunningham et al., 2002; Rogenhagen and Jokat, 2000; Rogenhagen et al., 2004, Escutia et al., 2005; Scheuer et al., 2006a,b; Maldonado et al., 2006, 2007; Leitchenkov, et al., 2007; Uenzelmann-Neben, 2007; Weigelt et al., 2009).

These studies established detailed horizon stratigraphy mostly for shelf processes or palaeo-bottom current circulation. The broad cross-region perspective of sediment distribution on the shelf and deep sea and what it reveals about the greenhouse to icehouse ice sheet development remain largely unresolved.

The seismic data network around Antarctica expanded during the last two decades and most of it is now publically available (Wardell et al., 2007; Fig. 3-1). Several local scale studies around Antarctica, referenced below, investigated the shelf and deep sea

### 3. Background

seismic reflection sedimentary record to answer questions related to past ocean current development and ice sheet dynamics.

However, large-scale cross-basin and cross-regional studies that bind these smaller studies together are still lacking. For example: until recently it was not possible to connect the seismic horizon stratigraphy in the southwestern Weddell Sea with that of the northwestern Weddell Sea and Scotia Sea (red oval, Fig. 3-1), but with the data acquired from Spain under Institute collaboration, these links can now be made. More recent multichannel seismic (MCS) data acquisition by AWI during the 2010 expedition on the Pacific margin of West Antarctica (ANT-XXVI/3; Gohl, 2010), provided profiles that now link the Ross Sea seismic network with that of the Amundsen Sea (red oval, Fig. 3-1).

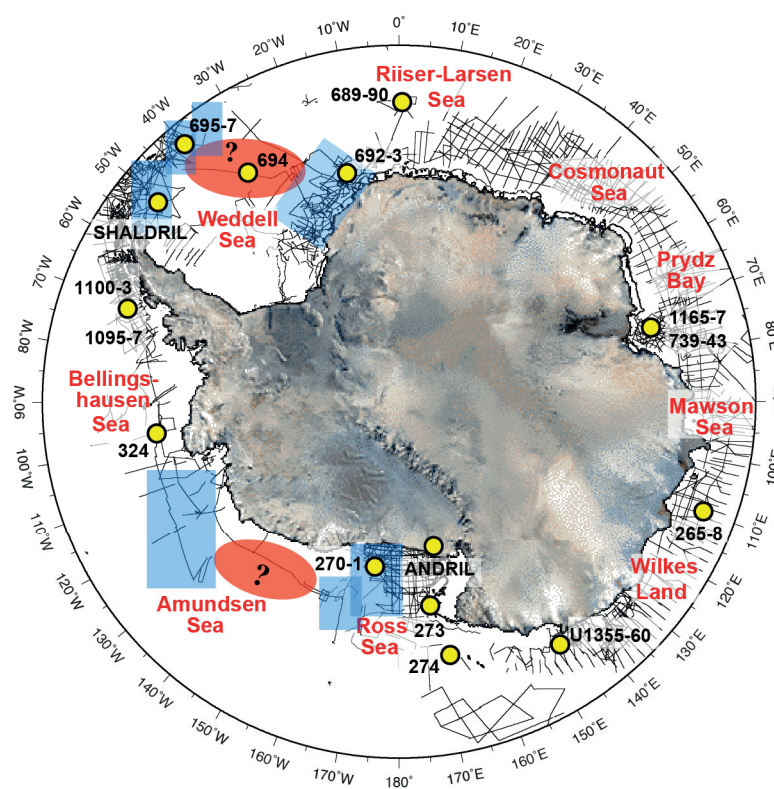


**Fig. 3-1.** Tracks of existing marine multichannel seismic (MCS) profiles around Antarctica available in the SCAR Seismic Data Library System (SDLS in Wardell et al., 2007; black lines).

Localised studies are broadly demarcated by the blue rectangles. Linking transects for the Weddell Sea and Amundsen Sea constructed in this research, are marked by the red ovals and question marks.

Various boreholes around Antarctica are shown as yellow dots: ANDRIL, SHALDRIL, Deep Sea Drilling Program (DSDP) numbers 265-274 and 324, Ocean Drilling Program (ODP) numbers 689-697 and 1095-1103, and International Ocean Drilling Program (IODP) numbers U1355-60. Ice surface taken from ETOPO1. Map modified after M. Breitzke and K. Gohl, AWI.

From this new and archive information, we can now begin to make cross-basin and cross-regional stratigraphic correlations of the deep sea and shelf sediments. However, four aspects make it difficult to do margin-wide seismic horizon correlations over 1000s of kilometres without assumptions:

- i. Persistent perennial sea ice, especially in the Weddell and Ross Sea, limit seismic reflection data acquisition and often dictate the distribution of lines.

- ii. Seafloor multiples on the shelf and sparse data, especially in the Ross Sea and Amundsen Sea region, make the correlation of shelf-slope-deep sea transitions problematic.
- iii. Limited age control on seismic horizons due to sparsely distributed deep-sea borehole information, or the complete absence thereof (e.g. in the Amundsen Sea).
- iv. Mass sediment transport processes on the shelf like turbidites or debris flows disturb the sedimentary layers and produce discontinuous, disturbed reflections in the seismic record that are challenging to trace over long distances.

The current deep sea pre-glacial to glacial work in each of the primary offshore Antarctic regions is briefly described to provide the context for this research and its contributions. The main studies on the Pacific margin of West Antarctica are considered and much supporting information drawn from the nearest and deepest distal basin borehole ODP Leg 318 Site U1356 (Escutia et al., 2011).

### **3.1.1 Weddell Sea**

In the Scotia Sea and northwestern Weddell Sea (Fig. 3-1), two Oligocene–early Miocene pre-glacial seismic units were identified (e.g. Sh5, Sh4; WD5, WD4 in Maldonado et al., 2005, 2006). A prominent horizon called “reflector c” was traced continuously between the Scotia Sea and northwestern Weddell Sea, and correlated with some of the ODP Leg 113 boreholes (Maldonado et al., 1998, 2003, 2005, 2006; Bohoyo, 2004; Bohoyo et al., 2002).

This major regional discontinuity were given a tentative age of 12.1–12.6 Ma and was interpreted to be coeval with the major Miocene glaciation (Mi4), a lowering of sea level (Ser3) and the initiation of the permanent east/west Antarctic ice-sheets in full-glacial conditions (Maldonado et al., 2006). Reflector “c” was also inferred to suggest a major event in the dynamics of bottom water circulation, representing the connection between the Scotia Sea and the Weddell Sea across the South Scotia Ridge (Maldonado et al., 2006). Transitional units were not interpreted.

MCS profiles across the Pacific margin of the Antarctic Peninsula showed a highly dynamic late Miocene Antarctic Peninsula ice sheet that repeatedly grounded to the shelf edge (Bart et al., 2005). This was followed by a series of oblique Pliocene-Pleistocene progradational sequences produced by ice sheet retreat and advance cycles during the glacial maximum or full glacial regime (Larter and Barker, 1989).

### 3. Background

---

Later work compared MCS data across ODP/DSDP boreholes in the Antarctic Peninsula, Prydz Bay, Wilkes Land, Weddell Sea, Eastern and Western Ross Sea (Fig. 3-1; Rebesco and Camerlenghi, 2008). Margin-wide erosion, subsequent progradation on the continental shelf, stratal downlap on the continental slope and major mass wasting deposits on the continental rise were identified in the MCS data. Dated at about 3 Ma in the Antarctic Peninsula and Prydz Bay margins, these sequences were related to late Pliocene climatic change that induced the transition of the Antarctic ice sheet regime from polythermal to present polar cold, dry-based conditions (Rebesco and Camerlenghi, 2008).

A seismic stratigraphy model and sediment thickness grid for the southeastern Weddell Sea, between the Crary Fan and Explora Escarpment (Fig. 7-2), was the initial attempt to separate pre-glacial and glacial sequences in the Weddell Sea (Rogenhagen and Jokat, 2000; Rogenhagen et al; 2004). Seismic horizons W1.5, W2 and W3 were interpreted as 114–136 million years old and deemed representative of pre-glacial sediments deposited during the separation of Antarctica, Africa and South America (König and Jokat, 2006), whereas seismic horizons W4 and W5 were interpreted as the Miocene-Pliocene-Pleistocene full glacial sequences.

Other seismic reflection studies looked at the shelf sequences (Miller et al., 1990), full glacial sequences across the Crary Fan (Bart et al, 1999) and reported drifts in the northwestern Weddell Sea that indicate early Miocene ocean bottom current activity (Michels et al., 2001; 2002).

#### 3.1.2 Bellingshausen Sea

Glacial sedimentation and shelf to deep-sea transport processes in the Bellingshausen Sea have been investigated by several researchers (Nitsche, 2000; Cunningham et al., 2002; Scheuer, 2006a,b Uenzelmann-Neben 2007; Weigelt et al., 2009).

Scheuer et al. (2006) compiled more than 10,000 km of single-channel and multichannel seismic reflection data and correlated the stratigraphic interpretation with borehole data (Bellingshausen Sea lines and DSDP leg 35 Site 324 and ODP Leg 178 Sites 1095 to 7, Figs. 3-1 and 3-2). They successfully mapped the glacial and pre-glacial sequences but it was not possible to expand the grids farther into the Amundsen Sea due to lack of data.

They identified two main sequences ascribed to frequent grounded ice advances to the shelf edge, which occurred about 10 million years ago (Horizons Be1 and Be2; Figure 2-3b) and resulted in a high sedimentation rate of 140-170 metres per million years (m/my). Their identified age of 10 Ma corresponds to the last time pCO<sub>2</sub> was at similar levels than today (arrow in Fig. 1-1, Ch. 1).

## BELLINGSHAUSEN SEA

Seismic stratigraphy and glacial sediment thickness grid (Scheuer et al., 2006a,b)

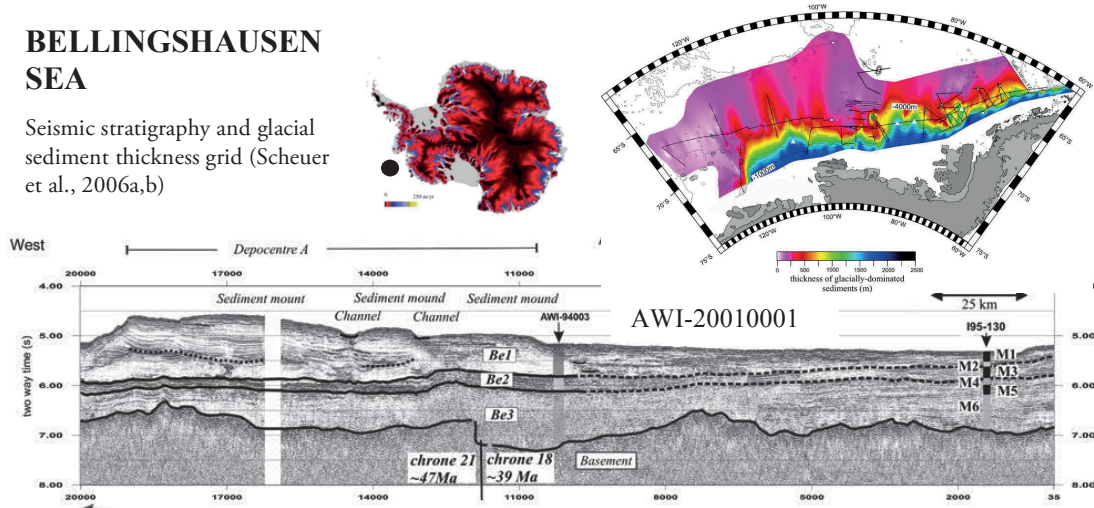


**Fig. 3-2.** Deep-sea glacial sediment thickness grid (top right) and multichannel seismic reflection line AWI-20010001 in Bellinghousen Sea (Scheuer et al., 2006a,b). Sequence Be3 was interpreted to represent the pre-glacial sediments, Be2 the transitional and Be1 the fully developed glacial sediment deposits with influences of bottom current sediment transport in the form of drifts and channels. The grid contains large distortion at the edges. Glacial sediment thickness range from 0-2500 m.

### 3.1.3 Amundsen Sea

Some of the main studies in the eastern Amundsen Sea (Cunningham et al., 2002; Nitsche, 2000; Uenzelmann-Neben et al., 1997, Uenzelmann-Neben and Gohl, 2012) interpreted a full glacial regime sequence, for example Fig. 2-3 in Ch. 2. Often a transitional boundary was picked as well, but not consistently. Examples of late Oligocene drifts have been observed in the Antarctic Peninsula (Rebesco et al., 2002, 2007), Weddell Sea (Maldonado et al., 2006) and Amundsen Sea (Uenzelmann-Neben and Gohl, 2012).

Since borehole data is sparse, the age-frame for the horizons remains speculative. Age data in the Amundsen Sea are obtained from linked analogues over vast distances e.g. from the Ross Sea as that is the next nearest data, albeit on the shelf (Fig. 3-1). Hence, we need to look farther along the Antarctic margin to find suitable deep sea borehole age data analogies, for example in Wilkes Land.

### 3.1.4 Wilkes Land

Recent drilling on the Wilkes Land margin and continental rise provide a long-term record of Cenozoic Antarctic glaciation, and much needed constraint on the age, nature and palaeo-deposition environment of glacial sequences in the seismic record, which was previously only inferred (Escutia et al., 2011). The seismic unconformity WL-U3 separates pre-glacial strata below, from the glacial strata above (Fig. 3-3; Fig. 2-4 in Ch. 2). This horizon was dated as being early Oligocene (33.5–30 million years old).



### 3. Background

Seismic unconformity WL-U5 marks the transition from a dynamic, to a persistent ice sheet (i.e. transitional to full glacial in Figs. 3-3 to 3-5) and was dated as mid-late Miocene (10–14 million years old; De Santis et al., 2003; Escutia et al; 2005, 2011). We draw extensively from this Wilkes Land basin age-model and horizon stratigraphy to test the Amundsen Sea basin interpretation. The Wilkes Land borehole data and age-model was chosen as most relevant, because it is the nearest deep sea basin borehole and more likely to include similar sediment deposition and transport processes, as opposed to the Ross Sea Shelf data. The main results for the relevant drill site in the Wilkes Land basin is therefore included here - for easier reference in the following chapters.

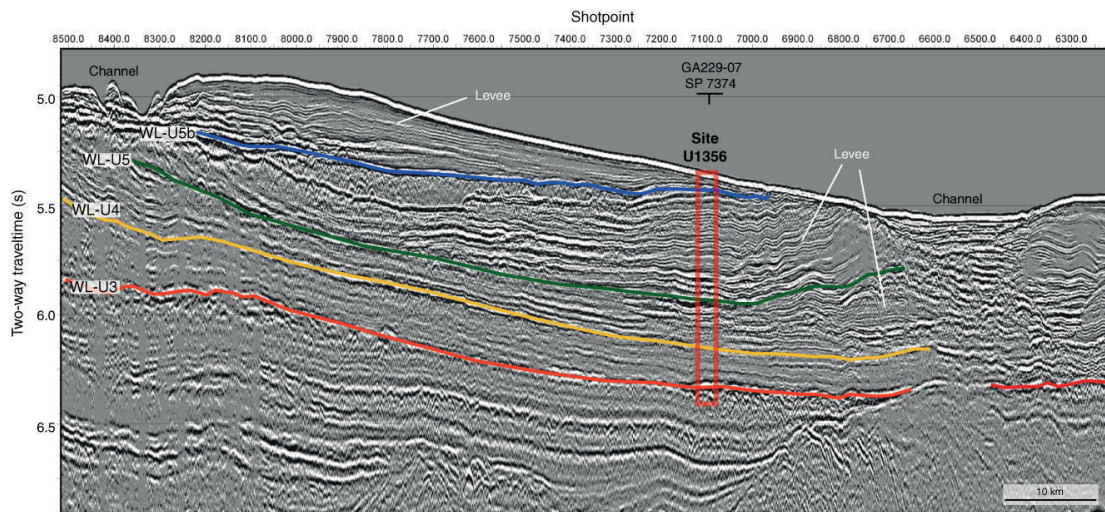


**Fig. 3-3.** Multichannel seismic reflection profile across Site U1356 showing regional unconformities WL-U3, WL-U4, and WL-U5. Red rectangle = approximate penetration achieved at Site U1356. Taken as published from Escutia et al., 2011; [http://publications.iodp.org/proceedings/318/101/101\\_.htm](http://publications.iodp.org/proceedings/318/101/101_.htm)

Regional unconformities/ Seismic units	Timing of glacial events	Wilkes Land glacial evolution
WL-S9	Pliocene-Pleistocene latest Miocene (?)	Persistent but oscillatory ? ice sheet
WL-U8	Pliocene (3 Ma) to mid-late Miocene (10-14 Ma)(?)	
WL-S8	late Miocene (?)	Transition from a dynamic to a persistent ice sheet
WL-U7	middle-late Miocene (?)	
WL-S7	middle-late Miocene (?)	
WL-U6	middle Miocene (?)	
WL-S6	middle Miocene (?)	
WL-U5	early Miocene (?)	Dynamic ice sheet
WL-S5	early Miocene (?)	
WL-U4	late Oligocene-early Miocene	First arrival of an ice sheet to the coast
WL-S4	early Oligocene (33.5-30 Ma) (?)	
WL-U3	early Oligocene to Late Cretaceous	Ice free

**Fig. 3-4** East Antarctic Ice Sheet evolution in the Wilkes Land margin and timing of events (modified from Escutia et al., 2005) inferred from continental shelf and rise stratigraphy (i.e., seismic regional unconformities and units). Taken as published from Escutia et al., 2011; [http://publications.iodp.org/proceedings/318/101/101\\_.htm](http://publications.iodp.org/proceedings/318/101/101_.htm)

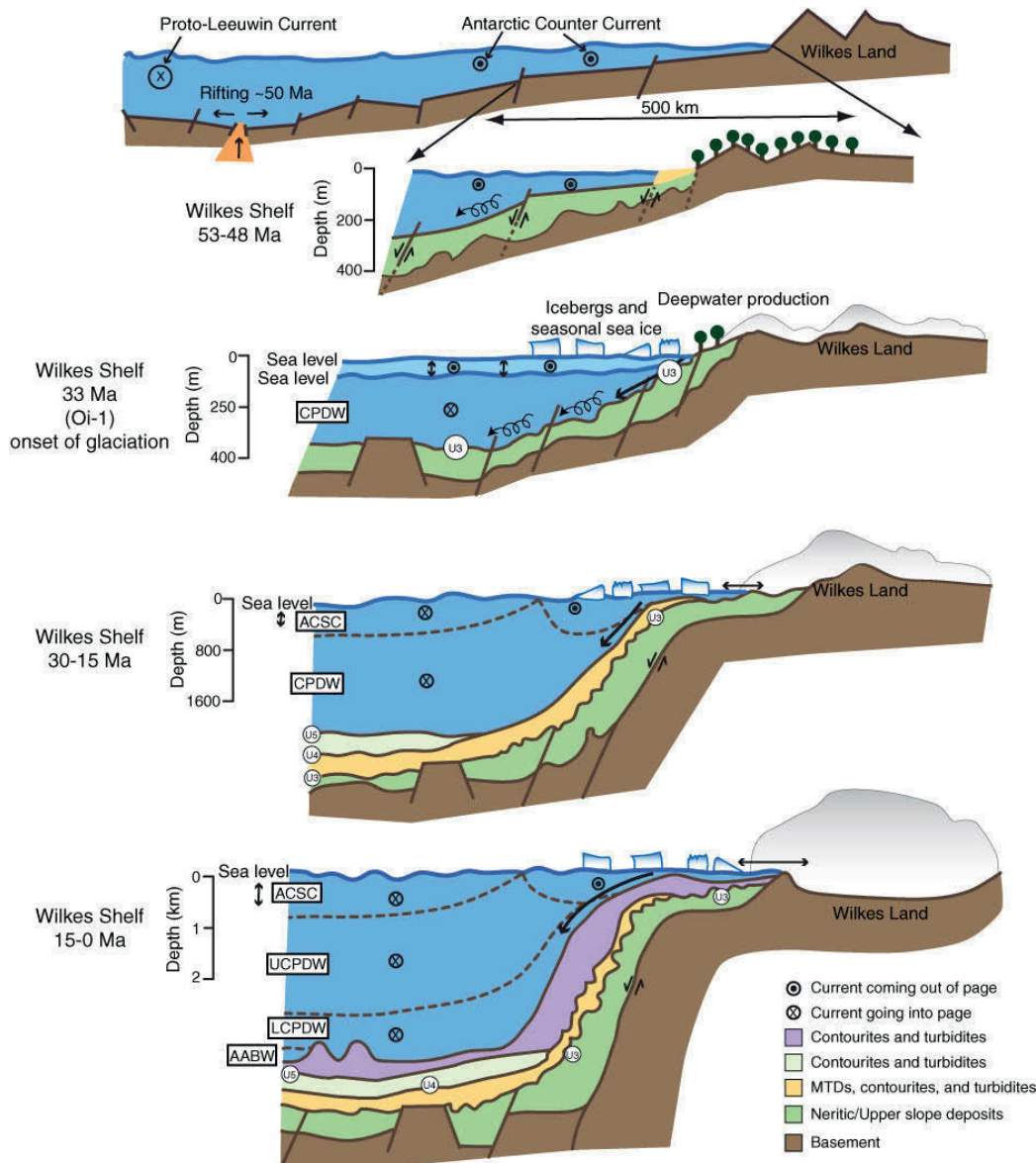


**Fig. 3-5.** Conceptual illustration of tectonic, geological, sedimentological, and climatic evolution of the Wilkes Land margin since the middle early Eocene (~54 Ma). U3, U4, and U5 refer to seismic unconformities WL-U3, WL-U4, and WL-U5. Oi-1 = Oligocene isotope Event 1, CPDW = Circumpolar Deep Water, ACSC = Antarctic Circumpolar Surface Water, UCPDW = Upper Circumpolar Deep Water, LCPDW = Lower Circumpolar Deep Water, AABW = Antarctic Bottom Water. MTD = mass transport debris flows. Taken as published from Escutia et al., 2011; [http://publications.iodp.org/proceedings/318/101/101\\_.htm](http://publications.iodp.org/proceedings/318/101/101_.htm)

### 3.2 Study area

This work focuses on studying sediment accumulation and deposition geometry by interpreting seismic profiles and incorporating magnetic anomaly data for basement age control. Sedimentation in the deep sea is relatively free from the influence of shelf processes like turbidites, debris flows and high pelagic fall-out. It is therefore an ideal, almost undisturbed record for distinguishing sequences associated with the changes from pre-glacial, transitional and full glacial climate regimes.



### 3. Background

In the first study area, a ~3300 km transect, starting in the eastern Weddell Sea, across the Peninsula and into the Scotia Sea (Fig. 3-6) was constructed to investigate if major glaciation events are expressed in offshore sediments, and to assess whether they are traceable on a cross-regional or margin-wide scale. Pre-glacial, transitional and full glacial dominated sequences were identified and tracked across the entire Weddell Sea and into the Scotia Sea. The WS-SS transect was also used to construct a new Weddell Sea basin-wide horizon stratigraphy model by tracing continuous reflector horizons between profiles without gaps. The results were published and can be found in Chapter 7.

In the second study area, the ~2000 km long Amundsen Sea – Ross Sea (AS-RS) transect (Fig. 3-6) was constructed from newly acquired data (Gohl, 2010; Fig. 3-1). Analogous to the WS-SS transect, the pre-glacial, transitional and full glacial sequences were identified based on the lateral and vertical variation in internal structure, geometry and acoustic properties. The sequence boundary horizons were traced continuously along each of the two transects and connected to analogue units in localized studies (Fig. 3-1). The AS-RS transect represents the first data link between the Amundsen Sea and Ross Sea seismic network. Work is on-going to produce the first margin-wide regional sedimentation grids, and so far, initial calculations suggest the glacial sequence thickness could be relatively constant along the margin (results to be published, see Ch. 6 and 9). Regional borehole age control in the Amundsen Sea is absent and therefore this first regional stratigraphy model is to be viewed as working hypothesis, until tested by deep-sea drilling. Borehole data from the Ross Sea and Wilkes Land provide the nearest age control model, and as it continues to link the AS-SS transect into an age frame, the collective results can become pivotal to further unravel the ice sheet development history.

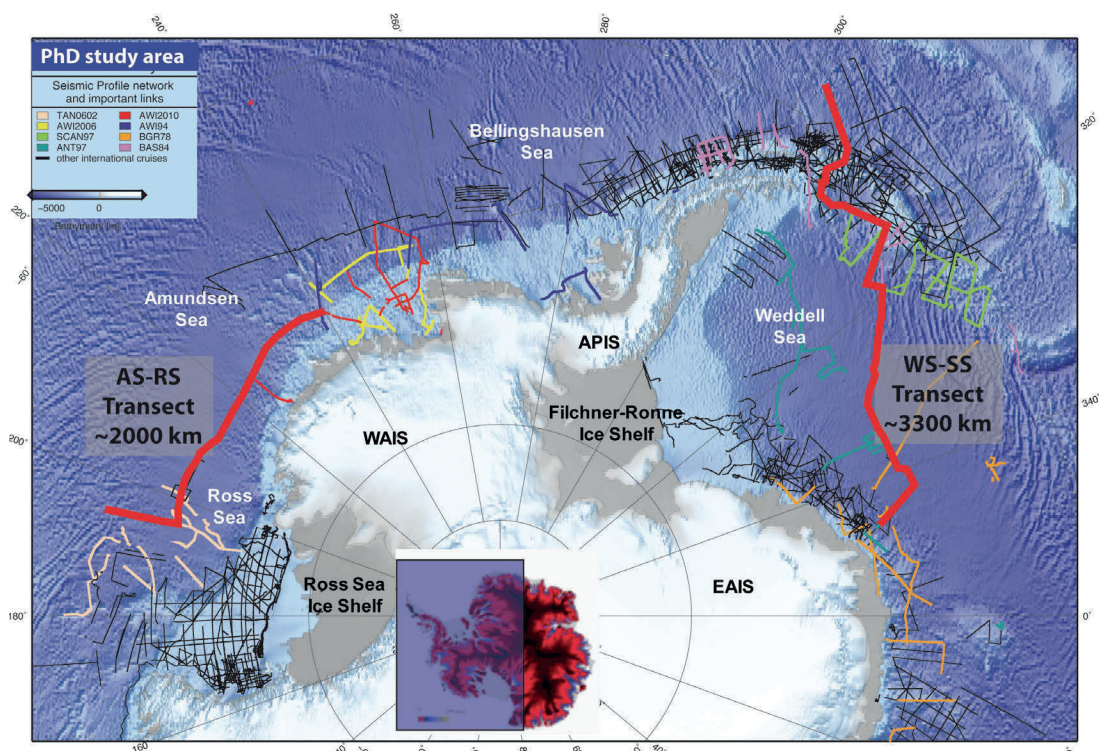


**Fig. 3-6.** Map of present study area showing the Weddell Sea – Scotia Sea transect and the Amundsen Sea – Ross Sea transect (thick red lines and annotated). Background image: global seafloor topography grid, version 13.1, Smith and Sandwell (1997) and for land, the ETOPO1 Global Relief Model (Amante and Eakins, 2009).



## 4 SEISMIC DATABASE AND METHODS

Key aspects:

- Sources of seismic data for the Weddell Sea – Scotia Sea transect
- Acquisition of seismic data for the Amundsen Sea – Ross Sea transect
- Processing of the acquired Amundsen Sea seismic data

### 4.1 Acquisition

Seismic profiles comprising the Weddell Sea – Scotia Sea transect (Ch. 3 and 7), were used as is and taken from the SDLS or received from collaborating Institutes. Profiles are stacked or post-stack time migrated data and no additional processing was done.

This chapter thus focuses on the acquisition and processing of selected seismic reflection profiles acquired during the ANT-XXVI/3 campaign (Gohl, 2010), which were used to construct the Amundsen Sea – Ross Sea transect described in Ch. 8.

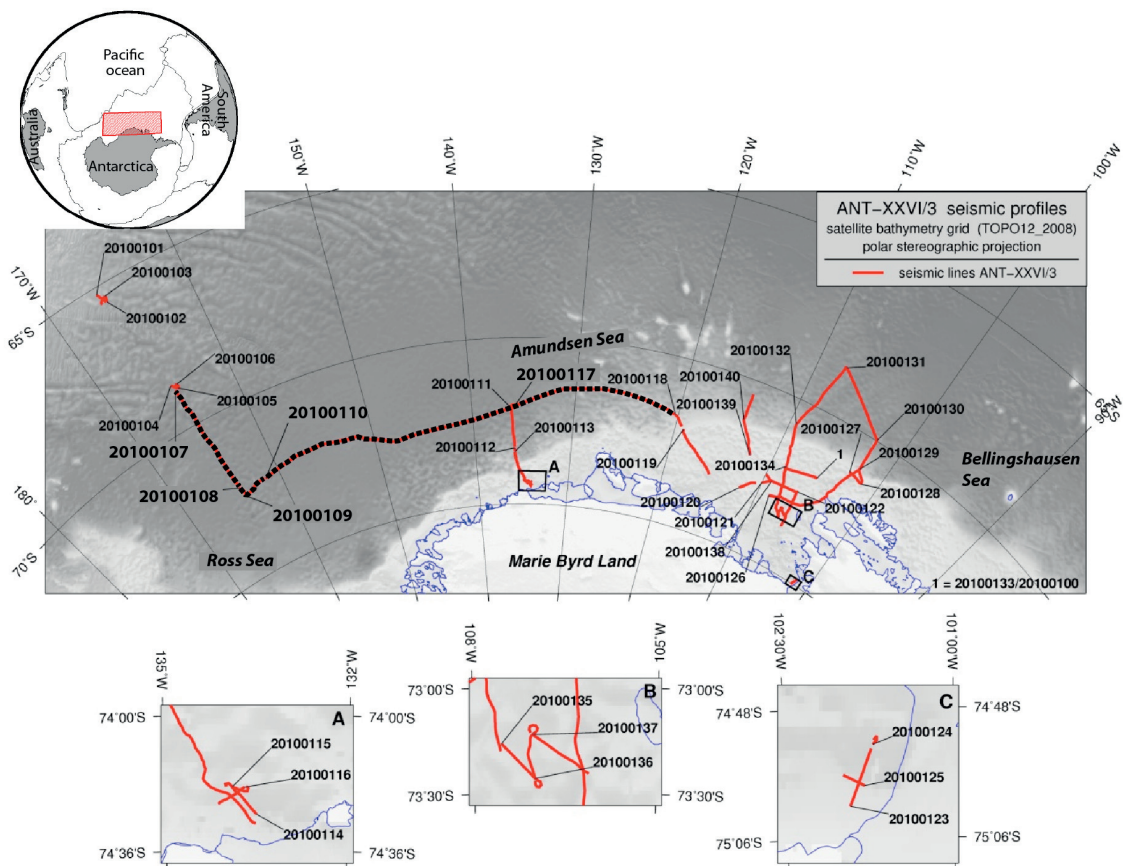


**Fig. 4-1.** Map of the Amundsen Sea research area. Red lines - multichannel seismic reflection profiles acquired during the ANT-XXVI/3 cruise with line numbers marking the start of each profile. Black and red dashed lines - profiles processed and interpreted in this thesis, labelled in bold. Map modified after Gohl (2010).

5032 km of multichannel seismic reflection profiles were recorded in the northeastern Ross Sea, Amundsen Sea and northernmost Bellingshausen Sea (Fig. 4-1; Gohl, 2010). Profiles AWI-20100107 – 110 and AWI-20100117 are relevant to this dissertation and collectively cover 2003 km (black dotted line in Fig. 4-1 and listed in Table 4-1).

#### 4.1.1 Method

Marine seismic reflection profiling involves deploying a source (airgun) and receiver (streamer with hydrophones) behind the ship in a particular configuration to create an acoustic image of the layers below the seafloor (Fig. 4-2a,d). The controlled source, comprising an airgun array (Fig. 4-2b), generates acoustic waves that travel through the water column, to the seafloor and into the layers below (Fig. 4-2a). At the interface between two materials with different acoustic impedances, some of the wave energy will reflect off the interface back to the receiver and some will refract through the interface (Fig. 4-2a). Measuring the travel time and amplitude of the waves between source and receiver, an image of the layers below the seafloor can be constructed (red box in Fig. 4-2a). The speed of these waves are governed by the acoustic impedance ( $Z$ ) of the medium through which they are travelling, defined by the equation:

$$Z = V\rho$$

where  $V$  is the seismic wave velocity and  $\rho$  (Greek rho) is the density of the layer (Yilmaz, 2001).

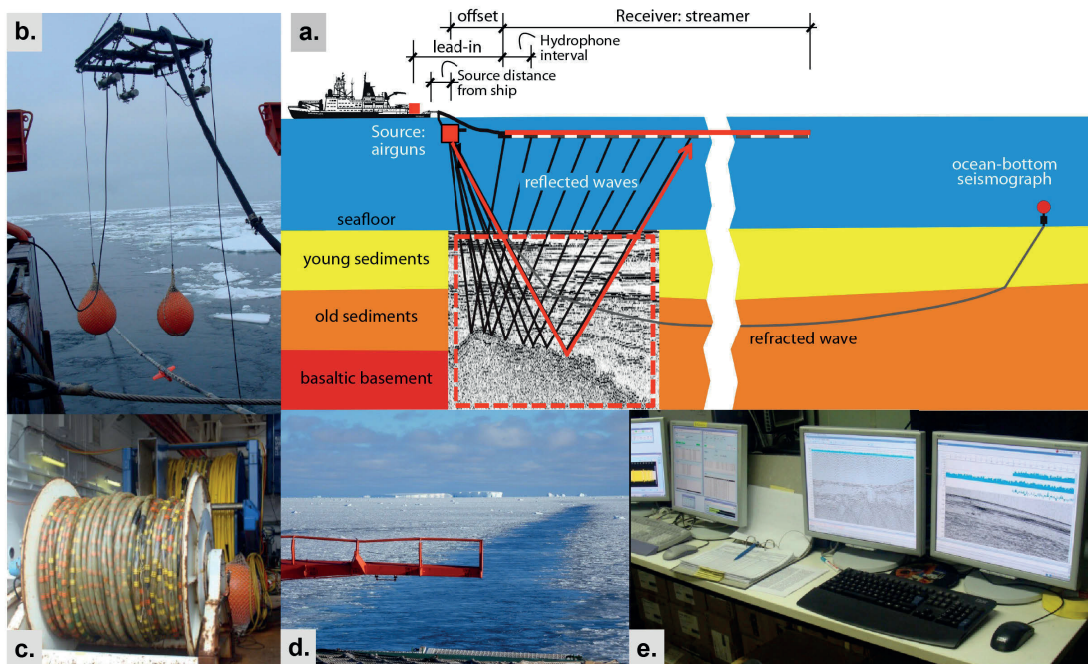


**Fig. 4-2.** Principles of the applied marine seismic reflection data acquisition method and equipment configuration. **a.** Schematic illustration of the airgun source (red square) and streamer receiver (horizontal red line) towed behind the RV *Polarstern*, and the simplified travel paths of the reflected seismic waves (red arrow and black lines) as well as refracted waves (gray line). Reconstruction of the travel paths of these rays creates an acoustic image with distinct reflections that can be related to the sediments and basement below (red dashed box and coloured layers). **b.** Deployment of the GI-gun cluster source hanging from a steel frame with two buoys mounted for balance, and the 3000 m streamer with a red depth-control bird (bottom centre of photo). **c.** Receivers used: 600 m PRAKLA streamer in the foreground and 3000 m Sentinel SERCEL streamer in the background. **d.** Data acquisition with equipment-in-tow behind the ship through relatively good sea-ice conditions. **e.** On-board quality control for the 3000 m streamer through real time display of shots and single channel data. All photos taken by A. Lindeque.

Such seismic images as are presented in Chapters 7 and 8, reveal the structure of the layers below the seafloor and can help us to understand the tectonic, sedimentation and ocean bottom current processes that played a role in their formation and deformation.

Table 4-1 . Seismic reflection data acquisition parameters for selected profiles from cruise ANT-XXVI/3.

Profile:	20100107	20100108	20100109	20100110	20100117
<b>Source:</b>					
No. of GI-Guns	3 x 2.7 ltr	3 x 2.7 ltr	3 x 2.7 ltr	2 x 2.7 ltr	2 x 2.7 ltr
Volume (L)	8.1	8.1	8.1	5.4	5.4
Shot mode delay (ms)	33	33	33	33	33
Shot interval (s)	12	12	12	12	12
<b>Receiver:</b>					
Streamer, Length (m)	SERCEL, 3000	PRAKLA, 600	PRAKLA, 600	SERCEL, 3000	SERCEL, 3000
No. of channels	240	96	96	240	240
Hydrophone interval (m)	12.5	6.25	6.25	12.5	12.5
Lead-in (m)	60	35	35	70	70
Stretch sections (m)	50 + 50 + 20	50 + 50 + 50	50 + 50 + 50	50 + 50 + 20	50 + 50 + 20
Distance, winch-to-airguns (m)	20	12	12	20	20
Offset, source-to-receiver (m)	160	173	173	170	170
<b>Recording:</b>					
Record length (s)	10	10	10	10	10
Sample rate (ms)	1	2	2	1	1
Shot no.	1–11920	1–1002	1–2695	1–27181	1–14286
<b>Profile length (km):</b>	390.4	33.9	89.4	917.6	571.5

#### 4.1.2 Source

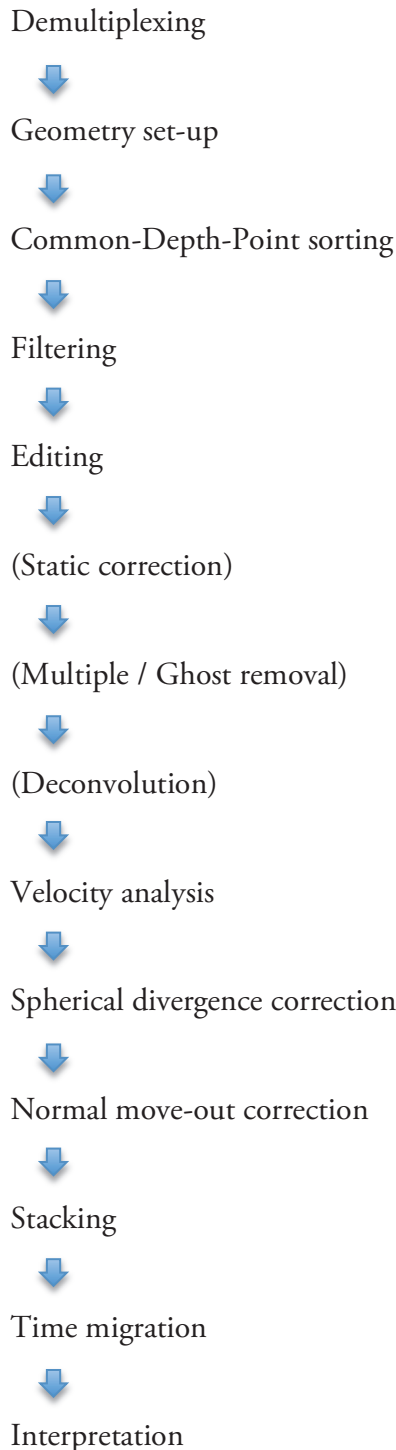
The 3 GI-Gun cluster source was towed at approximately 10 m behind the ship at a water depth of ~5 m and fired at 195 bar (Fig. 4-2b; Table 4-1). One GI-Gun contains two independent airguns, referred to as a “Generator” with a volume of 0.74 L or 45 inch<sup>3</sup> and an “Injector” with a volume of 1.72 L or 105 inch<sup>3</sup>. The “Injector” was fired 33 ms after the “Generator” to create an almost bubble-free signal and in doing so, enhanced the signal-to-noise ratio in the seismic data. With an average cruising speed of 5.4 knots and 12 s shot interval, the average shot spacing is about 33 m.

The airguns frequently showed air leaks and one or more had to be shut off for the remainder of the acquisition time (e.g. on profiles AWI-20100110 and AWI-20100117, Table 4-1). This somewhat decreased the signal penetration depth into the seafloor, but the overall data quality was still exceptionally good and basement clearly imaged in most cases. Complete shut downs were often necessary due to whale and seal occurrences close to the ship resulting in relatively small but significant data gaps on most of the profiles. After the whale or seal sighting status was cleared, soft-start procedures were applied for 15 minutes.

#### 4.1.3 Receiver

The receiver system for profiles 20100107, -110 and -117 consisted of a 3000 m long digital Sentinel SERCEL solid streamer with 240 channels (Fig. 4-2a, c; Table 4-1). 12 DigiCourse depth-control birds were mounted at regular intervals of ~200 m to keep the

streamer at a constant water depth of ~10 m (Fig. 3-2b). The eSQC-Pro was used for on-board quality control and displayed every shot record as well as single-channel 16 of the entire profile in real time (Fig. 4-2e). The single-channel, real time data, already showed clear reflectors and a high signal-to-noise ratio due to a calm sea and favourable sea-ice/polynia conditions. The SERCEL SEAL recording system stored the data in SEG-Y format on parallel LTO-2 tapes with an additional NAS backup system.



The receiver system for profiles AWI-20100108 and -109 comprised a 600 m long analogue PRAKLA streamer with 96 channels (Fig. 4-2c; Table 4-1). Varying streamer depths were considered during processing as no depth control system was deployed due to worsening sea-ice and weather conditions. The Geometrics EG/G 2400 recorder stored the data in SEG-D format on 3480 cartridge tapes. A thermo plotter printed the single channel 16 data of each profile in real time for on-board quality control and documentation.

## 4.2 Processing

The standard workflow chart on the left summarizes the processing steps applied to the selected profiles listed in Table 4-1. Steps in brackets were only applied to profiles AWI-20100108 and -109 due to the short streamer. The processing workflow steps are discussed in the following subsections and based on data examples.

### 4.2.1 Demultiplexing, geometry and sorting

During data acquisition the seismic reflection data for each shot were stored as a time sequential sequence and sampled across all channels for that time interval. Demultiplexing is the first step of seismic data processing, which resorts the data into sequential channel, or trace order for each shot. The SERCEL SEAL recording system performed demultiplexing internally, but demultiplexing for the 600 m PRAKLA streamer data were done separately in Paradigm's FOCUS™ processing software.

Next, the geometry for each profile was set-up by linking geographical data such as longitude, latitude, water depth, speed and course of the ship



to each shot, using time as the common denominator. All the rays from various shots that reflected off the same depth point on a layer surface, are grouped into a common depth point (CDP) gather, which is referred to as CDP sorting (Fig. 4-3). Profiles AWI-20100107, -110 and -117 have a CDP fold of 180, meaning each CDP trace represents the sum of 180 rays from 46 shots whereas profiles 20100108 and -109 have a CDP fold of 72 from 9 shots. The CDP spacing for all profiles is 25 m.

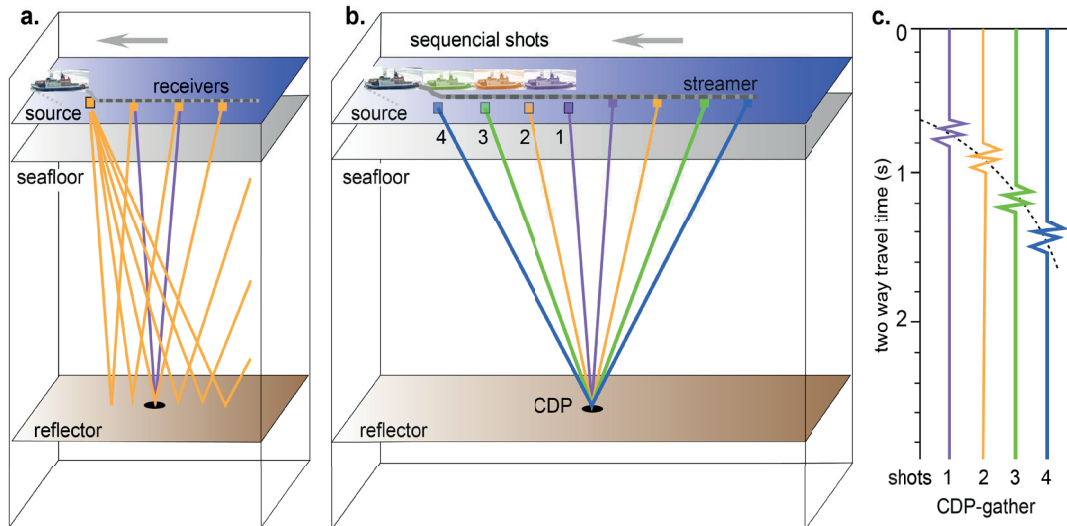


**Fig. 4-3.** Schematic diagram illustrating the principles of sorting shot data into common depth points (CDP) gathers. **a.** Reflected ray paths of shots 1 and 2 from several CDP's on one reflector layer below the seafloor. **b.** Reflected rays from shots 1 – 4 at a single CDP point. **c.** Rays from (b) are re-arranged into a 4-fold CDP gather and show the characteristic vertical offset called move-out, due to rays from later shots arriving at the streamer receivers with a time delay. Diagram modified after [http://www.oilandgasuk.co.uk/publications/britainsoffshoreoilandgas/Exploration/Discovering\\_the\\_Underground\\_Structure.cfm](http://www.oilandgasuk.co.uk/publications/britainsoffshoreoilandgas/Exploration/Discovering_the_Underground_Structure.cfm)

### 4.2.2 Filtering

A tapered high pass 5–10 Hz frequency filter was applied, allowing all frequencies above 10 Hz to pass through for further processing. This filter was chosen because it eliminates lower frequency noise from the ship and waves, but still allows the higher >200 Hz frequencies to pass, which are needed to resolve small-scale sedimentary structures.

### 4.2.3 Editing

Noisy and bad or dead channels were removed from each CDP gather (Fig. 4-4). No wrongly polarised traces were observed. Channels 2, 7, 8–10, 43, 70, 105–106 and 156159 were particularly noisy and therefore muted throughout further processing (Fig. 4-4).

### 4.2.4 Static correction

Lines AWI-20100108 and -109 were acquired during difficult sea ice conditions with the short streamer and as a precaution; depth control instruments were not fitted. Subsequently, the streamer was not always towed at the same depth, which caused a

#### 4. Seismic reflection data

vertical shift in the traces. This was corrected with a vertical shift equal to the distance to the ghost (Fig. 4-5).

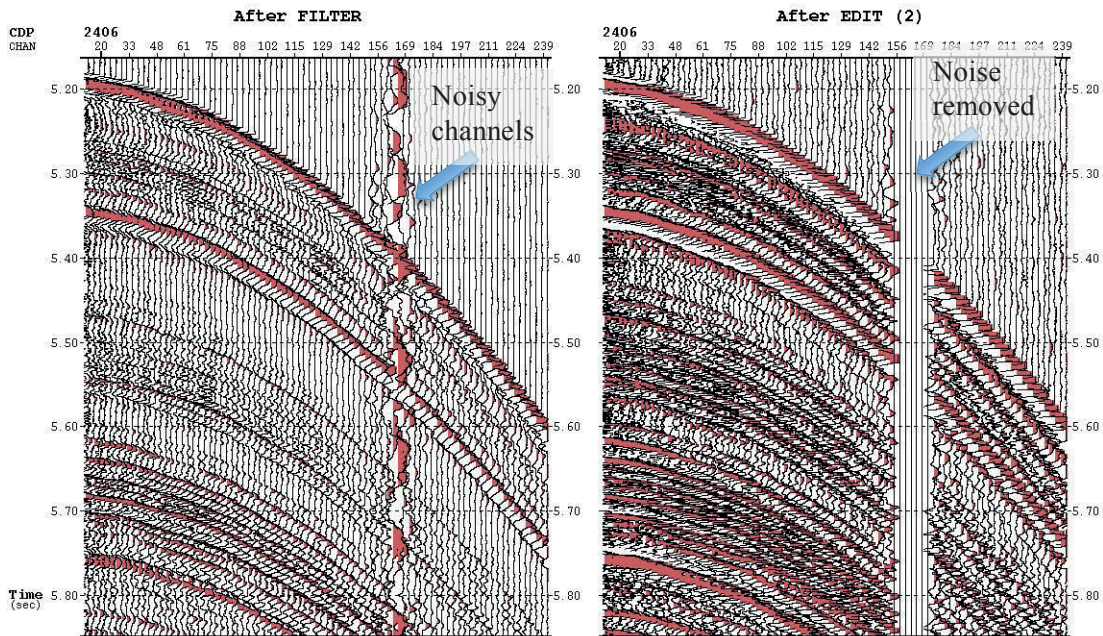


Fig. 4-4. Data example of the editing step during processing. Left – noise channels show a large and variable amplitude that is consistent for the length of the trace. Right – channels removed and replaced with zero amplitude traces.

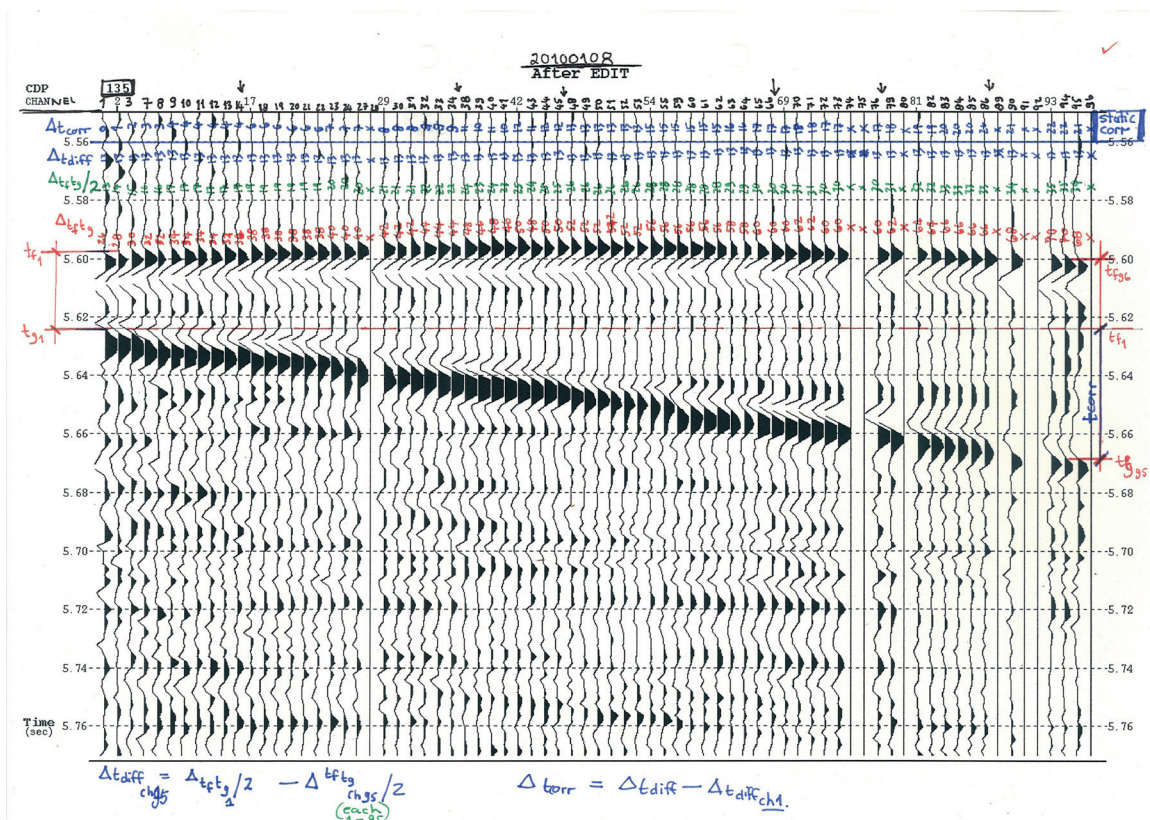


Fig. 4-5. Data example of the static correction calculation applied to AWI-20100108 and AWI-20100109. Note that the hyperbola trend does not decrease steadily to the right but shows an increase in the middle. Since the ghost is a multiple reflection between the seafloor surface and the streamer, its position was taken as guide to estimate how much static correction would need to be applied.



### 4.2.5 Multiple removal

The ghost in lines AWI-20100108 and -109 was effectively removed with an F-K filter. A 5-10 Hz high pass filter was applied and the remaining reflections overcorrected (Fig. 4-6). The F-K filter was applied and the normal move-out (NMO) over correction removed (Fig. 4.6). This effectively removed the ghost on both lines.

The profiles of the AS-RS transect lines AWI-20100107, -110 and -117, were towed in the deep sea (>4000 m water depth) using the 3000 m streamer. With the 3000 m streamer the ghost was indistinguishable from the primaries and the F-K filter unsuccessful in separating them. Hence, deconvolution was tested as an alternative method.

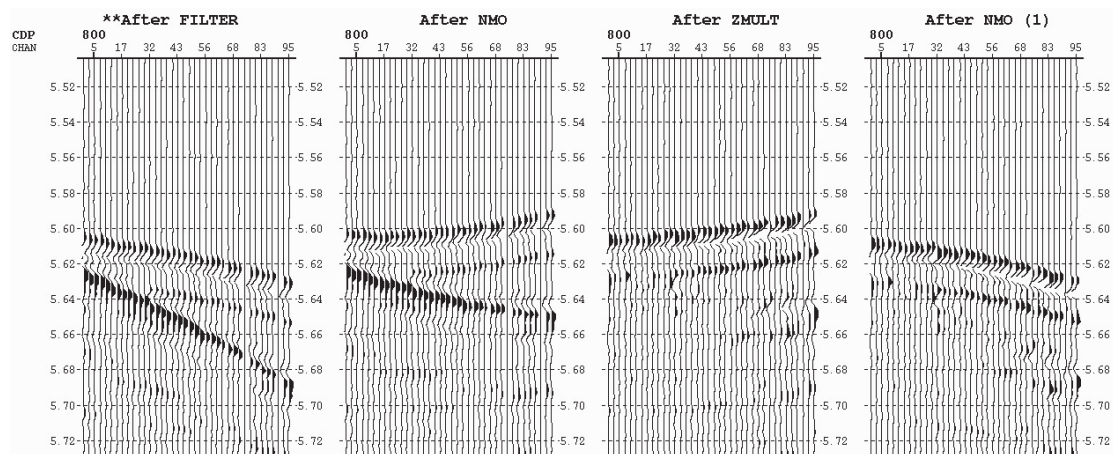


**Fig. 4-6.** Data example of the ghost removal during processing, from left to right: High-pass filter applied to remove noise; Ghost and primaries over corrected; F-K filter applied too remove under-corrected reflections; NMO over-correction removed.

### 4.2.6 Deconvolution

The impact of deconvolution on the seismic resolution is shown in Fig. 4-7. Both spiking and predictive deconvolution were tested. Spiking deconvolution effectively removed the ghost when using a 30 ms window, 100 ms operator length and 0.1% white noise. However, the seemingly finer, crispy and clearer reflection pattern in the deconvoluted data (Fig. 4-7 far right) is a result of boosting the higher frequencies while removing the streamer ghost in the upper reflections, but it is unclear if these finer reflections farther below are true or ringing artifacts. Deconvolution was therefore used in selected cases to more clearly image unconformities, drift feature geometry and seismic unit or sequence boundaries.

### 4.2.7 Migration

Velocity analyses were applied by picking sequence boundary horizons at every 50<sup>th</sup> CDP. After NMO correction and spherical divergence adjustment, a Kirchoff time migration was performed on the stacked section. A dip migration of 65 degrees and 90% of the NMO velocities were used, resulting in a post-stack-time-migrated (PSTM) image used for interpretation.



#### 4. Seismic reflection data

---

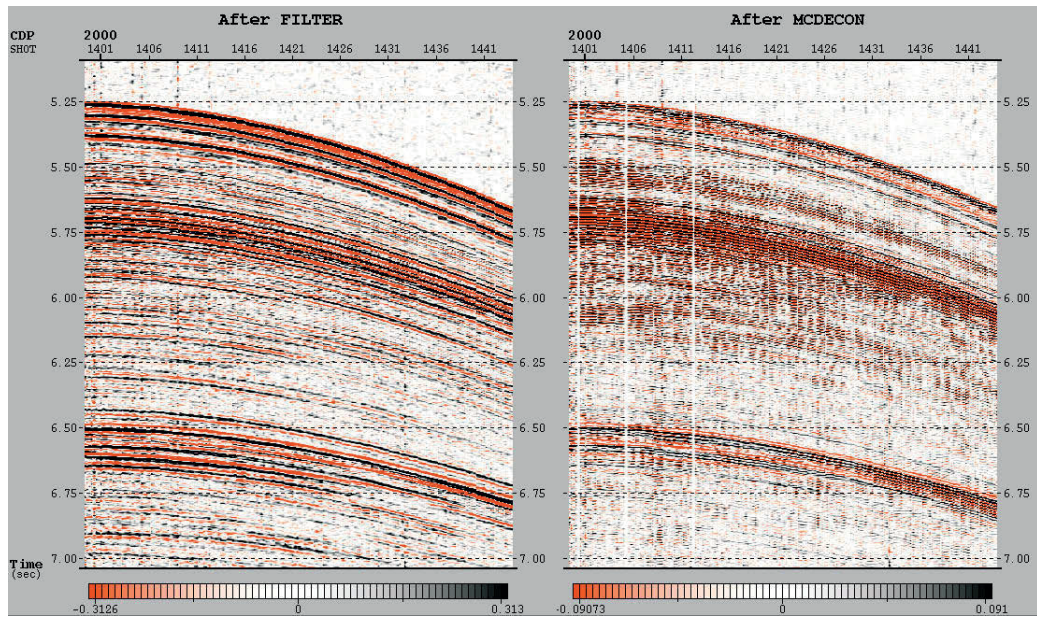


**Fig. 4-7.** Data example of the deconvolution applied to line AWI-20100117 for ghost removal during processing. Left – only the 5–10 Hz high pass filter applied; right – see the finer division of the reflections, but it can also be interpreted as a ringing artefact.

## 5 OTHER DATASETS AND METHODS

Key aspects:

- Borehole data from ODP and DSDP sources used for age control
  - Magnetic seafloor spreading anomalies used for additional age control
  - Refraction- and sonobuoy data used to expand and verify velocity model
- 

### 5.1 Borehole data

The ODP Leg 113 boreholes and selected SHALDRIL boreholes on the shelf were used for the age control of the stratigraphic horizons in the Weddell Sea – Scotia Sea transect. That analysis forms part of the paper 1 publication and to avoid repetition, the reader is referred to Fig. 7-3 and section 7.4.2 of Chapter 7 (paper 1).

For the Amundsen Sea – Ross Sea transect interpretation, DSDP Leg 28 sites 270–272 were used as guide to correlate the horizons from this study with the Ross Sea shelf stratigraphy, and to test the constructed age model. DSDP Leg 35 Sites 324, 323 and ODP Leg 178 Site 1095 were incorporated for supporting information on the horizon stratigraphy, sediment thickness and glacial deposits of the central basin.

The derived age model and type section interpretation was compared to IODP Leg 318 site U1356 and the coincident seismic line (Ch. 3), which serves as an analogue age model. Exactly how these boreholes were incorporated is explained in Chapter 8, section 8.4.3, which is part of the second paper manuscript and thus not repeated here.

### 5.2 Magnetic seafloor spreading anomaly data

Seismic profiles in the Weddell Sea – Scotia Sea transect were used for basement age control, but the public global magnetic seafloor spreading anomaly map had no data in this area. Consequently, it was necessary to compile the magnetic data for the Weddell Sea – Scotia Sea from several papers, scanned maps and point based georeferenced data sets. This compilation forms part of the first paper and the methodology is explained in Chapter 7, section 7.4.1 and Table 7-2. The digital data of this new magnetic seafloor spreading anomaly compilation for the Weddell Sea and Scotia Sea is available in the PANGAEA database, as an online supplement to the first paper (Ch. 7) and can be found at [doi:10.1594/PANGAEA.777453](https://doi.org/10.1594/PANGAEA.777453).

Basement age control for the Amundsen Sea basin was taken from Wobbe et al., (2012) and comprises airborne and ship borne magnetic data acquired during the same expedition as the seismic reflection data presented in this work (Fig. 4-1; ANT-XXVI/3; Gohl, 2010). The incorporation of this data is further discussed in section 8.4.4 of Chapter 8 (paper two).

### 5.3 Refraction data analysis

Past refraction data modelling in the eastern Amundsen Sea basin has been optimised for studies of the crust and treated the sediments as a single layer (Kalberg and Gohl, 2013). Since velocity information from borehole data is lacking, and available velocities had to be derived from stacking velocities, it was necessary to rework the model to deduce velocities for the various sediment layers (Figs. 5-1 to 5.4).

Layers were picked according to the main identified seismic sedimentary units and a simple 1D velocity model created using stations ST205 and ST206 (Figs. 5-1 to 5.4). These results were included as an online supplement to paper two and confirmed the range of velocities used for sediment thickness calculations presented in Chapter 8.

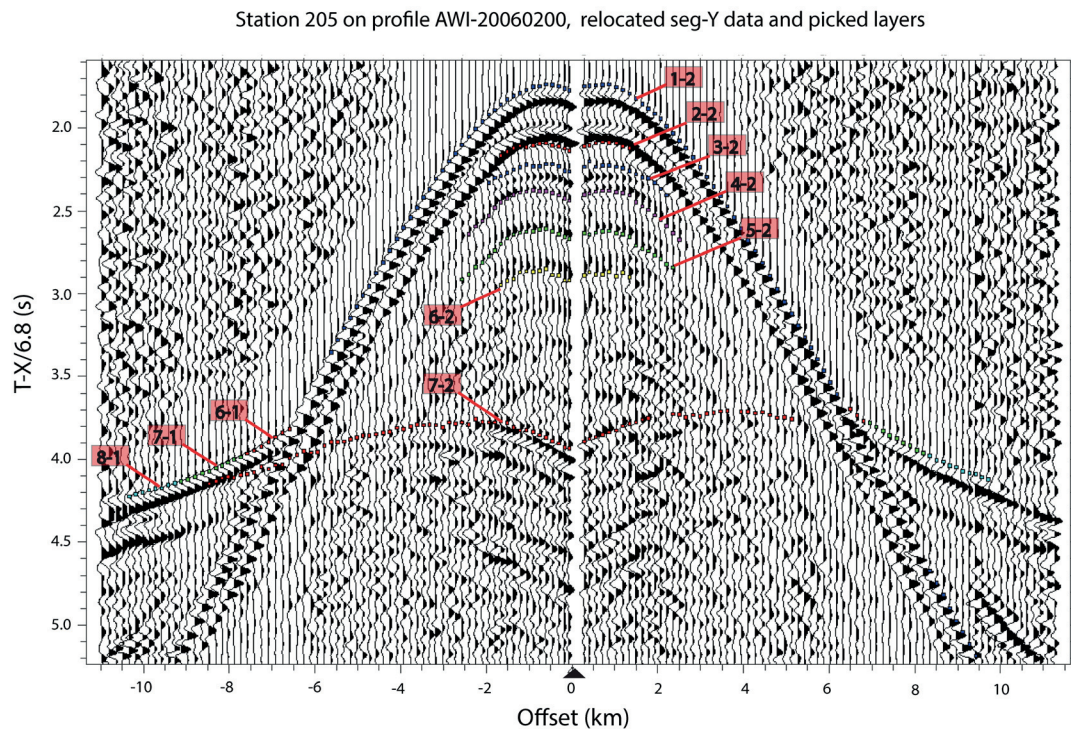


**Fig. 5-1.** Example of refraction data recorded at ocean-bottom seismograph (OBS) station ST205 on MCS profile AWI-20060200 (Fig. 8-1), located in the eastern Amundsen Sea. Travel time is reduced with a reduction velocity of 6.8 km/s for an optimised picking display. Coloured squares indicate the relevant boundary layers picked for ray-tracing (Fig. 5-2). Offset is distance from the OBS position.



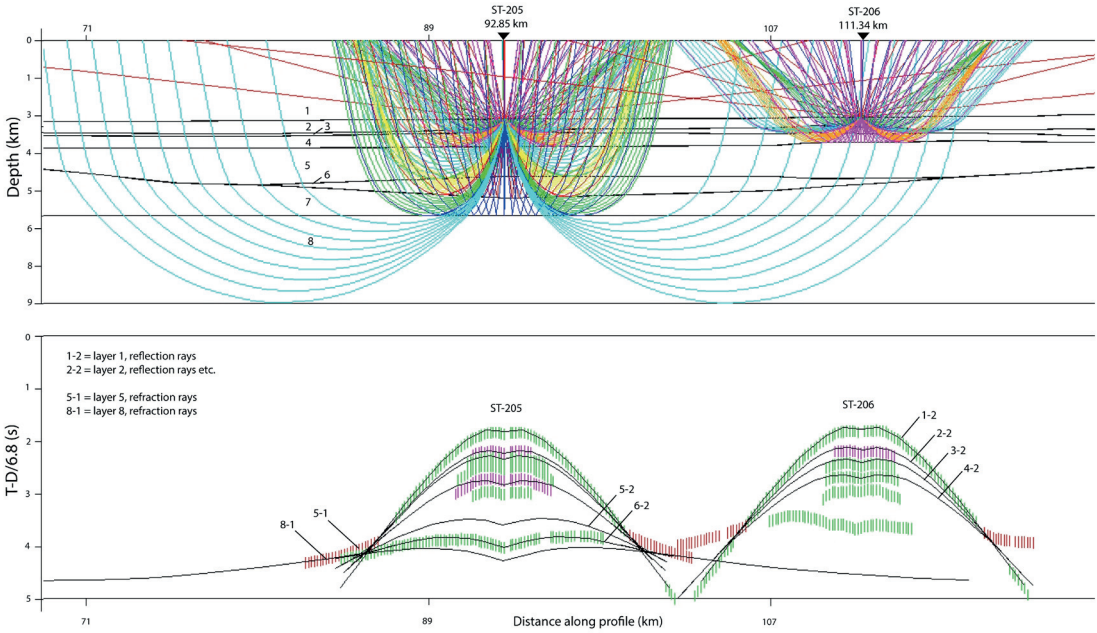


**Fig.5-2.** Ray tracing model, showing the ray path of the arrival picks at OBS stations ST205 and ST206. The picks have uncertainties (green and pink vertical bars), but from all the OBS stations along the profile, these two stations gave the more reasonable result for the sedimentary layers, which was the main focus of this analysis.

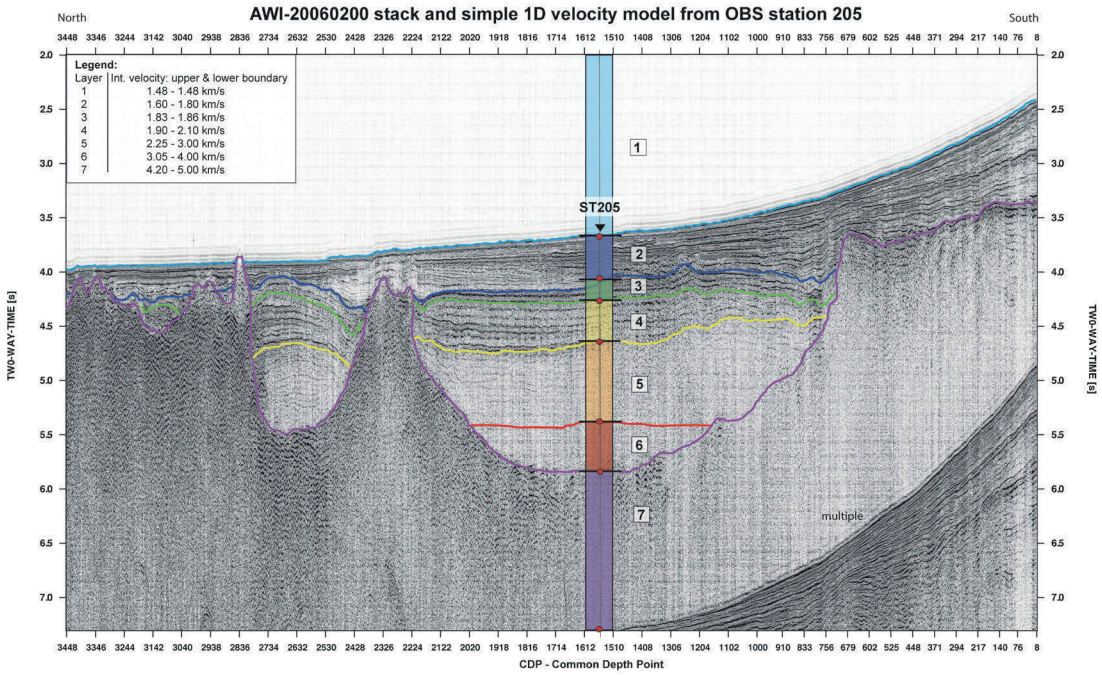


**Fig. 5-3.** Stacked multichannel seismic profile AWI-20060200, located in the eastern Amundsen Sea and on the eastern link of the Ant2010 and Ant94 MCS profiles (Fig. 8-1 in paper two). The interpreted, simplified sediment units are drawn in on the seismic image and the derived interval velocities, per unit, summarised in the table (inset). The line coincident OBS station ST205 is overlain. The interpreted seismic horizons are in agreement with the layers defined by the ray-tracing model.

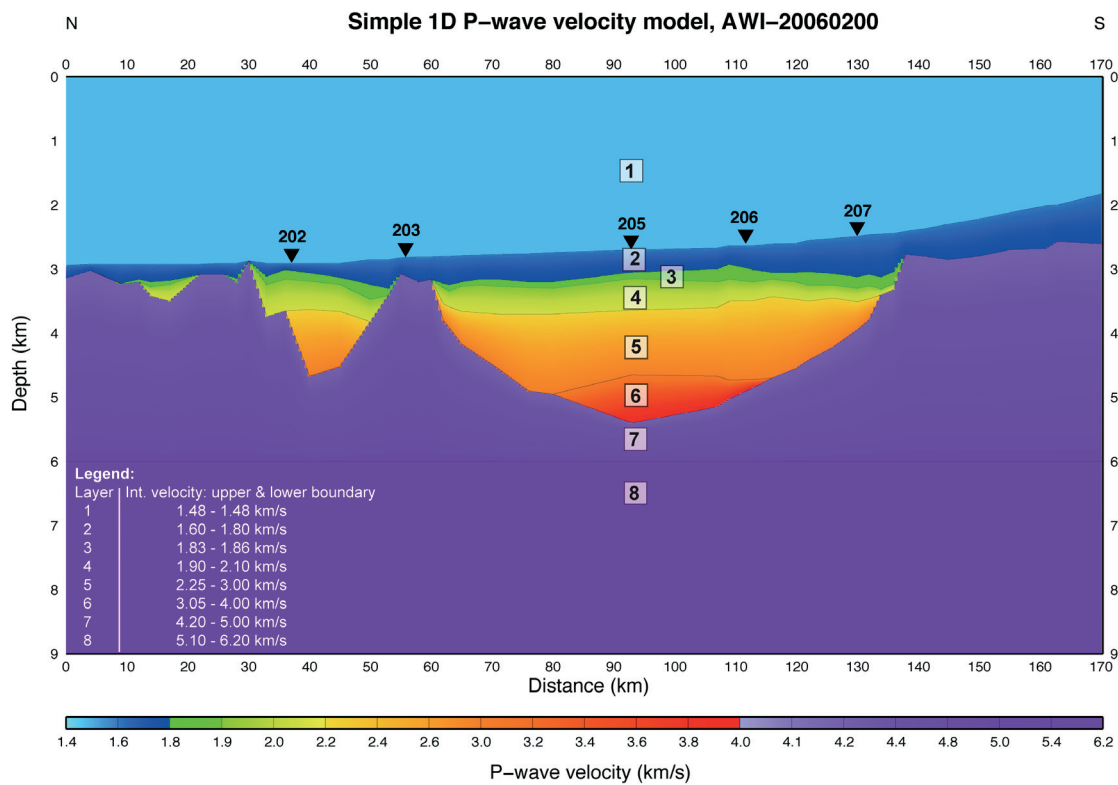


**Fig. 5-4.** Simple one dimensional P-wave velocity model, derived from picks at OBS stations 205 and 206. These interval velocities are the only control for the region and were used to estimate the sediment thickness (Fig. 4, Tables 3 and 4 in the paper). The derived interval velocities, per unit, are summarised in the table (inset).

## 5.4 Sonobuoy velocity data

During the GNS science New Zealand TAN0602 RV Tangaroa expedition in 2006, fourteen sonobuoys were deployed in the Ross Sea and western Amundsen Sea (Fig. 5-5). The measured velocities were made available to this project (Table 5-1) and are included in the online supplementary material to paper 2, together with the Tan0602 multichannel seismic data. The processing was done by GNS. The velocities are shown here for comparison to the NMO velocity model in Chapter 8, supplement 1.4 (paper two and online data).

All sonobuoy hydrophones were deployed to 300 m water depth and transmitted for 8 hrs. Originally the trace length for sonobuoys was set at 14 s (TWT) but was later extended to 16 s (Table 5-1).

All sonobuoys showed clearly reflected arrivals to offsets greater than 10 km but only sonobuoys 12 and 15 show refracted arrivals. All shot navigation and trace-offset information were incorporated into TAN0602 sonobuoy data during onboard processing, taking care to preserve the waveforms for analysis.

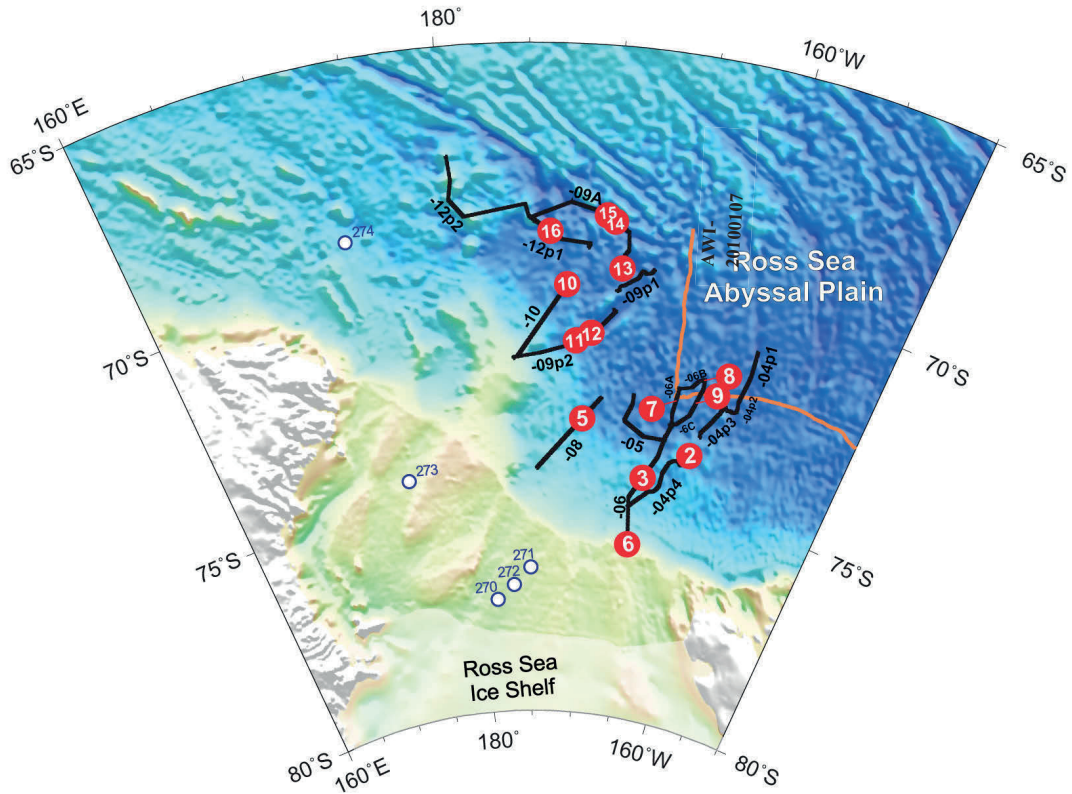


Fig. 5-5 Line geometry (annotated black line) and sonobuoy locations (numbered red circles) for TAN0602 seismic data. The ANT-XXVI/3 RV Polarstern lines are shown in brown.

Table 5-1 Summary of interval velocities for each sonobuoy in Fig 5-5

Sono2		Sono3		Sono5		Sono6		Sono7		Sono8	
TWT (ms)	Interval vel. (m/s)	TWT (ms)	Interval vel. (m/s)	TWT (ms)	Interval vel. (m/s)	TWT (ms)	Interval vel. (m/s)	TWT (ms)	Interval vel. (m/s)	TWT (ms)	Interval vel. (m/s)
0	1450	0	1450	0	1450	0	1450	0	1450	0	1450
4000	1450	4000	1450	4000	1450	4000	1450	4000	1450	4000	1450
5053	1797	4722	1886	5136	1890	5562	1725	5763	1609	5704	1700
6024	1818	5468	1775	5704	2322	6142	1974	6296	1976	6296	1998
6320	2531	5917	2394	6047	2951	6769	2505	7018	2735	6533	3128
6769	2976	6225	3251	6923	3813	7041	3285	12000	6684	6959	3686
7266	3679	7314	3767	12000	6458	7621	3454			12000	6594
12000	6745	12000	6669			12000	6989				

Sono9		Sono10		Sono11		Sono12		Sono13		Sono14	
TWT (ms)	Interval vel. (m/s)	TWT (ms)	Interval vel. (m/s)	TWT (ms)	Interval vel. (m/s)	TWT (ms)	Interval vel. (m/s)	TWT (ms)	Interval vel. (m/s)	TWT (ms)	Interval vel. (m/s)
0	1450	0	1450	0	1450	0	1450	0	1450	0	1450
4000	1450	4000	1450	4000	1450	4000	1450	4000	1450	4000	1450
5704	1700	5586	1700	5408	1696	5562	1689	5787	1670	5752	1696
6036	1979	6260	2169	6308	2216	6308	1903	6166	1939	6095	1867
6663	2744	6651	2280	6663	2314	7148	2288	6864	2207	6663	2247
7018	3935	7207	2816	7491	3020	8059	3703	7207	3501	6899	2728
12000	6617	7550	3162	12000	6932	12000	7309	12000	6784	7053	3246
		12000	6983							12000	6701

Sono15		Sono16	
TWT (ms)	Interval vel. (m/s)	TWT (ms)	Interval vel. (m/s)
0	1450	0	1450
4000	1450	4000	1450
5763	1683	5633	1750
6189	1856	6166	1880
7290	2474	6544	1862
7917	3846	7278	2850
12000	7208	12000	6832



## 6 CONTRIBUTIONS TO SCIENTIFIC PUBLICATIONS

---

This chapter summarizes contributions to journal publications, either as published in the journal, or in the format it is to be submitted in. They appear in chronological order.

### **6.1 Deep-sea pre-glacial to glacial sedimentation in the Weddell Sea and southern Scotia Sea from a cross-basin seismic transect.**

Lindeque, A., Martin, Y.M., Gohl, K., Maldonado, M., 2013.  
Marine Geology 336, 61–83, doi:10.1016/j.margeo.2012.11.004.

The Weddell Sea – Scotia Sea seismic transect stratigraphy is constrained by boreholes from ODP Leg 113, and basement ages are constrained by a compilation of all published magnetic seafloor spreading anomaly data in the Weddell and Scotia Seas. The combination of these datasets allows the construction of an initial age model from which sediment thicknesses, volumes and rates are derived. The findings increase our understanding of the Weddell Sea palaeocirculation and Antarctic ice sheet development. The paper contains a new compilation of all published magnetic seafloor spreading anomalies in the Weddell Sea Scotia region, available online in Pangaea.de and contributes to the world seafloor magnetic anomaly map.

I compiled the magnetic anomaly data, interpreted the ~3300 km multichannel seismic transect, created all the figures and wrote the manuscript. Y.M. Martin assisted with the seismic interpretation and improved the manuscript. K. Gohl supervised the project and commented on the manuscript. M. Maldonado supervised the project part of Y.M Martin and commented on the manuscript. The completed paper is Chapter 7.

### **6.2 Pre-glacial to glacial stratigraphy in the unexplored Amundsen Sea seep-sea basin: A first cross-regional correlation of deep-sea seismic reflection data.**

Lindeque, A., Gohl, K., Henrys, S., Wobbe, F., Davy, B.  
Manuscript intended for submission to the Palaeogeography, Palaeoclimatology, Palaeoecology journal. At the time of submitting the dissertation, the manuscript was with the co-authors for comment.



A revised and shortened version has subsequently been published as:

Lindeque, A., Gohl, K., Henrys, S., Wobbe, F., Davy, B., 2016. Seismic stratigraphy along the Amundsen Sea to Ross Sea continental rise: A cross-regional record of pre-glacial to glacial processes of the West Antarctic margin. *Palaeogeography, Palaeoclimatology, Palaeoecology*, 443, 183–202, doi:10.1016/j.palaeo.2015.11.017

The Amundsen Sea – Ross Sea transect is the first data across the previously unexplored central Amundsen Sea basin. Seismic units, interpreted to represent the pre-glacial to full glacial transition sequences, are compared to existing studies in the eastern Amundsen Sea and linked to deep-sea profiles in the Ross Sea, and pre-existing data in the eastern Ross Sea. A new age model is presented and in combination with the seismic interpretation, give insights into the basin geometry, first arrival of the ice sheets on the shelf and suggests the earlier onset of bottom current activity, already in pre-glacial times. This work forms the foundation for the subsequent two papers.

I processed all the data that comprise the AS–RS transect and was responsible for onboard quality control (QC) during data acquisition on the ANT-XXVI/3 expedition to the Amundsen Sea, Antarctica. I interpreted the multichannel seismic data, proposed the new Amundsen Sea basin stratigraphic nomenclature, created all the figures and wrote the manuscript. K. Gohl supervised the project, was Chief scientist on-board the ANT-26/3 expedition, and improved the manuscript. S. Henry provided the TAN0602 seismic data and sonobuoy data that link the seismic lines on the Ross Sea shelf with that in the Amundsen Sea basin. He also provided a preliminary interpretation of the shelf-slope link. F. Wobbe assisted with preparing the data for import into DUG Insight software for interpretation and commented on the manuscript. B. Davy participated in the ANT-XXVI/3 expedition, assisted with onboard QC during seismic data acquisition and commented on the manuscript. This papers' manuscript is Chapter 8.

### **6.3 Anomalous South Pacific lithosphere dynamics derived from new sediment thickness estimates off the West Antarctic margin.**

Wobbe, F., Lindeque, A., Gohl, K., 2014.

At the time of submitting the dissertation, the manuscript was submitted to *Global Planetary Change* and out for review.

It has subsequently been published as:

Wobbe, F., Lindeque, A. and Gohl, K., 2014. Anomalous South Pacific lithosphere dynamics derived from new total sediment thickness estimates off the

West Antarctic margin. *Global and Planetary Change*, 123 (A), 139–149, doi: 10.1016/j.gloplacha.2014.09.006.

The presented total sediment thickness grid is the first for the West Antarctic margin and extends the NGDC's 5 min arc grid of total ocean sediment thickness. The derived residual basement topography is used to understand the basement roughness. The palaeotopography reconstructions remain uncertain because the revised basement topography contradicts present-day dynamic topography models.

F. Wobbe analysed and gridded the data, derived the basement topography, and wrote the manuscript. I picked the acoustic basement and seafloor in the multichannel seismic data that were used to determine the sediment thickness, calculated the sediment thickness estimates, and assisted with the data processing and co-authoring of the manuscript. K. Gohl supervised the project and commented on the manuscript. This paper constitutes Chapter 9.

#### **6.4 Pre-glacial to glacial sediment thickness grids for the Pacific margin of West Antarctica.**

Lindeque, A., Wobbe, F., Gohl, K.

Manuscript for submission to *Geochemistry, Geophysics, Geosystems (G-Cubed)* as a Technical brief.

At the time of submitting the dissertation, the manuscript was with the co-authors for comment. It has subsequently been submitted and is out for review.

The presented grids identified the main depocentres on the West Antarctic margin and give an indication of how they shifted since the Cretaceous. The grids provide an initial quantification of volumes and sediment thicknesses for the Ross Sea, Amundsen Sea and Bellingshausen Sea – Antarctic Peninsula basin. The values are necessary for palaeotopography reconstructions, especially at the Eocene/Oligocene boundary and the mid-Miocene periods that are associated with large fluctuations in climate proxies.

I identified and picked the  $x$ ,  $y$ , two-way-time (TWT) coordinates for the basement, and the boundary horizons to the pre-glacial, transitional and full glacial sequences. These interpretation points were used for the sediment thickness grids and the isostatically corrected palaeotopography maps. I wrote the main manuscript whilst F. Wobbe merged the data, completed the gridding and volume estimate calculations, and commented on the manuscript. K. Gohl supervised the project and improved the manuscript. This paper is Chapter 10.

# WEDDELL SEA – SCOTIA SEA TRANSECT

Lindeque, A., Martin, Y.M., Gohl, K., Maldonado, M., 2013. Deep-sea pre-glacial to glacial sedimentation in the Weddell Sea and southern Scotia Sea from a cross-basin seismic transect. *Marine Geology* 336, 61–83, <http://dx.doi.org/10.1016/j.margeo.2012.11.004>.

#### Highlights:

- New seismostratigraphy and age model for the Weddell Sea and southern Scotia Sea
- Cross-basin correlation of Pre-glacial, transitional and full glacial sequences
- New sedimentation rate and sediment thickness estimates for the Weddell Sea basin
- Indications for a Cretaceous proto Weddell Gyre and Oligocene Antarctic ice sheet
- Indications for an Early Miocene expansion of the Antarctic Peninsula Ice Sheet

---

## 7.1 Abstract

Seismic identification of the pre-glacial, transitional and full glacial components in the deep-sea sedimentary record is necessary to understand the ice sheet development of Antarctica and to build circum-Antarctic sediment thickness grids for palaeotopography/-bathymetry reconstructions, which constrain palaeoclimate models.

A ~3300 km long Weddell Sea to Scotia Sea multichannel seismic reflection data transect was constructed to define the first basin-wide seismostratigraphy and to identify the pre-glacial to glacial components. Seven main seismic units were mapped: Of these, WS-S1, WS-S2 and WS-S3 comprise the inferred Cretaceous–Palaeocene pre-glacial regime (>27 Ma in our age model), WS-S4 the Eocene–Oligocene transitional regime (27–11 Ma) and WS-S5, WS-S6, WS-S7 the Miocene–Pleistocene full glacial climate regime (11–1 Ma). Sparse borehole data from ODP Leg 113 and SHALDRIL constrain the ages of the upper three seismic units and seafloor spreading magnetic anomalies compiled from literature constrain the basement ages in the presented age model.

The new horizons and stratigraphy often contradict local studies and show an increase in age from southeast to the northwest. The up to 1130 m thick pre-glacial seismic units form a mound in the central Weddell Sea basin and in conjunction with the eroded flank geometry, allow the interpretation of a Cretaceous proto-Weddell Gyre bottom current.

The base reflector of the transitional seismic unit has a model age of 26.6–15.5 Ma from southeast to northwest, suggesting similar southeast to northwest initial ice sheet propagation to the outer shelf.

We interpret an Eocene East Antarctic Ice Sheet expansion, Oligocene grounding of the West Antarctic Ice Sheet and Early Miocene grounding of the Antarctic Peninsula Ice Sheet. The transitional regime sedimentation rates in the central and northwestern Weddell Sea (6–10 cm/ky) are higher than in the pre-glacial (1–3 cm/ky) and full glacial regimes (4–8 cm/ky). The pre-glacial to glacial rates are highest in the Jane- and Powell Basins (10–12 cm/ky). Total sediment volume in the Weddell Sea deep-sea basin is estimated at  $3.3\text{--}3.9\times 10^6$  km<sup>3</sup>.

**Keywords:** Antarctica, Weddell Gyre, Ice sheet expansion, seismic reflection data, seismic stratigraphy

## 7.2 Introduction

Seismic deep-sea sediment thicknesses, distribution patterns and deposition characteristics reveal the erosional, transport and deposition processes that were active during Antarctica's transition from a warm, pre-glacial to a cold, glacial climate. The geometry, distribution and thickness of sediment sequences produced by these processes can provide insight into the ice sheet development and palaeocirculation of the Weddell Sea. Additionally, sediment thickness grids are needed for palaeotopography (Lythe et al., 2001; Le Brocq et al., 2010; Wilson et al., 2011) and palaeobathymetry (Brown et al., 2006; Hayes et al., 2009) reconstructions at epochs with similar or higher atmospheric (Pagani et al., 2005; Tripathi et al., 2009; 2011). These palaeosurface reconstructions provide boundary conditions for palaeoclimate models (e.g. Pollard and DeConto, 2009), which focus on predicting ice sheet behaviour under continued increase of pCO<sub>2</sub> levels.

Identification of these pre-glacial to glacial components in the deep-sea seismic sedimentary records is largely unresolved for the Weddell Sea basin and cross-regional stratigraphic grids for the West Antarctic margin are still absent. As a result, sediment thickness is largely omitted in palaeobathymetry reconstructions (e.g. Brown et al., 2006), or if considered, contain data from the 1970's (Hayes and La Brecque, 1991; Hayes et al., 2009) and few data points (Laske and Masters, 1997), which distort the grids. Tracing continuous horizons over large (>500 km) distances in seamless seismic data are thus needed to develop a basin-wide stratigraphy, identify the pre-glacial to glacial components in the deep-sea sedimentary record and estimate sediment thickness and volume. Previous seismic reflection studies presented seismostratigraphy models for the southern Scotia Sea (e.g. Maldonado et al., 1998, 2003, 2005; Fig. 7-1), the Antarctic Peninsula (e.g. Larter and Barker, 1989; Rebesco and Camerlenghi, 2008; Smith and Anderson, 2010), the Jane and Powell Basins in the northwestern Weddell Sea

(e.g. Coren et al., 1997; Bohoyo et al., 2002; Bohoyo, 2004; Fig. 7-1), and the southeastern Weddell Sea basin (Hinz and Kristoffersen, 1987; Miller et al., 1990; Rogenhagen and Jokat, 2000; Rogenhagen et al., 2004; Fig. 7-1).

These identified three pre-glacial seismic stratigraphic units in the Weddell Sea and one in the Scotia Sea (Pw5, SH5, Sh5, SOM-C, fourth column in Table 7-1 and references in footnote) span the Jurassic to the end of the Oligocene. Three glacial regime units in the Weddell Sea and four in the Scotia Sea, Jane and Powell Basins were also identified. In contrast to the pre-glacial units, the glacial units were deposited over a comparatively short period of time (~21 Ma) during the Miocene to late Pleistocene. These studies are however local scaled, stratigraphically disconnected and use different nomenclatures, making it difficult to construct regional and cross-regional sediment thickness grids.

Rooted in a ~3300 km long transect, hereafter referred to as the Weddell Sea–Scotia Sea (WS–SS) seismic transect, this study aims to: (i) define a basin-wide seismic stratigraphic model for the Weddell Sea that is correlated to the southern Scotia Sea stratigraphy and tested against local studies and sparse boreholes; (ii) identify the pre-glacial (PG), transitional (T) and full glacial (FG) components in the deep-sea sediment record; (iii) quantify the sediment thicknesses, lateral age variation and tentative sedimentation rates of these components; (iv) consider the implications the findings might have for understanding the pre-glacial to glacial development of Antarctica amidst changes in climate, tectonics, and ocean circulation.

We define the pre-glacial regime as warm, predominantly ice sheet free conditions and open-ocean. The transitional regime describes a colder alpine-type climate and periods of ephemeral continental scale ice sheets that initially grounded on the outer shelf after multiple cycles of advance and retreat. The full glacial regime denotes a cold polar climate and the expansion of the ice sheets to the coast that permanently grounded on the outer shelf. Smaller advance and retreat cycles occurred, but the ice sheets remain grounded.

The WS–SS seismic transect focuses on the deep-sea sedimentary record because there the reflections are less disturbed or influenced by changes in sea level and glacial processes, making it easier to trace horizons over long distances. The thickness and geometry of the seismic sequences can give an indication of high sediment influx to the deep-sea, triggered for example by expanding ice sheets pushing sediments off the outer shelf, onto the slope and rise.

The proposed age model provides a working hypothesis for further unravelling of the past ice-sheet dynamics and ocean circulation in the Weddell Sea that can be tested by future deep-sea drilling.



### 7.3 Tectonic, palaeoceanographic and palaeoclimate setting

The Weddell Sea basin experienced approximately 150 Ma of tectonic, palaeoceanographic and palaeoclimate history that spans the Mesozoic Gondwana break-up to the present (Table 7-1).

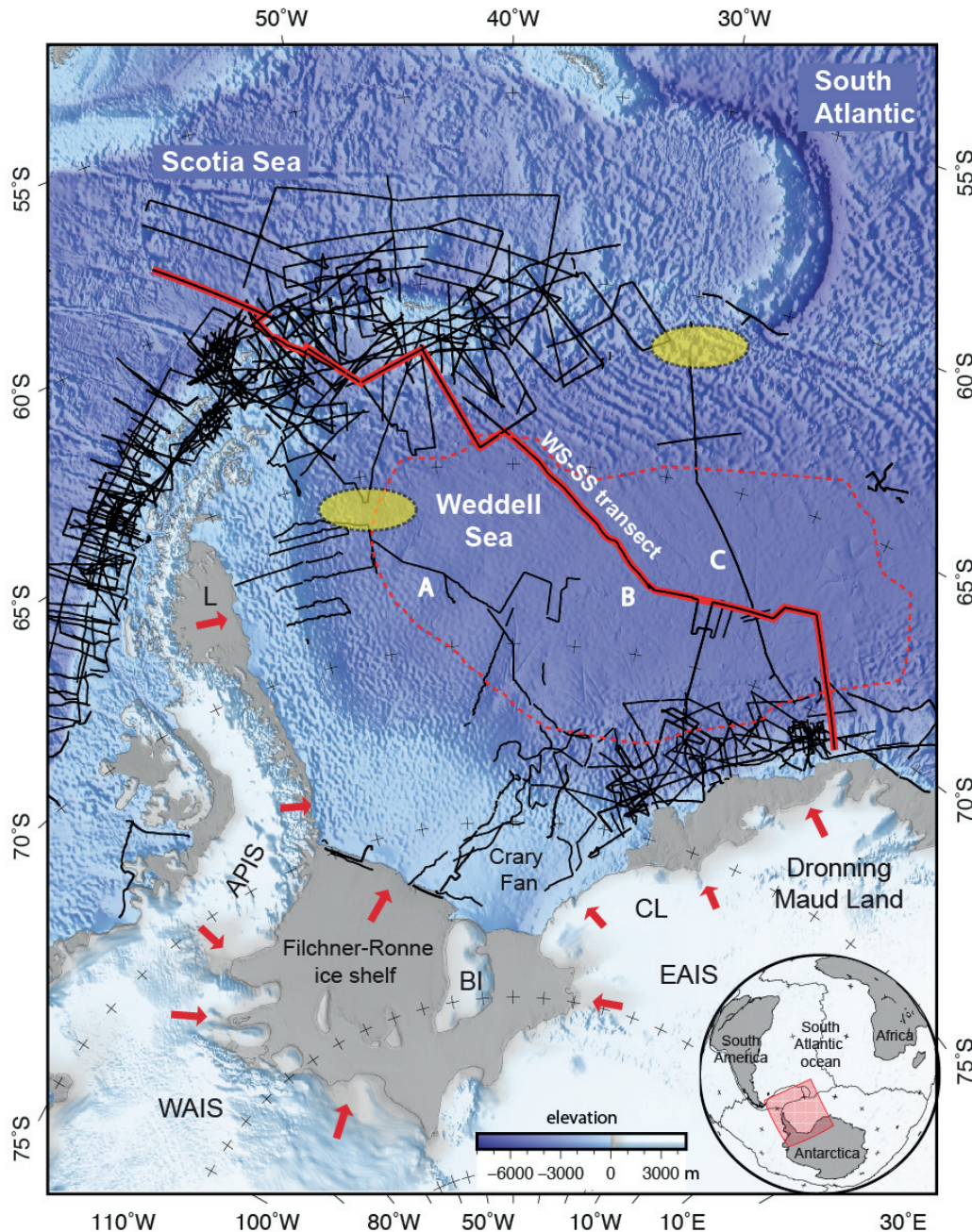


**Fig. 7-1** Overview map of the Weddell Sea basin (WSB, red dotted outline) study area with all seismic profiles from the Seismic Data Library (black lines) and the WS-SS seismic transect (thick red line, marked B). Yellow ovals demarcate seismic data gaps in two alternative cross-basin transects A and C. Background image: global seafloor topography grid, version 13.1, Smith and Sandwell (1997) and for land the ETOPO1 Global Relief Model (Amante and Eakins, 2009). Red arrows indicate general ice flow drainage directions of the Antarctic Peninsula Ice Sheet (APIS), West Antarctic Ice Sheet (WAIS) and East Antarctic Ice Sheet (EAIS) after Bentley et al., 2010; Jamieson et al., 2010; Pritchard et al., 2009; Rignot et al., 2008. L – Larsen ice shelf, BI – Berkner Island, CL – Coats Land. Globe insert: plate boundaries and study area (red square)



**Table 7-1** Deposition of seismic stratigraphic units in the Weddell and Scotia Seas during changes in tectonics, glaciation, climate and ocean circulation.

Epoch	Age (Ma)	Chron*	Seismic stratigraphic units, prefix indicates basin	Changes in tectonics, glaciation, sea level, climate and ocean circulation from literature
Pleist.	0.0	C1y	SH1 (2.4–1.6 Ma) <sup>1,2</sup> SOM-A (ODP695,6,7) <sup>3</sup>	Multiple grounding and retreat cycles of the APIS, WAIS and EAIS <sup>1,2,4,5,6</sup> Spreading in eastern Scotia Sea ends (C2o, 1.96 Ma) <sup>10</sup>
	2.6	C2Ay	S1,Pr1,Sh1,Pw1,J1,WD1 <sup>4</sup> <b>reflector a (3.8–3.5 Ma)<sup>4</sup></b>	Intensified deep-water production, sheeted facies and contourite deposits <sup>2,4,11</sup> Spreading in central Scotia Sea ends (C2A, 3.3 Ma) <sup>10,12</sup>
Pliocene	3.6	C2Ary	S1–S3 progradation <sup>5,6</sup> SH2 (5.5–2.4 Ma) <sup>1,2</sup>	Major sea level decrease (Za2) <sup>1,3</sup> Grounding cycles of APIS on the continental shelf more frequent <sup>2,5,7,14</sup>
	5.3	C3ry	SOM-B (ODP695,6,7, Hz2) <sup>3,7</sup> S4–S6 (6 Ma) <sup>5</sup> S2,Pr2,Sh2,Pw2,J2,WD2 <sup>4</sup> SH3 (8.2–5.5 Ma) <sup>1,2</sup> <b>reflector b (6.8–6.4 Ma)<sup>4,7</sup></b>	pCO <sub>2</sub> fluctuates (200–400ppm, 12–0.01 Ma) <sup>15,16</sup> Peninsula Pacific margin ridge-trench collisions <sup>5,6</sup> sea level increase (6.3 Ma, Tor3/Me1) <sup>13</sup> Spreading in eastern Scotia sea starts (C4n.1o, 7.6 Ma) <sup>10</sup> Uplift at South Scotia Fracture Zone and Antarctic Peninsula ~8 Ma ago <sup>59</sup> High WSBW activity, expanding WAIS <sup>4,11</sup> APIS grounding cycles (7.94–5.12 Ma) <sup>17</sup> Northward expansion of APIS (S4, S3), relatively thin sheet or small ice caps <sup>1,2</sup> Grounding cycles of EAIS and WAIS on the continental shelf <sup>2,4,18</sup> Spreading in western Scotia Sea ends (C5n.2m, 10.5 Ma) <sup>19</sup> Spreading in central Scotia Sea ends (C5n.2o, 10.95 Ma) <sup>20</sup> Initial incursions of Weddell Sea Bottom Water (WSBW) into Scotia Sea <sup>4</sup>
Miocene	11.6	C5r.3ry	W5 (12 Ma, ODP692,3) <sup>8,9</sup> S3,Pr3,Sh3,Pw3,J3,WD3 <sup>4</sup> <b>reflector c (12.6–12.1 Ma)<sup>7,4</sup></b> SH4 (13.8–8.2 Ma) <sup>1,2</sup> Pr4,J4 (14.1–12.1 Ma) <sup>4</sup> S4 (17.6–12.6 Ma) <sup>4</sup>	Permanent WAIS, bringing terrigenous sediments to margin <sup>1,2</sup> Miocene glaciation (Mi4), a lowering of sea level (Ser3) and permanent EAIS <sup>4,13,18</sup> Mid-Miocene climate optimum (16–15 Ma) and global temperature decrease ~8°C <sup>13,18</sup> Spreading in Jane Basin ends (C5Adm, 14.4 Ma) <sup>21,22</sup> Early expansions of APIS onto the continental shelf in the south <sup>2</sup> Bottom water circulation between Scotia Sea and Weddell Sea, WD4 drifts <sup>4</sup>
	16.0	C5Cn.1ny	Pr5,J5 (17.6–14.0 Ma) <sup>4</sup> Pw4,WD4 (18.5–12.6 Ma) <sup>4</sup> Sh4 (19.8–12.6 Ma) <sup>4</sup> S5 (20.7–17.6 Ma) <sup>4</sup>	Spreading in Scan Basin ends (C5Cn.3m, 16.6 Ma) <sup>21</sup> Spreading in Jane Basin and Scan basin starts (C5Dm, 17.6 Ma) <sup>21,22</sup> pCO <sub>2</sub> fluctuates (300 to 400ppm, 20–12 Ma) <sup>15</sup> Spreading in Weddell Sea (C6m, 19.2 Ma) <sup>21</sup> and Powell Basin ends (C6AAo, 21.1 Ma) <sup>23</sup>
Oligocene	23.0	C6Cn.2ry	WD5 (20.5–18.5 Ma) <sup>4</sup> Sh5 (28.0–19.0 Ma) <sup>4</sup> SOM-C (ODP695,6,7, Hz1) <sup>3,7</sup>	EAIS fully developed to shelf edge <sup>2,24–28</sup> Mi-1 Glaciation, warming 5–6°C <sup>18</sup> pCO <sub>2</sub> increase (~400–930ppm, 28–25 Ma) rapid decrease (~930–400ppm, 25–23 Ma) <sup>16</sup> Central Scotia Sea spreading starts (C8n.2o, 26.1 Ma) <sup>20</sup>
	28.4	C10n.1ry	Pw5 (32.0–18.0 Ma) <sup>4</sup>	pCO <sub>2</sub> decrease (1800–400ppm, 33–28 Ma) <sup>16</sup> sea level decrease by ~100m <sup>13</sup> Earliest observed glacial event on the Antarctic Peninsula (29.8 Ma) <sup>28</sup> Opening of the Powell Basin starts (C11n.1o, 29.7 Ma) <sup>22,25,60</sup> Opening of the Protector Basin (33.7–30.2 Ma) <sup>20,21,23</sup> or (17.4–13.8 Ma) <sup>61</sup> Seafloor spreading in western Scotia Sea starts (C12m, 30.9 Ma) <sup>19,20,29</sup> EAIS & WAIS formation (33–31 Ma) <sup>9,30,31,32</sup> Onset of the Antarctic Circumpolar Current (ACC) <sup>4,29,32,33</sup> Abrupt Eocene–Oligocene (ca. 33 Ma) cooling <sup>18,33,34</sup> clockwise gyre in Scotia Sea <sup>35</sup>
Eocene	33.8	C13ry	W4 (35 Ma, ODP692,3) <sup>8,9</sup> SH5 (37–32 Ma) <sup>1,2</sup>	pCO <sub>2</sub> decline (1750–700ppm, 38–33 Ma), temp ~4°C lower, orbital cycle changes <sup>33,36–39</sup> Spreading in Dove Basin ends (C15y, 34.7 Ma) <sup>40</sup> pCO <sub>2</sub> increase (750–1800 ppm, 35–33 Ma) <sup>16</sup> Initial continental/alpine glaciation on the Peninsula (49–32 Ma) <sup>2</sup> Oi-1 glaciation <sup>18</sup> small ephemeral ice sheets in west Antarctica, EAIS expansion <sup>7,34,41</sup> Drake Passage fully open, SAM - Antarctic Peninsula separation complete <sup>29,39,42</sup>
	37.2	C17n.1ry		Penetration of Pacific water through Drake Passage <sup>43</sup> Opening of Dove Basin starts (C18n.2o, 39.4 Ma) <sup>40</sup> pCO <sub>2</sub> increase (800 to 1800 ppm, 55–42 Ma) <sup>44</sup>
Eocene	48.6	C22ny		Complete change in deep ocean circulation, Antarctic Bottom Water forms (AABW) <sup>4</sup> Ridge-trench collisions on pacific margin of Peninsula starts (50 Ma) <sup>5</sup>
	55.8	C24rm		Drake Passage and Weddell Sea continues to open <sup>32,39,40</sup>
Paleo.	61.7	C27ny		Shallow gateways, watermass exchange between Weddell and Scotia Seas <sup>32,39,40</sup>
	65.5	C29rm		Falkland Plateau clearing the tip of Africa, opening of Drake Passage starts <sup>25</sup> Herringbone pattern anomalies form <sup>45,46,47</sup> Spreading in Weddell Sea changes to WNW–ESE <sup>45,46,47</sup>
Cretaceous	84.0	C34ny		pCO <sub>2</sub> decrease (>1800 to 800 ppm, 145–56 Ma) <sup>44</sup>
	99.6	C34nm	W3 (114 Ma, ODP692,3) <sup>8</sup> W2 (118 Ma, ODP692,3) <sup>8</sup> W1.5 (136 Ma, ODP692,3) <sup>8</sup> W3 (138–125 Ma) <sup>9</sup>	Opening of South Atlantic Ocean complete, (AFR–ANT separated) <sup>48</sup> Andenes Plateau <sup>49</sup> Weddell Sea rift <sup>50</sup> Polarstern Bank <sup>9</sup> Orion magnetic anomaly <sup>41,51,52,53</sup> Spreading in Weddell Sea now NNE–SSW and Anomaly-T forms <sup>52,54</sup> Indian and South Atlantic oceans broaden, but gateways still closed <sup>25</sup> Shear margin becomes transpressional <sup>45</sup> First oceanic crust in Weddell Sea (M17, 142 Ma) <sup>25</sup>
Jurassic	145.9	M19ry	W1 (160–145 Ma) <sup>8,9</sup>	Explora Escarpment, Explora wedge and Explora Anomaly form <sup>25,50,55,56,57</sup> N–S extension and stretching in front Dronning Maud Land, no seafloor yet <sup>25,48,58</sup>
	154.9	M25Ary		South America (SAM) - southern Africa (AFR) separates from Antarctica (ANT) <sup>25,48,49</sup>

**Abbreviations:** Epoch: Pleist. = Pleistocene, Paleo. = Paleocene, L = late, M = middle, E = early; \*Chron: Gradstein et al., 2004 appended with m (middle), y (young),

see Table 3 for chrons along the WS–SS transect; APIS = Antarctic Peninsula Ice Sheet, WAIS = West Antarctic Ice Sheet, EAIS = East Antarctic Ice Sheet, WSBW = Weddell Sea Bottom Water. Sediment unit prefixes: S = Scotia Sea, Pr = Protector Basin, Sh = near Shackleton Ridge, Pw = Powell Basin, SOM = South Orkney Microcontinent, J = Jane Basin, SH = SHALDRIL II James Ross Basin, WD = northwestern Weddell Sea, W = southeastern Weddell Sea; pCO<sub>2</sub> ppm = partial pressure atmospheric CO<sub>2</sub> in parts per million.

**References:** <sup>1</sup>Anderson et al., 2006 <sup>2</sup>Smith & Anderson, 2010 <sup>3</sup>Busetti et al., 2000 <sup>4</sup>Maldonado et al., 2006 <sup>5</sup>Larter & Barker, 1989 <sup>6</sup>Larter & Cunningham, 1993 <sup>7</sup>Barker & Kenneth, 1988 <sup>8</sup>Rogenhagen et al., 2004 <sup>9</sup>Miller et al., 1990 <sup>10</sup>BAS, 1985 <sup>11</sup>Maldonado et al., 2000 <sup>12</sup>Livormore et al., 2000 <sup>13</sup>Haq & Schutter, 1987 <sup>14</sup>Bart & Anderson, 1995 <sup>15</sup>Tripathi et al., 2009 <sup>16</sup>Pagani et al., 2005 <sup>17</sup>Bart et al., 2005 <sup>18</sup>Zachos et al., 2001 <sup>19</sup>Maldonado et al., 2007 <sup>20</sup>Eagles et al., 2005 <sup>21</sup>Bohoyo et al., 2002 <sup>22</sup>Bohoyo, 2004 <sup>23</sup>Eagles & Livormore, 2002 <sup>24</sup>Anderson, 1999 <sup>25</sup>Konig and Jokat, 2006 <sup>26</sup>Zachos & Kump, 2005 <sup>27</sup>Lear et al., 2008 <sup>28</sup>Dingle & Lavelle, 1998 <sup>29</sup>Barker et al., 1991 <sup>30</sup>Oszko, 1997 <sup>31</sup>Kennet et al., 1975 <sup>32</sup>Lawver & Gahagan, 1998, 2003 <sup>33</sup>Pollard & DeConto, 2009 <sup>34</sup>Barker, 2001 <sup>35</sup>Maldonado et al., 2003 <sup>36</sup>DeConto & Pollard, 2003 <sup>37</sup>Coxall, 2005 <sup>38</sup>Barker & Thomas, 2004 <sup>39</sup>Livormore et al., 2005 <sup>40</sup>Eagles et al., 2006 <sup>41</sup>LaBrecque et al., 1986 <sup>42</sup>Bohoyo et al., 2007 <sup>43</sup>Scher & Martin, 2006 <sup>44</sup>Berner & Kothavala, 2001 <sup>45</sup>Livormore & Hunter, 1996 <sup>46</sup>Rogenhagen & Jokat, 2000 <sup>47</sup>Ghidella et al., 2002 <sup>48</sup>Jokat et al., 2003 <sup>49</sup>Jokat et al., 1996 <sup>50</sup>Hinz & Kristoffersen, 1987 <sup>51</sup>Kristoffersen & Haugland, 1986 <sup>52</sup>LaBrecque & Ghidella, 1997 <sup>53</sup>Ferris et al., 2000 <sup>54</sup>Rogenhagen & Jokat, 2002 <sup>55</sup>Hunter et al., 1996 <sup>56</sup>Hinz & Krause, 1982 <sup>57</sup>Hinz, 1981 <sup>58</sup>Ghidella & LaBrecque, 1997 <sup>59</sup>Livormore et al., 2004 <sup>60</sup>Surifach et al., 1996 <sup>61</sup>Galindo-Zaldívar et al., 2006

eastern SS  
 uplift  
 western & central Scotia Sea (SS) opening  
 ACC onset  
 EAIS & WAIS expands  
 paleo Scotia gyre  
 Drake Passage opening  
 Weddell Sea opening  
 EAIS & WAIS expanding up to continental shelf edge, grounding cycles  
 APIS development  
 grounding

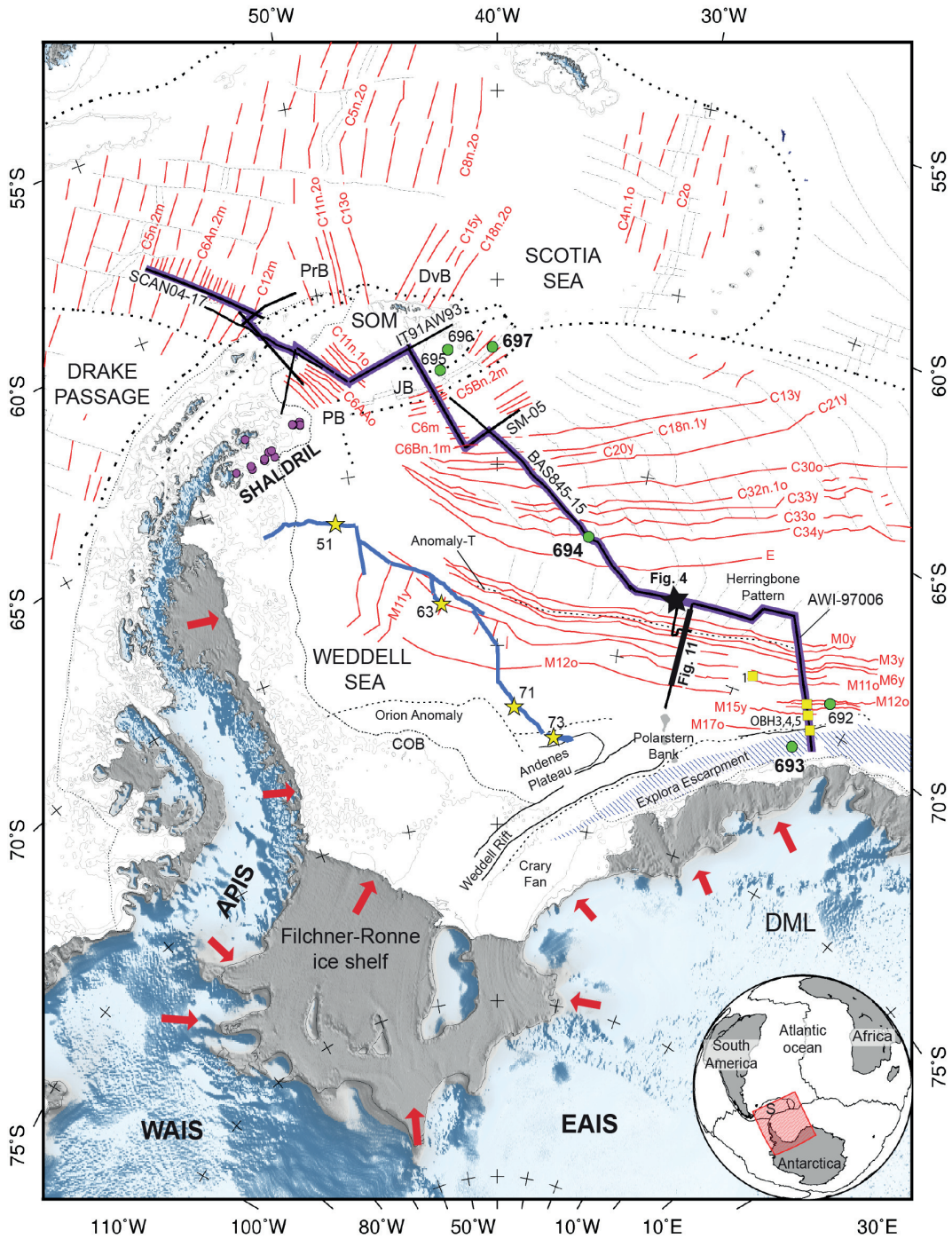


**Fig. 7-2** Magnetic anomaly map compilation for the Weddell Sea and Scotia Sea region and the WS-SS seismic transect (purple line), simplified tectonic features, boreholes and velocity stations, in a polar stereographic projection. Red arrows and background image for land are the same as for Fig. 7-1. Datasets: red lines = Isochrons of magnetic spreading anomalies compiled from literature, labelled with our standardized chron nomenclature (Table 7-2); green circles = ODP leg 113 boreholes, bold numbers = boreholes in Fig. 7-3 used for the stratigraphic correlation; purple circles = SHALDRIL boreholes; stars and blue line = seismic recording stations and seismic reflection profiles from Rogenhagen and Jokat (2000); yellow squares = archive sonobuoy data (Hinz and Krause, 1982) and Ocean Bottom Hydrophone (OBH) stations after Ritzmann (1998). Tectonic features: thick dotted black lines = plate boundaries; grey dashed lines = transform faults and flow lines; double dotted lines = spreading ridges. Geographic features: COB = Continent Ocean Boundary, DML = Dronning Maud Land, DvB = Dove Basin, JB = Jane Basin, PB = Powell Basin, PrB = Protector Basin, SOM = South Orkney Micro continent.

Tectonic seafloor spreading in the Weddell Sea started at ~147 Ma and continued into the Eocene. Sedimentation initially started in the Weddell Sea from ~138 Ma onwards (Miller et al., 1990; Rogenhagen et al., 2004), as Africa and Antarctica separated (e.g. Rogenhagen and Jokat, 2002; König and Jokat, 2006; Table 7-1). During the Early Eocene, Antarctica had a warm climate with high pCO<sub>2</sub> concentrations (>1800 ppm) and sea level was about 150 m higher than today (e.g. Zachos et al., 2001; Miller et al., 2008). Sediment deposits formed in the Antarctic Peninsula indicate shallow water gateways (seismic lithology unit SH5 at ~37 Ma onwards in Table 7-1; Anderson, 2006; Smith and Anderson, 2010; Anderson et al., 2011). This was followed by Oligocene sedimentation in the Powell Basin and western Scotia Sea (e.g. seismic stratigraphic units Pw5, Sh5, Maldonado et al., 2006) during the completion of the seismic Weddell Sea opening (e.g. Bohoyo et al., 2002; König and Jokat, 2006; Table 7-1; Fig. 7-1).

The Eocene–Oligocene transition at ~33 Ma signifies a period of several major changes: Antarctica's climate changed from warm and relatively ice-sheet free to cold and ice-covered, as temperatures decreased by about 4 °C; pCO<sub>2</sub> declined rapidly from 1750 to 700 ppm and orbital cycles changed (Barker, 2001; Zachos et al., 2001; DeConto and Pollard, 2003; Barker and Thomas, 2004; Coxall et al., 2005; Livermore et al., 2005; Pollard and DeConto, 2009); the Antarctic Circumpolar Current (ACC) developed (Lawver and Gahagan, 1998, 2003; Miller et al., 2008) as the Weddell Sea and Drake Passage opened and western Scotia Sea started to open (Bohoyo et al., 2002; Ghidella et al., 2002; König and Jokat, 2006; Maldonado et al., 2006); ephemeral ice sheets formed the initial East Antarctic Ice Sheet (EAIS) and West Antarctic Ice Sheet (WAIS) on higher elevations (LaBrecque et al., 1986; Barker et al., 1988; Miller et al., 1990; Oszko, 1997; Barker, 2001) as well as small ice-caps on the northern Antarctic Peninsula (Dingle and Lavelle, 1998; Smith and Anderson, 2010; Anderson et al., 2011).

In the Miocene (23.0–5.3 Ma), the EAIS, WAIS and Antarctic Peninsula Ice Sheet (APIS) growth accelerated and these ice sheets expanded to the outer shelf (dark grey bar on the right in Table 7-1, after e.g. Barker et al., 1988; Larter and Barker, 1989; Dingle and Lavelle, 1998; Barker, 2001; Zachos et al., 2001; Maldonado et al., 2006; Miller et al., 2008; Smith and Anderson, 2010; Davies et al., 2012). Atmospheric pCO<sub>2</sub> levels decreased further and more rapidly from ~930 to 400 ppm during 25–23 Ma (Zachos et al., 2001; Pagani et al., 2005; Zachos and Kump, 2005; Tripathi et al., 2009, 2011). Sea level decreased by ~100 m (e.g. Haq and Schutter, 2008) and ocean bottom water circulation intensified between the Weddell and Scotia Seas as the ACC system developed fully (e.g. Maldonado et al., 2006).

From the Pliocene–Pleistocene, after ~5.3 Ma, smaller glacial and interglacial, climate and sea-level cycles occurred in the Quaternary but the EAIS, WAIS and APIS repeatedly extended to the outer shelf in a tectonic and ocean circulation setting similar than today (Table 7-1).



## 7.4 Datasets and Methods

The WS–SS seismic transect is a first approach to identify the pre-glacial (PG), transitional (T) and full glacial (FG) components of the deep-sea sediment record in the Weddell Sea and southern Scotia Sea (Fig. 7-1). All three Antarctic ice sheets, the WAIS, EAIS and APIS, drain into the Weddell Sea (red arrows, Fig. 7-1) making this basin a unique area to study deep-sea sediment transport and depositional processes related to ice sheet growth and demise. Magnetic seafloor spreading anomalies, seismic reflection data and ODP boreholes (Fig. 7-2) were used to construct an age model and estimate sedimentation rates in the following manner:

### 7.4.1 Magnetic anomaly isochron compilation

To constrain basement ages, obtain a spreading age range for each basin that the WS–SS seismic transect crosses and to deduce the ages of the oldest sediments that lie on the basement, we compiled a cross-basin and cross regional seafloor spreading magnetic anomaly isochron map (Fig. 7-2; Table 7-2; Ch. 5) for the Weddell Sea and Scotia Sea from published literature (BAS, 1985; LaBrecque and Ghidella, 1997; Nankivell, 1997; Surinách et al., 1997; Lodolo et al., 1998, 2010; Bohoyo et al., 2002, 2007; Eagles and Livermore, 2002; Ghidella et al., 2002; Kovacs et al., 2002; Eagles et al., 2005, 2006; Galindo-Zaldívar et al., 2006; König and Jokat, 2006; Maldonado et al., 2007; Eagles, 2010). This map compilation has not been published before and is available in the PANGAEA.de database (Lindeque et al., 2012).

Where available, magnetic anomaly picks were sourced from authors and imported into GIS ArcMap 10 (e.g. König and Jokat, 2006). In regions where actual magnetic data picks were unavailable, published anomaly and isochron maps (e.g. Bohoyo et al., 2002; Maldonado et al., 2007) were georeferenced and the isochrons precisely digitized. Conflicting opinions do exist between studies in the same basin e.g. in the Powell Basin between Eagles and Livermore (2002) and Surinách et al. (1997) due to ambiguous data and allow for alternative age interpretations. In such cases, the most recent publication or best fit with the regional trend was favoured. The digitized isochrons were combined with the isochrons from the data picks and exported as an ESRI shapefile that was geospatially superimposed on the transect (thin red lines in Fig. 7-2; Ch. 5). All data picks and maps were used as published.

Chron nomenclature and ages in literature (Chron-L, Age-L in Table 7-2) often varied between authors who applied different time scales (e.g. Cande and Kent, 1995 versus Gradstein et al., 1994). We thus standardized the nomenclature of the final selected isochrons to the Gradstein et al. (2004) timescale. Chrons were appended with o=old, m=middle, y=young, to indicate which part of the modelled magnetic anomaly was picked in the original literature before assigning the updated chron nomenclature (respectively named Chron and Age in Table 7-2).

**Table 7-2** Isochrons of magnetic spreading anomalies crossing the Weddell Sea - Scotia Sea (WS-SS) seismic transect, see Figure 2.

This study		Literature		Profile number	This study		Literature		Profile number
Chron	Age	Chron-L	Age-L		Chron	Age	Chron-L	Age-L	
<b>Scotia Sea</b>					<b>Northeastern Weddell Sea</b>				
C5n.2m	10.5	C5n	9.8	SCAN04-17 <sup>1</sup>	C6m	19.2	C6n	19.5	SM04 <sup>2</sup>
C5An.2m	12.3	C5An	12.3	SCAN04-17 <sup>1</sup>	C6An.1m	20.1	C6An.1n	20.0	SM04 <sup>2</sup>
C5Bn.2m	15.1	C5Bn.2n	15.1	SCAN04-17 <sup>1</sup>	C6An.2m	20.5	C6An.2n	20.4	SM04 <sup>2</sup>
C5Cn.2m	16.4	C5Cn	16.4	SCAN04-17 <sup>1</sup>	C6Bn.1m	22.6	C6Bn	22.0	SM04 <sup>2</sup>
C5Dm	17.4	C5Dn	17.3	SCAN04-17 <sup>1</sup>	C6Cn.3m	23.3	C6Cn	24.0	SM04 <sup>2</sup>
C5Em	18.3	C5En	18.2	SCAN04-17 <sup>1</sup>	C7n.2m	24.4	C7n	25.0	SM04 <sup>2</sup>
C6m	19.2	C6n	19.2	SCAN04-17 <sup>1</sup>	<b>Central Weddell Sea</b>				
C6An.2m	20.5	C6An.2n	20.0	SCAN04-17 <sup>1</sup>	C13y	33.3	C13	33.1	BAS845-15 <sup>5</sup>
C6Bn.2m	22.1	C6Bn	21.9	SCAN04-17 <sup>1</sup>	C18n.1y	38.0	C18	38.4	BAS845-15 <sup>5</sup>
C6Cn.2m	23.0	C6Cn	23.0	SCAN04-17 <sup>1</sup>	C20y	41.6	C20	42.5	BAS845-15 <sup>5</sup>
C7n.2m	24.4	C7n	24.1	SCAN04-17 <sup>1</sup>	C21y	45.3	C21	46.2, 47.9	BAS845-15 <sup>5,6</sup>
C7Am	25.4	C7An	25.0	SCAN04-17 <sup>1</sup>	C30o	67.7	C30	67.6	BAS845-15 <sup>6</sup>
C8n.2m	25.8	C8n	25.4	SCAN04-17 <sup>1</sup>	C32n.1o	71.2	C32n.1	71.3	BAS845-15 <sup>7</sup>
C9m	27.3	C9n, C9	27.2, 27.7	SCAN04-17 <sup>1,4</sup>	C33y	73.6	C33	73.6	BAS845-15 <sup>7</sup>
C10n.1y	28.1	C10	28.0	M05 <sup>4</sup>	C33o	79.5	C33r	79.0	BAS845-15 <sup>7</sup>
C10n.2y	28.5	C10n	28.5	SCAN04-17 <sup>1</sup>	C34y	84.0	C34	83.0	BAS845-15 <sup>8</sup>
C11n.1m	29.6	C11n	29.5	SCAN04-17 <sup>1</sup>	E	93.0	E	93.0	BAS845-15 <sup>5</sup>
C12m	30.9	C12n	30.9	SCAN04-17 <sup>1</sup>	<b>Southwestern Weddell Sea</b>				
<b>Powell Basin</b>					M0y	124.6	M0	118, 121	97006 <sup>9</sup> , 10 <sup>9</sup> , 30 <sup>9</sup>
C6AAo	21.1	C6AA	21.8	IT89AW41 <sup>3</sup>	M1o	127.2	M1n	122.0	97006 <sup>9</sup> , 10 <sup>9</sup> , 30 <sup>9</sup>
C6Cn.3o	23.4	C6C	24.1	IT91AW90 <sup>3</sup>	M3y	127.6	M3	123.0	97006 <sup>9</sup> , 10 <sup>9</sup> , 28 <sup>9</sup> , 30 <sup>9</sup>
C7n.2o	24.5	C7	24.7	IT91AW92 <sup>3</sup>	M5y	129.8	M4	125.4	97006 <sup>9</sup> , 10 <sup>9</sup> , 29 <sup>9</sup>
C8n.2o	26.1	C8	26.5	IT91AW93 <sup>3</sup>	M6y	131.2	M5	127.0	97006 <sup>9</sup>
C9o	27.8	C9	27.9	IT91AW93 <sup>3</sup>	M10y	133.5	M10	130.2	97006 <sup>5</sup> , 10 <sup>5</sup>
C10n.1o	28.4	C10	28.5	IT91AW93 <sup>3</sup>	M11y	135.7	M10Nr	131.5	97006 <sup>9</sup> , 10 <sup>8</sup>
C11n.1o	29.7	C11	29.7	IT91AW93 <sup>3</sup>	M12o	137.8	M11, M12	133, 134	97006 <sup>8,9</sup> , 10 <sup>8,9</sup>
<b>Jane Basin</b>					M12r.1y	138.6	M12.1N	135.6	97006 <sup>9</sup>
C5ADm	14.4	C5ADn	14.4	SM04 <sup>2</sup>	M13o	139.3	M13	136.6	97006 <sup>9</sup>
C5Bn.2m	15.1	C5Bn.2n	15.1	SM04 <sup>2</sup>	M15y	140.4	M15n	138.3	97006 <sup>9</sup>
C5Cn.3m	16.6	C5Cn	16.6	SM04 <sup>2</sup>	M17o	142.8	M17	142.3	96110 <sup>9</sup>
C5Dm	17.4	C5Dn	17.6	SM04 <sup>2</sup>					

**Timescale:** Chron and Age (this study) taken from Gradstein et al., 2004. Ages appended with old (o), middle (m) and young (y); Chron-L and Age-L (literature) from: C5n to C33r, Cande and Kent, 1995; C34 to E, Gradstein et al., 1984; M0 to M17, Kent and Gradstein 1986; Gradstein et al., 1998.

**References:** <sup>1</sup>Maldonado et al., 2007; <sup>2</sup>Bohoyo et al., 2002; <sup>3</sup>Eagles and Livermore, 2002; <sup>4</sup>Lodolo et al., 1998; <sup>5</sup>Kovacs et al., 2002; <sup>6</sup>Ghidella et al., 2002; <sup>7</sup>Nankivell et al., 1997; <sup>8</sup>LaBrecque and Ghidella, 1997; <sup>9</sup>König and Jokat, 2006. All ages are in Ma.

The ages of the C-chron series slightly changed between the Gradstein et al. (2004) scale (used in this study) and the Cande and Kent (1995) scale. More significant age changes occurred in the M-series (Table 7-2) for example: chron M0y is now 124.6 Ma according to the Gradstein et al. (2004) scale, but was previously 118–121 Ma in the Cande and Kent (1995) scale used in Rogenhagen et al. (2004).

#### 7.4.2 Borehole stratigraphy

We projected Ocean Drilling Program (ODP) Leg 113 borehole sites 693, 694 and 697 (Barker et al., 1988) into the WS–SS seismic transect (Figs. 7-2 and 7-3). The projection path was chosen parallel to the contour or bathymetric feature (e.g. shelf edge,

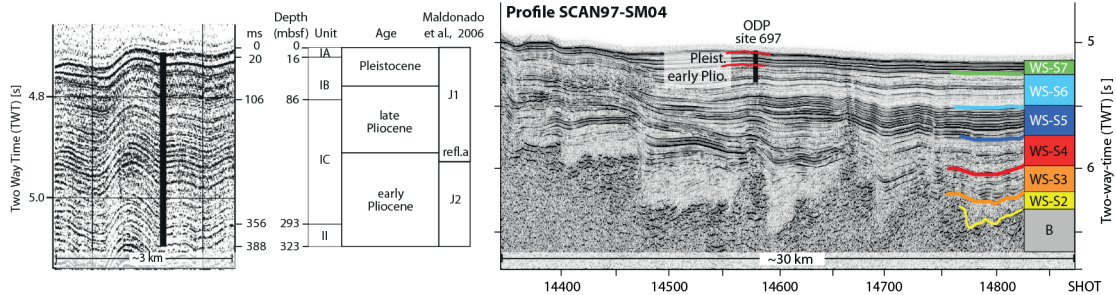


7. Weddell Sea basin

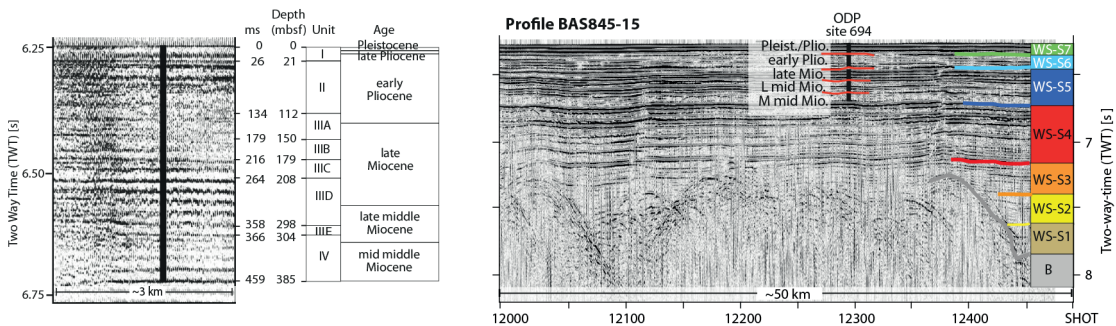
basin or ridge) in order to ensure the most accurate correlation. Site 693 lies ~65 km to the west of the transect, site 694 is line coincident and site 967 lies ~200 km to the east of the transect (Fig. 7-2). To compensate for these large offsets, the borehole horizons were matched to horizons in coincident seismic lines and traced along a series of crossing seismic tie lines until the horizon could be matched to equivalent reflectors in the WS–SS seismic transect data in order to obtain a stratigraphic age constrain for the upper 300 m (Fig. 7-3).

The following seismic tie lines were used: for site 697, lines IT91AW93, SM04 and SM05; none for site 694 as it lies directly on the transect; and for site 693, lines BGR78018, BGR78019, BGR86006 and BGR87097.

**A) ODP leg 113 site 697**



**B) ODP leg 113 site 694**



**C) ODP leg 113 site 693**

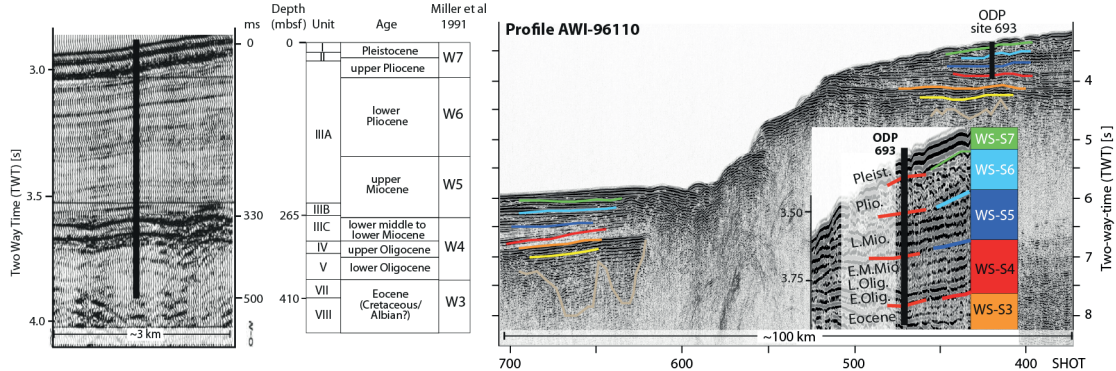


**Fig. 7-3.** Integration of nearby relevant borehole data. A, B, C: Left and middle images - Stratigraphy of ODP Leg 113 drill sites 697, 694 and 693 (Barker et al., 1988; for location see Fig. 7-2) with time scale and depth of main horizons as well as horizons interpreted in literature. Images on the right: extracts of WS-SS transect seismic data at the projected borehole position with our proposed Weddell Sea stratigraphy annotated. Units interpreted to represent glacial processes, are labeled in white. Plio. = Pliocene, Pleist. = Pleistocene, Mio. = Miocene, Olig. = Oligocene.

Most of the seismic lines used are available in the Seismic Data Library System (SDLS; Wardell et al., 2007). Recent SHALDRIL boreholes on the Antarctic Peninsula (Smith and Anderson, 2011) were also incorporated and connected to the transect via tie lines IT91AW90, M08, BAS84-154 to cruise NBP0602A.

### 7.4.3 Seismic characterization

A transect of continuous seismic data through the central Weddell Sea basin and parallel to the margin was required to ensure the most representative deep-sea data for interpretation. Multichannel seismic (MCS) reflection profiles collected on several expeditions of various organisations in the SDLS databank (Wardell et al., 2007), collectively form three transects across Transects A and C provide seismic reflection data from the southeastern to northwestern Weddell Sea, but do not connect to or cross any seismic profiles at the Antarctic Peninsula, and hence were considered unsuitable for the objectives of this work (yellow ovals in Fig. 7-1 mark data gaps).

The middle transect (B) was chosen for tracing the horizons because there are no data gaps between profiles and the transect is most representative of the deep-sea sedimentary archive, because it runs more or less through the middle of the Weddell Sea basin (red dashed outline in Fig. 7-1).

Typical seismic characteristics defined in other studies through drilling and seismic reflection data (e.g. Bellingshausen Sea: Scheuer et al., 2006; Cosmonaut Sea: Leitchenkov et al., 2007, 2008; Wilkes Land: DeSantis et al., 2003; Escutia et al., 2011) were used as a guide to identify the pre-glacial to glacial units; briefly summarised as follows:

The pre-glacial seismic facies are usually the first layers the central Weddell Sea (A, B, C in Fig. 7-1) above basement. They show diagnostic low amplitude to transparent reflectivity and stronger discontinuous reflectors therein, appearing light grey to almost white in the seismic image. The transitional regime depicts a change in the deposition processes since reflectors are now closer spaced, horizontal and mostly continuous with medium amplitude. These characteristics often result in a medium grey appearance in seismic sections without gain adjustment on display. The continuous, high amplitude reflectors represent the full glacial sequence. Deposits from sporadic down-slope sediment transport generally result in complex internal structures and form turbidite channel-levee systems, or chaotic bodies in the case of debris-flow processes. Persistent bottom-currents that flow along-slope or oblique to the contours develop various types of contourites of which the sheeted and mounded drifts are the most prominent in this case. This sequence typically appears dark grey to black in seismic images and is the first layers below the seafloor. Using these characteristic seismic facies changes, borehole correlation (Figs. 7-2 and 7-3) and other seismic stratigraphy models in the southeastern (Miller et al., 1990) and the northwestern Weddell Sea (Maldonado et al., 2006) as guidelines, we

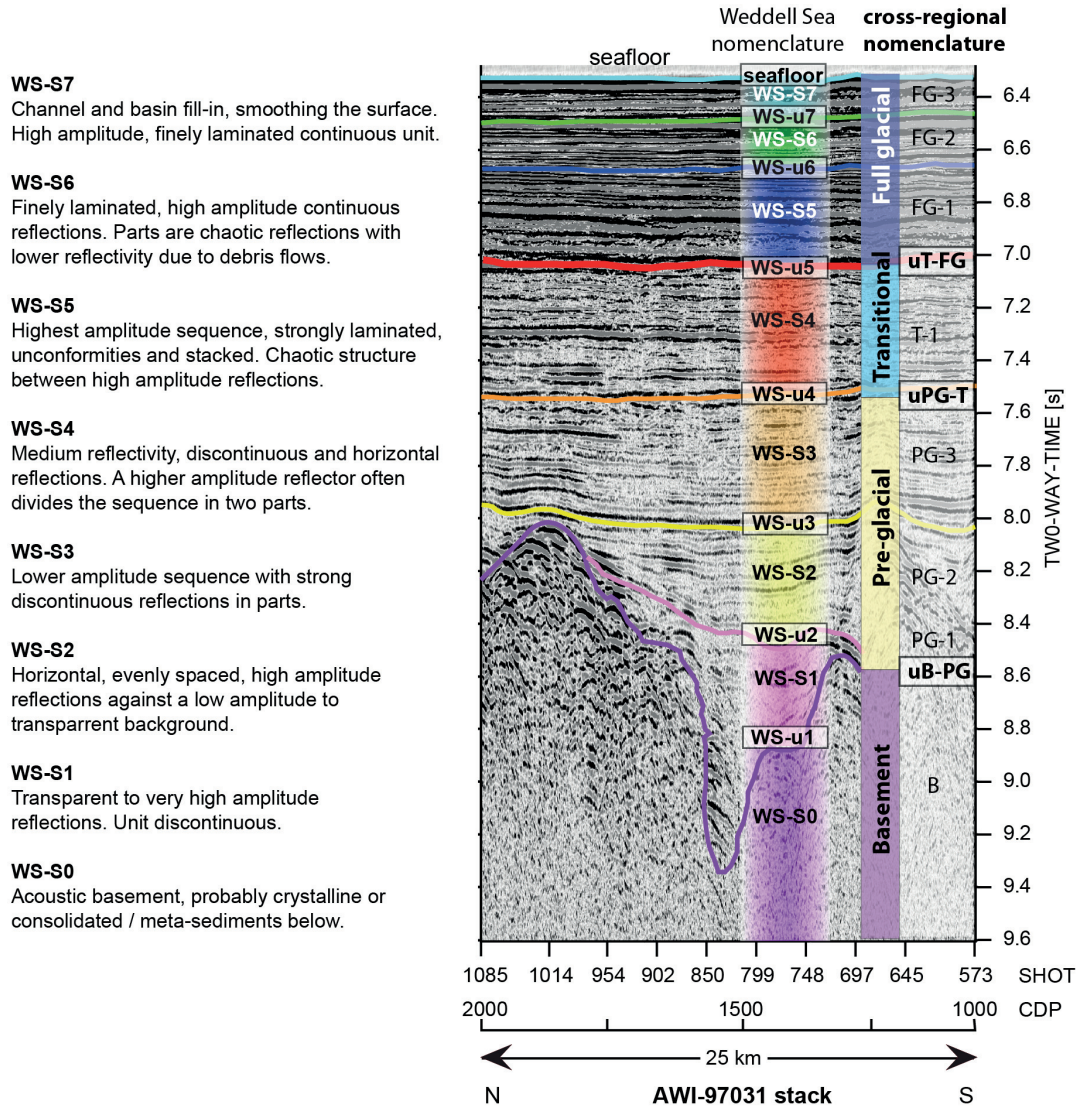


**Fig. 7-4.** Reference section, with the proposed Weddell Sea and circum-Antarctic stratigraphy superimposed on a typical seismic reflection image from the WS-SS transect. For location see Fig. 7-2. Vertical exaggeration is ~6x. The seismic characteristics of each unit are listed on the left. Sediment units for the Weddell Sea stratigraphy are numbered WS-S1 to WS-S7 from bottom to top and separated by base reflectors or unconformities (WS-u1 to WS-u7). The simplified circum-Antarctic stratigraphy defines sequences interpreted to represent acoustic basement (B), pre-glacial (PG), transitional (T) and full glacial (FG) processes, separated by the associated base reflector discontinuities or unconformities (uB-PG, uPG-T and uT-FG).

compiled a type section for the WS-SS seismic transect data (Fig. 7-4). A part of profile AWI-97030 was chosen from several other good example sections because: (1) it lies in the deeper part of the basin, (2) is close enough for correlations to the slope, (3) is a good representation of the changes in seismic facies, and (4) all the seismic units are present. See location of the type section in Fig. 7-2. We assigned a new bottom-to-top stratigraphy nomenclature for the Weddell Sea and proposed circum-Antarctic units (Fig. 7-4). The resulting model seismic stratigraphy was used as a template to interpret, or re-interpret the rest of the WS-SS seismic transect data. Twenty-three MCS profiles were used to construct the ~3300 km long WS-SS seismic transect (Fig. 7-1; Table 7-3).



**Table 7-3** Seismic reflection profiles used to construct the Weddell Sea - Scotia Sea (WS-SS) seismic transect.

Profile	Cruise	CDP spacing [m]	Source (# airguns x volume [L])	Streamer (channels/ length[m])	Profile length [km]	Processing stage of seismic data used	Area	Institute, References
SCAN04-17	SCAN-2004	25	7 x 16.40	96/2400	390	migrated	Scotia Sea	a, 1
M31	HESANT-92/93	6.25	6 x 15.26	96/1200	197	migrated	Scotia Sea	a, 2, 3
M05	HESANT-92/93	6.25	6 x 15.26	96/1200	304	migrated	Powell Basin	a, 2, 3
IT89AW41	IT90AP	12.5	18 x 2.51	120/2975	206	stack	Powell Basin	b, 4
IT91AW90	IT91AP	25	18 x 2.68	120/2975	208	stack	Powell Basin	b, 4
IT91AW91	IT91AP	25	18 x 2.68	120/2975	147	stack	Powell Basin	b, 4
IT91AW92	IT91AP	25	18 x 2.68	120/2975	56	stack	Jane Basin	b, 4
IT91AW93	IT91AP	25	18 x 2.68	120/2975	374	stack	Jane Basin	b, 5
SM04	SCAN-97	12.5	5 x 22.4	96/2400	362	migrated	Jane Basin	a, 2, 6, 7, 8
SM05	SCAN-97	12.5	5 x 22.4	96/2400	231	migrated	Jane Basin	a, 2, 6, 7
BAS845-15	BAS-84	25	4 x 8.5	48/2400	832	stack	central Weddell Sea	c, 9
AWI-97032	ANT-XIV/3	25	6 x 18	96/2400	27	stack	eastern Weddell Sea	d, 10, 11, 12
AWI-97031	ANT-XIV/3	25	6 x 18	96/2400	138	stack	eastern Weddell Sea	d, 10, 11, 12
AWI-97030	ANT-XIV/3	25	7 x 3 / 6 x 3	96/2400	109	stack	eastern Weddell Sea	d, 10, 11, 12
AWI-97029	ANT-XIV/3	25	7 x 21	96/2400	14	stack	eastern Weddell Sea	d, 10, 11, 12
AWI-97028	ANT-XIV/3	25	7 x 21	96/2400	16	stack	eastern Weddell Sea	d, 10, 11, 12
AWI-97027	ANT-XIV/3	25	7 x 21	96/2400	43	stack	eastern Weddell Sea	d, 10, 11, 12
AWI-97010	ANT-XIV/3	25	6 x 18	96/2400	335	stack	eastern Weddell Sea	d, 10, 11, 12
AWI-97009	ANT-XIV/3	25	6 x 18	96/2400	194	stack	eastern Weddell Sea	d, 10, 11, 12
AWI-97008	ANT-XIV/3	25	6 x 18	96/2400	49	stack	eastern Weddell Sea	d, 10, 11, 12
AWI-97007	ANT-XIV/3	25	6 x 18	96/2400	99	stack	eastern Weddell Sea	d, 10, 11, 12
AWI-97006	ANT-XIV/3	25	7 x 3 / 6 x 3	96/2400	312	stack	eastern Weddell Sea	d, 10, 11, 12
AWI-96110	ANT-XIII/3	50	1 x 32.6 & 60	96/2400	224	stack	eastern Weddell Sea	d, 13
				<b>Total km</b>	<b>4867</b>			

**Institutes:**

<sup>a</sup>Instituto Andaluz de Ciencias de la Tierra (IACT) and Consejo Superior de Investigaciones Científicas (CSIC), Spain; <sup>b</sup>Istituto Nazionale di Oceanografia e di Geofisica Sperimentale (OGS), Spain; <sup>c</sup>British Antarctic Survey (BAS), United Kingdom; <sup>d</sup>Alfred Wegener Institute for Polar and Marine Research (AWI), Germany. Profile names as in SDLS database (Wardell et al., 2007).

**References:**

in order of appearance along the transect: <sup>1</sup>Maldonado et al., 2007; <sup>2</sup>Maldonado et al., 2006; <sup>3</sup>Maldonado et al., 1993; <sup>4</sup>Coren et al., 1997; <sup>5</sup>Busetti et al., 2000; <sup>6</sup>Bohoyo, 2004; <sup>7</sup>Maldonado et al., 2003; <sup>8</sup>Maldonado et al., 2005; <sup>9</sup>Larter and Cunningham, 1993; <sup>10</sup>Rogenhagen, 2000; <sup>11</sup>Rogenhagen and Jokat, 2000; <sup>12</sup>Rogenhagen et al., 2004; <sup>13</sup>Ritzmann, 1998.

All navigation data and some of the seismic reflection data (IT91 and BAS845 cruises) are public domain legacy data in the SDLS. Seismic data of profiles AWI-970x were in-house at AWI, and SEG-Y data of the Spanish lines (cruises SCAN-2004, HESANT-92/93, and SCAN-97) were provided for this study from the cooperating Institute (Table 7-3). The MCS data are unmigrated or migrated stacked time sections and used as received without additional processing or conversion into a depth section. The 23 profiles were joined at the exact line intersections from northwest to southeast, resulting in a basin-wide seamless seismic reflection profile (Fig. 7-5a and 7-6a; online supplementary data to paper; Appendix A-1). No time and phase shifts were necessary to match the profiles. The magnetic spreading anomaly isochrons (Fig. 7-2) and nearby ODP leg 113 boreholes (Fig. 7-3) were projected into the transect seismic image (red dashed lines and black arrows in Fig. 7-5a and 7-6a) to constrain the interpretation and basement age. The interpretation of the upper units was tested against borehole stratigraphic correlations (Fig. 7-3) and type section (Fig. 7-4).

Thereafter we traced the strongest, undisturbed and most prominent seismic reflections and discontinuities, which define the basal boundaries of the sequences in the reference section, for the full transect length and present a basin-wide stratigraphy (Fig. 7-5b and 7-6b; online supplementary data to paper; Appendix A-1).

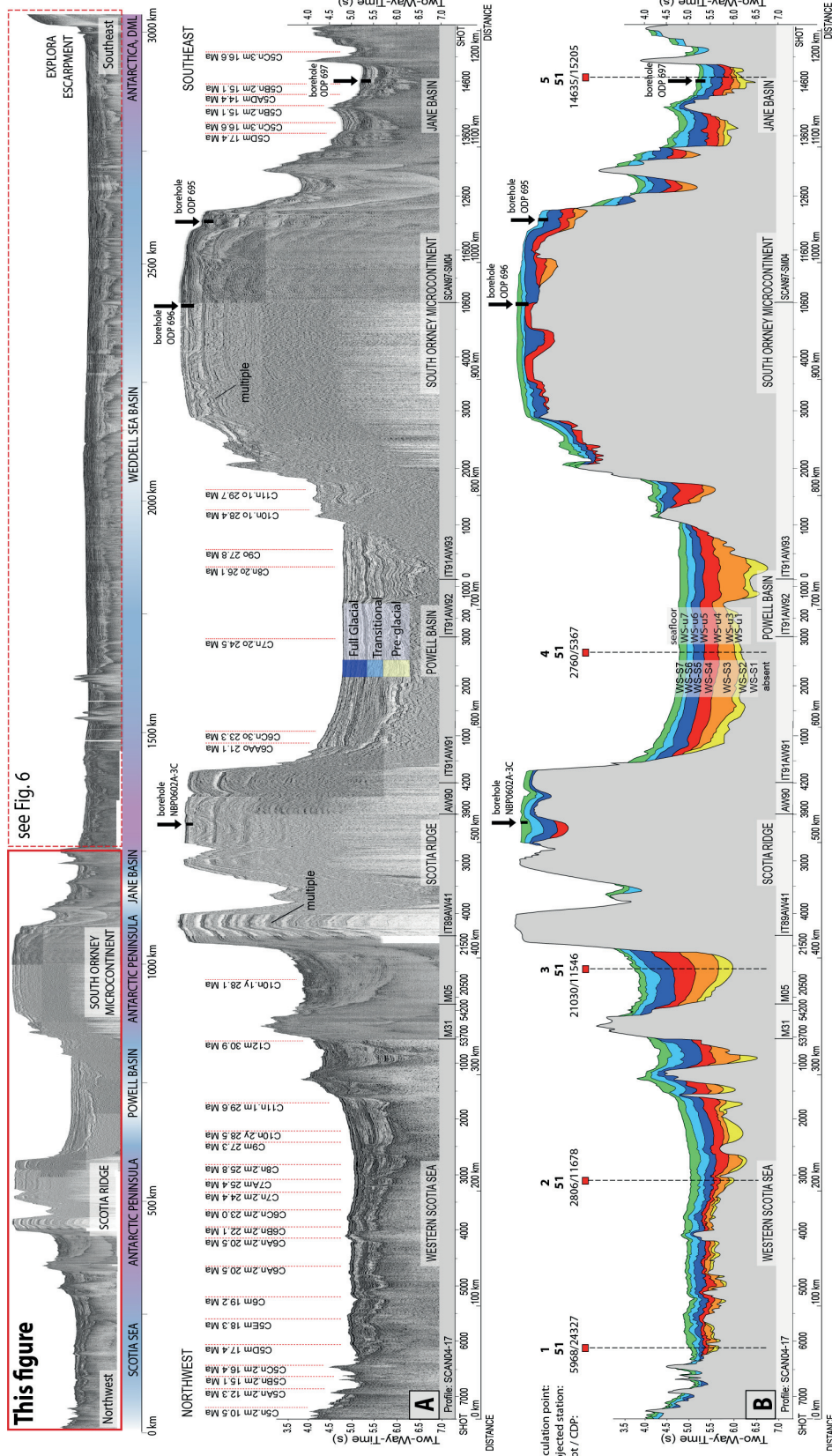


**Fig. 7-5.** Multichannel seismic acoustic image and interpretive line drawing of the deep-sea sedimentary archive along the WS-SS seismic transect. Top: Overview of the entire transect with the part illustrated in (A) and (B) below, marked with the solid line red box. (A) Seamless multichannel seismic acoustic image of the Southern Scotia Sea – Jane Basin segment represented in a time section. Profiles and shot numbers are listed in the bar below. Red dashed drop-down lines represent magnetic anomalies crossing the WS- SS transect (see Fig. 7-2 and Table 7-2). (B) Interpretive line drawing of the seismic image in (A) and the sequences identified according to the reference section (see Fig. 7-4). Profiles and shot numbers are listed in the bar below. Red squares and dashed drop-down lines represent points selected for sediment thickness and sedimentation rate calculations.



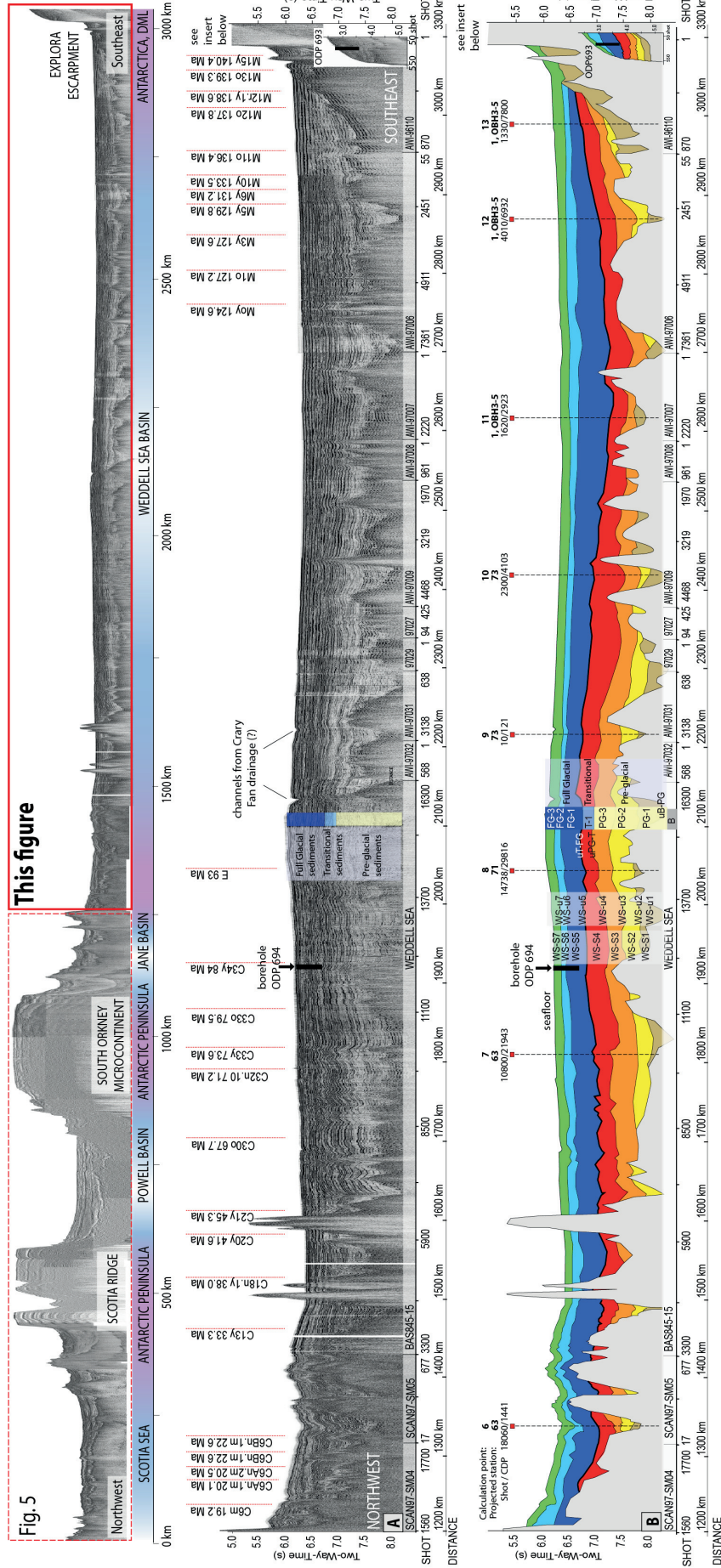


**Fig. 7-6.** Multichannel seismic acoustic image and interpretive line drawing of the deep-sea sedimentary archive along the WS-SS seismic transect continued. Top: overview of the entire transect with the part illustrated in (A) and (B) below, marked with the solid line red box. (A) Seamless multichannel seismic acoustic image of the northwestern, central and southeastern Weddell Sea segments, represented in a time section. Individual profiles and shot numbers used are listed in the bar below. Red dashed dropdown lines represent magnetic anomalies crossing the WS-SS transect (see Fig. 7-2 and Table 7-2). (B) Interpretive line drawing of the seismic image in (a) and the sequences identified according to the reference section (see Fig. 7-4). The profiles and shot numbers are listed in the bar below. Red squares and dashed drop-down lines represent points selected for sediment thickness and sedimentation rate calculations. Black arrows between points 8 and 9 indicate channel-levee geomorphology, possibly related to the Cray Fan drainage channel-system (Michels 2001, 2002) or bottom current activity.

## 7. Weddell Sea basin

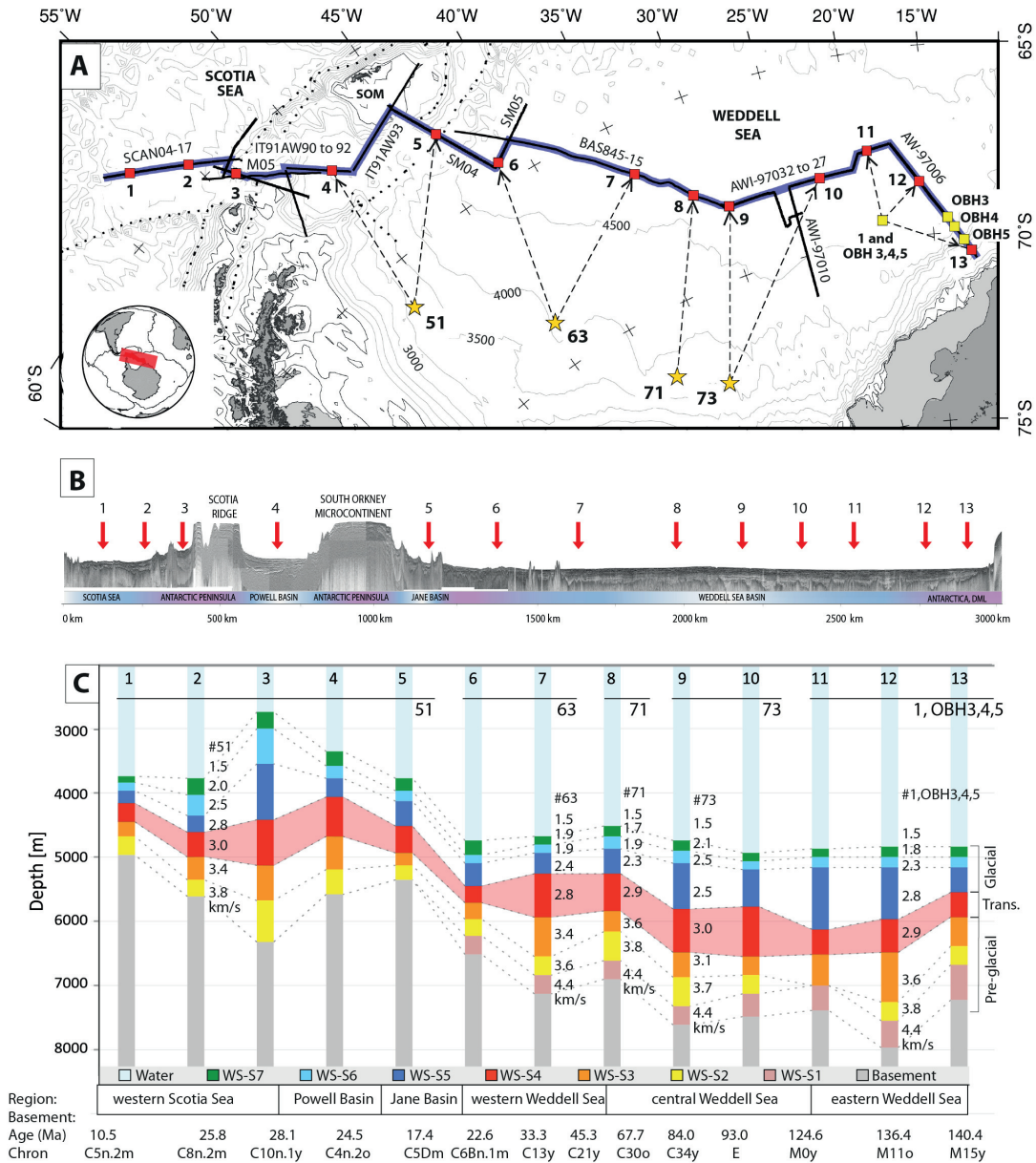


**Fig. 7-7.** Sediment thickness calculations for selected points on the WS-SS seismic transect. **(A)** Overview map showing the projection of each interval velocity station (yellow stars and squares) into the transect and matched to the 13 representative points (marked with red squares and numbered). **(B)** Overview of the seamless seismic reflection image of the WS-SS transect and the 13 selected points (red drop-down arrows). **(C)** Diagram of the sediment thickness (m) calculated at each point and the velocity data used, see text. Sediment units are listed below and identical to those identified in Figs. 7-5 and 7-6. The regional location of each point and the nearest magnetic chrons (Fig. 7-2 and Table 7-2) are annotated below.

### 7.4.4 Sediment thickness estimates

Sediment thickness-depth sections were constructed from 13 points along the WS-SS seismic profile (Fig. 7-5 to 7-7). These particular points were chosen so as to represent the major changes in the seismic facies and basin geometry, and are therefore not equidistant. Interval velocities from wide-angle seismic refraction data provide the nearest velocity information (Rogenhagen and Jokat, 2000, yellow stars Fig. 7-1) and were

supplemented by velocity data deduced from sonobuoy (station 1, Hinz and Krause, 1982) and ocean bottom hydrophones (OBH3, 4, 5, Ritzmann, 1998) experiment observations. The velocity model from station 1 divided the sediments into two units and the velocity model at OBH 3, 4 and 5, divided deep-sea sediments into three or four units. This was problematic because an average velocity for each seismic unit was needed. To resolve it, the data from these four stations were combined into one velocity function and applied to points 11, 12 and 13 (Fig. 7-7c). The sediment layer division of Rogenhagen et al. (2004) often varied from our interpreted WS–SS stratigraphy and an interpolated velocity was calculated for each sedimentary unit in proportion to the thickness. The full velocity model is available as an online supplementary data to paper.

Uncertainties in the sediment thickness of up to 70 m occur since the two-way-time picks can differ by one or two reflections (~30 ms) depending on visual interpretation. The uncertainty in interval velocities from refraction data is qualitatively estimated at ~0.1 km/s. Interval velocity in the same seismic unit change over distance due to increased compaction from more overburden and therefore using velocity data ~500 km from the transect introduce further uncertainties. Even so, the interval velocity model used was compiled from all available data nearest to the transect and in the Weddell Sea basin.

We minimize these uncertainties by assigning similar velocities to units with the same seismic facies characteristics. Velocity information from station 51 was used to calculate sediment thickness at points 1 to 5; station 63 for points 6 and 7; station 71 for point 8; and station 73 for points 9 and 10 (Fig. 7-7b and 7-7c). The resulting depth-sediment

**Table 7-4** Sediment thickness and sedimentation rate estimates at selected points on the WS-SS seismic transect, derived from the data in Figs. 1, 2 and 6 to 10.

Point	Region	Sediment thickness (m)				Sedimentation rate (cm/ky)		
		Total	Pre-glacial	Transitional	Glacial	Pre-glacial	Transitional	Glacial
1		1221	498	295	428	8.7	12.8	4.4
2	Scotia Sea	1827	626	378	824	7.4	6.9	7.0
3		3582	1172	726	1684	10.7	11.2	16.0
4	Powell Basin	2227	918	625	683	10.4	10.8	7.0
5	Jane Basin	1580	441	389	749	10.5	11.5	9.9
6	northwestern	1756	803	269	685	10.7	5.7	6.3
7	Weddell Sea	2455	1205	666	583	2.4	9.5	4.2
8	central	2386	1058	571	757	1.5	9.8	4.4
9	Weddell Sea	2872	1130	656	1085	1.4	8.2	7.8
10		2531	923	780	827	1.1	6.1	6.1
11		2524	894	383	1248	1.5	1.2	4.7
12	southeastern	3136	1481	522	1132	1.4	6.4	6.4
13	Weddell Sea	2405	1298	392	715	1.2	4.4	4.1

m = meters, m/my = meters per one million years, ms = milliseconds, red = minimum values, blue = maximum values

Pre-glacial: Seismic stratigraphic units WS-S1, WS-S2 and WS-S3 shown in Figures 6 and 7

Transitional: unit WS-S4 and Glacial: units WS-S5, WS-S6 and WS-S7

Uncertainty in sediment thickness ~30 ms, equating to 50 m for the upper and 70 m for the lower sediments

Uncertainty in interval velocity estimates from refraction data ~0.1 km/s and ~0.3 cm/ky for sedimentation rates



thickness diagram is shown in Fig. 7-7c and the sediment thickness for the pre-glacial to glacial units at each point are summarised in Table 7-4 and an online supplementary data to paper.

### 7.4.5 Age model and sedimentation rates

Our study is of basin-wide scale and since boreholes are few and far between, we constructed a hypothetical working age model as follows: a simplified Gradstein et al. (2004) geological time scale was re-drawn to a measurable vertical scale (Fig. 7-8, far left). The spreading age-range for each basin on the WS–SS seismic transect was taken from the magnetic anomaly compilation (Fig. 7-2 and Table 7-2) and drawn against the time scale (Fig. 7-8, black bars labelled SW, SS, JB, PB and WS). The nearest isochron was taken at each of the 13 points used for the sediment thickness calculation, or linearly interpolated between the two closest anomalies, and matched to the time scale.

The interpreted seismic stratigraphy (Fig. 7-5b and 7-6b) at these points were drawn on the time-diagram and vertically stretched so that the basement age, as well as the ages of the upper two units obtained from the boreholes (Fig. 7-3), matched the time-scale. The relative time span for the deposition of each unit was estimated by projecting the first and last occurrence of each unit back into the time scale (colour bars, Fig. 7-8).

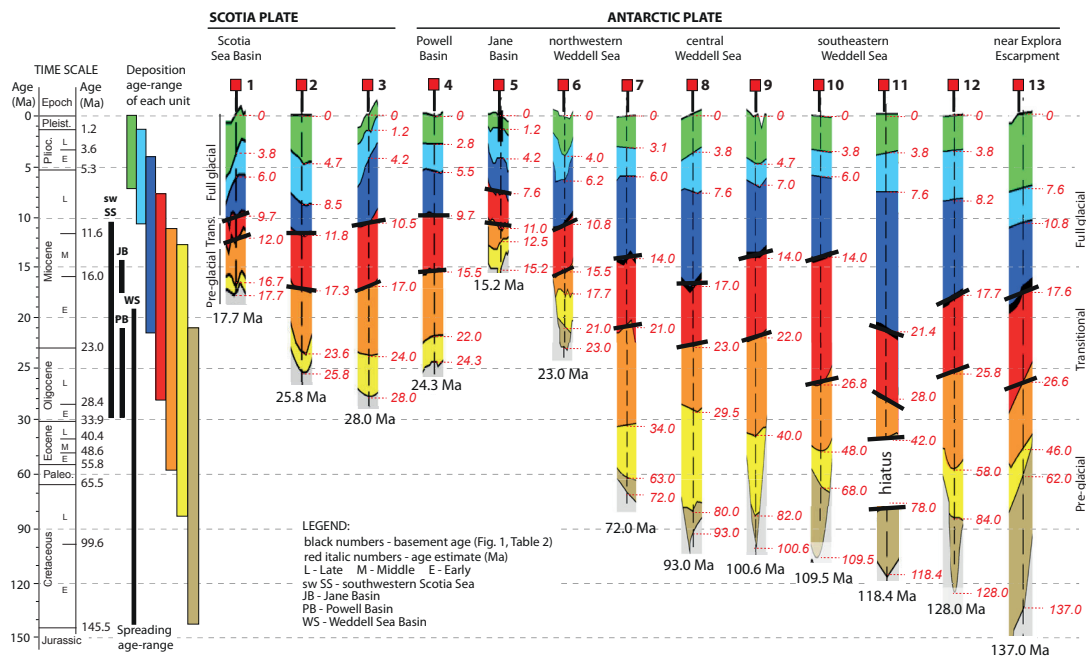


**Fig. 7-8.** Age model and associated sediment deposition along the WS-SS seismic transect. From left to right: Time scale of Epochs and boundary ages modified after Gradstein et al. (2004); Black bars = age-range obtained from the magnetic spreading anomaly isochron compilation (Fig. 7-2) for each basin. Colour bars = age-range of the deposition for each unit identified in the seismic data (Figs. 7-5 and 7-6), deduced from the first and last occurrence of each unit in the 13 scaled sections to the right, stratigraphy annotated. Thick black lines in the sections indicate the lower (uPG-T) and upper (uT-FG) boundaries of the pre-glacial to full glacial transitional unit. The vertical scale of the type sections represents time and not sediment thickness. The tentative age for each horizon is annotated in red and read off from the time scale on the left. Basement Age model and associated sediment deposition along the WS-SS seismic transect. From left to right: Time scale of Epochs and boundary ages modified after Gradstein et al. (2004); Black bars = age-range obtained from the magnetic spreading anomaly isochron compilation (Fig. 7-2) for each basin.

Each colour matches the corresponding seismic stratigraphic unit in the representative sections. The age range for each unit was used in combination with the sediment thickness estimates (Fig. 7-7) to deduce the sedimentation rates (Fig. 7-9).

## 7.5 Observations, results and interpretation

### 7.5.1 Basement ages

The compiled magnetic spreading anomaly isochron map (Fig. 7-2; Table 7-2; Ch. 5) constrained the basement ages as follows: Weddell Sea basin, 142.8–19.2 Ma (M17o–C6m); southwest Scotia Sea basin, 30.9–10.5 Ma (C12m–C5n.2 m); Powell Basin, 29.7–21.1 Ma (C11n.1o–C6AAo) and Jane basin, 17.4–14.4 Ma (C5Dn–C5ADn). The oldest magnetic anomalies occur in the southeast (Explora Escarpment), becoming younger towards the northwest part of the basin, near the Antarctic Peninsula. The lateral spreading age range for the Weddell Sea basement implies that sediments in contact with the basement should be younger than 124 Ma in the southwest or 14 Ma in the northwestern Weddell Sea. The magnetic isochrons crossing the WS–SS transect constrained the basement ages for the 13 selected points used to construct the age model (thin red lines in Fig. 7-2; red drop down lines in Fig. 7-5 and 7-6; listed ages below the 13 points in Fig. 7-8).

### 7.5.2 Borehole correlation

The WS–SS seismic transect seismic data matched the key stratigraphic boundaries in ODP Leg 113 sites 693, 694 and 697 well (Fig. 7-2). The upper part of WS-S3 was constrained to an Eocene age (site 693), WS-S4 Oligocene to Miocene (site 693), WS-S5 late to middle Miocene (all sites), and WS-S6 and WS-S7 constrained to Pliocene and Pleistocene respectively for all sites (Fig. 7-2). Through the seismic tie lines, our interpreted units WS-S2 to WS-S7 correlated well to units identified in the SHALDRIL boreholes as well (Fig. 7-10).

### 7.5.3 Seismic characterization and horizon stratigraphy

Through the borehole stratigraphy (Fig. 7-3) and the reference type-section (Fig. 7-4), we traced continuous horizons across adjacent profiles along the ~3300 km transect to produce a seamless correlation and a new stratigraphy (Fig. 7-5b and 7-6b). Two stratigraphic nomenclature models are proposed: The first is the nomenclature for the Weddell Sea, using the prefix WS and appended with “S” for seismic stratigraphic unit (units WS-S1 to WS-S7) and “u” to indicate the base reflection or horizon also referred to as an unconformity or discontinuity (WS-u1 to WS-u7 in Fig. 7-5b and 7-6b).



The second nomenclature is suggested for circum-Antarctic correlation of the pre-glacial to glacial components (PG, T and FG, numbered from bottom to top in Fig. 7-4). The second system allows the interpretation of additional units that can still be grouped under the appropriate PG, T or FG component for the construction of cross-regional isopach grids, irrespective of the regional stratigraphy. The acoustic basement topography near the Antarctic Peninsula is mostly rugged, ridges occur and some seamounts break through to the seafloor (e.g. profiles SCAN04-17, M31 and M05 in Fig. 7-5a; northwestern most part of profile BAS845-15, Fig. 7-6a). The Weddell Sea basement topography is less rugged with smaller valleys, but lies more or less on the same average level. In the absence of deep boreholes, the interpretation of basement is based on the seismic reflection data. For clarity, faults were not interpreted. Our resulting acoustic basement horizon (WS-u1) compares well with the refraction data and derived crustal model of Rogenhagen and Jokat (2002).

The seismic reflectivity of units WS-S1 till WS-S7 (Fig. 7-5a and 7-6a) match those of each unit described in the type section (Fig. 7-4) very well and show negligible lateral variation between the northwestern and southeastern Weddell Sea, or the smaller Jane and Powell Basins. All units are laterally continuous and well stratified with reflectors that are mostly coherent, horizontal and undisturbed, and easy to trace over long distances. Layering is parallel to the seafloor except in the middle of the Weddell Sea basin where the older, lower amplitude units appear to form a mound. The mound is especially recognisable to the Southeast of borehole 694 in the seismic image (Fig. 7-6a).

The PG sequence WS-S1, WS-S2 and WS-S3, is bounded by the acoustic basement reflection WS-u1 below and reflector WS-u4 above (Fig. 7-6a; Appendix A-1). WS-u4 or uPG-T marks a prominent change in seismic facies from low amplitude, more transparent, laterally discontinuous reflectors in the sequence below, to more continuous, higher amplitude, parallel reflections in the sequence above (Fig. 7-5a and 7-6a; online supplementary data to paper; Appendix A-1).

The T sequence consists of one seismic unit, WS-S4 and is bounded by reflector WS-u4 below and WS-u5 above, alternately referred to as horizons uPG-T and uT-FG (Fig. 7-5 and 7-6). Although thinner seismic units can be distinguished within WS-S4, the seismic facies characteristics are similar and grouped as one unit here. WS-u5 was picked as the top boundary horizon for this sequence because in the seismic data we see the lower reflective T-unit package below this reflection, rapidly transitioning into a sequence of high amplitude, closely spaced, horizontal reflections above (Fig. 7-6a). It is a thick strong high amplitude reflection that could easily be traced across the basin and merge with several unconformities above, especially near the flanks of the basin (Fig. 7-6a and 7-11; Appendix A-1). We interpreted these seismic characteristics to represent the first sedimentary sequences transported down-slope and onto the abyssal plain via the first ice sheet advancements to the outer shelf.

The FG sequence consists of three seismic units, WS-S5, -S6 and -S7 and is bounded by horizon WS-u5, the T to FG period unconformity (uT-FG) below, and the seafloor reflection above (Fig. 7-6). We assume the change in seismic facies and more complex internal structures (e.g. drifts) represent change in depositional processes. Hence we interpret the sharp transition to represent the onset of the full glacial regime processes and transition to a modern polar ice sheet, consistent with observations around the Antarctic Peninsula (e.g. Diviacco et al., 2006; Rebesco et al., 2006; Rebesco and Camerlenghi, 2008).

The initial FG unit (WS-S5 or FG-1), drapes over this pre-glacial and transitional sequences mound and fills the basin low in the southeastern Weddell Sea (observed from point 10 to 13, Fig. 7-6). Thinner units WS-S6 and WS-S7 were deposited on the smoothed bathymetry as two horizontal bands of high amplitude finely laminated reflectors.

#### 7.5.4 Sediment thickness

The lateral variations in sediment thickness are described for each unit in the Weddell Sea basin, from bottom to top and old to young, referring to Figs. 7-5 to 7-7 and an online supplementary data to paper:

WS-S1 is absent in the Scotia Sea, Jane and Powell Basins, but continuous throughout the Weddell Sea basin (WSB). It increases in thickness from 282 m in the northwest (point 6, Fig. 7-7) to 545 m in the southeast at point 13.

WS-S2 ranges from 273 to 640 m in the Scotia Sea (points 1–3), 395 m in the Powell Basin (point 4) and 247 m in the Jane basin (point 5). An interesting trend is seen in the Weddell Sea basin, where WS-S2 is thickest in the centre (474 m at point 9 to 302 m at point 7) and thinner on both flanks (266 m at point 6 and 285–293 m at points 12 and 13, Fig. 7-7). Notably WS-S2 is absent at point 11.

WS-S3 is continuous along the entire transect and becomes thicker from the northwest to the southeast: 224 m thick at point 1 and thickening to 532 m at point 3 in the Scotia Sea, 524 m in the Powel basin, thinnest in the Jane basin (139 m) and ranges from 255 to 778 m (points 6 to 12, Fig. 7-7) in the Weddell Sea basin.

Collectively, WS-S1, WS-S2 and WS-S3 comprise the pre-glacial (PG) sequence, which ranges in total thickness from 441 to 1481 m (Table 7-4). A westward thickening of PG sediments was expected in the Weddell Sea basin, but instead we found a higher mound in the middle (between points 7 and 10 in Fig. 7-6b) flanked by a deeper basin in the southeast (points 10 to 13 in Fig. 7-6b) and a thicker part near the continental slope at the Explora Escarpment.

WS-S4 or the transitional unit (T-1) varies in thickness throughout the Scotia Sea and Weddell Sea (red band in Fig. 7-6 and 7-7). The thinnest part is observed at point 6 (267

m) and the thickest part at point 10 (780 m) in the northwestern Weddell Sea (Table 7-4). WS-S4 seems to have partly filled in the palaeo basin low in the southeast (points 7 to 13) and thins over the mound.

WS-S5 is the most prominent and the first full glacial sequence (dark blue unit in Fig. 7-5b and 7-6b). It is laterally massive, thick and continuous. Similar to WS-S1 to WS-S4, WS-S5 thickens towards the Antarctic Peninsula shelf in the Scotia Sea (185–851 m from points 1 to 3). The thickness of WS-S5 is relatively constant in the northwestern Weddell Sea (280–398 m), but thickens to 974 m in the southeastern Weddell Sea (point 11) and filled the remaining palaeo basin low (points 9 to 13 in Fig. 7-7; online supplementary data to paper). WS-S5 seemed to mostly smooth out the Weddell Sea pre-glacial to transitional mound-and-flanking basin palaeotopography.

WS-S6 is 122–208 m thick across the Weddell Sea and 140–560 m thick in the Scotia Sea, following the same trend as units WS-S2 to WS-S5. The thickest parts occur in the centre of the Weddell Sea where it drapes over the mound (point 9, 209 m) and at either flank near the shelf (186 m at point 13 and 170 m at point 5; Fig. 7-7; online supplementary data to paper). WS-S7 is the thinnest unit in the entire sedimentary sequence and shows little lateral variation in sediment thickness between the Scotia Sea (103–273 m) and Weddell Sea basin (126–215 m). Units WS-S5, WS-S6 and WS-S7 comprise the fully developed glacial (FG) sequence, which ranges in total thickness from 428 to 1684 m in the Scotia Sea and 583–1248 m in the Weddell Sea (Table 7-4; Fig. 7-7).

The total sediment thickness in the Scotia Sea ranges from 1218 to 3762 m, and in the Weddell Sea from 1745 to 3123 m (Table 7-4). We estimate the deep-sea Weddell basin to have a minimum area of  $\sim 1.3 \times 10^6$  km<sup>2</sup> and a maximum area of  $\sim 1.5 \times 10^6$  km<sup>2</sup> (red outline in Fig. 7-1, inset). The shelf areas were not incorporated due to lack of data in front of the Filchner–Ronne Ice shelf. Taking an average sediment thickness of  $\sim 2.5$  km (Table 7-4) a first order minimum estimate of the total sediment volume for Weddell deep-sea basin would be  $3.3 \times 10^6$  km<sup>3</sup> and a conservative maximum volume estimate  $3.9 \times 10^6$  km<sup>3</sup>. Under the assumption that the pre-glacial to fully glacial units occur throughout the Weddell Sea basin, we use the average thickness of each component (PG=923 m, T=478 m, FG=769 m; Table 7-4) and the minimum and maximum basin area to estimate sediment volumes. Minimum volumes are: PG= $1.2 \times 10^6$  km<sup>3</sup>, T= $0.6 \times 10^6$  km<sup>3</sup> and FG= $1.0 \times 10^6$  km<sup>3</sup> and the conservative maximum volumes: PG= $1.4 \times 10^6$  km<sup>3</sup>, T= $0.7 \times 10^6$  km<sup>3</sup> and FG= $1.2 \times 10^6$  km<sup>3</sup>.

### 7.5.5 Age model

In our age model Weddell Sea basement age is estimated at 137 Ma in the southeastern part of the transect and becomes progressively younger ( $\sim 23$  Ma) towards the northwest (Fig. 7-8). WS-S1 has the largest age range of all the units. In the southeast

near the Explora Escarpment it is 137–62 Ma at point 13 and ~23 Ma in the northwest (point 6 in Fig. 7-8). Units WS-S2 and WS-S3 both follow a similar trend as WS-S1 and become younger to the northwest as well (84.0–17.7 Ma and 58.0–15.5 Ma at points 13 to 6, Fig. 7-8). A hiatus of ~36 Ma occurs at point 11 where unit WS-S2 is absent, probably due to erosion. The lower boundary of the transitional unit (horizon WS-u4 or uPG-T) decreases in age from 26.8 Ma in the southeastern Weddell Sea (point 13 in Fig. 7-8) and to 15.5 Ma in the northwestern Weddell Sea (point 6), being slightly younger in the Jane basin (11 Ma). The uPG-T horizon shows lateral age variation in the Scotia Sea of 17.3–12.0 Ma, the oldest part near the Antarctic Peninsula and becoming younger to the northwest (points 1–3, Fig. 7-8).

The upper boundary of the transitional unit (horizon WS-u5 or uT-FG), interpreted to represent the advancing ice sheets grounding on the outer shelf for long periods in a full glacial regime, also youngs from southeast to northwest (17.7–10.8 Ma at points 13 to 6, Fig. 7-8). We observe an older outlier age of ~26.8 Ma at point 11 in the Weddell Sea basin and a younger age of ~7.6 Ma at point 5 in the Jane Basin. Horizon WS-u6 has a tentative age of ~10.6 Ma in the southeastern Weddell Sea basin (point 13) and becomes increasingly younger up to 6.0 Ma in the northwest (point 7, Fig. 7-8). The model age of ~7.6 Ma at point 11 for WS-u6 fits with the regional trend. Horizon WS-u7 shows a modelled lateral age variation of 3.8–1.2 Ma (points 1 to 4, Fig. 7-8).

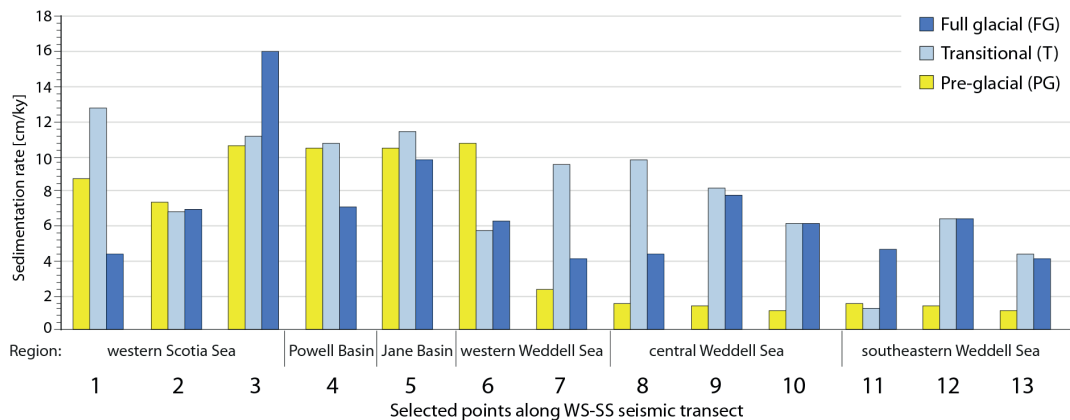


**Fig. 7-9.** Sedimentation rates for the pre-glacial (PG), transitional (T) and full glacial (FG) regimes at the 13 selected points along the WS-SS seismic transect (for location see Fig. 7-7a). Calculations are based on the sediment thickness in Fig. 7-7 and online supplement 4, the interpreted seismic reflection data (Figs. 7-5 and 7-6) and the hypothetical age model in Fig. 7-8. Rates are given in cm/ky and listed in Table 7-4 and online supplement 5.

### 7.5.6 Sedimentation rates

The age model was used in combination with the derived sediment thickness estimates (Fig. 7-7; Table 7-4) to deduce sedimentation rates for the pre-glacial, transitional and full glacial components of the deep-sea sediment archive in the Weddell Sea basin (Table

7-4; Fig. 7-9). Since there are uncertainties in our age model due to the absence of borehole age-control, we only comment the sedimentation rate trends. The pre-glacial sedimentation rates at points 4–6 in the Powell Basin, Jane Basin and northwestern Weddell Sea are the highest (10–11 cm/ky, Table 7-4; yellow bars in Fig. 7-9) and almost an order of magnitude higher than the rates in the central Weddell Sea (1.1–1.6 cm/ky). Although the Weddell Sea pre-glacial units are the thickest (894–1481 m), the sedimentation rates are the lowest.

The transitional sedimentation rates range from 1 to 10 cm/ky in the Weddell Sea and 7–13 cm/ky in the Scotia Sea (Table 7-4; middle bars in Fig. 7-9) and are almost an order of magnitude higher than the pre-glacial rates. An anomalous transitional sedimentation rate of 1.2 cm/ky occurs at point 11, the same place where the hiatus and eroded WS-S2 unit are observed (Fig. 7-8). In the central and northwestern Weddell Sea the transitional sedimentation rates are amongst the highest (8–10 cm/ky). Higher transitional sedimentation rates occur on the flanks of the Weddell Sea basin as expected (points 7–9 and 12; Fig. 7-9; Table 7-4) since it is closer to sediment supply from land.

The full glacial sedimentation rates are the highest at points 3 and 5 in the Scotia Sea and Jane Basin (~16 cm/ky and 10 cm/ky) and at points 9 and 11 in the Weddell Sea (~7–8 cm/ky, Fig. 7-9; Table 7-4).

### 7.6 Discussion

The new basin-wide seismic stratigraphy and assignment of seismic units to PG, T or FG components rest on the basic premise that glacial sediment input and transport is recorded in the seismic strata. Based on our age model, the seven identified horizons increase in age from the southeastern to the northwestern Weddell Sea. This result is different from local scale studies where a uniform age for each horizon is often assumed (Miller et al., 1990; Rogenhagen et al., 2004; Maldonado et al., 2006).

For the pre-glacial units this lateral increase-in-age trend can be ascribed to sediments being deposited synchronous to seafloor spreading and formation of the Weddell Sea basin. However, in the transitional and full glacial units it is presumed to represent the lateral increase in sediment supply and consequential increase in down-slope and along-slope sediment transport processes. Such increases are often related to ice sheet advance and intensification of bottom currents.

We compare our findings to previous work and discuss our observations in the context of implications for understanding the bottom water ocean circulation changes and ice sheet development in the pre-glacial to glacial climate transition.



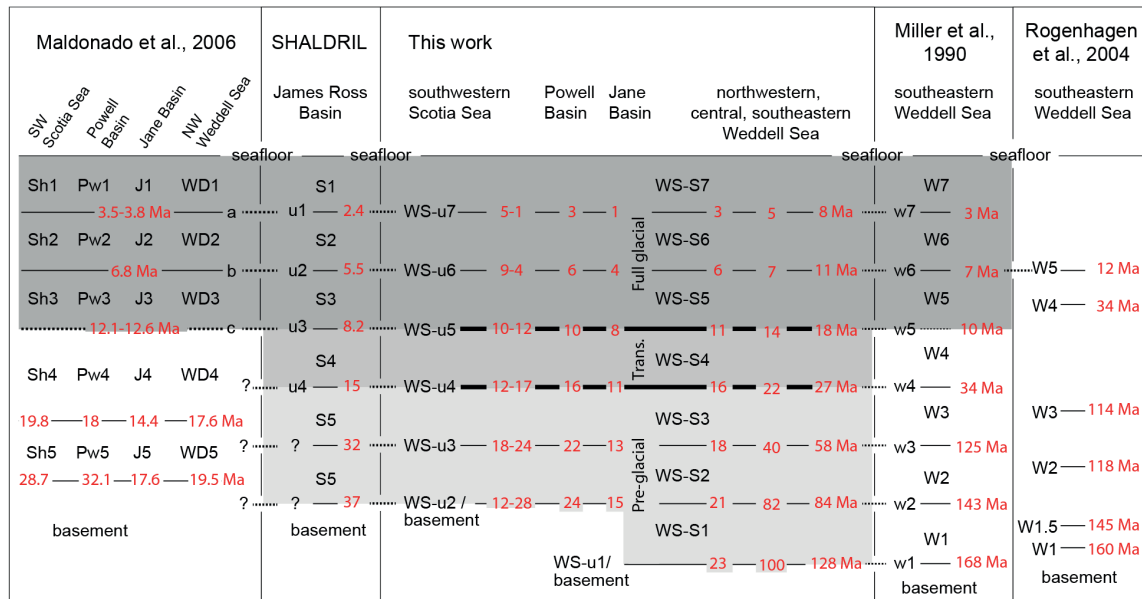


**Fig. 7-10.** Seismic stratigraphy correlation chart linking seismic units and horizons from this paper, to previous studies in the Weddell Sea and Scotia Sea. Thin black lines = mapped horizons in all studies; thick black lines = lower boundary of the proposed transitional and full glacial units, this paper; Dashed lines = correlated seismic horizons according to matching reflectors; red numbers = ages of the horizons, showing the lateral variation in age across the basins. Light grey = pre-glacial units; Medium grey = transitional units; Dark grey = full glacial units. SHALDRIL refers to Anderson (2006), Smith and Anderson (2010; 2011), Anderson and Wellner (2011), and Bohaty et al. (2011).

### 7.6.1 Pre-glacial (PG) regime

Previous seismic stratigraphy work in the Scotia Sea, the Powell and Jane Basins, and in the northwestern Weddell Sea identified two pre-glacial seismic units assigned to Oligocene–early Miocene age (e.g. Sh5, Sh4; Pw5, Pw4; J5, J4; WD5, WD4 in Fig. 7-10). We identified additional prominent horizontal reflections in the central Weddell Sea (profile BAS645-15, Fig. 7-6) and upon tracing them as well as boundary horizon WS-u4 into the northwestern Weddell Sea, Powell and Jane Basins and southern Scotia Sea, found that they mismatched this previous work (Fig. 7-10). We consequently re-divided the PG seismic sequence into three units instead of the previous two, labelled bottom up as WS-S1, WS-S2 and WS-S3 (Figs. 7-6 and 7-10). The boundary horizons of these units (WS-u1, WS-u2, WS-u3) were traced farther into the southeastern Weddell Sea and matched all horizons in the seismic stratigraphy of Miller et al., 1990 (Fig. 7-10), but disagree with seismic stratigraphy model of Rogenhagen et al. (2004).

Contrary to Rogenhagen et al. (2004), we re-interpret the basement reflector WS-u1 up to ~0.5 s deeper, below the series of strong horizontal reflectors directly above basement (Figs. 7-10 and 7-11). This was done because in our opinion these could either be older consolidated sediments or lava flows, especially considering that the thickest part lies near the Explora Escarpment.

Horizons WS-u2 and WS-u3 matched the seismic stratigraphy of SHALDRIL and Maldonado et al. (2006) in the northwestern Weddell Sea (Fig. 7-10). These two

horizons were farther traced across the central Weddell Sea and into the southeastern part of the basin, where it mismatched horizons W2 and W3 in Rogenhagen et al. (2004) and we interpreted at different positions based the cross-basin correlation in continuous data and on observed unconformities (Figs. 7-10 and 7-11).

The PG horizons all show a lateral variation in age in the southern Scotia Sea, Jane and Powell Basins, northwestern and southeastern Weddell Sea (Fig. 7-10) and our age range compares well to previous tentative age estimates (Figs. 7-8 and 7-10; Maldonado et al., 2006; Miller et al., 1990). The PG ages in the northwestern Weddell Sea (Figs. 7-8 and 7-10) are consistent with late Oligocene pre-glacial strata (28.4–23.3 Ma) drilled in SHALDRIL Hole 3C (Bohaty et al., 2011; Fig. 7-3).

The southeastern Weddell Sea basement is the oldest (up to ~145 Ma, M17; Fig. 7-1; Table 7-2) and nearest to the shelf at Dronning Maud Land. We would therefore expect to find the thickest sediments and highest sedimentation rates on the slope near this continental margin. Instead, we found a ~1130 m thick mound in the centre of the Weddell Sea basin on much younger basement (93–45 Ma, Figs. 7-1 and 7-6; Tables 7-2 and 7-4). The depositional geometry on both the northwestern and southeastern flanks of the mound have a basin shape (Figs. 7-6 and 7-12a). If the basin-like depressions were due to differential compaction, the reflectors would be offset or curved in the seismic image, but this is not observed. It also leaves the thinner units (~790 m) to the east of the mound and the partial absence of unit WS-S2 at point 11 unaccounted for.

We consider alternative processes that may cause high sediment transport to the deep-sea. A typical mechanism is ice rafting and ice sheets pushing sediments onto the slope and rise as they ground on the outer shelf. However, given the warm climate and ice minimum conditions (Zachos et al., 2001) inferred for the Cretaceous–Eocene pre-glacial seismic sequence, mass sediment transport due to expanding ice sheets becomes an unlikely process and we have to consider other explanations. High bio-productivity and mortality could cause high pelagic fall-out and could account for high sediment supply in the deep-sea, but fail to explain the mound and basin-like depressions. Tectonic uplift and an underlying basement high or low are also excluded because, although the Weddell Sea basement is highly variable and uneven (Fig. 7-6) when averaged, it remains on a similar level.

Thinner units (790 m) to the east of the mound (Fig. 7-6 and 7-12a), the partial absence of unit WS-S2 and the anomalously low transitional sedimentation rate of 1.2 cm/ky at point 11 (Fig. 7-6 and 7-8), collectively allow the interpretation that bottom current erosion may have caused this mound-basin depositional geometry.

Such bottom currents could have been caused by down-slope sediment influx from the Crary Fan (Kuvaas and Kristoffersen, 1991; Bart et al., 1999; Michels et al., 2001, 2002) or a Cretaceous–Eocene proto-Weddell Gyre that build the mound in the centre whilst eroding the flanks asymmetrically.

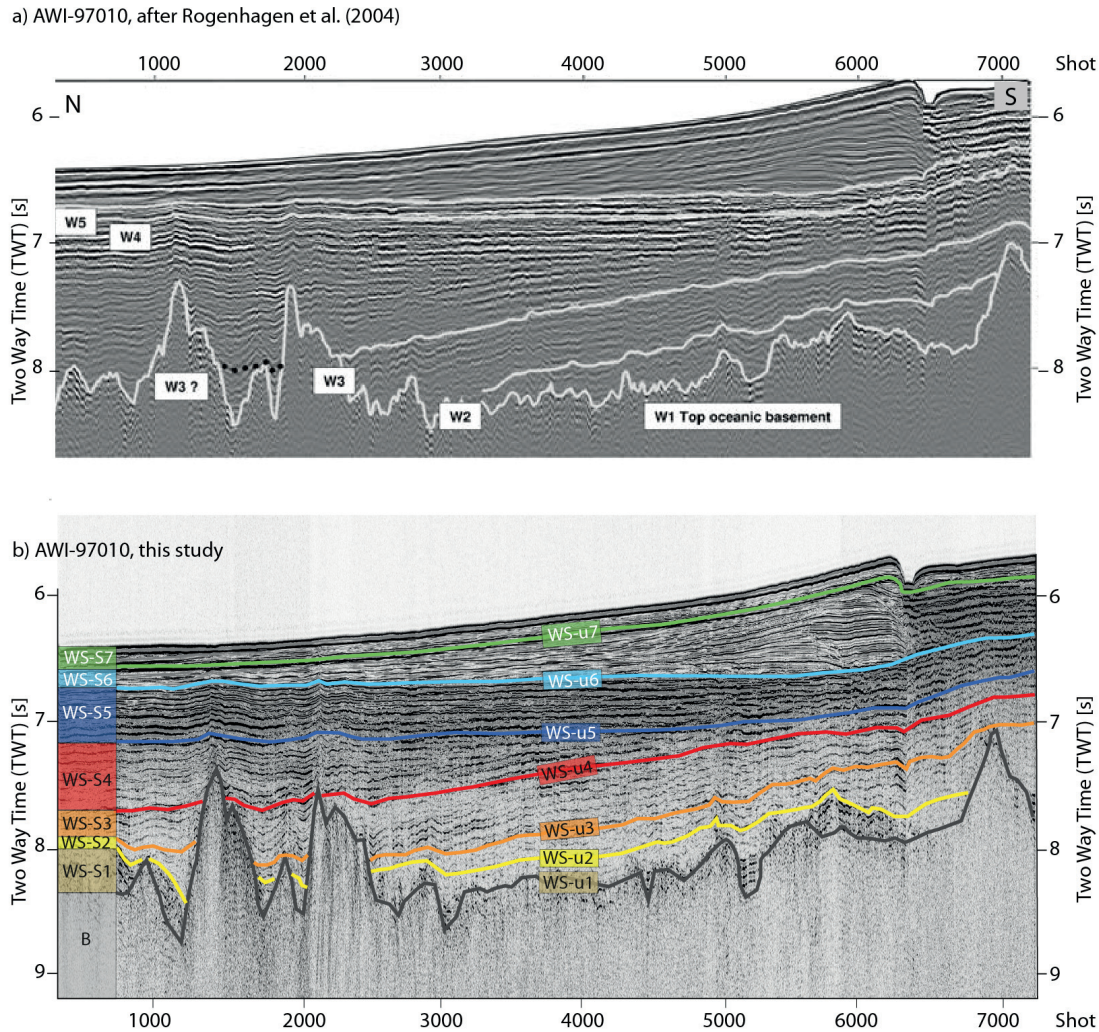


**Fig. 7-11.** Interpretation of multichannel seismic line AWI-97006 in time domain comparing the horizon stratigraphy of Rogenhagen et al. (2004) in (A) with the new Weddell Sea seismic units identified in the WS-SS transect (B). See Fig. 7-2 for location. Note the difference between W4 and our WS-u5 - both horizons were interpreted to represent the full glacial onset. W4 was replaced with WS-u5 because of a large-scale unconformity mapped between shots 4000–6000. Similarly WS-u4 were newly interpreted based on the unconformity between shots 2000–4000 and ~7.5 s TWT. The lower units were also subdivided and the basement interpreted below prominent reflectors just above, e.g. at shots 5000 – 6000 and ~8 s TWT.

We consider it unlikely that the Crary Fan downslope current could solely account for the mound-basin geometry for the following reasons: Michels et al. (2001, 2002) observed combined contourite–turbidite sedimentation patterns at the western and southeastern Weddell Sea margin (south of 70°S) for the transitional (W4) and full glacial sequences (their regional unconformity W5). Pre-glacial sediments were not considered in their study. Of the three identified main Crary Fan down-slope channels, each about 2–5 km wide, two could perhaps be interpreted in the WS–SS transect between points 8 and 9 (black arrows Fig. 7-6).

However, these are at least two orders of magnitude smaller than the basin-wide features observed in the transect, unpronounced and constrained to uppermost the Pliocene–present day layers. Additionally the WS–SS transect lies more than 500 km (or

5° north of the slope and Crary Fan extent (Kuvaas and Kristoffersen, 1991; Bart et al., 1999; Michels et al., 2001, 2002). We thus favour the proposed proto-Weddell Gyre hypothesis as the most likely dominant process responsible for the depositional geometry.

The fact that the depression is deeper and the units thinner on the southeastern flank than on the northwestern flank, may be consistent with the up-current side and hence with a clockwise circulation (Fig. 7-12a). To our knowledge a proto-Weddell Gyre has not been proposed before, but Eocene–Oligocene proto-Antarctic Bottom Water and Weddell Sea Deep Water masses has been inferred for pre-glacial regimes at Maud Rise, from  $\delta^{18}\text{O}$ , and mineral and grain analyses in ODP leg 113 site 690 (Diester-Haass. et al., 1996).

Contourites were used to determine bottom current direction around the Antarctic Peninsula for transitional and full glacial deposits (e.g. Maldonado et al., 2005; Uenzelmann-Neben, 2006). Although typical contourite drift structures are not clearly observed in the WS–SS transect seismic data; the seismic profiles are too sparse to exclude their existence in the pre-glacial central Weddell deep-sea units. Further analyses of the two parallel transects (A and C in Fig. 7-1) are ongoing and might shed more light on the proto-gyre circulation direction. The driving force of the proto-gyre circulation remains unclear as well. The ACC is not fully developed because South America was still connected to Antarctica with shallow water gateways (Fig. 7-12a; Livermore et al., 2007), but Weddell Bottom Water could have formed due to sea ice. Either way, the mound feature is prominent enough that it warrants future investigation.

### 7.6.2 Transitional (T) regime

The base reflector of the transitional unit, WS-u5, was traced from the northwestern Weddell Sea into the Jane Basin, Powell Basin and the Scotia Sea, where it exactly matched with horizon “c” of Maldonado et al. (2006; Fig. 7-10). Based on seismic facies changes and downlap terminations, they postulated that horizon “c” represents an erosional surface signalling the incursion of bottom water exchange between the Scotia and Weddell Sea and coeval to the Mi4 glaciation. WS-u5 and WS-u4 partially correlates to S3 (~8 Ma) in the SHALDRIL boreholes identified as the start of the PG to FG transitional sequence at the Antarctic Peninsula (Fig. 7-3; Smith and Anderson, 2010, 2011; Bohaty et al., 2011).

Our model age of ~17.6 Ma (point 13 in Fig. 7-8) is also consistent with the ODP leg 113 site 693 borehole age of early mid-Miocene– Late Miocene of 16–11 Ma (Figs. 7-3 and 7-10). Tracing WS-u5 into the southeastern Weddell Sea it matched horizon w5 of Miller et al. (1990) but mismatched the W4 marker horizon (Rogenhagen et al., 2004) that represents the onset of the FG regime in the deep-sea (Figs. 7-10 and 7-11). We re-interpret W4 of Rogenhagen et al. (2004) in the southeastern Weddell Sea and place it ~0.75 s deeper (WS-u5, dark blue line in Fig. 7-11).



Which depositional processes active in the Eocene–Oligocene transitional climate associated with high sediment transport may have formed this WS-S4 unit? Previous seismic stratigraphy studies postulated that ephemeral ice caps and small ice sheets formed on high elevations in the West Antarctica, with the EAIS periodically grounding on parts the outer shelf and increasing sediment supply to the deep-sea (e.g. Miller et al., 1990; Oszko, 1997; red polygons and arrows in Fig. 7-12b). Isolated gravel and terrigenous sand grains in ODP Leg 113 site 689 and 690 at Maud Rise, offshore north of Dronning Maud Land, provided evidence for a grounded Eocene EAIS since ~45.5 Ma, probably with a more temperate rather than polar character (e.g. Ehrmann and Mackensen, 1992).

If it is the case that only the EAIS grounded during the Eocene–Oligocene, the highest sediment supply would presumably be in front of the Crary Fan and on the slope and rise of the southeastern Weddell Sea near the Explora Escarpment (Fig. 7-1), with little or no ice sheet related sediment supply at the Antarctic Peninsula. The effect would be transitional deposits that are thicker in the southeast than in the northwestern part of the Weddell Sea basin and the Antarctic Peninsula. On the contrary, we observe that unit WS-S4 is thickest in the northwestern Weddell Sea (~806 m), 400–600 m thick in the central and southeastern Weddell Sea and thinnest over the peak of the mound (~383 m; Fig. 7-7; Table 7-4; online supplementary data to paper). WS-S4 drapes over the mound and partly fills in the basin depressions to either side, whilst being continuous along the entire WS–SS transect and probably basin-wide (Fig. 7-6; Appendix A-1).

It is likely that bottom current processes could have redistributed sediments from the southeastern EAIS source region to the central and northwestern Weddell Sea, thus maintaining the eroded basin geometry to the east of the mound. The transitional unit displays no along-slope drift or contourite structures but was interpreted as a sheeted drift. Bottom current processes alone cannot account for the WS-S4 geometry. The continuous occurrence and thicker WS-S4 deposits in the northwestern Weddell Sea can also be explained by along-slope sediment supply from the proto-Weddell Gyre circulation, down-slope supply by an advancing ephemeral EAIS, and from advancing ice sheets in the North–West i.e. WAIS and the southern APIS.

SHALDRIL boreholes and seismic records on the southern margin of the Joinville Plateau show glacial marine sedimentary processes dominated sedimentation since the late Oligocene and a phased APIS expansion from south to north across the Peninsula in the late Miocene (e.g. Smith and Anderson, 2010, 2011; Bohaty et al., 2011) or Oligocene (Davies et al., 2012). High transitional sedimentation rates around the Antarctic Peninsula (11 cm/ky) and northwestern Weddell Sea (6–10 cm/ky; Fig. 7-9; Table 7-4) and the age variation of the initial ice grounding boundary horizon, uPG-T (27–16 Ma; WS-u4 in Fig. 7-10) across the Weddell Sea, allow the interpretation that the southern part of the APIS probably already grounded in the early Miocene or even Oligocene, and the WAIS in the Oligocene.



## 7. Weddell Sea basin

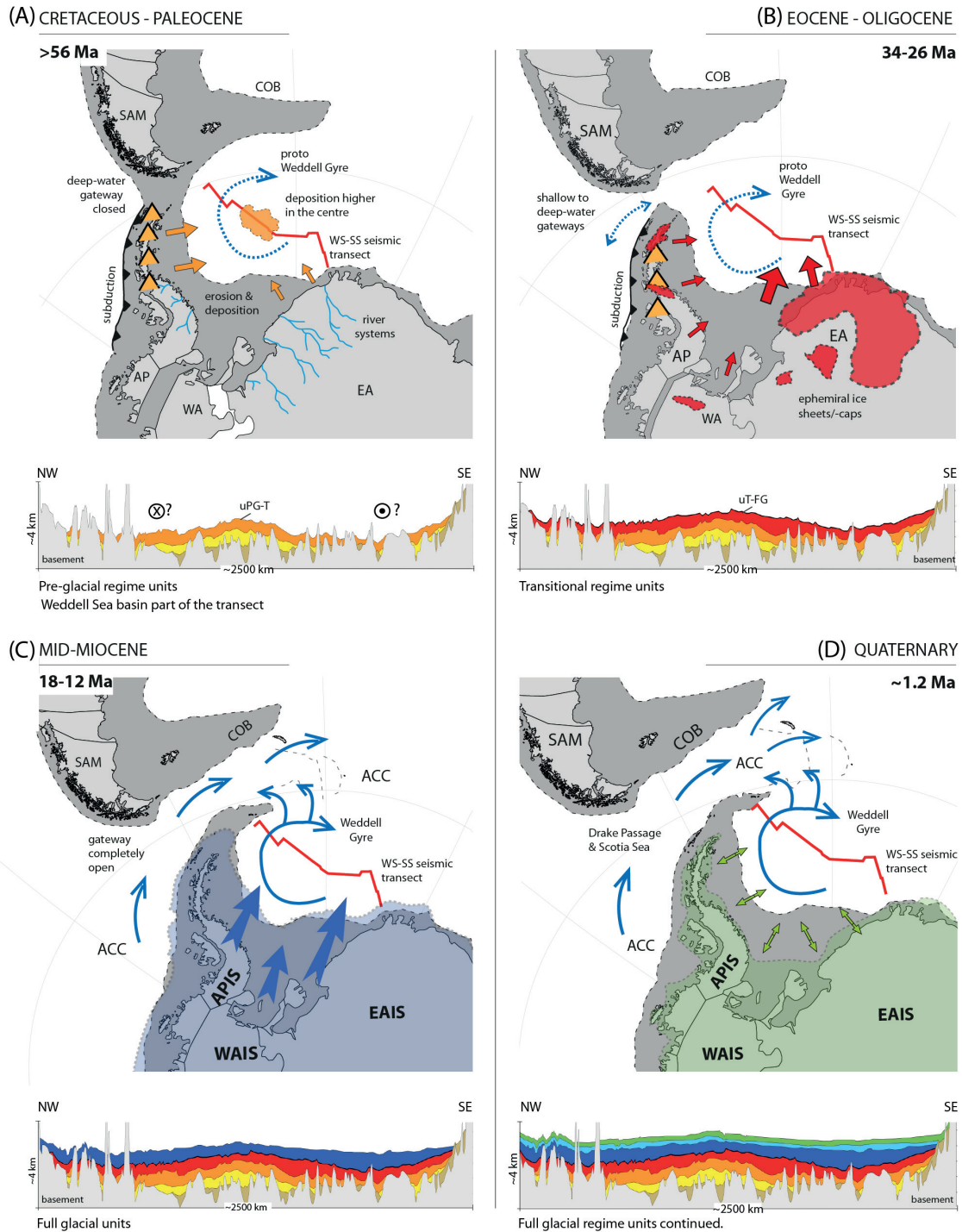


**Fig. 7-12.** Model showing the role of plate-tectonic motion, pre-glacial sedimentation, ice sheet development and ocean circulation in the greater Weddell Sea region, since the Cretaceous. Rivers, mountains, ice caps, ice sheet boundaries and the WS-SS transect are schematic interpretations. Diagrams below represent Weddell Sea Basin part of the transect. Plate reconstruction adapted from GPlates (Boyden et al., 2011) and associated sediment deposition for each regime, is illustrated in the diagram below. **(A)** Pre-glacial regime. COB = continent ocean boundary, SAM = South American plate, AP = Antarctic Peninsula, WA = West Antarctica, EA = East Antarctica. Orange triangles = mountain building in the Antarctic Peninsula, subsequent erosion and deep-sea deposition (orange arrows). Blue dashed line = the proto Weddell Sea Gyre, red line = Weddell Sea part of the WS-SS seismic transect, orange cloud = higher sediment deposition of PG-units near the centre. **(B)** Transitional regime. Red polygons = ice caps and smaller ice sheet development on the highlands of EA, the northern tip of the AP and WA. Red arrows indicate high sediment supply. **(C)** Full glacial regime. Transparent blue polygon = EAIS, WAIS and APIS, fully developed and grounded on the continental shelf; Thick blue arrows = high volume of sediment transport; Weddell Gyre and ACC = fully developed Antarctic Circum-polar Current (simplified after Livermore et al. (2007)). **(D)** Full glacial regime cont. Green arrows = smaller ice sheet advance and retreat cycles while ice sheets (transparent green polygon) still remain grounded on the outer shelf.

Sampling, drilling and multichannel seismic reflection data analyses of Drift 7 on the Pacific margin of the Peninsula, suggest down-slope transport as a result of the growth of the Antarctic Peninsula ice sheet in the Early Miocene (~15 Ma and 9.5 Ma; Uenzelmann-Neben, 2006). This early Miocene/ Oligocene APIS and Oligocene WAIS expansion is not adequately reproduced by palaeoclimate models that suggested a late Miocene – early Pliocene APIS grounding (7.94–5.12 Ma, Bart et al., 2005; Pollard and 2011).

### 7.6.3 Full glacial (FG) regime

In the Scotia Sea, Jane Basin, Powell Basin and northwestern Weddell Sea, seismic horizons WS-u5, -u6 and -u7 identified in this study match the horizons “c”, “b” and “a” of Maldonado et al. (2006; Fig. 7-10). Our interpreted horizons show a lateral age variation contrasting the uniform ages assigned in Maldonado et al. (2006; Fig. 7-10). Seismic units WS-S5, WS-S6 and WS-S7, listed from old to young, consistently matched the upper three units in the southern Scotia Sea (Sh3–Sh1), Powell Basin (Pw3–Pw1), Jane Basin (J3–J1) and northwestern Weddell Sea (WD3–WD1) mapped in previous studies (Fig. 7-10). Horizon WS-u6's age of ~5.5 Ma in the Powell Basin (Figs. 7-8 and 7-10) is in broad agreement with the base-age of S2 (~5.5 Ma) dated in the nearby SHALDRIL cores, even though the latter lies on the shelf (Fig. 7-10; Smith and Anderson, 2010; Bohaty et al., 2011). WS-u7 is correlated to reflector “a” in Maldonado et al. (2006) dated in their study at 3.5–3.8 Ma from ODP Leg 113 site 695–697 (see Fig. 7-2 for borehole locations). Our age range 3.8–1.2 Ma is also in good agreement to the base-age of S1 (2.4 Ma) in the SHALDRIL cores (Fig. 7-10; Smith and Anderson, 2010; Bohaty et al., 2011).

In the southeastern Weddell Sea, horizons WS-u6 and WS-u7 matched horizons w6 and w7 of Miller et al. (1990), dated at late Miocene (~7 Ma) and late Pliocene (~3 Ma) in ODP Leg 113 sites 692 and 693 (Figs. 7-2c and 7-10). Horizon WS-u6 is correlated with horizon W5 of Rogenhagen et al. (2004) and our tentative model age of 10.8–8.2 Ma for the southeastern Weddell Sea broadly agrees with their older extrapolated age of ~12 Ma (Figs. 7-10 and 7-11). Horizon WS-u7 was absent in the Rogenhagen et al. (2004) model and is newly interpreted on the AWI-97 profiles (Figs. 7-6 and 7-11; Table 7-3) to match horizons traced from ODP Leg 113 site 694 (Fig. 7-3).

Taking into account the geometry, lateral variation in sediment thickness and sedimentation rates of the transitional unit along the WS–SS transect, we infer from our observations which depositional processes in the Miocene – Quaternary may have played a role in the deposition of these units. WS-S5 filled the basin lows on either side of the inferred mound and levelled the basin bathymetry (dark blue unit, Figs. 7-6 and 7-12c). If the mound formed in response to an assumed proto-Weddell Gyre that intensified in the Miocene glacial regime, it poses the question of why the full-glacial units do not reflect mound geometry as well.

Reason for this change in geometry could be that the Weddell Gyre erosion capacity changed due to the development of the ACC (Table 7-1; Fig. 7-12c) or that the glacial/ice sheet till particles became too large to be transported by bottom currents over long distances. Sediments created by glacial process would have larger grain sizes, thus be heavier and require more energy to transport than pelagic fall-out. We consider it most likely that sedimentation rates were much higher than the erosion rate due to increased sediment supply and deposition to the deep-sea. Even after full glacial conditions were developed on the continent, there were still significant volumes of fine sediments being produced and deposited around the continent. It is generally observed that sedimentation rates increased during the early phases of glaciation, which is expected.

ODP site 697 in Jane Basin reported a sedimentation rate of 4.4 cm/ky for the upper 200 m, increasing down core to 10 cm/ky for the interval of 250–300 m (Barker et al., 1988; Gersonde et al., 1990; Ramsay and Baldauf, 1990). Our estimated rate of 9.9 cm/ky for the full glacial unit (~749 m thick) in the Jane Basin compares extremely well to the ODP rates and to 10 cm/ky reported in Maldonado et al. (2006).

Sediment transport by expanding ice sheets is the most probable process capable of rapidly eroding sediments on land and the continental shelf, transporting it to the outer shelf and as the ice sheets grounded, pushed massive volumes of sediments over the edge in a bulldoze effect. Such increased supply to the deep-sea would balanced the gyre or bottom current erosion and result in a smoothed out basin geometry. An alternative interpretation, although speculative, is that the proto-Weddell Gyre was constrained during its initial development to the margins of the basin and flowed mostly as a density nepheloid layer. The particles that escaped from this nepheloid layer were deposited in the central basin plain.

ODP Leg 113 site 694 lies in the central Weddell Sea and on profile BAS845-15 of the WS–SS transect (Fig. 7-2). The matched seismic stratigraphy of this borehole and our transect (Fig. 7-3), constrained unit WS-S5 and reflectors WS-u5, WS-u6 to middle–late Miocene age in our age model (Fig. 7-8). The borehole log also reported glacial turbidite units and present evidence of deep-sea glacial sediment transport during this time, implying that grounded ice sheets were already present in the Miocene that drained into the Weddell Sea basin (Fig. 7-12c). Miocene continental scale ice sheets in Antarctica were also documented in other borehole and seismic reflection data (e.g. Barker et al., 1988; Miller et al., 1990; Zachos et al., 2001; Maldonado et al., 2005, 2006; Leitchenkov et al., 2008; Anderson et al., 2011; Escutia et al., 2011).

Units WS-S6 and WS-S7 were deposited in the Pliocene – Pleistocene (Fig. 7-3) and have an estimated average thickness of 158 m and 165 m, respectively across the Weddell Sea basin (Fig. 7-7; online supplementary data to paper). Even though these units are ascribed to the same glacial driven depositional processes as the on average 542 m thick WS-S5 unit below, they appear much thinner (Fig. 7-6b).

One possibility could be that the initial full glacial ice sheet advancements and retreats already eroded most of the terrigenous and shelf sediments, which were created by the river systems and other erosional processes in the pre-glacial and transitional regimes. Hence resulting in lower sediment supply due to established ice sheets and bedrock erosion and smaller interglacial cycles (Fig. 7-12d).

## 7.7 Conclusions

The interpretation of the deep-sea sedimentary record along the ~3300 km WS–SS seismic transect contribute to our understanding of the Cretaceous to Quaternary evolution of the Antarctic ice sheets in the Weddell Sea basin. The main contributions are summarized in the following conclusions:

1. We developed a new seismic horizon stratigraphy for the Weddell Sea and southern Scotia Sea using boundary conditions from various datasets. Lower units (WS-S1, WS-S2, WS-S3 and WS-S4) were newly interpreted or re-interpreted. The upper 3 units (WS-S5, WS-S6 and WS-S7) are consistent with local scale studies.
2. The pre-glacial (WS-u1 to WS-u4), transitional (WS-u4 to WS-u5) and full glacial (WS-u5 to seafloor) boundary horizons were identified in the Weddell Sea basin and traced into the Jane and Powell Basins and southern Scotia Sea. The proposed seismic unit divisions are consistent with localized seismic stratigraphy studies around Antarctica in the Bellingshausen Sea (e.g. Scheuer et al., 2006), Wilkes Land (e.g. Escutia et al., 2011) East Antarctica (Leitchenkov et al., 2007), Scotia Sea and Antarctic Peninsula basins (Maldonado et al., 2006) and Weddell Sea (Miller et al., 1990), but disagrees with the stratigraphy of Rogenhagen et al. (2004).
3. Average values for the complete pre-glacial sequence in the Weddell Sea (excluding Jane and Powell Basins): sediment thickness = 1100 m, sedimentation rate = 2.7 cm/ky, volume =  $1.3 \times 10^6$  km<sup>3</sup>; the transitional sequence: sediment thickness = 530 m, sedimentation rate = 6.4 cm/ky, volume =  $0.7 \times 10^6$  km<sup>3</sup> and; the complete full glacial sequence: sediment thickness = 880 m, sedimentation rate = 5.5 cm/ky, volume =  $1.1 \times 10^6$  km<sup>3</sup>.
4. In the pre-glacial sequence (WS-S1, WS-S2 and WS-S3), a deposition mound-and-eroded-flank basin geometry lateral variation in sediment thickness, and sedimentation rates calculated from published interval velocity data support a Cretaceous proto-Weddell Gyre hypothesis. A deeper depression on the east of the mound, ascribed to higher erosion hints at a probable clockwise circulation, but in the absence of clear drift structures an anti-clockwise circulation cannot be excluded.

5. The transitional unit (WS-S4 or T-1) is interpreted to represent high sediment supply through accelerated down-slope mass sediment transport deposits such as turbidites, considered indicative of advancing ice sheets grounding on the outer shelf. The cross-basin occurrence and lateral age variation of this unit ( $\sim 27$  Ma in the southeastern Weddell Sea to  $\sim 11$  Ma in the northwest) imply initial Oligocene grounding of the WAIS and initial early Miocene grounding of the APIS.
6. In the full glacial sequence, the up to 975 m thick WS-S5 unit is continuous and fills the depressions on either side of the mound-and-eroded-flank topography of the pre-glacial and transitional regimes. WS-S5 represents increased deep-sea sediment deposition due to amplified downslope sediment supply in response to advancing ice sheets permanently grounding on the outer shelf. The lateral continuity and age of this unit (18–6 Ma from southeast to northwest) implies concurrent advancement and grounding of the EAIS, WAIS and APIS during the late to early Miocene.
7. The even distribution of the full glacial sequence along the transect suggests that early ice sheet/ice caps/glaciers must have transported sediments not only from the Ronne–Filchner outflow system but also from the Antarctic Peninsula. This is consistent with Smith and Anderson (2010) and implies expansion of the southern APIS to the outer shelf, earlier than the Pleistocene predicted in palaeoclimate models (e.g. Pollard and DeConto, 2009).
8. The younger glacial units WS-S6 and WS-S7 reflect decreased sediment supply to the basin, which is consistent with a reduction in sediment supply following the establishment of a polar glacial regime.

Our Weddell Sea basin seismic stratigraphy rests on the assumption that changes in the observed seismic pattern represent pre-glacial, transitional and full glacial sequences. The presented age model has been derived from all available age information, geophysical and stratigraphic data. The greatest uncertainties lie in the velocity model and estimated horizon ages. Even so, we consider these results a best estimate for deriving a working hypothesis although the lateral horizon ages within the sedimentary column are only constrained by secondary information. The identification of pre-glacial to glacial components in the deep-sea sediment archive enabled an initial quantification of sediment volumes and thicknesses and rates, which are useful to constrain future palaeobathymetry and palaeotopography reconstructions.

Supplementary data to this article can be found online at: <http://dx.doi.org/10.1016/j.margeo.2012.11.004> and [doi:10.1594/PANGAEA.777453](https://doi.org/10.1594/PANGAEA.777453).



## 7.8 Acknowledgements

The YMM and AM thank the “Ministerio de Ciencia e Innovación” of Spain for support through the FPI programme and CGL2004-05646/ANT, CTM2008-06386-C02/ANT and CTM2011-30241-CO2-01 projects. The study benefited greatly from a three-month research visit of YMM to the Alfred Wegener Institute. We thank M. Rebesco and J. Anderson for their thorough evaluation and reviews of this paper. Colleagues J. Grützner, C. Läderach, M. Mieth and G. Uenzelmann-Neben are sincerely thanked for fruitful discussions that improved the manuscript significantly. This project has been funded through the Priority Program 1158 ‘Antarctic Research’ of the Deutsche Forschungsgemeinschaft under project number GO 724/10-1 (AL and KG) and contributes to the Circum-Antarctic Stratigraphy and Palaeobathymetry project (CASP), a Scientific Committee on Antarctic Research – Antarctic Climate Evolution (SCAR-ACE) working group. In memory to Peter Barker who passed away this year (25.06.2012), for his contributions as Principal Investigator on RRS Discovery Cruise 154 which collected line BAS845-15 line, the critical link in the WS-SS transect, and as Co-Chief Scientist on ODP Leg 113, which provided most of the available age control.

## 7.9 References

- Amante, C., Eakins, B.W., 2009. ETOPO1 1 Arc-Minute Global Relief Model: Procedures, Data Sources and Analysis. NOAA Technical Memorandum NESDIS NGDC-24, 19 pp.
- Anderson, J.B., 1999. Antarctic Marine Geology. Cambridge University Press, Cambridge, 289 pp.
- Anderson, J.B. (Ed.), 2006. SHALDRIL II Cruise Report. <http://shaldril.rice.edu/>, 369 pp.
- Anderson, J.B., Wellner, J.S. (Eds.), 2011. Tectonic, Climatic, and Cryospheric Evolution of the Antarctic Peninsula. Geopress, American Geophysical Union, Washington DC, USA. <http://dx.doi.org/10.1029/SP063>, 218 pp.
- Anderson, J.B., Warny, S., Askin, R., Wellner, J., Bohaty, S., Smith, T., 2011. Cenozoic cryosphere expansion and the demise of Antarctica's last refugium. *Proceedings of the National Academy of Science* 108, 11299–11726.
- Barker, P.F., 2001. Scotia Sea regional tectonic evolution: implications for mantle flow and palaeocirculation. *Earth-Science Reviews* 55, 1–39.
- Barker, P.F., Thomas, E., 2004. Origin, signature and palaeoclimate influence of the Antarctic Circumpolar Current. *Earth-Science Reviews* 55, 1–39. <http://dx.doi.org/10.1016/j.earscirev.2003.10.003>.
- Barker, P.F., Kennett, J.P., et al., 1988. *Proceedings of the Ocean Drilling Program, Scientific Results Leg 113*. Ocean Drilling Program, College Station, Texas, USA. <http://dx.doi.org/10.2973/odp.proc.ir.113.1988,774> pp.
- Barker, P.F., Dalziel, I.W.D., Storey, B.C., 1991. Tectonic development of the Scotia Arc region. In: Tingey, R.J. (Ed.), *Geology of Antarctica*. Oxford University Press, Oxford, 215–248.
- Bart, P.J., De Batist, M., Jokat, W., 1999. Interglacial collapse of Crary trough-mouth Fan, Weddell Sea, Antarctica: implications for Antarctic glacial history. *Journal of Sedimentary Research* 69 (6), 1276–1289. <http://dx.doi.org/10.1306/D4268B5D-2B26-11D7-8648000102C1865D>.
- Bart, P.J., Egan, D., Warny, S.A., 2005. Direct constraints on Antarctic Peninsula Ice Sheet grounding events between 5.12 and 7.94 Ma. *Journal of Geophysical Research* 110, F04008. <http://dx.doi.org/10.1029/2004JF000254>.
- BAS, 1985. Tectonic map of Scotia Arc, sheet 3, scale 1:3,000,000. British Antarctic Survey, Cambridge.
- Bentley, M.J., Fogwill, C.J., Le Brocq, A.M., Hubbard, A.L., Sugden, D.E., Dunai, T.J., Freeman, S.P.H.T., 2010. Deglacial history of the West Antarctic Ice Sheet in the Weddell Sea embayment: constraints on past ice volume change. *Geology* 38 (5), 411–414.
- Berner, R.A., Kothavala, Z., 2001. GEOCARB III: A revised model of atmospheric CO<sub>2</sub> over Phanerozoic time. *American Journal of Science* 304, 397–437.

- Bohaty, S.M., Kulhanek, D.K., Wise Jr., S.W., Jemison, K., Warny, S., Sjunneskog, C., 2011. Age Assessment of Eocene-Pliocene Drill Cores Recovered During the SHALDRIL II Expedition, Antarctic Peninsula. In: Anderson, J.B., Wellner, J.S. (Eds.), *Tectonic, Climatic, and Cryospheric Evolution of the Antarctic Peninsula*. Special Publication, 63. American Geophysical Union, 63–113. <http://dx.doi.org/10.1029/2010SP001049>.
- Bohoyo, F., 2004. Fragmentación continental y desarrollo de cuencas oceánicas en el sector meridional del Arco de Scotia, Antártida. Ph. D Thesis, University of Granada, Granada, 252 pp.
- Bohoyo, F., Galindo-Zaldívar, J., Maldonado, A., Schreider, A.A., Suriñach, E., 2002. Basin development subsequent to ridge-trench collision: the Jane Basin, Antarctica. *Marine Geophysical Research* 23, 413–421. <http://dx.doi.org/10.1023/B:MARI.0000018194.18098.0d>.
- Bohoyo, F., Galindo-Zaldívar, J., Jabaloy, A., Maldonado, A., Rodríguez-Fernández, J., Schreider, A., Suriñach, E., 2007. Extensional deformation and development of deep basins associated with the sinistral transcurrent fault zone of the Scotia–Antarctic plate boundary. *Geological Society, London, Special Publications* 290, 203–217. <http://dx.doi.org/10.1144/SP290.6>.
- Boyden, J., Müller, R., Gurnis, M., Torsvik, T., Clark, J., Turner, M., Ivey-Law, H., Watson, R., Cannon, J., 2011. Next-generation plate-tectonic reconstructions using GPlates. In: Keller, G., Baru, C. (Eds.), *Geoinformatics: Cyber infrastructure for the Solid Earth Sciences*. Cambridge University Press, 95–114.
- Brown, B., Gaina, C., Müller, R.D., 2006. Circum-Antarctic palaeobathymetry. *Palaeogeography, Palaeoclimatology, Palaeoecology* 231, 158–168. <http://dx.doi.org/10.1016/j.palaeo.2005.07.033>.
- Busetti, M., Zanolla, C., Marchetti, A., 2000. Geological structure of the South Orkney microcontinent. *Terra Antarctica* 8 (2), 71–78.
- Cande, S.C., Kent, D.V., 1995. Revised calibration of the geomagnetic polarity timescale for the Late Cretaceous and Cenozoic. *Journal of Geophysical Research* 100 (B4), 6093–6095.
- Coren, F., Geccone, G., Lodolo, E., Zanolla, C., Zitellini, N., Bonazzi, C., Centonze, J., 1997. Morphology, seismic structure and tectonic development of the Powell Basin, Antarctica. *Journal of the Geological Society* 154, 849–862.
- Coxall, H.K., Wilson, P.A., Palike, H., Lear, C.H., Backman, J., 2005. Rapid stepwise onset of Antarctic glaciation and deeper calcite compensation in the Pacific Ocean. *Nature* 433, 53–57. <http://dx.doi.org/10.1038/nature03135>.
- Davies, B.J., Hambrey, M.J., Smellie, J.L., Crrivick, J.L., Glasser, N.F., 2012. Antarctic Peninsula ice sheet evolution during the Cenozoic era. *Quaternary Science Reviews* 31, 30–66. <http://dx.doi.org/10.1016/j.quascirev.2011.10.012>.
- DeConto, R.M., Pollard, D., 2003. Rapid Cenozoic glaciation of Antarctica induced by declining atmospheric CO<sub>2</sub>. *Nature* 421, 245–249. <http://dx.doi.org/10.1038/nature01290>.
- DeSantis, L., Brancolini, G., Donda, F., 2003. Seismo-stratigraphic analysis of the Wilkes Land continental margin (East Antarctica): influence of glacially driven processes on the Cenozoic deposition. *Deep Sea Research Part II: Topical Studies in Oceanography* 50 (8–9), 1563–1594. [http://dx.doi.org/10.1016/S0967-0645\(03\)00079-1](http://dx.doi.org/10.1016/S0967-0645(03)00079-1).
- Dierster-Haass, L., Robert, C., Charnley, H., 1996. The Eocene-Oligocene preglacial–glacial transition in the Atlantic sector of the Southern Ocean (ODP Site 690). *Marine Geology* 31, 123–149. *SSDI* 0025-3227(95)00174-3.
- Dingle, R.V., Lavelle, M., 1998. Late Cretaceous-Cenozoic climatic variations of the northern Antarctic Peninsula: new geo-chemical evidence and review. *Palaeogeography, Palaeoclimatology, Palaeoecology* 141, 215–232. [http://dx.doi.org/10.1016/S0031-0182\(98\)00056-X](http://dx.doi.org/10.1016/S0031-0182(98)00056-X).
- Diviacco, P., Rebesco, M., Camerlenghi, A., 2006. Late Pliocene mega debris flow deposit and related fluid escapes identified on the Antarctic Peninsula continental margin by seismic reflection data analysis. *Marine Geophysical Research* 27 (2), 109–128. <http://dx.doi.org/10.1007/s11001-005-3136-8>.
- Eagles, G., 2010. The age and origin of the central Scotia Sea. *Geophysical Journal International* 183 (2), 587–600. <http://dx.doi.org/10.1111/j.1365-246X.2010.04781.x>.
- Eagles, G., Livermore, R.A., 2002. Opening history of Powell Basin, Antarctic Peninsula. *Marine Geology* 195–205. [http://dx.doi.org/10.1016/S0025-3227\(02\)00191-3](http://dx.doi.org/10.1016/S0025-3227(02)00191-3).
- Eagles, G., Livermore, R.A., Fairhead, J.D., Morris, P., 2005. Tectonic evolution of the west Scotia Sea. *Journal of Geophysical Research* 110, B02401. <http://dx.doi.org/10.1029/JB2004003154>.
- Eagles, G., Livermore, R.A., Morris, P., 2006. Small basins in the Scotia Sea: the Eocene Drake Passage gateway. *Earth and Planetary Science Letters* 242, 343–353. <http://dx.doi.org/10.1016/j.epsl.2005.11.060>.

- Escutia, C., Brinkhuis, H., Klaus, A., and the Expedition 318 Scientists, 2011. Proceedings IODP leg 318. Integrated Ocean Drilling Program Management International, Inc., Tokyo. <http://dx.doi.org/10.2204/iodp.proc.318.2011>.
- Ferris, J.K., Vaughan, A.P.M., Storey, B.C., 2000. Relics of a complex triple junction in the Weddell Sea embayment, Antarctica. *Earth and Planetary Science Letters* 178, 215–230.
- Galindo-Zaldívar, J., Bohoyo, F., Maldonado, A., Schreider, A., Surinách, E., Vázquez, J.T., 2006. Propagating rift during the opening of a small oceanic basin: the Protector Basin (Scotia Arc, Antarctica). *Earth and Planetary Science Letters* 241, 398–412. <http://dx.doi.org/10.1016/j.epsl.2005.11.056>.
- Gersonde, R., Burckle, L.H., 1990. Neogene diatom biostratigraphy of ODP Leg 113, Weddell Sea (Antarctic Ocean). In: Barker, P.F., Kennett, J.P. (Eds.), *Proceedings of the Ocean Drilling Program Science Results*, 761–789. College Station, Texas, USA.
- Ghidella, M., La Brecque, J., 1997. The Jurassic conjugate margins of the Weddell Sea: considerations based on magnetic, gravity and paleobathymetry data. In: Ricci, C. (Ed.), *The Antarctic region: Geological Evolution and Processes*. Terra Antarctica Publication, 441–451.
- Ghidella, M.E., Yáñez, G., LaBrecque, J.L., 2002. Revised tectonic implications for the magnetic anomalies of the western Weddell Sea. *Tectonophysics* 347, 65–86. [http://dx.doi.org/10.1016/S0040-1951\(01\)00238-4](http://dx.doi.org/10.1016/S0040-1951(01)00238-4).
- Gradstein, F.M., Agterberg, F.P., Ogg, J.G., Hardenbol, J., van Veen, P., Thierry, T., Huang, Z., 1994. A Mesozoic time scale. *Journal of Geophysical Research* 99 (B12), 24051–24074.
- Gradstein, F.M., Ogg, J.G., Smith, A.G., Bleeker, W., Lourens, L.J., 2004. A new Geologic Time Scale, with special reference to Precambrian and Neogene. *Episodes* 27, 83–100.
- Haq, B.U., Schutter, S.R., 2008. A chronology of Paleozoic sea-level changes. *Science* 322 (5898), 64–68. <http://dx.doi.org/10.1126/science.1161648>.
- Hayes, D.E., La Brecque, J.L., 1991. Sediment isopachs: circum-Antarctic to 30°S. In: Hayes, D.E. (Ed.), *Marine Geological and Geophysical Atlas of the Circum-Antarctic to 30°S*. Antarctic Research Series, 54. American Geophysical Union, Washington, D. C., 29–35.
- Hayes, D.E., Zhang, C., Weissel, R.A., 2009. Modeling Paleobathymetry in the Southern Ocean. *EOS, Transactions of the American Geophysical Union* 90 (19), 165–172.
- Hinz, K., 1981. A hypothesis of terrestrial catastrophes - Wedges of very thick ocean-ward dipping layers beneath passive continental margins - Their origin and paleoenvironmental significance. *Geologisches Jahrbuch*. E22, 3–28.
- Hinz, K., Krause, W., 1982. The continental margin of Queen Maud Land/Antarctica: seismic sequences, structural elements and geological development. *Geologisches Jahrbuch* E23, 17–41.
- Hinz, K., Kristoffersen, Y., 1987. Antarctica, recent advances in the understanding of the continental shelf. *Geologisches Jahrbuch* E37, 3–54.
- Hunter, R.J., Johnson, A.C., Aleshkova, N.D., 1996. Aeromagnetic data from the southern Weddell Sea embayment and adjacent areas: Synthesis and interpretation. In: Storey, B.C., King, E.C., Livermore, R.A. (Eds.), *Weddell Sea Tectonics and Gondwana Break-up: Geological Society Special Publication*, London, 108, 143–154.
- Jamieson, S.S.R., Sugden, D.E., Hulton, N.R.J., 2010. The evolution of the subglacial landscape of Antarctica. *Earth and Planetary Science Letters* 293, 1–27. <http://dx.doi.org/10.1016/j.epsl.2010.02.012>.
- Jokat, W., Hübscher, C., Meyer, U., Oszko, L., Schöne, T., Versteeg, W., Miller, H., 1996. The continental margin off East Antarctica between 10°W and 30°W. In: Storey, B., King, E.C., Livermore, R.A. (Eds.), *Weddell Sea Tectonics and Gondwana Break-up: Geological Society Special Publication*, London, 108, 129–141.
- Jokat, W., Boebel, T., König, M., Meyer, U., 2003. Timing and geometry of early Gondwana breakup. *Journal of Geophysical Research* 108 (B9), 2428. <http://dx.doi.org/10.1029/2002JB001802>.
- Kent, D.V., Gradstein, F.M., 1986. A Jurassic to recent chronology. In: Vogt, P.R., Tucholke, B.E. (Eds.), *The Geology of North America, Volume M. The Western North Atlantic Region*, Geological Society of America.
- Kennett, J.P., Houtz, R.E., Andrews, P.B., Edwards, A.R., Gostin, V.A., Hajos, M., Hampton, M., Jenkins, D.G., Margolis, S.V., Owenshine, A.T., Perch-Nielsen, K., 1975. Cenozoic paleoceanography in the southwest Pacific Ocean, Antarctic glaciation, and the development of the circum-Antarctic current. In: Kennett, J.P., Houtz, R.E. (Eds.), *Initial Report DSDP 29*. US Government Printing Office, Washington, 1155–1169.

- König, M., Jokat, W., 2006. The Mesozoic breakup of the Weddell Sea. *Journal of Geophysical Research* 111 (B12102). <http://dx.doi.org/10.1029/2005JB004035>.
- Kovacs, L.C., Morris, P., Brozena, J., Tikku, A., 2002. Seafloor spreading in the Weddell Seas from magnetic and gravity data. *Tectonophysics* 347, 43–64. [http://dx.doi.org/10.1016/S0040-1951\(01\)00237-2](http://dx.doi.org/10.1016/S0040-1951(01)00237-2).
- Kristoffersen, Y., Haugland, K., 1986. Geophysical evidence for East Antarctic plate boundary in the Weddell Sea. *Nature* 322, 538–541. <http://dx.doi.org/10.1038/322538a0>.
- Kuvaas, B., Kristoffersen, Y., 1991. The Crary Fan: a trough-mouth fan on the Weddell Sea Continental Margin, Antarctica. *Marine Geology* 97, 345–362.
- LaBrecque, J.L., Ghidella, M.E., 1997. Bathymetry, depth to magnetic basement, and sediment thickness estimates from aerogeophysical data over the western Weddell Sea. *Journal of Geophysical Research* 102, 7929–7945. <http://dx.doi.org/10.1029/96JB01264>.
- LaBrecque, J.L., Cande, S., Bell, R., Raymond, C., Brozena, J., Keller, M., Parra, J.C., Yáñez, G., 1986. Aerogeophysical survey yields new data in the Weddell Sea. *Antarctic Journal Review* 21, 69–71.
- Larter, R.D., Barker, P.F., 1989. Seismic stratigraphy of the Antarctic Peninsula Pacific margin: a record of Pliocene-Pleistocene ice volume and paleoclimate. *Geology* 17, 731–734. [http://dx.doi.org/10.1130/0091-7613\(1989\)017b0731:SSOTAP>2.3.CO;2](http://dx.doi.org/10.1130/0091-7613(1989)017b0731:SSOTAP>2.3.CO;2).
- Larter, R.D., Cunningham, A.P., 1993. The depositional pattern and distribution of glacial–interglacial sequences on the Antarctic Peninsula Pacific margin. *Marine Geology* 109, 203–219. [http://dx.doi.org/10.1016/0025-3227\(93\)90061-Y](http://dx.doi.org/10.1016/0025-3227(93)90061-Y).
- Laske, G., Masters, G., 1997. A global digital map of sediment thickness. *EOS, Transactions American Geophysical Union* 78 (46), F483 (Fall Meeting Supplement).
- Lawver, L.A., Gahagan, L.M., 1998. Opening of Drake Passage and its impact on Cenozoic ocean circulation. In: Crowley, T.J., Burke, K.C. (Eds.), *Tectonic Boundary Conditions for Climate Reconstructions*. Oxford Monographs on Geology and Geophysics. Oxford University Press, Oxford, 212–223.
- Lawver, L.A., Gahagan, L., 2003. Evolution of Cenozoic Seaways in the circum-Antarctic region. *Palaeogeography, Palaeoclimatology, Palaeoecology* 198, 11–37. [http://dx.doi.org/10.1016/S0031-0182\(03\)00392-4](http://dx.doi.org/10.1016/S0031-0182(03)00392-4).
- Le Brocq, A.M., Payne, A.J., Vieli, A., 2010. An improved Antarctic dataset for high resolution numerical ice sheet models (ALBMAP v1). *Earth System Science Data Discussions* 3, 195–230. <http://dx.doi.org/10.5194/essdd-3-195-2010> ([www.earth-systsci-data-discuss.net/3/195/2010/](http://www.earth-systsci-data-discuss.net/3/195/2010/)).
- Lear, C.H., Bailey, T.R., Pearson, P.N., Coxall, H.K., Rosenthal, Y., 2008. Cooling and ice growth across the Eocene–Oligocene transition. *Geology* 36, 251–254. <http://dx.doi.org/10.1130/G24584A.1>.
- Leitchenkov, G.L., Guseva, Y.B., Gandyukhin, V.V., 2007. Cenozoic environmental changes along the East Antarctic continental margin inferred from regional seismic stratigraphy. In: Cooper, A.K., Raymond, C.R. (Eds.), *Antarctica: A Keystone in a Changing World–Online Proceedings of the 10th ISAES: USGS Open-File Report 2007-1047, Short Research Paper 005*. <http://dx.doi.org/10.3133/of2007-1047.srp005>.
- Leitchenkov, G., Guseva, J., Gandyukhin, V., Grikurov, G., Kristoffersen, Y., Sand, M., Golynsky, A., Aleshkova, N., 2008. Crustal structure and tectonic provinces of the Riiser-Larsen Sea area (East Antarctica): results of Geophysical studies. *Marine Geophysical Research* 29, 135–158. <http://dx.doi.org/10.1007/s11011-008-9051-z>.
- Lindeque, A., Martos, Y.M., Gohl, K., Maldonado, A., 2012. Seafloor Spreading Magnetic Anomaly Isochron Map Compilation for the Weddell Sea and Scotia Sea. <http://dx.doi.org/10.1594/PANGAEA.777453>. ([www.pangea.de](http://www.pangea.de)).
- Livermore, R.A., Hunter, R.J., 1996. Mesozoic seafloor spreading in the southern Weddell Sea. In: Storey, B., King, E.C., Livermore, R.A. (Eds.), *Weddell Sea Tectonics and Gondwana Break-up: Geological Society Special Publication*, London, 108, 227–241.
- Livermore, R.A., Balanyá, J.C., Maldonado, A., Martínez, J.M., Rodríguez-Fernández, J., Sanz de Galdeano, C., Galindo-Zaldívar, J., Jabaloy, A., Barnolas, A., Somoza, L., Hernández, J., Suriñach, E., Viseras, C., 2000. Autopsy on a dead spreading centre: the Phoenix Ridge, Drake Passage, Antarctica. *Geology* 18, 607–610. [http://dx.doi.org/10.1130/0091-7613\(2000\)28b607:AOADSC>2.0.CO;2](http://dx.doi.org/10.1130/0091-7613(2000)28b607:AOADSC>2.0.CO;2).
- Livermore, R., Nankivell, A., Eagles, G., Morris, P., 2005. Paleogene opening of Drake Passage. *Earth and Planetary Science Letters* 236, 459–470. <http://dx.doi.org/10.1016/j.epsl.2005.03.027>.



- Livermore, R.A., Hillenbrand, C.-D., Meredith, M., Eagles, G., 2007. Drake Passage and Cenozoic climate: an open and shut case? *Geochemistry, Geophysics, Geosystems* 8, Q01005. <http://dx.doi.org/10.1029/2005GC001224>.
- Lodolo, E., Coren, F., Schreider, A.A., Ceccone, G., 1998. Geophysical evidence of a relict oceanic crust in the southwestern Scotia Sea. *Marine Geophysical Research* 19, 439–450. <http://dx.doi.org/10.1023/A:1004355707951>.
- Lodolo, E., Civile, D., Vuan, A., Tassone, A., Geletti, R., 2010. The Scotia–Antarctica plate boundary from 35°W to 45°W. *Earth and Planetary Science Letters* 293, 200–215. <http://dx.doi.org/10.1016/j.epsl.2009.12.045>.
- Lythe, M.B., Vaughan, G.D., the BEDMAP Consortium, 2001. BEDMAP: a new ice thickness and subglacial topographic model of Antarctica. *Journal of Geophysical Research* 106, 11335–11351. <http://dx.doi.org/10.1029/2000JB900449>.
- Maldonado, A., Aldaya, F., Balanyá, J.C., Galindo Zaldívar, J., Livermore, R.A., Monseñe, F.M., Rodríguez-Fernández, J., Roussanov, M., Sanz de Galdeano, C., Suriñach, E., Viseras, C., 1993. Tectonics and paleoceanography in the northern sector of the Antarctic Peninsula: preliminary results of HESANT1992/93 cruise with the B/O HESPERIDES. *Scientia Marina* 57 (1), 79–89.
- Maldonado, A., Zitellini, N., Leitchenkov, G., Balanyá, J.C., Coren, F., Galindo-Zaldívar, J., Lodolo, E., Jabaloy, A., Zanolla, C., Rodríguez-Fernández, J., Vinnikovskaya, O., 1998. Small ocean basin development along the Scotia–Antarctica plate boundary and in the northern Weddell Sea. *Tectonophysics* 296, 371–402.
- Maldonado, A., Balanyá, J.C., Barnolas, A., Galindo-Zaldívar, J., Hernández, J., Jabaloy, A., Livermore, R., Martínez-Martínez, J.M., Rodríguez-Fernández, J., Sanz de Galdeano, C., Somoza, L., Suriñach, E., Viseras, C., 2000. Tectonics of an extinct ridge-transform intersection, Drake Passage (Antarctica). *Marine Geophysical Research* 21, 43–68. <http://dx.doi.org/10.1023/A:1004762311398>.
- Maldonado, A., Barnolas, A., Bohoyo, F., Galindo-Zaldívar, J., Hernández-Molina, J., Lobo, F., Rodríguez-Fernández, J., Somoza, L., Vázquez, J.T., 2003. Contourite deposits in the central Scotia Sea: the importance of the Antarctic Circumpolar Current and Weddell Gyre flows. *Palaeogeography, Palaeoclimatology, Palaeoecology* 198, 187–221. [http://dx.doi.org/10.1016/S0031-0182\(03\)00401-2](http://dx.doi.org/10.1016/S0031-0182(03)00401-2).
- Maldonado, A., Barnolas, A., Bohoyo, F., Escutia, C., Galindo-Zaldívar, J., Hernández-Molina, F.J., Jabaloy, A., Lobo, F.J., Nelson, C.H., Rodríguez-Fernández, J., Somoza, L., Vázquez, J.T., 2005. Miocene to recent contourite drifts development in the northern Weddell Sea (Antarctica). *Global Planet Change* 45, 99–129.
- Maldonado, A., Bohoyo, F., Galindo-Zaldívar, J., Hernández-Molina, F.J., Jabaloy, A., Lobo, F.J., Rodríguez-Fernández, J., Suriñach, E., Vázquez, J.T., 2006. Ocean basins near the Scotia-Antarctic plate boundary: influence of tectonics and paleoceanography on the Cenozoic deposits. *Marine Geophysical Research* 27, 83–107. <http://dx.doi.org/10.1007/s11001-006-9003-4>.
- Maldonado, A., Bohoyo, F., Galindo-Zaldívar, J., Hernández-Molina, F.J., Lobo, F.J., Shreyder, A.A., Suriñach, E., 2007. Early opening of Drake Passage: regional seismic stratigraphy and paleoceanographic implications, in Antarctica: A Keystone in a Changing World. Extended Abstract EA57, online Proceedings of the 10th International Symposium on Antarctic Sciences (ISAES). In: Cooper, A.K., Raymond, C.R., et al. (Eds.), USGS Open-File Report (<http://pubs.usgs.gov/of/2007/1047/ea/of2007-1047ea057.pdf>).
- Michels, K.H., Rogenhagen, J., Kuhn, G., 2001. Recognition of contour-current influence in mixed contourite–turbidite sequences of the western Weddell Sea, Antarctica. *Marine Geophysical Research* 22, 465–485. <http://dx.doi.org/10.1023/A:1016303817273>.
- Michels, K.H., Kuhn, G., Hillenbrand, C.-D., Diekmann, B., Fütterer, D.K., Grobe, H., Uenzelmann-Neben, G., 2002. The southern Weddell Sea: combined contourite–turbidite sedimentation at the southeastern margin of the Weddell Gyre. In: Stow, D.A.V., Pudsey, C., Howe, J.C., Faugères, J.-C., Viana, A.R. (Eds.), Geological Society of London, *Memoirs*, 22, 305–323. <http://dx.doi.org/10.1144/GSL.MEM.2002.022.01.32>.
- Miller, H., Henriot, J.P., Kaul, N., Moons, A., 1990. A fine-scale stratigraphy of the eastern margin of the Weddell Sea. In: Bleil, U., Thiede, J. (Eds.), *Geological History of the Polar Oceans: Arctic Versus Antarctic*. Kluwer Academic Publishers, 131–161.
- Miller, K.G., Wright, J.D., Katz, M.E., Browning, J.V., Cramer, B.S., Wade, B.S., Mizintseva, S.F., 2008. A view of Antarctic ice-sheet evolution from sea level and deep-sea isotope changes during the Late Cretaceous-Cenozoic. In: Cooper, A.K., Barrett, P.J., Stagg, H., Storey, B., Stump, E., Wise, W.,



- the 10th ISAES editorial team (Eds.), Proceedings of the 10th International Symposium on Antarctic Earth Sciences. The National Academic Press, Washington, DC. <http://dx.doi.org/10.3133/of2007-1047.kp06>.
- Nankivell, A.P., 1997. Tectonic evolution of the Southern Ocean. PhD thesis, Oxford University.
- Oszko, L., 1997. Tectonic structures and glaciomarine sedimentation in the South-Eastern Weddell Sea from seismic reflection data. *Berichte zur Polarforschung (Reports on Polar Research)*, 222. Alfred Wegener Institut für Polar und Meeresforschung, Bremerhaven, Germany. PhD thesis, University of Bremen. [hdl:10013/epic.12931](http://hdl.handle.net/10013/epic.12931).
- Pagani, M., Zachos, J., Freeman, K.H., Tipple, B., Bohaty, S., 2005. Marked decline in atmospheric carbon dioxide concentrations during the Paleogene. *Science* 309 (5734), 600–603. <http://dx.doi.org/10.1126/science.1110063>.
- Pollard, D., DeConto, R.M., 2009. Modelling West Antarctic ice sheet growth and collapse through the past five million years. *Nature* 458, 320–323. <http://dx.doi.org/10.1038/nature07809>.
- Pritchard, H.D., Arthern, R.J., Vaughan, D.G., Edwards, 2009. Extensive dynamic thinning on the margins of the Greenland and Antarctic ice sheets. *Nature* 461, 971–975. <http://dx.doi.org/10.1038/nature08471>.
- Ramsay, A.T.S., Baldauf, J.G., 1990. A reassessment of the Southern Ocean biochronology. *Memoirs of the Geological Society of America* 18, 1–122.
- Rebesco, M., Camerlenghi, A., 2008. Late Pliocene margin development and mega debris flow deposits on the Antarctic continental margins: evidence of the onset of the modern Antarctic Ice Sheet? *Palaeogeography, Palaeoclimatology, Palaeoecology* 260, 149–167.
- Rebesco, M., Camerlenghi, A., Geletti, R., Canals, M., 2006. Margin architecture reveals the transition to the modern Antarctic ice sheet ca. 3 Ma. *Geology* 34, 301–304. <http://dx.doi.org/10.1130/G22000.1>.
- Rignot, E.J., Bamber, J.L., van den Broeke, M.R., Davis, C., Li, Y., van de Berg, W., van Meijgaard, 2008. Recent Antarctic ice mass loss from radar interferometry and regional climate modelling. *Nature Geoscience* 1. <http://dx.doi.org/10.1038/ngeo102>.
- Ritzmann, O., 1998. Refraktionsseismische Untersuchungen am Kontinentalrand der Ostantarktis. Diploma thesis (unpublished), Rheinische Friedrich-Wilhelms Universität, Bonn.
- Rogenhagen, J., Jokat, W., 2000. The sedimentary structure in the western Weddell Sea. *Marine Geology* 168, 45–60. [http://dx.doi.org/10.1016/S0025-3227\(00\)00048-7](http://dx.doi.org/10.1016/S0025-3227(00)00048-7).
- Rogenhagen, J., Jokat, W., 2002. Origin of the gravity ridges and Anomaly-T in the southern Weddell Sea. In: Gamble, J.A., Skinner, D.N.B., Henrys, S. (Eds.), *Antarctica at the Close of a Millennium, Proceedings of the 8th International Symposium on Antarctic Earth Sciences*. Royal Society of New Zealand, Wellington, 227–231.
- Rogenhagen, J., Jokat, W., Hinz, K., Kristoffersen, Y., 2004. Improved seismic stratigraphy of the Mesozoic Weddell Sea. *Marine Geophysical Researches* 25, 265–282. <http://dx.doi.org/10.1007/s11001-005-1335-y>.
- Scher, H.D., Martin, E.E., 2006. Timing and climatic consequences of the opening of Drake Passage. *Science* 312, 428–430.
- Scheuer, C., Gohl, K., Eagles, G., 2006. Gridded isopach maps from the South Pacific and their use in interpreting the sedimentation history of the West Antarctic continental margin. *Geochemistry, Geophysics, Geosystems* 7, Q11015. <http://dx.doi.org/10.1029/2006GC001315>.
- Smith, R.T., Anderson, J.B., 2010. Ice-sheet evolution in James Ross basin, Weddell Sea margin of the Antarctic Peninsula: the seismic stratigraphic record. *Geological Society of America Bulletin* 122 (5/6), 830–842. <http://dx.doi.org/10.1130/B26486.1>.
- Smith, R.T., Anderson, J.B., 2011. Seismic stratigraphy of the Joinville Plateau: implications for regional climate evolution. In: Anderson, J.B., Wellner, J.S. (Eds.), *Tectonic, Climatic, and Cryospheric Evolution of the Antarctic Peninsula*. Geopress, American Geophysical Union, Washington DC, USA, 51–61. <http://dx.doi.org/10.1029/2010SP000980>.
- Smith, W.H.F., Sandwell, D.T., 1997. Global seafloor topography from satellite altimetry and ship depth soundings. *Science* 277, 1957–1962.
- Surinách, E., Galindo-Zaldívar, J., Maldonado, A., Livermore, R., 1997. Large amplitude magnetic anomalies in the northern sector of the Powell Basin, NE Antarctic Peninsula. *Marine Geophysical Research* 19, 65–80. <http://dx.doi.org/10.1023/A:1004240931967>.
- Tripathi, A.K., Roberts, C.D., Eagle, R.A., 2009. Coupling of CO<sub>2</sub> and ice sheet stability over major climate transitions of the last 20 million years. *Science* 326, 1394–1397. <http://dx.doi.org/10.1016/j.gca.2011.01.018>.

- Tripati, A.K., Roberts, C.D., Eagle, R.A., Li, G., 2011. A 20 million year record of planktic foraminiferal B/Ca ratios: systematics and uncertainties in pCO<sub>2</sub> reconstructions. *Geochimica et Cosmochimica Acta* 75 (10), 2582–2610. <http://dx.doi.org/10.1016/j.gca.2011.01.018>.
- Uenzelmann-Neben, G., 2006. Depositional patterns at Drift 7, Antarctic Peninsula: along- slope versus down-slope sediment transport as indicators for oceanic currents and climatic conditions. *Marine Geology* 233, 49–62. <http://dx.doi.org/10.1016/j.margeo.2006.08.008>.
- Wardell, N., Childs, J.R., Cooper, A.K., 2007. Advances through collaboration: sharing seismic reflection data via the Antarctic Seismic Data Library System for Cooperative Research (SDLS). In: Cooper, A.K., Raymond, C.R. (Eds.), *Antarctica: A Keystone in a Changing World—Online Proceedings of the 10th ISAES: USGS Open-File Report 2007-1047, Short Research Paper 001*. <http://dx.doi.org/10.3133/of2007-1047.srp001> (4 pp.).
- Wilson, D.S., Jamieson, S.S.R., Barrett, P.J., Leitchenkov, G., Gohl, K., Larter, R.D., 2011. Antarctic topography at the Eocene–Oligocene boundary. *Palaeogeography, Palaeoclimatology, Palaeoecology*. <http://dx.doi.org/10.1016/j.palaeo.2011.05.028>.
- Zachos, J.C., Kump, L.R., 2005. Carbon cycle feedbacks and the initiation of Antarctic glaciation in the earliest Oligocene. *Global and Planetary Change* 47, 51–66. <http://dx.doi.org/10.1016/j.gloplacha.2005.01.001>.
- Zachos, J., Pagani, M., Sloan, L., Thomas, E., Billups, K., 2001. Trends, rhythms, and aberrations in global climate 65 Ma to present. *Science* 292/5517, 686–693. <http://dx.doi.org/10.1126/science.1059412>.



# Chapter 8

## SECOND PAPER

### AMUNDSEN SEA – ROSS SEA TRANSECT

Lindeque, A., Gohl, K., Henrys, S., Wobbe, F., Davy B., 2014. Pre-glacial to glacial stratigraphy in the unexplored Amundsen Sea deep-sea basin: A first cross-regional correlation of deep-sea seismic reflection data. Manuscript prepared for submission to *Palaeogeography, Palaeoclimatology, Palaeoecology*.

#### Highlights:

- Two new seismic reflection datasets across the Amundsen Sea and Ross Sea.
- First direct Amundsen Sea – Ross Sea seismic horizon stratigraphy correlation.
- Separation of the pre-glacial, transitional and full glacial sediment components.
- Total sediment volume  $2.8$  to  $3.3 \times 10^6 \text{ km}^3$  and total sediment thickness  $\sim 4$  km.
- Drifts in the pre-glacial and transitional units indicate Eocene bottom currents.

---

## 8.1 Abstract

Characterization of changes in seismic reflectivity patterns and changes in geometry provide insight into -slope sediment transport processes that can be connected back to bottom current development and ice sheet growth/demise across tectonic time scales. Separating the pre-glacial, transitional and full glacial components in the offshore sedimentary record can therefore provide clues on when the ice sheets first reached the shelf. In addition, quantifying the sediment volumes can help constrain palaeobathymetry and palaeotopography reconstructions used in climate-ice sheet modelling.

Amongst the seismic reflection data acquired during the 2010 *RV Polarstern* ANT-XXVI/3 and 2006 *RV Tangaroa* TAN-2006 expeditions, a  $\sim 2000$  km long Amundsen Sea – Ross Sea transect across a previously unsurveyed sector, provides the first opportunity to directly link key pre-glacial to glacial seismic stratigraphy horizons on the continental rise and -shelf of the Amundsen Sea, with that of the Ross Sea. 10 main seismic units were mapped: AS-S1, AS-S2, AS-S3 constitutes the inferred Cretaceous to Eocene pre-glacial sequence (70–38 Ma in our age model), AS-S4 to AS-6 the Eocene to mid-Miocene transitional sequence (38–15.5 Ma) and AS-S7 to AS-S11 the mid-Miocene to Pleistocene full glacial climate sequence (15.5–1 Ma).

The first direct seismic horizon stratigraphy link from the Ross Sea slope and continental rise, to the far eastern Amundsen Sea continental rise and slope has been established. The top pre-glacial boundary horizon AS-u3/uPG-T, links to RSU6 and the base of Unit II respectively, and is interpreted as the first arrival of the WAIS on the shelf. The top transitional boundary AS-u6/uT-FG, links to RSU4 and base of Unit III, interpreted as the

onset of the full-glacial regime. Sparse borehole information from IODP Leg 318 site 1356 and DSDP Leg 28 Sites 270–272 support the constructed age model, and link AS-u3/uPG-T to WL-u3, RSU6 and AS-u6/uT-FG to WL-U5, RSU4. Magnetic seafloor spreading anomaly data provide age control for the basement in the constructed age model. The 71 Ma old basin accumulated up to ~3.9 km (3 s TWT) sediments in the centre near the Endeavour fracture zone, without decompaction applied. The total basin area is 1.2 to 1.4 x 10<sup>6</sup> km<sup>2</sup> and the total sediment volume 2.83 to 3.0 x 10<sup>6</sup> km<sup>3</sup>, using an average sediment thickness of 2357 m.

Seismic facies geometry analysis suggests: (i) Paleogene–Eocene bottom current activity. (ii) Eocene grounding of the West Antarctic ice sheet. (iii) An anomalous part of the basin just West of the Proto-Antipodes fracture zone that could be stretched continental crust. (iv) Evidence for tectonic uplift at part (iii), and (iv) Total sediment thickness of 3.9 km and total volume estimate 2.83 to 3.30 x 10<sup>6</sup> km<sup>3</sup>. The pre-glacial (up to 34 Ma Eocene/Oligocene), Transitional (34–15.5 Ma, Eocene to mid-Miocene) and full glacial (<15.5 Ma) climate regime sediment volumes are estimated at: PG = 1.5 to 1.8 x 10<sup>6</sup> km<sup>3</sup>, T = 0.8 to 1.0 x 10<sup>6</sup> km<sup>3</sup> and FG = 0.8 to 0.9 x 10<sup>6</sup> km<sup>3</sup>.

**Keywords:**

West Antarctica, seismic horizon stratigraphy, glacial development, bottom-currents, sediment thickness

## 8.2 Introduction

At the stages where continental scale ice sheets expanded and grounded on the continental shelf, erosion and rapid transport moved massive amounts of sediments from inland to the coast, shelf, slope and deep-sea. Such increased sediment supply and changes in transport/depositional processes combine to form sedimentary features that can be identified in seismic reflection images, and based on the geometry and amplitude of the reflections, be related back to a general depositional environment or process.

The sedimentary sequences and structural elements along continental rises and margins contain records of the transport and depositional history that allow analyses of the palaeo-environmental and palaeoclimate conditions. The polar continental margins in particular, exhibit sedimentary records of the onset and dynamics of the continental ice sheets. On the Pacific margin of Antarctica, the sediment record captured the last 90 million years of ice sheet and bottom current development history.

The sediment transport and depositions processes changed within the context of tectonic reorganisation and ocean-bottom current evolution, intertwined with changes in palaeotopography (Wilson et al., 2012, 2013; Fig. 1-2 in Ch.1), atmospheric pCO<sub>2</sub>, sea level



and sea-surface temperature during Antarctica's greenhouse to ice house climate change (Fig. 1-1 in Ch. 1; Zachos et al., 2001; Pagani et al., 2005; Haq and Schutter, 2008; Tripathi et al., 2009, 2011).

Evidence for ice sheet related increased sediment supply and deposition have been observed in marine seismic reflection images around Antarctic continental rises (e.g. Nitsche et al., 1997, 2000; De Santis et al., 2003; Rogenhagen et al., 2004; Maldonado et al., 2006; Scheuer et al., 2006; Leitchenkov et al., 2007; Escutia et al., 2005, 2011; Uenzelmann-Neben and Gohl, 2012; Lindeque et al., 2013). These studies are often localised, but circum-Antarctic palaeobathymetric (Hayes et al., 2009) and palaeotopography mass-balance reconstructions are needed to improve ice-sheet modelling (Fig. 8-1; Fig. 1-1 in Ch. 1; Le Brocq et al., 2010; Wilson et al., 2012). This information for the central Amundsen Sea and eastern Ross Sea continental rises are still lacking due to the absence of information on the sediment record, seismic data and age control through drilling data.

Open questions that need to be considered in studying the sedimentary record of the as yet underexplored Amundsen Sea and eastern Ross Sea continental rises include:

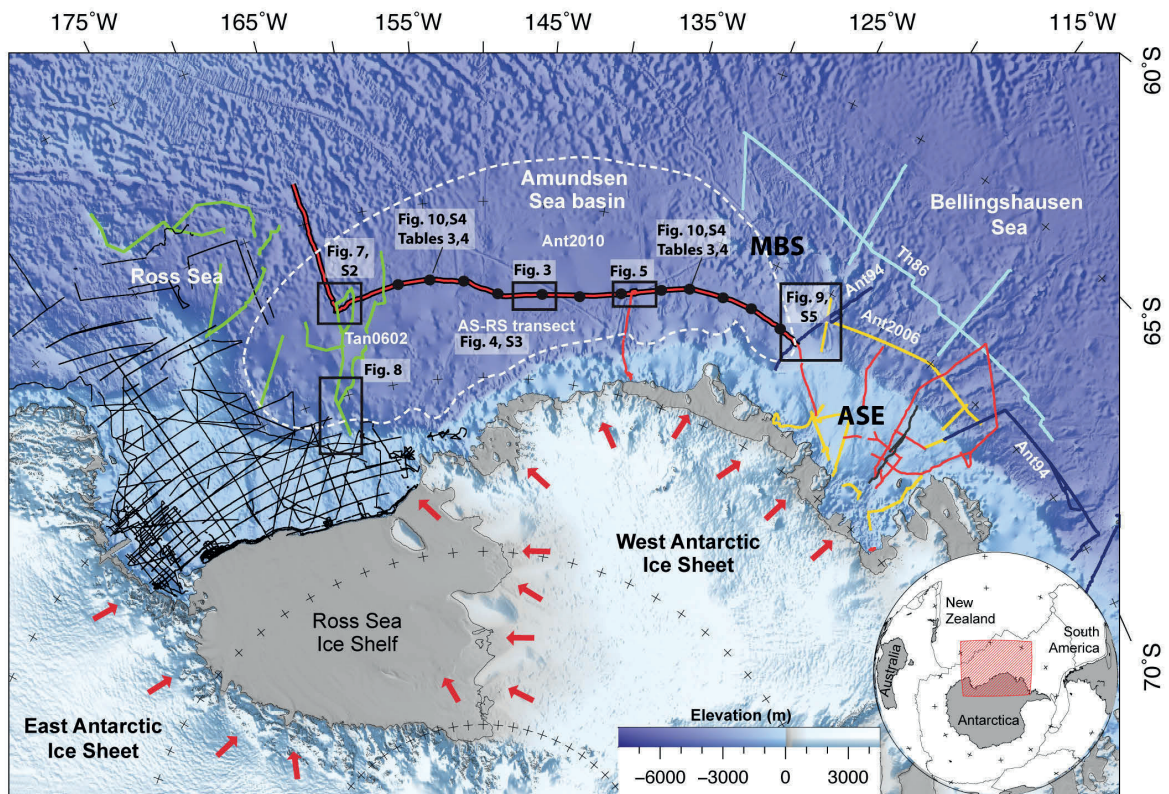


**Fig. 8-1** Overview map of the Amundsen Sea basin study area (ASB, white dashed line) with seismic surveys referred to in this paper demarcated as: AWI-2010 – red; TAN-2006 – green; Ant2006 – yellow; Ant94 – navy; other international lines are Th86 – light blue, and on the Ross Sea shelf – black. The AS-RS transect is shown in the thick black/red line through the ASB (Fig. 8-4; Appendix B-1). The locations of the figures are demarcated by the black squares and annotated. The black dots represent the 12 points used for the sediment thickness estimates (Figs. 8-4 and 8-10; Appendix B-1, B-2; Ch. 5; Tables 8-3 and 8-4). Background image: International Bathymetric Chart of the Southern Ocean (IBCSO) Version 1.0 digital bathymetric model (DBM), online supplement to Arndt J.E., et al. (2013). Red arrows indicate the general ice flow drainage directions of the West Antarctic Ice Sheet (WAIS) and East Antarctic Ice Sheet (EAIS) after Bamber et al. (2009).

- Which part of the sediment record indicates the onset of the glacially dominated environment of West Antarctica and is it possible to estimate when this might have taken place?
- Where are the major deposition centres for the pre-glacial to glacial periods and what processes may have caused their formation? Did the centres move over time?
- Is there a difference in the deep-sea sediment transport processes or a shift in deposition between the Amundsen Sea and Ross Sea, and if so why?
- What evidence is there to reveal the development of past bottom current formation?
- If there is regional variation in acoustic basement topography and if so, what can it reveal about the tectonic history of the Amundsen Sea basin development?
- How much sediment was eroded off the land and deposited in the deep-sea basin in total, or at times of key climate change such as the Eocene/Oligocene boundary? Can the lateral continuation of units, sediment thicknesses and sediment volumes be quantified for palaeotopography and palaeobathymetry reconstructions?

Acquisition of seismic reflection data on the Amundsen Sea – Ross Sea continental rise in 2006 (*RV Tangaroa* TAN-2006 survey) and in 2010 (*RV Polarstern* ANT-XXVI/3 survey; Gohl et al., 2010) provide the first seismic link across the previously unsurveyed central and western Amundsen Sea sector (115°W to 170°W; Fig. 8-1), and presents an opportunity to establish a preliminary, direct seismic horizon stratigraphic correlation across two major WAIS drainage outlet basins that address some of these open questions.

In this work the pre-glacial climate regime is defined as being relatively warm and predominantly ice sheet free, except for smaller glaciers in high altitudes, and open-ocean conditions without major sea-ice cover. The transitional regime refers to a colder climate, analogous to the present day Alpine climates, with regional scale ice sheets with multiple advance/retreat cycles to/from coastal areas and inner shelves, and only perennial regional sea-ice cover. The full glacial climate regime describes a climate in West Antarctica, in which continental scale ice sheets expanded to the coastal regions and grounded on the middle to outer shelf during glacial maxima.

### 8.3 Tectonic and palaeoclimate setting

#### 8.3.1 Rifting and basin development

The Amundsen Sea basin formation started in the late Cretaceous (~84 Ma, C34y) during continental rifting before initial oceanic crust formed as the Campbell Plateau and Chatham

**Table 8-1.** Chronological summary of the seismic stratigraphic sequences or units in the Pacific margin of West Antarctica, deposited during changes in tectonics, glaciation, climate and ocean circulation.

Epoch	Age (Ma)	Chron*	Bounding unconformities	Seismic sequence or units	Changes in tectonics, glaciation, sea level, climate and ocean circulation from literature		
Pleist.	0.0	C1n		RSS-8 <sup>5,13,14</sup>	Multiple grounded ice sheet advance and retreat cycles of the WAIS and EAIS <sup>20,51</sup> Amundsen Sea shelf show megascale lineations and grounding zone wedges <sup>9</sup>	EAIS & WAIS expanding up to continental shelf edge, grounding cycles Full glacial (FG) climate regime	
	1.5 <sup>14</sup>		RSU1 <sup>5,13,14</sup>				
Pliocene	L 2.6	C2n		ASS-6 (Plio.–Pleist.) <sup>3</sup> Unit IV (4–0 Ma) <sup>12</sup> RSS-7 <sup>5,13,14</sup>	Multiple grounded ice sheet advance and retreat cycles of the WAIS and EAIS <sup>20,51</sup> Mass transport deposits and levee-drifts <sup>12</sup> Less consolidated aggradational material deposited on shelf and slopes <sup>3,4,8,9,14,21</sup>		
	3.3 <sup>14</sup>		RSU2 <sup>5,13,14</sup>		Sub-glacial erosional phases <sup>3,5,22</sup>		
	E 3.6	C2r	ASS-u5 <sup>3</sup>		Major sea level decrease (Za2) <sup>51</sup> Continued WAIS & EAIS oscillation <sup>20</sup> , progradational building of the shelf <sup>5,12,13</sup>		
Miocene	L 5.3	C3r		ASS-5 (L.Mio.–E.Plio.) <sup>3</sup> RSS-6 <sup>5,13,14</sup>	Atmospheric pCO <sub>2</sub> fluctuates (200–400ppm, 12–0.01 Ma) Temp ~3° higher than today <sup>51,37</sup> Sediment drifts and mass transport deposits in the deep sea, ice sheet expansion <sup>12</sup> Oscillating WAIS & EAIS advance/retreat cycles on the shelf, older strata truncated <sup>3,5,8,9,35</sup>		
	10.0 <sup>14</sup>		RSU3 <sup>5,13,14</sup>				
	M 11.6	C5r	ASS-u4 <sup>3</sup>	ASS-4 (M.Mio.) <sup>3</sup> Unit III (15–4 Ma) <sup>12</sup> RSS-5 <sup>5,13,14</sup> WL-S9 <sup>11</sup>	Sub-glacial erosional phases <sup>3,5,22</sup> Progradational sequences interpreted as glacial advance cycle to the outer shelf <sup>3,5,8,11,13,14</sup> Large elongate sediment drifts and channel-levees formed on seafloor <sup>12</sup> Marked increase in sediment supply <sup>11,15</sup>		
	15.5 <sup>14</sup>		WL-u8 <sup>11,15</sup> ASS-u3 <sup>3</sup> RSU4 <sup>5,13,14</sup>	<b>T/FG boundary</b> <sup>14,17</sup>	Transition from dynamic, to persistent continental scale ice sheets <sup>11,13-15,35,36</sup> Miocene glaciation (Mi4), a lowering of sea level (Ser3) and permanent EAIS <sup>51,10,25</sup> Mid–Miocene climate optimum (16–15 Ma) and global temperature decrease ~8°C <sup>13,18</sup>		
	E 16.0	C5Cn	ASS-3 (E–M.Mio.) <sup>3</sup> Unit II (21–15 Ma) <sup>12</sup> RSS-4 <sup>5,13,14</sup> WL-S5 to -S8 <sup>11,15</sup>	Major increase in sediment transport across shelf edge to slope <sup>3,5,12-14</sup> Continued ice sheets advance/retreat cycles at the coast, first advances to the shelf <sup>23</sup> Elongate drifts and levee drifts deposits, intensified bottom water circulation <sup>12</sup> Sub-glacial erosional phases <sup>3,5,22</sup>			
	18.0 <sup>14</sup>		WL-u4 to -u7 <sup>11,15</sup> RSU4a <sup>5,13,14</sup> ASS-u2 <sup>3</sup>		Continental ice sheets expand to the coast and multiple advance/retreat cycles occur <sup>5,11,18,34</sup>		
	20.0		RSU5 <sup>5,13,14</sup>	RSS-3 <sup>5,13,14</sup>	Atmospheric pCO <sub>2</sub> fluctuates (300 to 400ppm, 20–12 Ma) <sup>51,33</sup> Mi-1 Glaciation, warming 5–6°C <sup>25,51</sup>		
	Oligocene	L 23.0	C6Cn		WL-S4 <sup>11,15</sup>		Atmospheric pCO <sub>2</sub> decrease (1800–400ppm, 33–23 Ma) <sup>23,51</sup> sealevel decrease by ~100m <sup>51</sup> Transpressional and translateral motion along former Bellingshausen plate boundary <sup>1,2</sup> or possibly WARS activity <sup>3</sup>
		E 28.4	C10n		RSS-2 <sup>5,13,14</sup>		Onset of the Antarctic Circumpolar Current (ACC) <sup>21,30,32</sup> Ice caps on elevated land areas expand, forming dynamic continental ice sheets <sup>26,27,29,30,31</sup>
		29.0 <sup>14</sup>		RSU6 <sup>5,13,14</sup>	<b>PG/T boundary</b> <sup>14,17</sup>		Oi-1 glaciation (at ~34 Ma) <sup>51,21,25</sup> Global climate cooling
Eocene	L 33.8	C13r	WL-u3 <sup>11,15</sup>	Unit I (60–21 Ma) <sup>12</sup> ASS-2 (L.Cret.–Olig.) <sup>3</sup> WL-S3 <sup>11,15</sup>	<b>First formation of the WAIS</b> <sup>38</sup> <b>Bottom currents in the Amundsen Sea, elongate sediment drifts build-up</b> <sup>12,17</sup> Atmospheric pCO <sub>2</sub> declines (1750–700ppm, 38–33 Ma), temp ~4°C lower than today <sup>51,28</sup> Faulted & folded units suggest convergent, transpressional passive rifting margin <sup>3</sup> Youngest magnetic seafloor spreading anomaly in the Amundsen Sea deep-sea basin <sup>1,4</sup> North-south orientated strike-slip motion <sup>3</sup> , full spreading rates decreased to 30–40 mm/Myr <sup>1</sup> Atmospheric pCO <sub>2</sub> increase (800 to 1800 ppm, 55–42 Ma) <sup>51,24</sup> Full spreading rates steadily decreasing from 60–70 mm/Myr <sup>1</sup>		
	M 42.0	C20n <sup>1</sup>					
	E 45.0	C20r <sup>1</sup>					
Paleo.	L 55.8	C24r			<b>Proto-Ross Sea gyre develops</b> <sup>19</sup> <b>surface waters cool</b> <sup>16</sup> <b>bottom water circulation</b> <sup>12</sup>		
	E 61.7	C27r <sup>1</sup>			Independent motion of Bellingshausen plate ends, becomes part of West Antarctic plate <sup>1,2</sup>		
Cretaceous	L 65.5	C29r	ASS-u1 <sup>3</sup>		Emplacement of Marie Byrd Seamounts (65–55 Ma) <sup>16</sup>		
	69.0	C31r <sup>1,2</sup>			Shift in Pacific Plate motion, transform faults bend left <sup>1</sup>		
	74.0	C32r.2r <sup>1,2</sup>			Bellingshausen plate rotation shifts to counter-clockwise <sup>1,4</sup> , spreading rate 60–70 mm/Myr <sup>1,2</sup>		
	80.0	C33r <sup>1,2</sup>		RSS-1 <sup>5,13,14</sup> volcanics	Antarctic passive margin west of the Proto Antipodes Fracture Zone formed <sup>1</sup>		
	E 84.0	C34y <sup>1,2</sup>		WL-S1 <sup>11,15</sup> volcanics	Bellingshausen plate moves independently forming ~670 km wide COT zone <sup>1</sup> Seafloor spreading propagates from Amundsen Sea West, Ross Sea opens <sup>1</sup>		
90.0			ASS-1 (E.Cret.) <sup>3</sup>	Initial oceanic crust forms in the Amundsen Sea basin, divergent margin <sup>1</sup> Continental rifting, beginning of break-up between Zealandia & Marie Byrd Land <sup>1,2</sup>			

**Abbreviations:** Pleist. - Pleistocene, Paleo. - Paleocene, L - late, M - middle, E - early; \*Chron: Gradstein et al., 2004 unless otherwise indicated. WAIS = West Antarctic Ice Sheet  
EAIS - East Antarctic Ice Sheet, WARS - West Antarctic Rift System. Prefixes: RSS - Ross Sea Shelf, ASS - Amundsen Sea Shelf, WL - Wilkes Land.  
pCO<sub>2</sub> ppm - partial pressure atmospheric CO<sub>2</sub> in parts per million

**References:** <sup>1</sup>Wobbe et al., 2012 <sup>2</sup>Eagles et al., 2004 <sup>3</sup>Gohl et al., 2013 <sup>4</sup>Müller et al., 2007 <sup>5</sup>De Santis et al., 1999 <sup>6</sup>Nitsche et al., 2000 <sup>7</sup>Dowdeswell et al., 2004, 2006 <sup>8</sup>Weigelt et al., 2009 <sup>9</sup>Klages et al., 2013 <sup>10</sup>Haq & Schutter, 2008 <sup>11</sup>Escutia et al., 2005, 2011 <sup>12</sup>Uenzelmann-Neben & Gohl, 2012 <sup>13</sup>Brancolini et al., 1995 <sup>14</sup>Brancolini & Leitchenkov, 2010 <sup>15</sup>De Santis et al., 2003 <sup>16</sup>Kipf et al., 2013 <sup>17</sup>This paper <sup>18</sup>Anderson, 1999 <sup>19</sup>Huber et al., 2004 <sup>20</sup>Miller et al., 2008 <sup>21</sup>Pollard & de Conto 2009 <sup>22</sup>Lowe and Anderson, 2002 <sup>23</sup>Haywood et al., 2009 <sup>24</sup>Berner & Kothavala 2001 <sup>25</sup>Zachos et al., 2001 <sup>26</sup>Barker, 2001 <sup>27</sup>LaBrecque et al., 1986 <sup>28</sup>Livermore et al., 2005 <sup>29</sup>Miller et al., 1990 <sup>30</sup>Lawver & Gahagan, 2003 <sup>31</sup>Ozko 1997 <sup>32</sup>Barker et al., 1991 <sup>33</sup>Pagani et al., 2005 <sup>34</sup>Lear et al., 2008 <sup>35</sup>Anderson, 2006 <sup>36</sup>Smith & Anderson, 2010 <sup>37</sup>Tripathi et al., 2009, 2011 <sup>38</sup>Wilson et al., 2013 <sup>51</sup>electronic supplement, S1.

Rise of New Zealand separated from the Pacific margin of West Antarctica at western Thurston Island and Marie Byrd Land between 90 and 83 Ma (Fig. 8-2; Table 8-1; e.g. Eagles et al., 2004; Wobbe et al. 2012). The basin opening propagated from East (older) to West (younger). In the East, multi-stage wide-mode rifting dominated (Wobbe et al., 2012; Kalberg and Gohl, 2013) whilst narrow-mode extension took place in the eastern Ross Sea (Luyendyk et al., 2003; Davey and De Santis, 2006; Jordan et al., 2010).

Between about 80 and 62 Ma, (C34y and c27o in Fig. 8-2) the Bellingshausen plate (BHP) moved independently from the Antarctic plate along the Proto-Antipodes fracture zone (Fig. 8-2; Larter et al., 2002; Eagles et al., 2004; Wobbe et al., 2012).

The southern margin of the BHP formed a diffuse, possibly distributed plate boundary zone crossing the Amundsen Sea Embayment (Fig. 8-2; Fig 9f in Wobbe et al; 2013). By 61 Ma, the BHP was incorporated into the Antarctic plate (Table 8-1; Cande et al., 2000; Eagles et al., 2004; Wobbe et al., 2012).

Shortly after the BHP demise, the Marie Byrd Seamounts (Figs. 8-1, 8-2; MBS) were emplaced until the early Cenozoic (65–56 Ma; Kipf et al., 2013; Table 8-1). Recent gravity and seismic refraction data modelling in the Amundsen Sea Embayment and eastern Amundsen Sea continental rise (line AWI-20060200, Fig. 8-2) suggest that MBS emplacement was accompanied by magmatic underplating due to partial melting (Kalberg and Gohl, 2013). Near the far eastern part of the Amundsen Sea basin, Apatite-He age trends indicate a major fault system was active during or after the Oligocene, but the extent thereof is uncertain (Lindow et al., 2011; Wobbe et al., 2012).

The remaining Oligocene, Eocene and Miocene stages of the basin development comprised on going passive margin rifting, which widened the Amundsen Sea basin to its present day geometry and extent (Figs. 8-1, 8-2).

### 8.3.2 Palaeoclimate development

Several palaeoclimate events occurred during the rifting and tectonic evolution of the Amundsen Sea basin, summarised in Table 8-1 and online supplement 1.1. The Cretaceous-Palaeocene climate (> 55.8 Ma) is thought to have been warm and relatively ice-free, with atmospheric CO<sub>2</sub> in the region of 900 ppm (Bernier and Kothavala, 2001, GEOCarb III), eustatic sea level ~200 m higher, and sea surface temperature (SST) 2–3° warmer than today (Haq et al., 1987; Haq and Schutter, 2008; Fig. 1-1 in Ch. 1).

Most of West Antarctica was elevated above sea level (Wilson et al., 2012; ANTscape G. Eagles, personal communication, 2011; Fig. 1-2 in Ch. 1) and the ocean gateways between East Antarctica and Australia (Tasmanian gateway) and between South America and the Antarctic Peninsula (Drake Passage/Scotia Sea gateway) were still closed (e.g. Bijl et al., 2013; Eagles and Jokat, 2014). A proto Amundsen Sea / Ross Sea gyre may have developed towards the late Palaeocene (Huber et al., 2004) and surface waters cooled sufficiently to initiate bottom water circulation (Uenzelmann-Neben and Gohl, 2012).



Initial stage deposits on the Pacific margin of East Antarctica comprised lava flows (units RSS-1 in the Ross Sea, WL-S1 on the Wilkes land margin; Table 8-1 and references therein) recognisable in multichannel seismic images (e.g. De Santis et al., 1999; Escutia et al., 2005).

In the early Eocene (55.8–42 Ma), atmospheric CO<sub>2</sub> doubled (1800 ppm) and the SST increased by a further 3° (Table 8-1; Fig. 1-1 in Ch. 1). These higher palaeoclimate indicators coincide with the maximum age extent of the Amundsen Sea basin. After 42 Ma, the atmospheric pCO<sub>2</sub> rapidly decreased (to 700 ppm, 38–33 Ma) and SST fell to only being 1° higher than today (Fig. 1-1 in Ch. 1). Shallow to deep water gateways developed in the Tasmanian and Drake Passage/Scotia Sea gateways while Antarctic's climate became increasingly cooler. By the Late Eocene/Oligocene transition, the first West Antarctic Ice sheet (WAIS) formed (Wilson et al., 2013; Table 8-1) and bottom currents in the Amundsen Sea intensified to such an extent that elongate sediment drifts formed in the eastern part (seismic Unit I in Table 8-1; Uenzelman-Neben and Gohl, 2012).

Compared to 70 Ma, the West Antarctica land topography was now significantly eroded and more parts in the Ross Sea shelf submerged (Fig. 1-2 in Ch. 1; Wilson et al., 2012; 2013). The Eocene/Oligocene transition is marked by high amplitude regional unconformities, visible in the Ross Sea and Wilkes Land seismic images (RSU6, WL-u3 in Table 8-1; De Santis et al., 1999; Escutia et al., 2005). Borehole information from IODP Leg 318 Site U1356 (Fig. 8-2 inset) confirmed the WL-u3 boundary as marking a transition from a warm ice-sheet free climate, hereafter referred to as Pre-glacial (PG) climate regime, to a colder climate with an dynamic ice sheet arrival at the coast (Escutia et al., 2011), hereafter referred to as a Transitional (T) climate regime (PG/T boundary, Table 8-1).

From the Oligocene to mid-Miocene (34–15.5 Ma) atmospheric pCO<sub>2</sub> spiked from 700 ppm to 1700 ppm (34–31 Ma) and fell again to ~500 ppm at 15 Ma (Table 8-1; Fig. 1-1 in Ch. 1; Tripate et al., 2009; 2011). Sea level decreased consistently to ~100 m higher than today, whereas SST stayed similar to present day temperatures (Haq and Schutter, 2008; Fig 1-1 in Ch. 1). The Southern Ocean gateways fully opened to deep-water passages, and the Antarctic Circumpolar Current (ACC) developed.

This period is marked by an increased amount of sediment deposition: seismic units RSS-3, RSS-4 in the Ross Sea (Table 8-1; Brancolini et al., 1995; De Santis et al., 1999; Brancolini and Leitchenkov, 2010); WL-S5 and WL-S4 in Wilkes Land (De Santis et al., 2003; Escutia et al., 2005; 2011) and Unit II in the eastern Amundsen Sea (Uenzelmann-Neben and Gohl, 2012). Elongate drifts and levee drift deposits in the eastern Amundsen Sea increased in response to intensified bottom water circulation (Uenzelmann-Neben and Gohl, 2012). In addition, sediment transport across the shelf and slope increased as the continental scale ice sheets had numerous advance/retreat cycles at the coast and advanced onto the inner shelf (De Santis et al., 1999; Brancolini et al., 1995; Haywood et al., 2009; Brancolini and Leitchenkov, 2010; Uenzelmann-Neben and Gohl, 2012; Gohl et al., 2013b).

By the mid-Miocene climate optimum (15.5 Ma in Table 8-1) the transitional climate regime developed into the current icehouse polar climate as SST and sea level continued to



fall, while atmospheric  $p\text{CO}_2$  level stayed between 200–400 ppm (T/FG boundary in Table 8-1; Fig. 1-1 and references therein; Anderson 1999).

The ice-house climate, hereafter referred to as the Full glacial (FG) climate regime, span the mid-Miocene to the present-day and is dominated by multiple grounded advance and retreat cycles of the West Antarctic Ice Sheet (WAIS) and East Antarctic Ice Sheet (EAIS) onto the outer shelf (Miller et al., 2008), and the building of progradational sequences (De Santis et al., 1999; Brancolini and Leitchenkov, 2010; Gohl et al., 2013b).

The ACC and Antarctic Bottom Water (AABW) circulation developed fully (Uenzelmann-Neben and Gohl, 2012) and the Antarctic topography changed, especially in West Antarctic and the Ross Sea, where much of the region were now submerged (see Fig. 1-2 in Ch. 1, compare the area in the red square in 34 Ma (Wilson et al., 2012; 2013) to the present-day topography (BEDMAP Lythe et al., 2001; ALBMAP Le Brocq et al., 2010)).

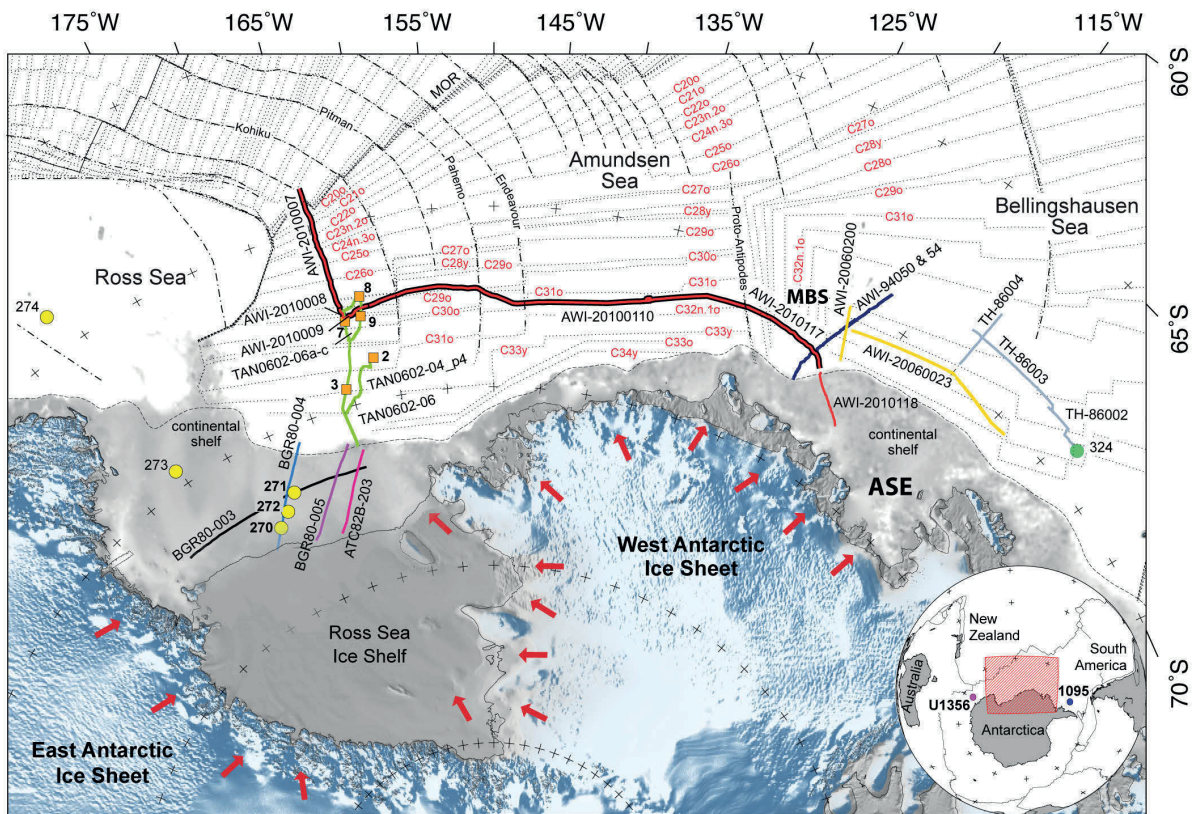


**Fig. 8-2.** Isochron compilation map for the Amundsen Sea and Ross Sea region modified after Wobbe et al. (2012). Isochrons are labelled in red and appended with o – old or y – young. Dashed lines – Fracture zones that cross the AS-RS transect (thick red/black line). Selected tie lines used in this work are annotated and summarised in Table 8-2. Main seismic surveys are AWI-2010 – red; Tan0602 – green; Ant2006 – yellow; Ant94 – navy; selected lines from BGR80 – labelled. Supporting age information was drawn from boreholes: yellow circles – DSDP Leg 28 drill sites 270, 271, 272; green circle – DSDP Leg 35 Site 324; and further afield, show on the inset: blue circle - ODP Leg 178 Site 1095; purple circle – IODP Leg 318 Sites U1356 and U1359. Velocity data for sediment thickness estimates were taken from selected Tan0602 sonobuoys – orange squares (Ch. 5), interval velocities from the AS-RS transect seismic data (Tables 8-3, 8-4; online supplement 1.2), and ocean-bottom seismograph (OBS) measurements on line AWI-20060200, annotated (Ch. 5; Kalberg and Gohl, 2013). Red arrows and background image for land are the same as for Fig. 8-1. MBS – Marie Byrd Seamounts.

The Full glacial climate seismic sequence comprise: units RSS-5 to RSS-8 in the eastern Ross Sea (Table 8-1; Brancolini et al., 1995; De Santis et al., 1999; Brancolini and Leitchenkov, 2010); WL-S9 in Wilkes Land (De Santis et al., 2003; Escutia et al., 2005; 2011) and Units III and IV in the eastern Amundsen Sea (Uenzelmann-Neben and Gohl, 2012). Borehole information from IODP Leg 318 Site U1356 (Fig. 8-2 inset) confirmed the WL-U5 boundary as marking a transition from dynamic to a persistent ice sheet (Table 8-1; Escutia et al., 2011).

## 8.4 Database and Methods

### 8.4.1 Seismic reflection data

The multichannel seismic profiles AWI-2010xxxx used to construct the AS–RS transect were acquired during the ANT-XXVI/3 *RV Polarstern* expedition (Figs. 8-1, 8-2; Table 8-2; Gohl, 2010). Exceptionally favourable sea-ice conditions allowed the acquisition of a continuous ~2000 km profile along the -72°S latitude, and a previously unsurveyed sector of the Pacific margin of West Antarctica. The TAN0206-xx lines in Figs. 8-1, 8-2 and Table 8-2 were acquired during the 2006 *RV Tangaroa* expedition and complement the AWI-2010 lines.

This combined dataset now links existing deep sea seismic data in the eastern Amundsen Sea (Nitsche et al., 1997, 2000; Scheuer et al., 2006; Gohl, 2007; Uenzelmann-Neben and Gohl, 2012) with some of the eastern Ross Sea shelf data in the eastern Ross Sea (Figs. 8-1, 8-2; Fritsch, 1980; Anderson and Bartek, 1992; ANTOSTRAT, 1995; Brancolini et al., 1995; De Santis et al., 1995, 1999; Brancolini and Leitchenkov, 2010), via an initial TAN0602–BGR80 shelf-slope link (Fig. 8-2). The acquisition and processing parameters for the ANT-XXVI/3 survey, hereafter referred to as the AWI-2010 survey and the TAN0206 survey are described below. Additional lines used in this work are summarised in Table 8-2 and elaborated upon in section 8.4.3 and 8.5.2.

#### 8.4.1.1 *The AWI-2010 survey on the RV Polarstern*

Most of the AWI-2010xx profiles used to construct the AS–RS transect (Figs. 8-1, 8-2; Table 8-2) were acquired using a 3000 m long SERCEL Sentinel streamer as receiver, with 240 active channels and towed at a nominal depth of 10 m. Profiles AWI-20100108 and AWI-20100109 are the exceptions where the long streamer was replaced with an older, analogue 600 m long Prakla streamer with 96 channels due to changing sea-ice conditions. These two profiles are short (34 km and 54 km respectively, Table 8-2) and had a minimal impact on the overall transect data quality or continuity. In all cases, the source consisted of two to three GI-Guns of 4.8–7.2 litres (300–450 in<sup>3</sup>) total volume, fixed to a steel frame and towed ~7 m behind the vessel in ~3 m water-depth. Shots were fired at a 12-second interval

in true GI-mode and at 195 bar nominal operational pressure. Data were sampled at a 1 ms and recorded to 10 s trace length using the on-board SEAL recording system (SERCEL). Restrictions by the German Federal Environmental Agency prevented the use of a larger airgun source needed to image the basement beneath very thick sedimentary layers. Consequently, basement was poorly imaged in some cases, especially in profile AWI-20100117 in the East.

Some data gaps occur due to stopping acquisition when marine mammals were observed close to the vessel and appear as white strips in the seismic images. A large data gap of ~50 km exist between shot points 14075–15535 and common-mid-point (CMP) 19312–21314 on line AWI-20100110 (Fig. 8-3), due to a fault in the recording system. However, because the seismic units and reflectors are continuous, dominantly horizontal and undisturbed over vast distances, they matched up precisely on either side of the data gap without applying a static shift and it was possible to omit the data gap. This facilitated an improved visualisation of the data and continuity of the seismic interpretation across this most central part of the Amundsen Sea basin.

**Table 8-2.**

Post-stack time migrated seismic reflection profiles used in this study, totalling 5412 line km. Lines are listed in order of appearance, from west to east, as shown on the map in Fig. 1. See text for the processing details on the AWI-2010 and the TAN0602 data.

Profile	Cruise, year, ship	Profile length [km]	Length (msec)	Sample Rate (msec)	First SP	Last SP	First CDP	Last CDP	Source (# airguns, total volume)	Receiver (streamer length [m], channels)
BGR80-003	BGR-80, 1980, E	612.6	8000	4	1	12253	-	-	G-gun array, 23.5 l	2400 m, 48
BGR80-004	BGR-80, 1980, E	617.8	9000	4	1	12355	-	-	G-gun array, 23.5 l	2400 m, 48
BGR80-005	BGR-80, 1980, E	320.5	8000	4	1	6409	-	-	G-gun array, 23.5 l	2400 m, 48
ATC82B-203	ATC-82B, 1982, F	287.9	9000	4	1	5758	-	-	tuned airray, 36 l	2000 m, 48
TAN06020-06	TAN-0602, 2006, T	306.1	12000	2	1001	7150	100	12342	4 GI-guns, 9.8 l	200 m, 32
TAN0602-04p4	TAN-0602, 2006, T	245.3	12000	2	8501	13979	100	9910	4 GI-guns, 9.8 l	100 m, 16
TAN0602-06A	TAN-0602, 2006, T	150.4	12000	2	1001	4011	100	6116	4 GI-guns, 9.8 l	200 m, 32
TAN0602-06B	TAN-0602, 2006, T	72.2	12000	2	1001	2459	100	2988	4 GI-guns, 9.8 l	200 m, 32
TAN0602-06C	TAN-0602, 2006, T	160.3	12000	2	1001	4612	100	6512	4 GI-guns, 9.8 l	200 m, 32
AWI-20100107	ANT-XXVI/3, 2010, PS	390.4	10000	1	1	11920	66	15742	3 GI-guns, 7.5 l	3000 m, 256
AWI-20100108	ANT-XXVI/3, 2010, PS	33.9	10000	2	1	1002	17	1386	3 GI-guns, 7.5 l	600 m, 96
AWI-20100109	ANT-XXVI/3, 2010, PS	89.4	10000	2	1	2695	17	3606	3 GI-guns, 7.5 l	600 m, 96
AWI-20100110	ANT-XXVI/3, 2010, PS	917.6	10000	1	1	27181	66	36829	3 GI-guns, 7.5 l	3000 m, 256
AWI-20100117	ANT-XXVI/3, 2010, PS	571.5	10000	1	1	17465	66	22987	3 GI-guns, 7.5 l	3000 m, 256
AWI-94050	ANT-XI/3, 1994, PS	175.7	10000	2	1	4153	18	7046	8 GI-guns, 24 l	600 m, 96
AWI-94054	ANT-XI/3, 1994, PS	290.2	10000	2	1	6740	18	11623	8 GI-guns, 24 l	600 m, 96
AWI-20060200	ANT-XXIII/4, 2006, PS	170.3	8000	4	1	1111	8	3448	8 G-guns, 68.2 l	600 m, 96

**References:** BGR-80xx lines - Fritsch (1980), Hinz and Block (1985) and ANTOSTRAT (1995); ATC-82xx line - Wannesson et al. (1985); AWI-94xx lines - Gohl et al. (1997), Nitsche et al. (1997, 2000), Uenzelmann-Neben et al. (2007); AWI-2006xx - Gohl (2007), Uenzelmann-Neben and Gohl (2012), Kalberg and Gohl (2014); online supplement S5. The AWI-2010xx and TAN-06xx lines pertain to this study.

**Abbreviations:** mig - migration, E - RV Explora, F - RV Francias, T - RV Tangaroa, PS - RV Polarstern.

Seismic processing followed a standard approach using the processing software FOCUS (by Paradigm). The data was not resampled and kept at 1 ms in all processing steps. After trace editing a high pass filter tapered at 5–10 Hz was applied, to allow higher frequencies and maximum resolution of the data. Channels 2, 7, 8–10, 43, 70, 105 and 106 were

particularly noisy and muted throughout the AWI-20100107, -110 and -107 lines. Both predictive and spiking deconvolution were tested for removing the ghost and internal multiples prior to velocity analyses. Spiking deconvolution effectively removed the ghost when using a 30 ms window, 100 ms operator length and 0.1% white noise, but introduced ringing artefacts in key parts of the deeper sequences and across major sequence boundaries after stacking. It was therefore only applied during velocity analyses and in selected cases to more clearly image unconformities, geometry of drifts, or the seismic unit boundaries.

Static corrections of up to 2 ms were applied to profiles AWI-20100108 and -109, because the 600 m streamer was not equipped with depth control devices due to sea-ice. The ghost on these two profiles was effectively removed with the application of an F-K filter.

Velocity analysis was applied at every 50<sup>th</sup> CDP and intervals were picked to match sequence boundary horizons closely. After normal-move-corrected (NMO) and spherical divergence adjustment, a Kirchoff time-migration was applied to the stacked section. A maximum migration angle of 65 degrees and 90% of the NMO velocities were used.

The interpretation of the seismic images is based on the change in seismic characteristics such reflectivity and variation of internal reflection geometries. No additional filters or amplitude scaling were applied to most sections, so that true amplitudes were largely preserved. In one case, AGC was partially applied on line AWI-20100117, between CDP's 15000 – 22988 to image the basement more clearly.

#### *8.4.1.2 The TAN0602 survey on the RV Tangaroa*

The RV Tangaroa acquired 3409 km of seismic data, and velocity data from 16 sonobuoys, during the 2006 TAN0602 marine geophysical survey in the Ross Sea conducted by NIWA and GNS Science of New Zealand (Fig. 8-1; Table 8-2; Ch. 5). Eleven seismic lines were acquired with a 300 m streamer with 48 channels (near offset ~129 m and far-offset ~422 m) towed at a nominal depth of 10 m. The source consisted of 4 GI-Guns (9.8 L) towed at 5 m depth and fired in true GI-mode, resulting in a shot spacing of 50 m. Recording was done for 12 s at a sample rate of 1 ms and a 10 Hz low-cut filter applied during acquisition.

The lines vary in geometry and acquisition parameters due to sea-ice conditions, which introduced additional noise and necessitated processing in parts. This particularly affected line TAN0602-04 where noise due to sea-ice conditions, and damage caused by the snagging and parting of the streamer by an iceberg, reduced sections of the 48 channel streamer to 16 on the whole array (Table 8-2). Channels 1, 7 and 33 were consistently noisy and were muted throughout.

Preliminary seismic data processing to final migrated stacks were done on-board using the shot point navigation. Zero traces were inserted for missing shots to account for <10 km wide gaps and jumps in the line geometry. Line gaps of >10 km were processed as separate lines (Fig. 8-2 and Ch. 5). A 25 m CMP spacing ensured a good signal-to-noise ratio.



A standard final processing flow was used in the GNS Science's in-house developed GLOBE CLARITAS seismic processing package and included: resampling the data down to 2 ms, applying a 225–250 Hz low pass filter, standard muting of noisy traces and data spikes before velocity analyses, followed by stacking. After stacking a band-pass filter of 4–24 Hz was applied and finite difference migration was done, with a dip migration of 45 degrees and 100% of the NMO velocities were used. The finite difference post-stack migration produced a clearer true-dip image.

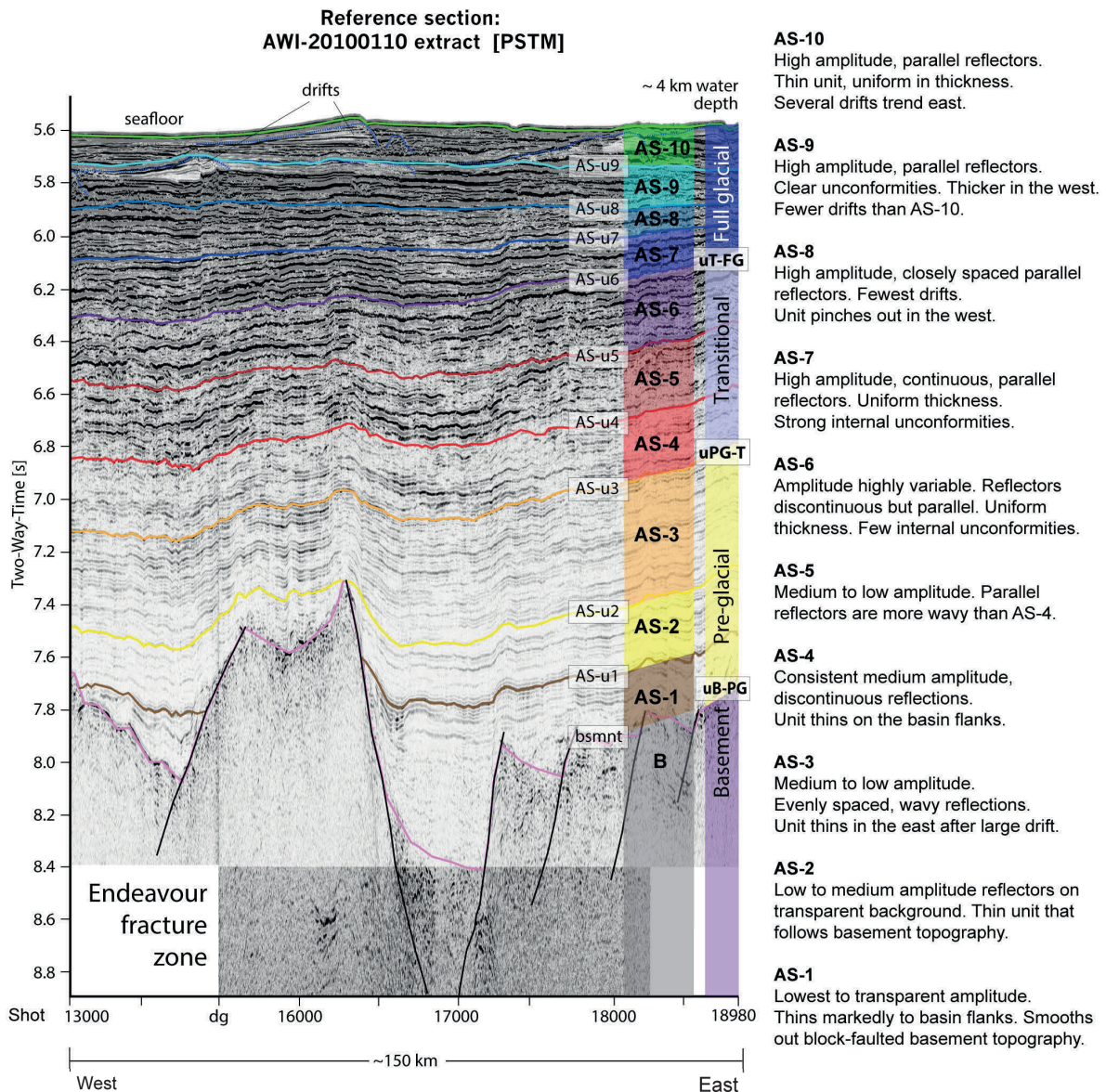


**Fig. 8-3.** Type section of the seismic reflection units observed in the Amundsen Sea basin, see Fig. 8-1 for location. The proposed Amundsen Sea basin and circum-Antarctic stratigraphy nomenclature are superimposed. Vertical exaggeration is ~ 50x. The characteristics of each seismic unit or sequence are listed on the right. The units are numbered from the basement upwards, AS-1 to AS-10 and separated by top of unit discontinuities, labelled AS-u1 to AS-u10. On the far right: The proposed circum-Antarctic stratigraphy sequences, interpreted to represent acoustic basement (B), pre-glacial (PG), transitional (T) and full glacial (FG) regime processes. Each sequence is separated by the associated base reflector discontinuities: uB-PG, uPG-T and uT-FG, respectively. dg – data gap between shot points 14075 – 15535, see text for explanation.



The 16 sonobuoys were deployed to a depth of 300 m and the transmission continued for eight hours. The trace length was initially at 14 s (sonobuoys 2, 3 and 5) then extended to 16 ms for the rest (Ch. 5). All sonobuoys, except 12 and 15, showed clear reflected arrivals to offsets of >10 km. A low cut frequency filter of 10 Hz and high cut frequency filter of 250 Hz was applied. The detailed acquisition, processing and analyses steps for the sonobuoys are in Ch. 5. The velocities at sonobuoy stations 8 and 5 are of particular relevance to this work (see section 8.4.3.3).

## 8.4.2 Interpretations approach

### 8.4.2.1 *Type section*

Prior to interpreting the all relevant AWI-2010 and TAN0602 lines (Table 8-2) and linking it with the interpretation of previous surveys, we independently identified the prominent horizons and unit boundaries observed in the processed seismic images, following an unbiased approach. To achieve this unbiased approach, we selected a representative type section in the central part of the Amundsen Sea basin, line AWI-20100110 (Figs. 8-1, 8-2), with the assumption that the sediments are likely to be the thickest and least disturbed, and thus would present the best possible opportunity to identify all the potential basin-wide units (Fig. 8-3; see Fig. 8-1 for location). In mapping the initial prominent first and second order boundary horizons, we looked for variation in seismic facies characteristics such as reflectivity, reflection continuity and internal geometry in the vertical axis of the type section image in Fig. 8-3.

### 8.4.2.2 *Seismic characterization*

Subsequently we compared our initial horizons in the type section interpretation to observations from several studies in other deep sea basins around Antarctica that identified pre-glacial to glacial sedimentary sequences in seismic reflection data, some of which are tied to drilling information (e.g. eastern Amundsen Sea: Nitsche et al., 1997, 2000; Uenzelmann-Neben and Gohl, 2012; Bellingshausen Sea: Scheuer et al., 2006; Weddell Sea: Maldonado et al., 2006; Lindeque et al., 2013; Riiser Larsen Sea: Leitchenkov et al., 2008; Cosmonaut Sea: Leitchenkov et al., 2007a; Mawson Sea: Leitchenkov et al., 2007b; Wilkes Land: De Santis et al., 2003; Escutia et al., 2011; Ross Sea: De Santis et al., 1995; Brancolini and Leitchenkov, 2010). Shelf studies were not considered under the premise that sediment processes on the shelf vary from those in the deep-sea basins and the resulting shelf stratigraphy would therefore be an unsuitable analogue for this objective. We used these collective interpretations and seismic horizon characteristics of the pre-glacial to glacial units, as analogues to assess if similar packages can be recognised in the Ross Sea and central Amundsen Sea deep-sea basins. The assumption being that if these sequences were identified on an almost circum-Antarctic scale in several of the deep-sea basins, two of these locations being on either side of the study area, it is very likely that similar sequences could be present.

In some parts of the eastern Amundsen Sea and around the Marie Byrd Seamounts, the FG and T sequences contain distinctive mass sediment transport bodies such as sheeted or mounded drifts – interpreted to have formed by contour and coast parallel bottom currents, and channel-levee systems – interpreted to have formed by mass sediment down-slope gravity-driven transport (e.g. Uenzelmann-Neben and Gohl, 2012). Hence, identifying drifts or channel-levees in the seismic images of the central Amundsen Sea could similarly give an indication of the palaeo-depositional processes and palaeo-bottom current activity in the central Amundsen Sea basin.

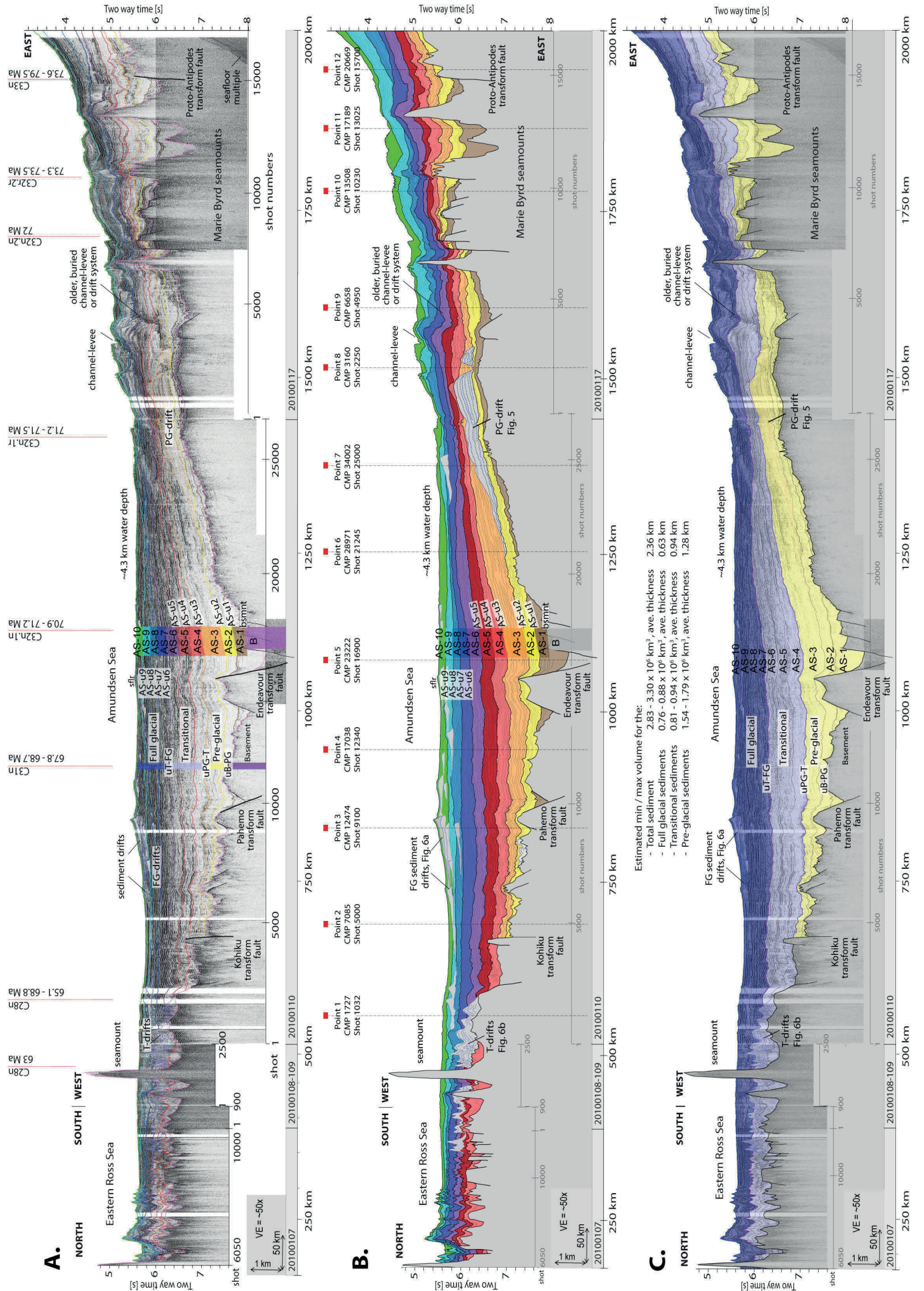
#### 8.4.2.3 *Horizon mapping*

The type section interpretation was expanded into the regional basin context through an ~2000 km long Amundsen Sea – Ross Sea (AS-RS) transect. The AS-RS transect was constructed from 8 pre-stack time migrated profiles of continuous seismic data from the AWI-2010 survey (Figs. 8-1, 8-2; Table 8-2; Gohl, 2010), shown in Figs. 8-4a and Appendix B-1. It runs approximately through the central axis of the basin length along the 72°S latitude and is the only seismic dataset that crosses full length of the Amundsen Sea deep-sea basin. Due to these aspects the data presented are currently the most representative data of this deep-sea basin sediment archive.

To test the initial unit boundary horizons interpretation in the type section (Fig. 8-3) within the extensive AS-RS transect, not only the marker horizons, but also every internal reflection were traced up to the farthest western and eastern flanks of the basin and for the full extent of the transect dataset. In so doing, we were able to identify low-angle onlap or downlap unconformities and depositional angle changes (Fig. 8-5).

Lastly we mapped the block-faulted basement, the corresponding fracture zones (Fig. 8-2, 8-4, Appendix B-1), and larger internal structures such as drifts and channel-levee systems (Fig. 8-6). From independent analyses of the central transect, we were in a position to assess if the unit boundaries and preliminary sequence boundaries correlate with the existing survey interpretations in the Ross Sea and eastern Amundsen Sea (Fig. 8-1).

**Fig. 8-4.** The Amundsen Sea – Ross Sea transect. (A) Seamless multichannel seismic acoustic image of the western, central and eastern Amundsen Sea and eastern Ross Sea, represented in a post-stack time migrated (PSTM) section. White strips in the seismic image signify data gaps, caused by recording stopped due to the presence of marine wildlife in a <1 km radius to the ship. Interpreted horizons, also referred to as sequence or unit boundaries, as identified according to the type section (Fig. 8-3) are overlain in various colours and annotated. Profile numbers, shot number range and kilometre scales are annotated below. Red dashed lines represent the magnetic anomalies crossing the AS-RS transect, taken from Wobbe et al. (2012; Fig. 8-2). (B) Interpretative line drawing of the PSTM seismic section in (a) with the seismic units and associated boundaries. These boundaries are defined by unconformities within the internal reflections (thin back lines in each unit, also see Fig. 8-5). A high-resolution version of this figure is available in Appendix B-1. Note the presence of drifts in units AS-3 (East), AS-5 (West), AS-8 (East and West), AS-9 (West and central) and AS-10 (West and central) shown in light grey. Red squared and dashed drop down lines represent points selected for sediment thickness and sedimentation rate calculations (Fig. 8-10; Tables 8-3 and 8-4; Ch. 5; Appendix B-2). (C) Seismic units in (b) represented as those deposited in the Pre-glacial (PG) climate regime – yellow polygon, the Transitional (T) climate regime – pale blue polygon, and full glacial (FG) climate regime – darker blue polygon. Each group is separated by a regional unconformity, labelled uPG-T and uT-FG, respectively.





### 8.4.3 Integrating pre-existing data

#### 8.4.3.1 *Seismic reflection surveys*

There are three points where the AS-RS transect ties into the regional seismic survey network. The first is at the western end of the AS-RS transect, between the ANT2010 and TAN0602 surveys, linking the Amundsen Sea deep-sea seismic profile network with that of the eastern Ross Sea (Fig. 8-2). Lines AWI-20100107 and AWI-20100108, connect to line TAN0602-06a, whereas line TAN0602-06c crosses line AWI-20100109 (Figs. 8-1, 8-2). This key seismic stratigraphic link is illustrated in 3D in Fig. 8-7. Since the TAN0602 dataset has no previously published interpretation, the AS-RS transect horizons were extended onto these lines.

The second key seismic stratigraphic link consists of the Ross Sea shelf-slope connection between the TAN0602 and AWI-2010 interpretation (this chapter), and the BGR80 interpretations (Fritsch, 1980; Hinz and Block 1985; ANTOSTRAT 1995) in particular, line BGR80-005 connecting to TAN0602-06 (Figs. 8-2, 8-8; Table 8-2).

Line ATC82B-203 (Fig. 8-2; Table 8-2; Wannesson et al., 1985) provided additional information on the shelf break where the reflections were obscured by multiples or unclear.

The BGR80-005 interpretation was used as published and the AS-u... unconformities were traced up the slope, across the shelf along lines BGR80-003 and BGR80-004 (Fig. 8-2; Table 8-2) and up to line PD-30 (Anderson and Bartek, 1992, interpretation used as is) to see if they matched. The Ross Sea shelf-slope link is an initial attempt to tie the shelf data with the greater Amundsen Sea deep-sea horizons. The correlation is shown in Fig. 8-8.

The third key seismic stratigraphic link lies in the eastern Amundsen Sea, on the far eastern end of the AS-RS transect (Figs. 8-1, 8-2). At this intersection, profile AWI-20100117 of the AS-RS transect crosses lines AWI-94050 and AWI-94054 (Table 8-2; Gohl et al., 1997; Nitsche et al., 1997, 2000; Uenzelmann-Neben and Gohl, 2012), linked to line AWI-20060200 (Table 8-2; Ch. 5; Gohl 2007; Uenzelmann-Neben and Gohl, 2012; Kalberg and Gohl, 2013). The eastern Amundsen Sea link correlation is illustrated in 3D in Fig. 8-9. The AWI-94050 and AWI-94054 horizons and interpretations were used as published (Uenzelmann-Neben and Gohl, 2012) and matched to the proposed central Amundsen Sea basin horizons (Figs. 8-3, 8-4; Appendix B-1). Line AWI-20060200 was newly interpreted because a detailed seismic horizon interpretation is unpublished (Ch. 5).

#### 8.4.3.2 *Borehole information*

Boreholes are absent in the central Amundsen Sea basin. We therefore used the borehole controlled age model from the outer eastern Ross Sea shelf, derived from DSDP Leg 28 Sites 270–272 (Figs. 8-1, 8-2; Hayes and Frakes, 1975) as a guide to estimate ages of interpreted slope and deep-sea horizons in the AS-RS transect, via a series of seamlessly linked profiles and extended horizons (Fig. 8-2; Table 8-2 and references therein).

To the West of the Ross Sea continental rise, the nearest deep-sea borehole is IODP Leg 318 Site U1356, off the Wilkes Land margin (Fig. 8-2 inset; Escutia et al., 2011) approximately 1300 km away from the most western point of the AS-RS transect. We used the seismic reflectivity characteristics of the dated, and biostratigraphically analysed pre-glacial, transitional and full-glacial sequences, as an analogue to place observations in the AS-RS Transect in a provisional age- and stratigraphic framework.

To the East of the Amundsen Sea, the nearest borehole DSDP Leg 35 Site 324 (e.g. Tucholke et al., 1976) is located in the Bellingshausen Sea, about 1000 km from the eastern most end of the AS-RS transect (Fig. 8-2). This drill site only provides information for the uppermost 200 m and found Pleistocene and Pliocene aged sediments. DSDP Leg 35 Site 323 lies on the abyssal plain and contain predominantly pelagic deposits. Neither of these two drill sites was considered useful for the objectives of this work. Farther to the East on the Antarctic Peninsula margin, ODP Leg 178 Site 1095 is more applicable (Fig. 8-2 inset; Barker et al., 2002). Sequences of mid-Miocene age in a sediment drift deposit were drilled and dated (e.g. Iwai et al., 2002; Uenzelman-Neben 2006). Although the drill site lies over 2000 km from the easternmost point of the interpreted AS-RS transect, it was used in Scheuer et al. (2006) and Uenzelmann-Neben and Gohl (2012) for the horizon correlation and age model verification in the Bellingshausen Sea (Figs. 8-1, 8-2), and was considered as supporting information.

#### *8.4.3.3 Velocity measurements for sediment thickness estimates*

Sediment thickness-depth sections were constructed from 12 points along the AS-RS seismic transect (Figs. 8-1, 8-4; Appendices B-1, B-2). The points were chosen to represent the trends of the changes in sediment thickness and basin geometry and are therefore irregularly spaced. Due to distant borehole information and absent refraction data in the central Amundsen Sea basin, it was necessary to use the interval velocities, derived from the RMS stacking velocities, in order to convert the sediment thickness from two-way-time to metres. Spiking deconvolution was applied in the velocity analyses in order to consistently pick the velocity intervals on the sequence boundaries. Supporting velocity information was extracted from sonobuoys 5 and 8 collected on the TAN0602 expedition (Fig. 8-2; Appendix B-2) and compared to a reworked refraction model of profile AWI-20060200 (Fig. 8-2; Ch. 5). Since refraction data is usually optimised for studies of the crust, the sediments in line AWI-20060200 is usually seen as a single layer (Kalberg and Gohl, 2013). It was thus necessary to recreate a simple 1D velocity model from stations ST205 and ST206, with layers picked according to the main identified seismic sedimentary units (Ch. 5). The interval velocities, derived from the stacking velocities (see the compiled velocity model in Appendix B-2), at each one of the 12 points, compare well to the interval velocities of refraction line AWI-20060200 (Ch. 5) even though the refraction line is ~1000 km from the transect and near to the upper slope. The velocities used are also consistent with the sonobuoy velocities in the Ross Sea (Ch. 5).



Uncertainties of up to 50 m in sediment thickness occur due to the TWT picks accuracy that can differ by half or a full phase cycle, depending on the visual interpretation. The uncertainties of interval velocities are estimated at 0.1 km/s.

### 8.4.4 Age model and sedimentation rate estimates

Due to the sparse or completely absent borehole information, there is no direct control on the basement age of the Amundsen Sea basement. Alternatively, oceanic basement age control was obtained from the magnetic seafloor spreading anomalies of Wobbe et al. (2012). The magnetic seafloor spreading anomaly isochrones that crosses the AS-RS transect are delineated as thin black dashed lines in Fig. 8-2 and the isochrones annotated in red, key fracture zones are labelled. These were used in conjunction with the seismic reflection data to derive a stratigraphic age model. The age model was constructed as follows:

Each of the 12 points used in the sediment thickness-depth sections (section 8.5.3) were assigned the age of the closest isochron, or the age was linearly interpolated between the two closest anomalies (Fig. 8-4; Appendix B-1). This age was then used to place the basement horizon in each of the 12 sections at the corresponding age position on the geological time scale, and the sections vertically stretched so that seafloor matched 0 time (Fig. 8-10). To estimate the relative depositional time span of each unit, the first and last occurrence of that unit was projected back onto the time scale (thin colour bars on the left in Fig. 8-10). The deduced age range for each unit was used in conjunction with the 12 point-based sediment thickness estimates (Table 8-3) to calculate the sedimentation rates (Table 8-4).

The age model and seismostratigraphy presented here are based on all available data in the region and provide a first provisional framework, which allows an improved analysis of the pre-glacial to glacial processes of West Antarctica, and, provides a basis for implementing palaeobathymetry grids as well as palaeo-ice sheet modelling.

## 8.5 Results

### 8.5.1 Seismic interpretation and horizon characteristics

#### *8.5.1.1 Type section and nomenclature definition*

The representative central section of the AS-RS transect (see Fig. 8-2 for location) and the assigned a new bottom-to-top seismic stratigraphy nomenclature are shown in Fig. 8-3, with the comparison to the type sections from three other Antarctic deep-sea basins summarised below. Prominent horizons or unconformities were assigned up-sequence as AS-u1, AS-u2 and so on. AS stands for Amundsen Sea and -ux for the discontinuity or unconformity horizon number. Similarly, the sequence units between two boundary horizons were assigned AS-1, AS-2 etc. and numbered up-sequence.

We started the interpretation with the delineation of the basement horizon and observed block faulting (bsmnt and black angular lines in Fig. 8-3). Continuing up from the basement, the first high amplitude, continuous reflector was assigned as AS-u1, followed by AS-u2. Both reflectors stood out prominently against the low amplitude to transparent background. The next unit boundaries were identified at reflectors AS-u3, AS-u4, and AS-u5, as amplitudes increased consistently up-sequence and the internal unit reflections geometry changed to more closely spaced.

AS-u6 is mapped along a low angle unconformity with onlap up-dip (between 6.2 – 6.4 s and shot numbers 17000–18000 in Fig. 8-3) and also marks a strong amplitude increase of all the units above this horizon. AS-u7 and AS-u8 are high-amplitude unconformities as well, and -u9 was chosen at the base of the drifts, but above what seems to be a truncated drift (at 5.75 s and shot numbers 15000–16500).

In concluding this step, we initially identified two horizons (AS-u4, AS-u6 in Fig. 8-3) as the preliminary boundary horizons for the first order sequences. However, it was still ambiguous at this stage if either AS-u4 or AS-u3 would be the lower 1<sup>st</sup> order sequence boundary. A more conservative approach was taken by favouring AS-u4, because the internal amplitudes of AS-u4 seemed higher (i.e. darker grey in the image) than AS-u3. This boundary horizon was re-evaluated again more closely in the comparison with other type sections around Antarctica and the regional transect mapping (section 8.4.2).

To identify the pre-glacial to glacial sequences and characteristics, we compare our type section to other type sections of deep-sea basins around Antarctica. These studies typically described the pre-glacial seismic sequence as the initial series of discontinuous reflections, showing low amplitude to transparent reflectivity and occurring just above the crystalline basement. Internal reflections are predominantly parallel to each other and the basement topography. If plotted in true amplitude, this sequence appears light grey to white on a grey scale seismic image e.g. units below WL-u3 in Escutia et al. (2011), unit WL-S3 in DeSantis et al. (2003, Figs. 8-3, 8-4) Unit I in Uenzelmann-Neben and Gohl (2012, line AWI-94054 in Fig. 8-2d) and units WS-S1 to WS-S3 in Lindeque et al. (2013, Figs. 8-4, 8-6 and Appendix B-1).

These studies described the reflectors in the transitional (T) sequence units as closer spaced, horizontal to wavy, and of medium amplitude with internal structure or discontinuities. Buried drifts and cut-and-fill geometries can occur infrequently. This sequence typically has a medium grey appearance if plotted without display filter adjustments e.g. WL-S4 and WL-S5 in Escutia et al. (2011) and DeSantis et al. (2003; Figs. 8-3, 8-4), Unit II in Uenzelmann-Neben and Gohl (2012, line AWI-94054 in Fig. 8-2d) and unit WS-S4 in Lindeque et al. (2013; Figs. 8-4, 8-6 and Appendix B-1).

The full glacial (FG) sequence units were mostly characterised the highest amplitude reflections and strong lateral continuity. Internal reflections are parallel and closely spaced, with a collective dark grey to partly black appearance on a greyscale seismic image of true amplitudes e.g. WL-S6 to WL-S8 in Escutia et al. (2011) and DeSantis et al. (2003; Figs. 8-

3, 8-4), Units III and IV in Uenzelmann-Neben and Gohl (2012, line AWI-94054 in Fig. 8-2d) and units WS-S5 to WS-S7 in Lindeque et al. (2013, Figs. 8-4, 8-6, Appendix B-1).

Using the seismic characteristics identified in these other studies as a guide, we visually identified the uPG-T and uT-FG boundaries in our type section, interpreted as separating the 1<sup>st</sup> order pre-glacial, transitional and full-glacial sequences (annotated in Fig. 8-3). The ambiguity around AS-u3 / AS-u4 became clearer and AS-u3 was favoured as the lower (uPG-T) 1<sup>st</sup> order sequence boundary instead. In the central Amundsen Sea type section (Fig. 8-3) we describe the pre-glacial, transitional and full glacial sequence as follows:

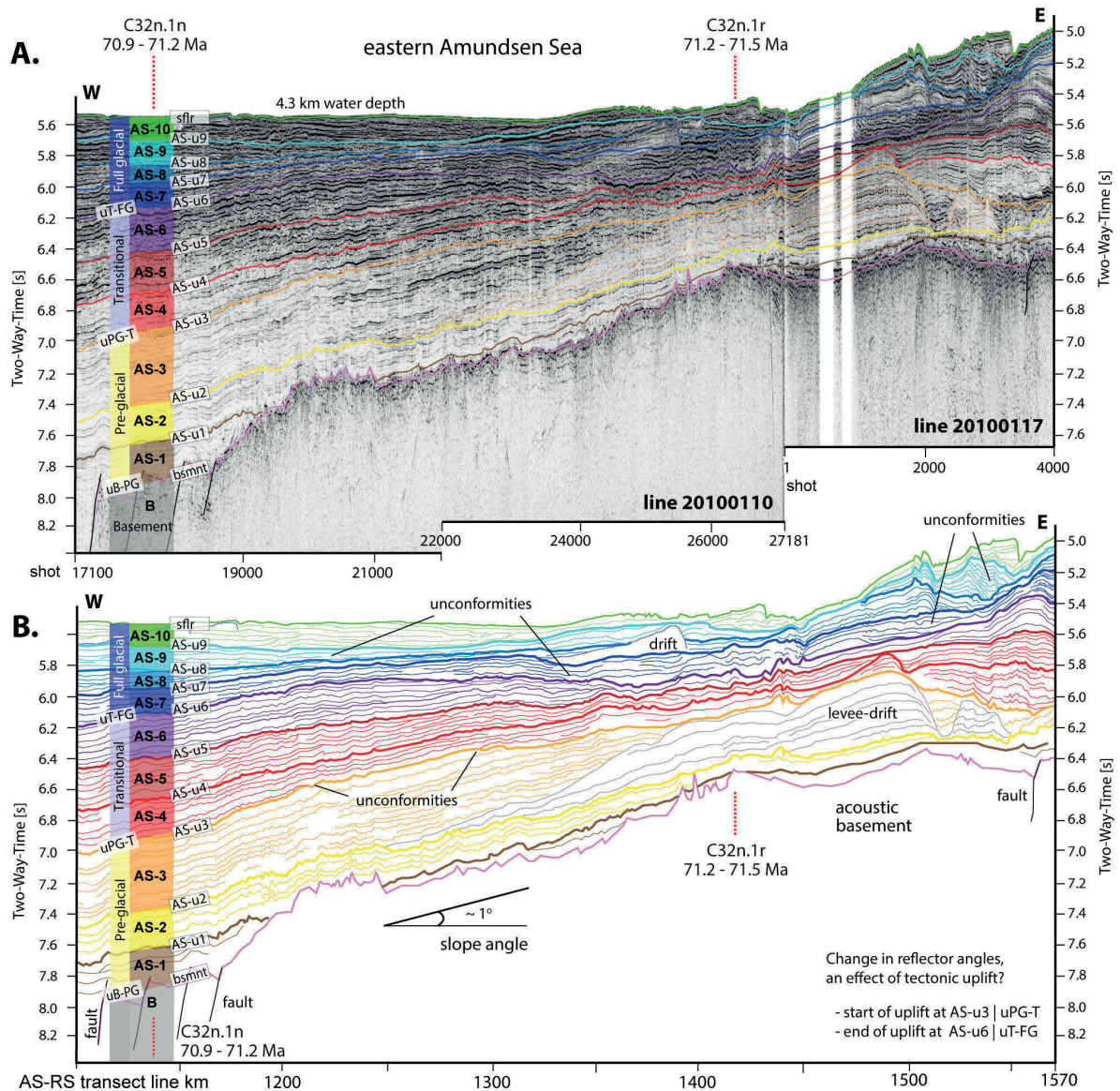


Fig. 8-5. Interpretation of an extract from the AS-RS transect (Fig. 8-4; Appendix B-1) to illustrate the low-angle onlap and downlap unconfomities observed in the PSTM image, used to determine the boundaries for the sequences deposited in the pre-glacial, transitional and full glacial climates regimes. (A) AS-RS transect multichannel seismic data image from lines AWI-2010110 and -117 (Figs. 8-1, 8-2, 8-4 and Appendix B-1) with the main seismic unit boundaries overlain and annotated. Red dashed lines represent the magnetic anomalies crossing the AS-RS transect, taken from Wobbe et al. (2012; Fig. 8-2). (B) Line drawing of the seismic image in (a) with the unconfomities annotated. Note how the reflector angles change: parallel to the basement slope up to AS-u3, then more angular up to AS-u6, and progressively more horizontal towards the top units. A 2<sup>nd</sup> order internal unconfomity occurs in AS-3, which terminates against the drift. Smaller scale internal unconfomities were mapped in the other units (annotated).

- The uniform pre-glacial sequence displays a low to transparent reflectivity and lack internal structure, which indicates well-sorted sediments, probably associated with river transport processes active in the greenhouse period of Antarctica.
- The glacial transitional sequence has medium to low amplitude reflectivity and the reflectors are discontinuous, parallel and evenly spaced. The higher amplitudes are probably due to poorer sorted material, associated with increased down-slope gravity-driven and along-slope bottom current driven sediment transport processes.
- The full glacial sequence shows the highest reflectivity and the reflectors are parallel and closely spaced. Drifts occur in AS-9 and AS-10. The high amplitudes are interpreted as being indicative of the continued supply of predominantly poorly sorted material through mass down-slope sediment transport processes as ice sheets oscillated on the shelf.

Even though these type sections in the Weddell Sea, eastern Amundsen Sea and Wilkes Land studies are far apart from each other, and from this study's central Amundsen Sea type section, the visual resemblances of the PG, T and FG sequences between the type sections, when placed directly next to each other, are striking.

#### *8.5.1.2 Seismic characterization and horizon stratigraphy*

We used the nomenclature and marker horizons from the type-section to map the remaining full length of the AS-RS transect and present new basin-wide seismic stratigraphy for the Amundsen Sea deep-sea basin (Figs. 8-4, 8-5 and Appendix B-1).

The acoustic basement topography is irregular and rugged along the western basin flank (line AWI-20100107 in Figs. 8-1, 8-2) as well as on the eastern Amundsen Sea flank (line AWI-20100117 in Figs. 8-1, 8-2). The basin geometry deepens towards middle of the transect, forming a classic 'saucer shape' and a valley in the centre (line km 1000 to 1200 in Fig. 8-4 a, b and Appendix B-1). To the left of the centre point (line km 700 to 1100), block faulting was mapped. The fracture zones predicted in the magnetic data (Wobbe et al., 2012) match major basement faults observed in the AS-RS transect seismic reflection data (Kohiko-, Pahemo- and Endeavour fracture zones, labelled in Fig. 8-2 and Fig. 8-4). Magnetic seafloor spreading anomalies crossing the transect are annotated in red dashed lines and labelled (Fig. 8-4a and Appendix B-1).

In the region to the left of the centre point (line km 1100 to ~1650) and up to the first seamount (near line km 1700 in Figs. 8-2, 8-4, 8-5 and Appendix B-1), the basement topography is anomalously smoother and without faulting. The slope angle of this anomalous part is ~1 degree (Fig. 8-5, vertical exaggeration ~110x).



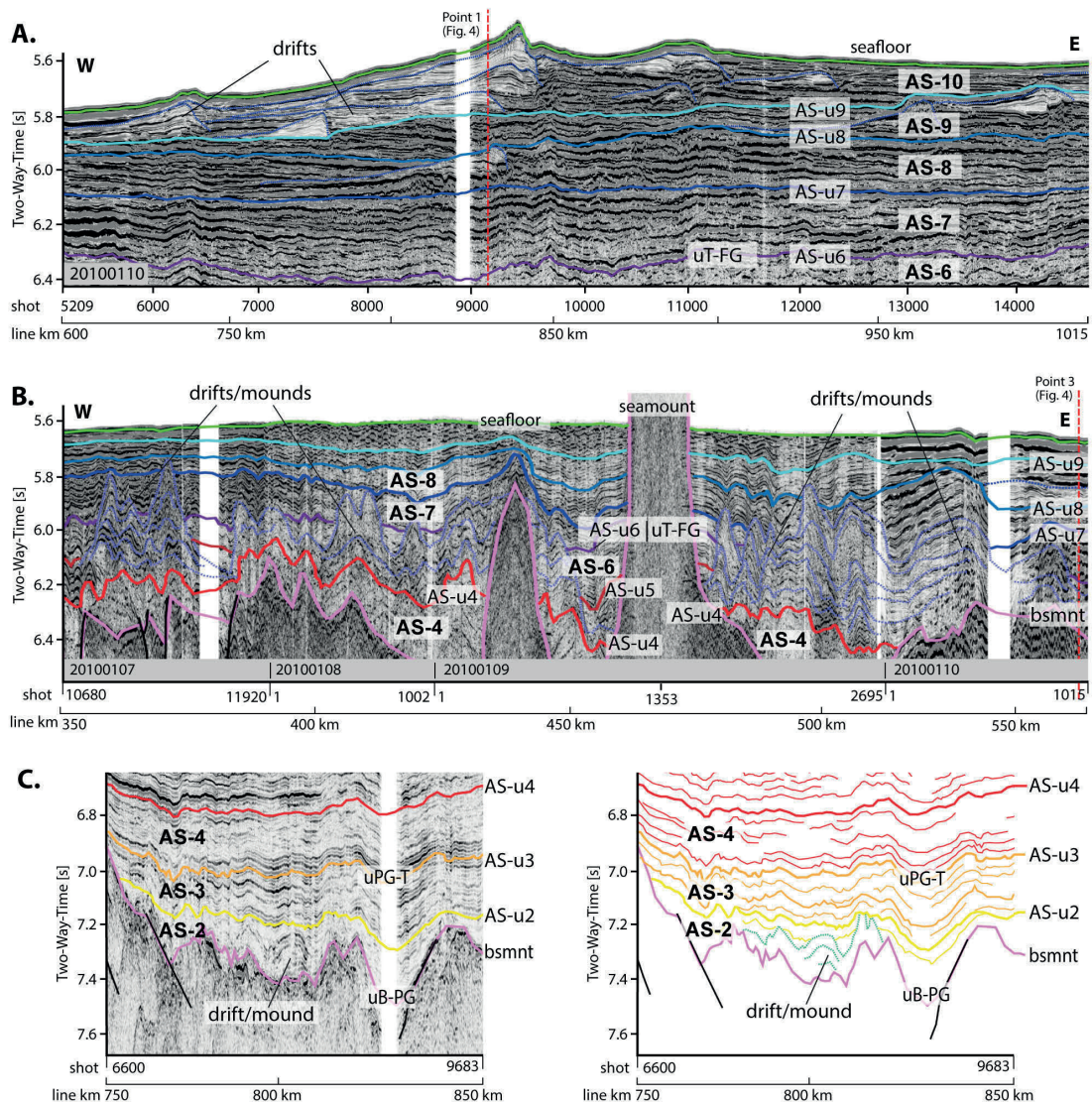


**Fig. 8-6.** Extracts of seismic images and interpretation from the AS-RS transect, highlighting the drifts or mounds observed in the pre-glacial, transitional and full glacial groups. (A) FG-drifts: Extract of the full-glacial sequences in line AWI-20100110, from shot 5209–14075 or CMP 7481–19312 (Fig. 8-4; Appendix B-1). The amount of drifts increases from one in AS-8, two in AS-9, to several stacked and more widely distributed ones in AS-10. The main base of the stacked drifts lies on AS-u9. Red dashed line – point 1 used for sediment thickness estimates (Fig. 8-4; Table 8-3). (B) T-drifts: Composite extract of the transitional sequences in lines AWI-20100107 to -110 (Fig. 8-4; Appendix B-1). The drifts or mounds, defined by the dashed lines, cut through units AS-5 and AS-6 as well across the transitional to full-glacial unconformity AS-u6/uT-FG, and even into the full-glacial unit AS-7. The amalgamated base of these drifts or mounds mostly lies on AS-u4 in the west and directly on the 63–65 Ma basement (Wobbe et al., 2012; Fig. 8-4; Appendix B-1) to the East. Red dashed line – point 3 used for sediment thickness estimates (Fig. 8-4; Table 8-3). (C) PG-drifts: Extract of the pre-glacial sequences in line AWI-20100110, from shot 6604–9683 or CMP 9508–13528, seismic image on the left and line interpretation drawing on the right. The buried drift or mound, defined by the green dashed lines in the line drawing, lies directly on the basement that is approximately 65–68 Ma old (Wobbe et al., 2012; Fig. 8-4, Appendix B-1).

The seismic reflectivity characteristics of units AS-1 to AS-10 in the AS-RS transect match the characteristics for each unit described in the type section (see point 4.1.1) well and lateral variation is negligible. All the marker horizons, AS-u1 to AS-u9, were laterally continuous and traceable over the ~2000 km transect distance. Every internal reflector was mapped over the full transect length and low-angle unconformities and onlaps or downlaps identified,

which increased confidence in deciding on the PG, T and FG sequence boundary horizons (Figs. 8-4b, 8-5b and think black lines in Appendix B-1b).

In general, the horizons are mostly parallel to the general basin geometry and basement trend, except above the anomalous part of the basin (line km 1100 to ~1650). This part was mapped in detail; see the line drawing in Fig. 8-5. Up to AS-u3, the reflections are parallel to the basement slope trend and the internal unit reflections onlap against a drift / channel-levee structure in AS-3 (delineated in dashed lines in Figs. 8-4, 8-5 and Appendix B-1). A prominent reflector occurs in the middle of AS-3 (6.4 – 6.8 s, shot 20000 – 25000 in Fig. 8-5b) and was first thought to be the unit boundary, possibly also the uPG-T boundary (section 8.4.2), but it pinches out against the large sedimentary drift body up-dip and is laterally discontinuous. It was therefore interpreted to only indicate a sub-unit within AS-3.

Above AS-u3, the reflections become increasingly angular with respect to the reflections below AS-u3, for example, the thinner red lines in unit AS-4 and AS-5 (Figs. 8-4b, 8-5b and thin black lines in Appendix B-1b). The internal unconformities are at their largest internal angles up to AS-u6, this is especially visible in the internal geometry of unit AS-6. Above AS-u6, the horizons trend changes to progressively more horizontal and parallel towards the top units, with complex internal geometry in the youngest unit, AS-u10 (green lines in Fig. 8-5b, between sflr and AS-u9).

After mapping all the marker horizons and every internal reflection, additional low angle unconformities were noticed, which confirmed the initial marker horizon decisions taken in the type section interpretation (section 8.4.2). It also cleared up the earlier ambiguity around AS-u3 (see annotated unconformities in Fig. 8-5b onlapping against AS-u3).

The resulting PG sequence AS-1 to AS-3, is bounded by the basement reflection (bsmnt) below and AS-u3 above (Figs. 8-4, 8-5 and Appendix B-1). AS-u3 or uPG-T was picked as the bottom boundary of this 1<sup>st</sup> order PG sequence because it: (i) marks a change in seismic facies from low amplitude and more transparent reflections below to more dense reflectivity patterns above, (ii) appears as a light grey to white unit on a grey scale seismic image that changes into medium grey appearance unit if plotted without display filter adjustments. This gradational change is consistent with the descriptions of the pre-glacial to transitional unit progression, seen in type sections in the other basins (section 8.5.1). (iii) AS-u3 also marks a change in the reflection angles (Fig. 8-5) and (iv) is demarcated from the low amplitude and different internal geometry units below by clear unconformities (Figs. 8-4b, 8-5b and Appendix B-1b).

The T sequence comprises AS-4, AS-5 and AS-6, bounded by AS-u3 / uPG-T below and AS-u6 / uT-FG above (Figs. 8-3, 8-4, 8-5 and Appendix B-1). AS-u6 was picked as the top boundary of this 1<sup>st</sup> order T sequence because marks a sharp change into the highest amplitude, finely layered reflective package above. The package has a medium grey appearance in the grey scale seismic image (Fig. 8-4a and Appendix B-1a). Again this is consistent with the descriptions of the pre-glacial to transitional unit progression, seen in type sections in the other basins (section 8.5.1). In addition, this horizon is a pronounced unconformable high amplitude reflector with reflections terminating against it and it

delineates a prominent change in the reflection angles on either side (Fig. 8-5), which may also indicate a tectonic uplift change. We interpret this sequence and associated seismic characteristics to indicate an rapid increase in the supply of large volumes of poorly sorted sediments, pushed across the shelf and spilled down the slope and into the abyssal plane, in a response to the first ice sheet advancements onto the shelf.

The FG sequence include units AS-7, AS-8, AS-9 and AS-10, bounded by AS-u6 / uT-FG below and the seafloor reflection (sflr) above. These units show more complex internal second and third order unconformities towards the top and several internal drift structures (annotated in Figs. 8-3, 8-4, 8-5, 8-6 and Appendix B-1). It is assumed that the increased occurrence of the complex internal drift structures represents changes in the depositional processes and bottom water circulation, consistent with the interpretations of Uenzelmann-Neben and Gohl (2012) in the adjacent farthest part of the eastern Amundsen Sea. This sequence package appears dark grey to black on the seismic image when plotted as grey scale, consistent with what was seen in the other type sections (section 8.5.1). The sharp transition at AS-u6 is thus interpreted to mark the onset of the full glacial polar climate regime and the establishment of a modern oscillatory polar ice sheet, consistent with the drilling information from the IODP Leg 318 Site U1356 (Fig. 8-2; Escutia et al., 2011).

### *8.5.1.3 Drifts*

Distinct mass sediment transport bodies are observed in the AS-RS transect seismic reflection data (grey wedge-shaped structures in Fig. 8-4, 8-5 and Appendix B-1; Fig 8-6) and are briefly described below in the context of the units within which they occur.

The pre-glacial sequence contains two sediment bodies. The first is large drift or buried channel-levee-drift system on the eastern flank of the basin. It occurs near the basement and within the older pre-glacial unit AS-3 with its base on AS-2 (Fig. 8-5, drift delineated in grey). It is ~3000 m long and almost 400 m high at the highest point (5.9 – 6.3 s TWT at line km 1475 in Fig. 8-6b). The internal seismic reflections are distinct and continuous, forming a parallel lamination that follows the overall drift geomorphology. The stoss side pinches out to the West.

The second sediment body is a smaller, approximately 80 km wide mound or drift, just to the left of the centre of the basin near the Pahemo fracture zone (line km 750 in Fig. 8-4b and Appendix B-1b). It lies directly on the 68–65 Ma basement and is constrained to AS-2 (Fig. 8-6c, line AWI-20100110, from shot 6604–9683 or CMP 9508–13528, green dashed lines in the line drawing on the right and seismic image on the left).



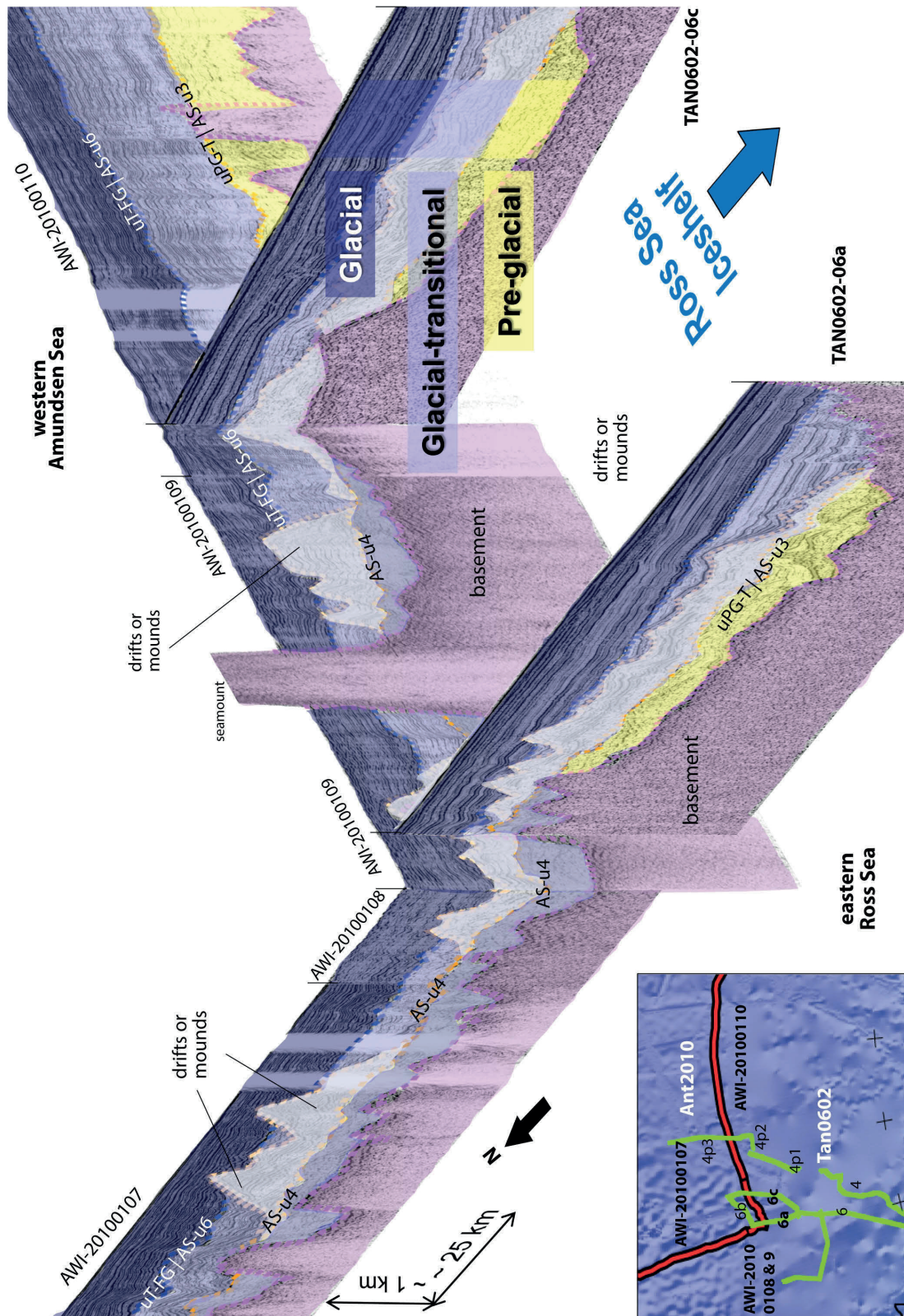


**Fig. 8-7.** 3D image illustrating the seismic stratigraphic link of the pre-glacial to glacial sequences between the TAN0602 data in the eastern Ross Sea and the corresponding horizons interpreted AWI-2010 survey in the western Amundsen Sea. The correlation of the pre-glacial to transitional unconformity, uPG-T (AS-u3) and the transitional to full-glacial unconformity uT-FG (AS-u6) are annotated. Note the drifts or mounds, in pale grey, terminating on AS-u4 or the basement and cutting through into the full glacial sequence (dark blue polygon), especially visible in line AWI-20100107 and TAN0602-6a. Inset: Location of the lines used for the 3D link construction annotated in bold, see Fig. 8-1 for the location in the larger study area. Thick red line with black border - the AS-RS transect (Fig. 8-4; Appendix B-1) comprising AWI-2010 seismic data, of which lines AWI-20100107, -108, -109 and a part of -110 were used in the 3D image, annotated. Green lines – the Tan0602 seismic data, of which extracts of lines 6a and 6b were used, annotated in bold. Background image and black lines are the same as in Fig. 8-1.



Smaller drifts or mounds occur in the transitional sequence and are concentrated on the western flank of the basin (outlines in grey in profiles AWI-20100107, -108 and -109 in Figs. 8-4b, 8-6b; Appendix B-1b). The base seems amalgamated and terminates on AS-u4, but the eastern part of the base lies directly on the 63–65 Myr old basement (Fig. 8-6b, line km 520 onwards, in line AWI-20100110). The tops extend into AS-5, AS-6 and AS-7 (line km 350 – 550 in Fig. 8-4b and Fig. 8-6b). The height is estimated as 400–500 m (Fig. 8-6b, 6.3 – 5.8 s TWT).

Fig. 8-6a illustrates an extract of the elongate sediment bodies observed in the full-glacial sequence in line AWI-20100110 (shot 5209–14075 or CMP 7481–19312; Fig. 8-4, Appendix B-1). The amount of drifts increases from one in AS-8, to two in AS-9, and to several stacked, more widely distributed ones in AS-10 (e.g. at shot 9000 and 5.6 – 5.9s TWT; Fig. 8-6a). The main base of the stacked drifts lies on AS-u9. The drifts are typically 50–100 km wide and 200–300 m high, and occur in the central and western parts of the basin. The drifts are usually confined to their respective seismic unit and may fill up part, or all of the unit thickness. The stoss side of all the drifts trend West. A stacked buried channel-levee system can be seen in all the units, just to the East of the large PG-drift (line km 1500 to 1600, Fig. 8-4, Appendix B-1).

### 8.5.2 Seismic stratigraphic links

#### 8.5.2.1 *AWI-2010-TAN-2006 Ross Sea*

The TAN-2006 and AWI-2010 surveys link seamlessly and no static shift was needed (Fig. 8-7). The horizons from the AS-RS transect were extended into lines TAN0602-06, -06a,b,c, -04, 04p1, p2, p4 (Table 8-2; Fig. 8-2; Fig. 8-7 inset). Both lines TAN0602-06a and -06c also have drifts or mounds in the transitional units that tie with the mounds seen in lines AW-20100108 and -109. These drifts are outlined in Fig. 8-7. The pre-glacial sequence represented by the yellow polygon in Fig. 8-7, pinch out against a basement high in the eastern Ross Sea (see bathymetry image in Fig. 8-1).

#### 8.5.2.2 *Ross Sea shelf-slope link*

Ross Sea shelf line ATC82B-203 (Wannesson et al., 1985) and line BGR80-005 (Fritsch, 1980) are the nearest to TAN0602-06, and due to limited lines are the only option as this stage to link the new Amundsen Sea dataset with that of the Ross Sea shelf (Fig. 8-2). The stratigraphy on the Ross Sea shelf was taken as published from Brancolini and Leitchenkov (2010). The link to line PD90-30 (Anderson and Bartek, 1992) and DSDP Leg sites 270, 271 and 272 (Fig. 8-1; Hayes and Frakes, 1975) via BGR80-003 and -004, were used as published as well (see Fig. 8-2 for line locations).

It is expected that the characteristics of the sedimentary units on the shelf and slope in the eastern Ross Sea would differ vastly in internal geometry from those in the deep-sea basin, and that the seismic correlation from the shelf across the slope to the rise would have large

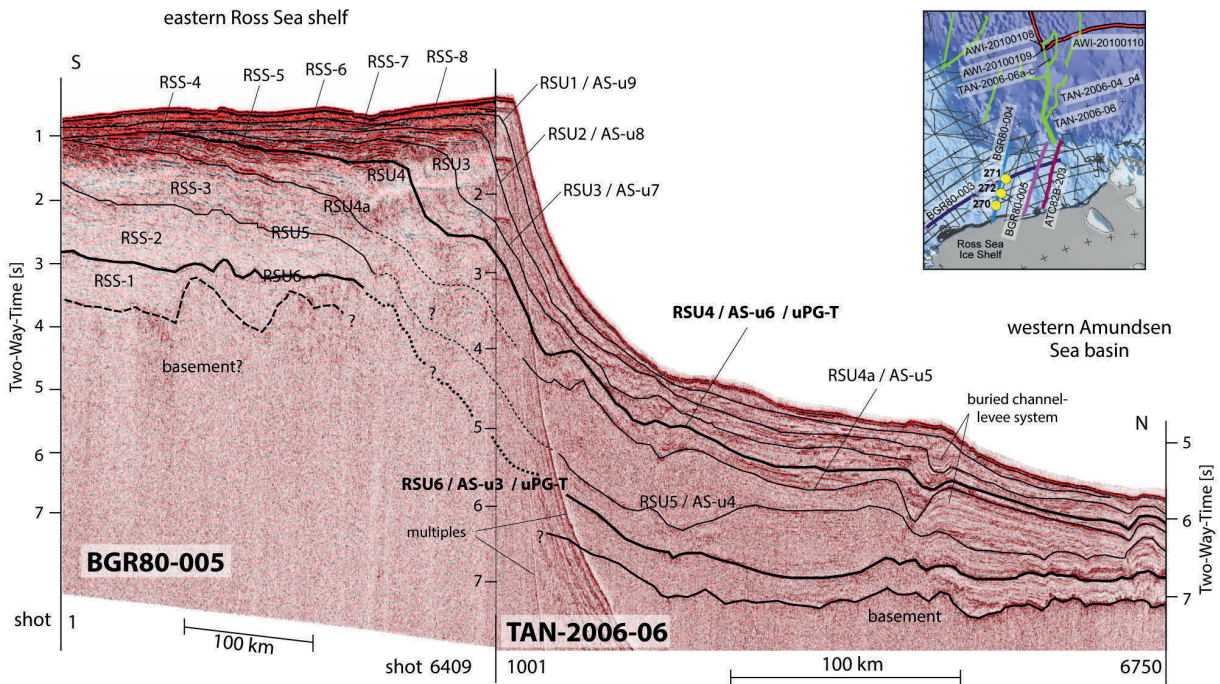


**Fig. 8-8.** 3D image illustrating the proposed shelf-to-slope seismic stratigraphic link between the TAN0602 data (line TAN0602-06) and the BGR80 data (line BGR80-005) in the eastern Ross Sea. See Table 8-2 for the key references and acquisition parameters of these lines. The correlation of the pre-glacial to transitional unconformity, uPG-T (AS-u3 / RSU6) and the transitional to full-glacial unconformity uT-FG (AS-u6 / RSU4) are annotated. The BGR80-005 stratigraphy was taken as published (Brancolini et al., 1995; Brancolini and Leitchenkov, 2010). Line PD90-30 (Anderson and Bartek, 1992) and DSDP Leg sites 270, 271 and 272 (Fig. 8-1; Hayes and Frakes, 1975) and correlated to line BGR80-005 (Fritsch, 1980) via a series of lines (see Fig. 8-2 and section 8.5.2). Inset: Location of the lines used for the 3D link construction, see Fig. 8-1 for the location in the larger study area. Red line with white parts – Tan0602 lines, the AWI-2010 and BGR80 lines are annotated, see Table 8-2. Background image and black lines same as in Fig. 8-1, but projected in to 3D-space and relief shaded.

uncertainties due to numerous spontaneous mass wasting and chaotic transport/deposition processes down-slope. As such, the sequence of unit and horizon ages may be the similar, but not the sedimentation processes.

However, bar a few slumping structures seen in the shelf-slope link seismic image, the AS-ux horizons in the TAN0602-06 line could be followed up through most of the multiples and linked to part of the Ross Sea shelf interpretations (Fig. 8-8). Even so, the shelf sequences are different from the deep-sea sequences in composition and depositional processing. In taking this conservative approach, we deemed only the age and nomenclature correlation of the horizons of relevance. Seafloor multiples made some of the correlation ambiguous, but nearby line ATC82B-203 provided useful information so that the correlation is fairly certain.

The RSU6 horizon correlates to the pre-glacial / transitional boundary AS-u3/uPG-T and RSU4 links to the full glacial transitional boundary AS-u6/uPG-T (Fig. 8-8). RSU-4a correlates with to AS-u4 and is considered part of the transitional sequences as opposed to a first-order sequence boundary. RSU-4a could also be similar to the strong reflector seen in AS-3 on the eastern basin flank around which some ambiguity exists (section 8.5.1.2; Fig. 8-5).



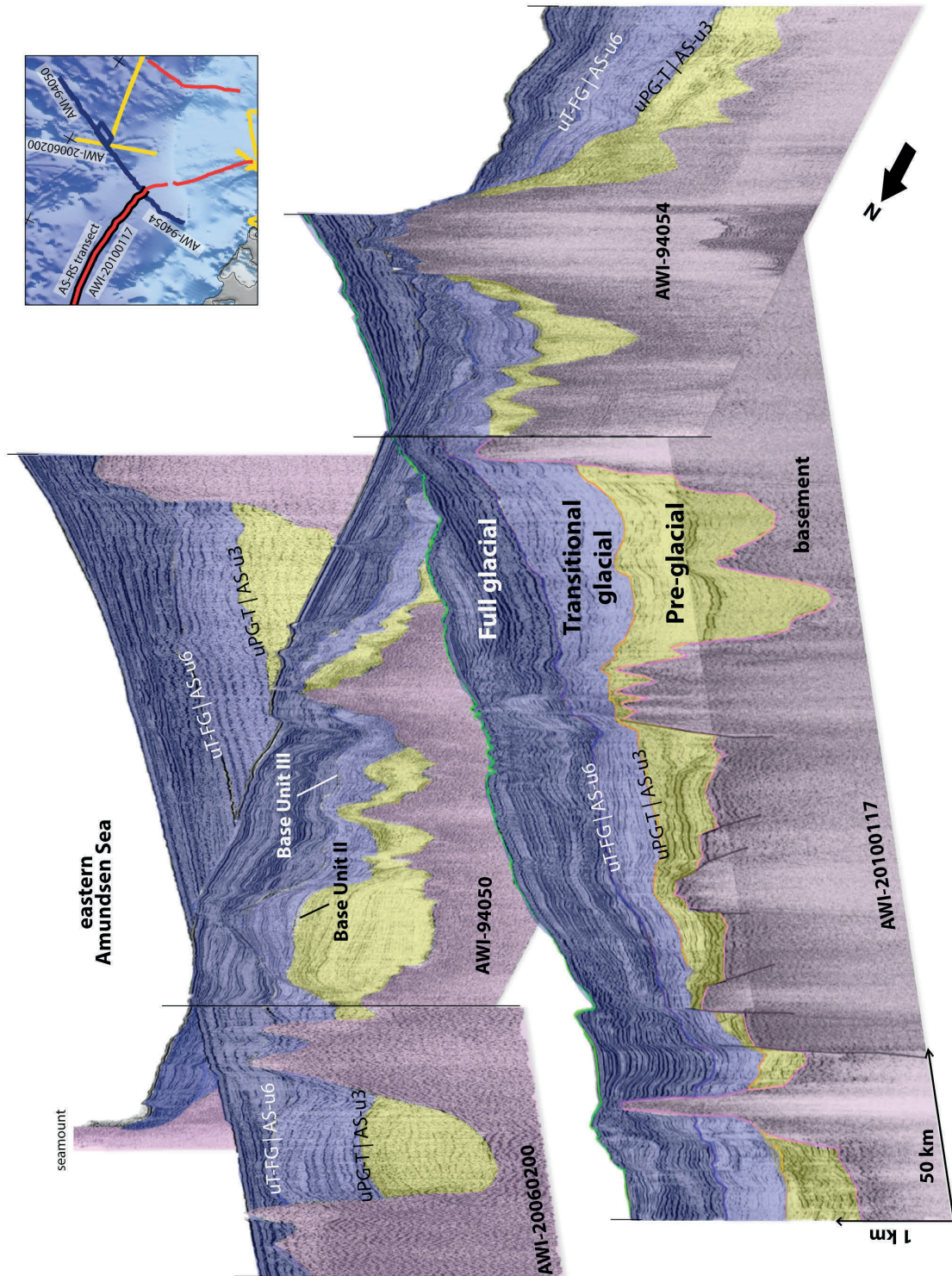


**Fig. 8-9.** 3D image illustrating the eastern Amundsen Sea seismic stratigraphic link of the pre-glacial to glacial sequences, as interpreted in the AS-RS transect (line AWI-20100117 part) and correlated to the corresponding horizons in the legacy Ant94 seismic data (lines AWI-94050 and AWI-94054) and Ant96 seismic data (line AWI-20060200, Ch. 5). Pink polygons – basement, yellow polygons – pre-glacial units, light blue-purple polygon in the middle – glacial transitional units, darker blue polygon up to seafloor – full glacial units. The correlation of the pre-glacial to transitional unconformity, uPG-T (AS-u3) and the transitional to full-glacial unconformity uT-FG (AS-u6) presented in this study is annotated in black and white, respectively. These two sequence boundaries respectively align with the bases of Unit II and Unit III in lines AWI-94050 and AWI-94054 (Uenzelmann-Neben and Gohl, 2012). Inset: Location of the lines used for the 3D link construction are annotated, see Fig. 8-1 for the location in the larger study area. Thick red line with black border – the AS-RS transect and AWI-2010 seismic data, eastern part of line AWI-20100117 shown, navy blue lines – the Ant94 seismic data of which lines AWI-94050 and AWI-94053 were used, yellow lines – the Ant96 seismic data of which line AWI-20060200 was used. Background image and black lines same as in Fig. 8-1.

Subsequently, we have taken the approach that RSU4a rather links to AS-u4 and is considered to be part of the transitional sequence, as oppose to a 1<sup>st</sup> order sequence boundary. RSS-8 pinches out downslope on line TAN0602-06 towards the north, near shot 6500 (Fig. 8-8). The slope-shelf correlation supports the proposed chrono-stratigraphy for the entire AS-RS transect. The correlations of the remaining RSUx to AS-x horizons are annotated in Fig. 8-8.

### 8.5.2.3 Eastern Amundsen Sea Link

Line AWI-20100117 forms the far eastern part of the AS-RS transect and crosses older seismic lines AWI-94054, AWI-94050 (Table 8-2; Gohl et al., 1997; Nitsche et al., 1997, 2000; Uenzelmann-Neben and Gohl, 2012) as well as AWI-20060200 (Fig. 8-2; Table 8-2; Ch. 5; Gohl 2007; Uenzelmann-Neben and Gohl, 2012; Kalberg and Gohl, 2013). The Neben & Gohl, (2012) correlates to the pre-glacial / transitional unconformity uPG-T/AS-u3 (Fig. 8-9). The base of Unit III corresponds to the transitional / full glacial boundary, uT-

FG/AS-u6 (Fig. 8-9). The units occur throughout the lines and a correlation without discrepancies or ambiguities was done.

**Table 8-3.**

Summary of the sediment thickness and velocities for each unit, as estimated at the 12 points along the AS-RS transect shown Fig. 4 and online supplement S3. The detailed calculations and velocity models used are in the online supplements S2, S4 and S5.

Group	Unit	Thickness (m)		Velocity range (m/s)	
		min	max	min	max
FG	AS-10	52.5	201.6	1690	1920
	AS-9	52.5	220.5	1750	2130
	AS-8	45.3	178.9	1876	2237
	AS-7	65.4	367.4	2043	2300
T	AS-6	47.5	393.2	2131	2357
	AS-5	89.8	419.5	2257	2432
	AS-4	115.2	359.8	2351	2674
PG	AS-3	108.7	680.0	2550	2917
	AS-2	67.5	519.0	3118	3245
	AS-1	133.5	1256.3	3574	3760

**Table 8-4.**

Summary of the sediment volumes and sedimentation rates for the Pre-glacial (PG), Transitional (T) and Full glacial (FG) components, as estimated at the 12 points along the AS-RS transect (Fig. 4 and online supplement S3). Estimated min/max area for the Amundsen Sea basin is  $1.2-1.4 \times 10^6 \text{ km}^2$  (Fig. 1).

	Thickness (m)			Volume ( $10^6 \text{ km}^3$ )		Sedimentation rate (cm/ky)	
	min	max	mean	min	max	min	max
Total sediment	805.1	3909.3	2357.2	2.83	3.30	1.01	2.97
FG sequence	373.6	888.9	631.3	0.76	0.88	1.49	3.56
T sequence	274.0	1069.3	671.7	0.81	0.94	1.01	2.49
PG sequence	358.4	2202.8	1280.6	1.54	1.79	0.61	2.17

### 8.5.3 Sediment thickness

The minimum, maximum and mean thickness of each AS-x unit, and the velocity range used to calculate the thickness is listed in Table 8-3. The detailed calculation of the sediment thickness at each one of the 12 points (black dots in Fig. 8-1) can be found in Appendix B-2 and the supporting sonobuoy and refraction velocity models in Ch. 5.

AS-1 is the thickest unit in the central part of the basin (~1.3 km thick; Table 8-3) at the Endeavour fracture zone where it fills up the rugged block faulted basement. It is therefore interpreted as a syn- or post rift sequence (brown unit at line km 1100 in Fig. 8-4). Little internal faulting is present and it



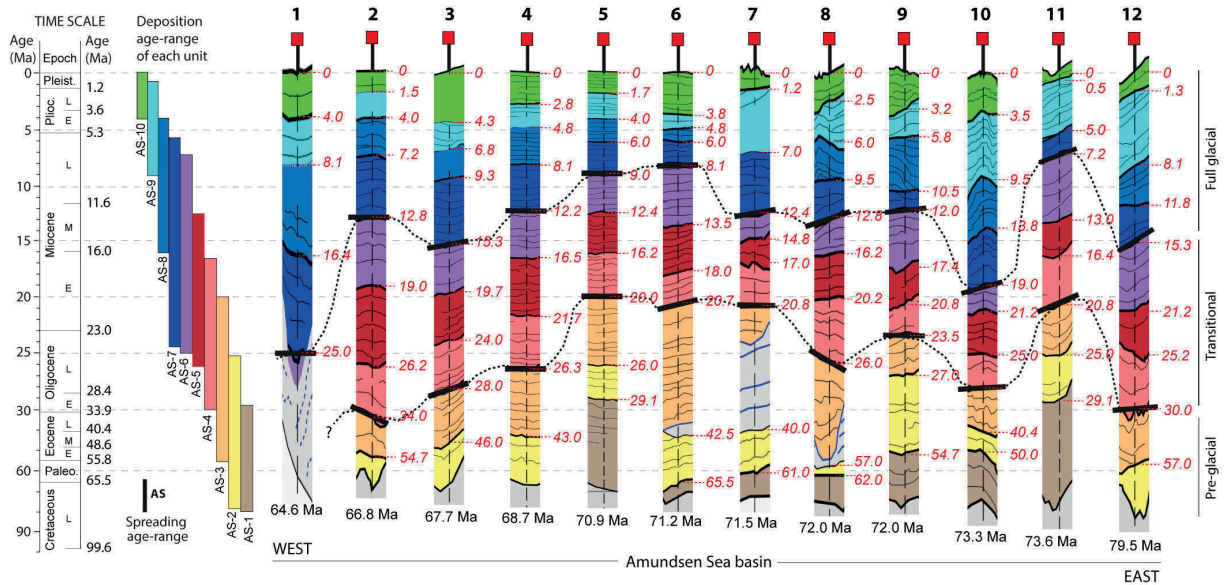


**Fig. 8-10** Age model and associated deposition along the AS-RS transect. From left to right: Time scale of Epochs and boundary ages after Gradstein et al. (2004), L – Late, M – Middle, E – Early. Narrow colour bars – first and last occurrence of each unit, projected onto the time scale. Broader colour columns – interpreted horizons, extracted from the 12 points along the AS-RS transect (Fig. 8-1; Appendix B-2) and represented as a section scaled to time (Fig. 8-4 and higher resolution A0 Appendix B-1). The vertical scale of these type sections represents time and not sediment thickness. Black bars depict interpreted top and bottom boundaries of the transitional (T) sediment component and the red italic numbers represent the tentative age estimate (Ma) for each horizon, read off from the time scale on the left. Black bar and black numbers below each column, summarises the basement ages at each point. AS – Amundsen Sea basin. The age range of the Amundsen Sea basin basement after Wobbe et al. (2012).

seems to have draped over the basement to even out some of the topography. AS-1 thins up the basin flanks (~133 m thick) and terminates at the Pahemo fracture zone in the West, and against the Proto-Antipodes fracture zone in the East. AS-2 follows the trend of AS-1, but is of a more uniform thickness in the centre of the basin (~500 m; Table 8-3; point 5 in Fig. 8-4b and Appendix B-2) where it levels on top of the block-faulted basement topography. It terminates to the East against the Kohiku fracture zone (point 2 in Fig. 8-4b and Appendix B-2). AS-3 is anomalously thick in the East where the levee-drift is located (680 m at point 6, Fig. 8-4b and Appendix B-1b, B-2b) and thins to the West to 108 m thick. Similar to AS-2, AS-3 terminates at the Kohiku fracture zone.

AS-4 varies between 155 and 360 m thick (Table 8-3; Appendix B-2b). It thins noticeably upslope, (between points 7 and 8, Fig. 8-4b and Appendix B-1b, B-2b). Similar to AS-4, units AS-5, AS-6 and AS-7 thin above the AS-2 PG-drift location to less than 100 m thick (Table 8-3; Appendix B-2) and then propagate into the buried channel-levee system where they thicken again. All three units have a maximum thickness in the order of 350–400 m (Table 8-3; Appendix B-2) and are parallel to each other as well as to the units above and below.

AS-8 varies greatly in thickness throughout the basin (45–179 m thick; Table 8-3) and is absent between line km 1750 and 2000 (Fig. 8-4a, b and Appendix B-2). Following the trend of units AS-4 to AS-6, it also thins markedly above the AS-2 drift location (between

points 7 and 8, Fig. 8-4b and Appendix B-1b, B-2b). AS-9 and AS-10 are similar in thickness ( $\sim 50$ – $200$  m thick; Table 8-3, Appendix B-2) and variable geometry. Both contain drifts, mostly concentrated where the Pahemo fracture zone crosses the transect (point 3 in Fig. 8-4b and Appendix B-1b). Units AS-4 to AS-10 are continuous along the entire transect, parallel to each other and in general, uniform in thickness up to the region above the anomalous basement topography and the AS-2 PG-drift.

The total sediment thickness ranges from 805 to 3909 m (Table 8-4) with the thickest part in the centre of the basin, as expected (Fig. 8-4, Appendix B-1). Under the assumption that all units occur throughout the Amundsen Sea basin extent, an area of  $1.2$  to  $1.4 \times 10^6$  km<sup>2</sup> delineated by the white dashed line in Fig. 8-1, we estimate the total sediment volume at  $2.83$  to  $3.30 \times 10^6$  km<sup>3</sup> (Table 8-4). Similarly, by taking the mean thickness of each 1<sup>st</sup> order sequence (PG – 1281 m, T – 672 m, T – 631 m) and the min/max of the basin area, we estimate the pre-glacial to glacial sediment volumes as: PG =  $1.5$  to  $1.8 \times 10^6$  km<sup>3</sup>, T =  $0.8$  to  $1.0 \times 10^6$  km<sup>3</sup> and FG =  $0.8$  to  $0.9 \times 10^6$  km<sup>3</sup> (Table 8-4).

#### 8.5.4 Sedimentation rates

Sedimentation rates and volume estimates for the pre-glacial, transitional and full-glacial sequences were determined by using the sequence age range (Fig. 8-10) and sediment thicknesses (Table 8-4; Appendix B-2). The age model contains large uncertainties because of the lack of borehole age-control. We therefore only outline the general trend for the 1<sup>st</sup> order pre-glacial, transitional and full glacial sequences. For the total sediment volume of  $2.8$  to  $3.3 \times 10^6$  km<sup>3</sup> in the Amundsen Sea basin a min/max sedimentation rate of  $1$ – $3$  cm/ky is estimated (Table 8-4). The pre-glacial sequence had the lowest min/max sedimentation rate estimate at  $0.6$ – $2.1$  cm/ky. The rate progressively increased to  $1.0$ – $2.5$  cm/ky for the transitional sequence and is the highest for the full glacial sequence ( $1.5$ – $3.6$  cm/ky).

## 8.6 Discussion

Since this is the first seismic horizon stratigraphy model for the central Amundsen Sea basin and the eastern Ross Sea basin, we need to look somewhat farther afield. We compare our results to previous work in order to place it into a provisional pre-glacial to glacial age- and stratigraphic framework with respect to changes in sedimentation processes, bottom water circulation and ice sheet development. The nearest three suitable boreholes Sites are  $1000$ – $2000$  km away from either end of our multichannel seismic dataset (section 8.4.3.2; Figs. 8-1, 8-2). We draw most information from IODP Leg 318 Site U1356,  $\sim 1300$  km away on the Wilkes Land margin (Fig. 8-2 inset; Escutia et al., 2011) because: (i) Pliocene to Eocene sediments were recovered from this  $1006$  m (b.s.f.) deep borehole; (ii) it is located on the continental rise as oppose to the shelf like DSDP Leg 28 Sites 270–272 (Figs. 8-1, 8-2;

Hayes and Frakes, 1975); (iii) the main objective was to date the regional unconformity WL-U3 in order to constrain the timing of the first arrival of the ice sheet to the margin in an ice-distal setting, and; (iv) their seismic type section shows a most remarkable resemblance to the Amundsen Sea ice-distal seismic facies (sections 8.4.2 and 8.5.1). Although their results pertain to the past dynamics of the East Antarctic Ice Sheet, it is the nearest available ice-distal analogue as there is no drilling information available for the continental rise off West Antarctica. The nearest borehole to the East of the AS-RS transect is ODP Leg 178 Site 1095, on Drift 7 in the Bellingshausen Sea off the western Antarctic Peninsula, which mostly provides information on the development of the Antarctic Peninsula Ice Sheet (APIS; Fig. 8-2 inset; Uenzelmann-Neben, 2006).

### 8.6.1 Pre-glacial (PG) sequence

Seafloor age in the Amundsen Sea basin becomes increasingly younger from 84 Ma (C34y) in the East to 42 Ma (C20n) in the northwest (Fig. 8-2; Table 8-1; Wobbe et al., 2012). In our age model, the selected 12 points along the transect range in basement age from 79.5 Ma at point 12 in the East, to 64.6 Ma at point 1 in the West (Fig. 8-4b; Fig. 8-10). This means sediments in direct contact with the basement from line km 500 to 2000 should be at least younger than 79.5–64 Myr.

In our constructed age model, AS-1 has an estimated age of 71–66 Ma (Figs. 8-10 and 8-11), which agrees with the age of the nearest magnetic seafloor spreading anomaly at the Endeavour fracture zone (71 Ma, C32n.1n; Figs. 8-2, 8-4 and Appendix B-1; Wobbe et al., 2012). AS-2 is estimated to be 65–42 Myr old and AS-3, 42–21 Myr. The older dates apply to the unit flanks and the younger age to the centre (Figs. 8-10, 8-11). Units AS-1, AS-2 and AS-3 collectively match Unit 1 of Uenzelmann-Neben and Gohl (2012) in the 3D seismic horizon correlation well (Fig. 8-9).

In the Cretaceous to Paleocene part of the pre-glacial climate regime (up to 55.8 Ma, Fig. 8-12a) the major deposition centre is located in the basin centre near the Endeavour fracture zone (labelled EFZ in Fig. 8-12a). Since sediment deposits occur more on the eastern flank of the basin and seem thicker on that side (up to 1.3 km for AS-1 and 519 m for AS-2, Table 8-3; Appendix B-2) it is inferred that the pre-glacial depo-centre was probably supplied from the southeast (orange arrows in Fig. 8-12a), possibly by complex river systems that eroded the elevated inland palaeotopography region of West Antarctica (Fig. 1-2 in Ch. 1). These systems could have transported the largest volume of the total sediments ( $1.5$  to  $1.8 \times 10^6$  km<sup>3</sup>; Table 8-4) into the sea at a deposition rate of 0.6–2.2 cm/ky (Table 8-4). The routes could have been along palaeotopographic lows, which could later define the flow stream channels of the subsequent ice sheet.

An approximately 80 km wide mound or drift West of the basin centre near the Pahemo fracture zone (annotated in the simplified section of the AS-RS transect in Fig. 8-12a). The mound or drift lies directly on the 68–65 Myr old basement and is constrained to AS-2 (Fig. 8-6c); hence it cannot be older than 67 Myr (Paleocene age). An early regional proto

bottom-current circulation possibly caused it, although the gateway Southern Ocean gateways were still closed. Huber et al. (2004) suggested the development of a proto-Ross sea gyre at 55.8 Ma (Table 8-1). It was not possible to deduct any current direction information from the geometry, but considering the likely bathymetry (Fig. 8-1 background image) and basement high to the West, an eastward flow direction is suggested (blue dashed arrow in 12a).

Wilkes Land Basin		Ross Sea shelf and slope			central Amundsen Sea basin			far eastern Amundsen Sea basin	
Escutia et al., 2011		De Santis et al., 1999	Brancolini et al., 1995	Brancolini & Leitchenkov 2010	This study			Uenzelmann-Neben 2006; Uenzelmann-Neben and Gohl 2012	Nitsche et al. (1997, 2000)
seafloor		seafloor			west	central	east	seafloor	
WL-U8	WL-S9	RSU1	RSS-8	2.5 — 1.5 Ma	AS-u9 — ~2 Ma	AS-10	~2 — ~1 Ma	Unit IV	
WL-U7	WL-S8	RSU2	RSS-7	4.0 — 3.3 Ma	AS-u8 — ~4 Ma	AS-9	~5 — ~8 Ma	4 Ma	Unit 1
WL-U6	WL-S7	RSU3	RSS-6	10.5 — 10.5 — 10 Ma	AS-u7 — ~9 Ma	AS-8	~6 — ~12 Ma	Unit III	
WL-U5	WL-S6	RSU4	RSS-5	14 — 10 Ma — 16.5 — 14.7 — 15.5 Ma	AS-u6 — ~15 Ma	AS-7	~9 — ~15 Ma	14 Ma	
WL-U4	WL-S5	RSU4a	RSS-4	17.0 — 18.5 — 18 Ma	AS-u5 — ~20 Ma	AS-6	~14 — ~21 Ma	Unit II	Unit 2
WL-S4		RSU5	RSS-3	21.0 — 30-22 — 20 Ma	AS-u4 — ~26 Ma	AS-5	~18 — ~25 Ma		
WL-U3	WL-S4	RSU6	RSS-2	33.5-30 Ma — 30.0 — 34-30 — 29 Ma	AS-u3 — ~34 Ma	AS-4	~21 — ~30 Ma	21 Ma	
					AS-u2 — ~55 Ma	AS-3	~43 — ~57 Ma	Unit I	Unit 3
basement			RSS-1 volcanics		AS-u1 — =	AS-2	~66 — =		
			basement		bsmnt — ~67 Ma	AS-1	~71 — ~80 Ma	60 Ma	
						basement		basement	basement

**Fig. 8-11.** Seismic stratigraphy correlation chart linking the boundary horizons and the identified seismic units presented in this paper, to previous studies in Ross Sea shelf and eastern Amundsen Sea basin. Thin black lines – discontinuities or boundary horizons mapped in each study; thick black lines – lower boundary of the proposed full glacial and transitional units, this paper; red numbers – ages of the horizons, showing the lateral variation across the basin from west to east. Darker grey block – units assigned to the full glacial component of the total sediments, light grey block – transitional units and lower white block, pre-glacial units.

Close to the Eocene–Oligocene transition (34 Ma), unit AS-3 was deposited with model ages of 43–21 Ma, 30 Ma and 34 Ma (Figs. 8-10, 8-11, 8-12b). AS-3 is the thickest unit in the PG sequence (680 m Table 8-3; Appendix B-2) and contains a large ~3000 m long, almost 400 m high levee-drift (Figs. 8-4, 8-5; Appendix B-1). The base of the levee-drift (PG-drift) terminates at the top boundary of AS-2, at unconformity AS-u2. If we project the last occurrence of AS-2 on the timescale (yellow band at points 6, 7 and 8 in Fig. 8-10) the base of the drift should be at least younger than 57–40 Myr (points 8 and 7) thereby placing it in the Eocene (Figs. 8-10, 8-11, 8-12). The stoss side of the drift trends West (Fig. 8-5) and this geometry suggests a bottom-current flow direction from West to East (blue dashed arrow in Fig. 8-12b; Stow et al., 2002; Shanmugam, 2006; Shanmugam and Camerlenghi, 2008). The occurrence of a larger and additional PG-drift confirms our earlier mound observation at >55.8 Ma (Fig. 8-12a) and the inference that bottom current circulation may have already been active in the Eocene and probably earlier.



Uenzelmann-Neben and Gohl (2012) observed drifts in Unit I (60–21 Ma, Fig. 8-11) near the Marie Byrd Seamounts, which also implies Paleogene bottom-current activity in this part of the basin. They infer that the likely cause and driving force was related to the proto Antarctic Bottom Water (AABW) being deflected against a basement high, the latter ascribed to have been caused by thermal uplift related to the emplacement of the Mary Byrd Seamount province. This may explain why it is the only drift in AS-3 and deposited at this particular location (see section 8.6.6 for the discussion on the basement geometry).

### 8.6.2 The uPG-T boundary process: arrival of the WAIS to the margin

Seismic stratigraphy work in the Wilkes Land distal basin identified the first arrival of the EAIS to the margin at 33.5–30 Ma, marked by regional unconformity WL-U3 (Fig. 8-11; Escutia et al., 2011). Comparing the type sections for the Amundsen Sea basin and the seismic line coincident on IODP Leg 318 Site U1356 (Fig. 8-2; Escutia et al., 2005, 2011; De Santis et al., 1995, 2003) it is visually evident that the lower seismic sequence are similar in amplitude, geometry and seismic character. We thus correlate our interpreted pre-glacial sequence unconformity AS-u3/uPG-T to WL-U3. The WL-U3 age is in good agreement with our estimated AS-u3/uPG-T model horizon age of 34–28 Ma for the basin flanks (lower black dashed line through points 1 to 3 and 9 to 12 in Fig. 8-10; Fig. 8-11).

From the seismic reflection shelf-slope correlation between the TAN0602-06 line and DSDP Leg 28 Sites 270–272, via lines BGR80-003, -004 and 005 (Figs. 8-2 and 8-8; Table 8-3), the pre-glacial sequence unconformity AS-u3/uPG-T correlates to RSU6. RSU6 has an age of 30–20 Ma, constrained by the DSDP Leg 28 boreholes, ~300 km from the AS-RS transect (Figs. 8-2, 8-10 and 8-11; Brancolini et al., 1995; De Santis et al., 1999; Brancolini and Leitchenkov, 2010). The RSU6 age is also in good agreement with our model age of 34–20 Ma and accounts for the younger age observed in the centre of the AS-u3/uPG-T horizon (points 5, 6, 7 in Fig. 8-10). It is speculated that the younger trend in the centre could be ascribed to a delay in the arrival of the ice sheet on the shelf at this part, perhaps due to elevated topography, such as a mountain range, that it had to overcome before it could reach the shelf. The reconstructed 34 Ma palaeotopography of West Antarctica does suggest an elevated land area opposite the centre of the transect (red square in Fig. 1-2; Wilson et al., 2012). Alternatively, low lying palaeo-river drainage systems from the PG climate regime may have directed the ice streams and drainage towards basin flanks instead.

In the eastern Amundsen Sea 3D seismic reflection correlation (Fig. 8-9), the pre-glacial sequence unconformity AS-u3/uPG-T in line AWI-20100117 of the AS-RS transect, matches the base of Unit II in line AWI-95054 (Figs. 8-2, 8-9, 8-11). The base of Unit II was assigned a hypothetical age of 21 Ma in Uenzelmann-Neben and Gohl (2012) by jump-correlation to the Ross Sea shelf horizon ages in De Santis et al. (1995). Our age-model however suggests an older age of at least early Oligocene, 30–28 Ma (Figs. 8-10 and 8-11). The Eocene/Oligocene transition age of 34 Ma for the uPG-T unconformity is favoured above the DSDP ages, because of the similar distal setting and thus similar processes. Based

on the seismic horizon mapping, the constructed age model and borehole information we infer an Eocene age of 34 Myr for the first arrival of the West Antarctic ice sheet to parts of the coast. An Eocene/Oligocene WAIS arrival toward the shelf is consistent with the reconstructed palaeotopography (Wilson et al., 2012) and inferred paleo-ice-sheet modelling (Wilson et al., 2013).

### 8.6.3 Transitional (T) sequence

By the mid-Miocene, the deep-water Tasmanian and Drake Passage/Scotia Sea gateways opened completely, enabling the development of the Antarctic Circum-Polar Current (ACC) (Fig. 8-12c; Table 8-1; Fig. 1-1). The WAIS reached the continental shelf and pushed sediments onto the slope and into the abyssal plane (red polygon in Fig. 8-12c). This is in agreement with higher amplitudes in units AS-4, -5 and -6 (Fig. 8-4; Appendix B-1) seen above AS-u3/uPG-T, which can be associated with larger sediment influx of poorly sorted material such as debris carried by advancing ice streams. The sedimentation rate also increased to 1-2.5 cm/ky (Table 8-4).

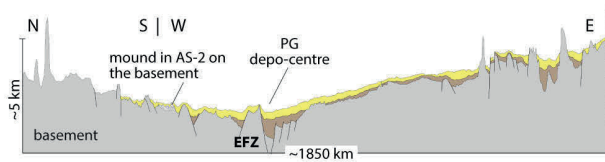
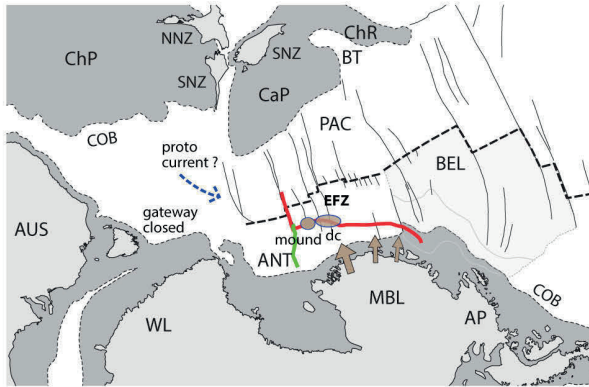
In the Ross Sea shelf-slope-rise seismic horizon correlation (Fig. 8-8), AS-u4 links to RSS-4a. Our model age of 26–18 Ma is in fair agreement with the 17 Ma age of De Santis et al. (1999), the 18.5 Ma age of Brancolini et al. (1995) and the 18 Ma age of Brancolini and Leitchenkov (2010). AS-4 correlates with RSS-3 and WL-S4 (Escutia et al., 2011), whereas AS-5 and AS-6 correlate to RSS-4 and WL-S5 (Figs. 8-8 and 8-11; section 8.5.2). In the eastern Amundsen Sea seismic horizon correlation (Fig. 8-9) AS-4 to AS-6 collectively correlates to unit II (Figs. 8-9 and 8-11; Nitsche et al., 1997, 2000; Uenzelmann-Neben and Gohl, 2012). However, our age model suggests an older age range of 30–15 Ma for the eastern Amundsen Sea basin flank (Figs. 8-10 and 8-11). Similar to the pre-glacial sequence, the ages on the basin flanks are older than in the centre. The sediment deposition is evenly distributed throughout the basin, but it appears thicker in the centre (up to 1070 m) and thins over the AS-2 PG drift and the anomalous basement topography.

Drifts occur on a basement high on the western flank of the basin (Fig. 8-4; Appendix B-1). The amalgamated base of the T-mounds/drifts lies on AS-u4, in AS-5, as well as on the basement. Hence, their ages should be at least younger than the youngest age of AS-4, which is 26–24 Myr (points 1 and 2, Fig. 8-4b and Fig. 8-10). ODP Leg 178 Site 1095 (Fig. 8-2 inset) reached sequences of mid-Miocene age in a sediment ice-distal drift deposit near the Antarctic Peninsula (e.g. Iwai et al., 2002; Uenzelmann-Neben, 2006).

Elongate drifts and levee drifts were mapped in the eastern Amundsen Sea in Unit II and inferred from the DSDP Leg 28 Sites 270–272 data in De Santis et al. (1999), to be 21–15 Myr old (Uenzelmann-Neben and Gohl, 2012). Again our age model, which is in closer proximity and more directly linked to the DSDP Leg 28 data, suggests the transitional drift deposits may be 5 to 10 Myr older. It was not possible to deduct any bottom-current direction information from the geometry and they could also be interpreted as sediment waves.

A. CRETACEOUS - PALEOCENE

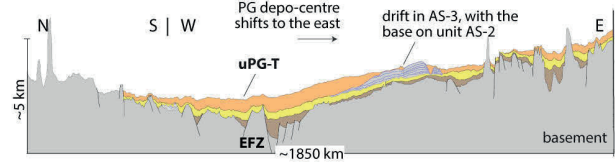
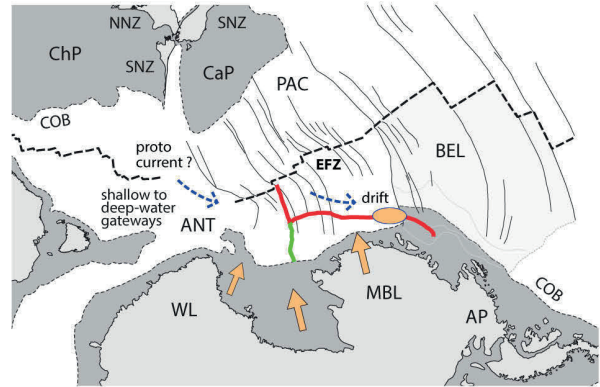
55.8 Ma



Pre-glacial regime units: AS-1, AS-2

B. EOCENE - OLIGOCENE

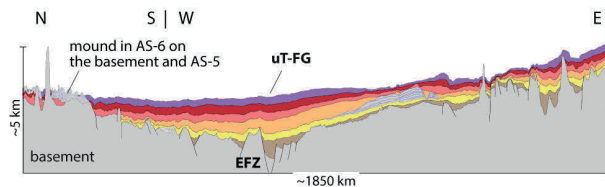
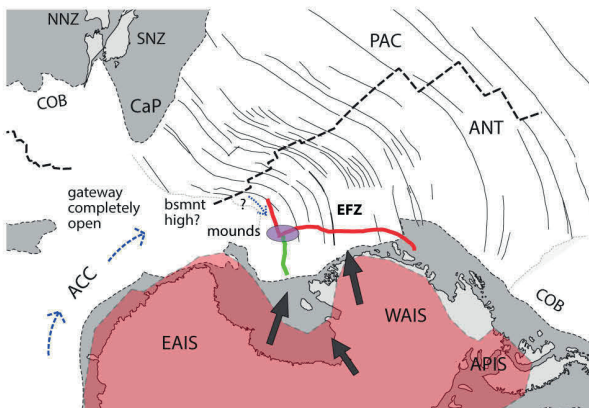
34.0 Ma



Pre-glacial regime units: AS-1, AS-2, AS-3

C. MID-MIOCENE

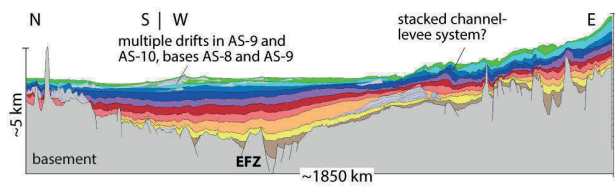
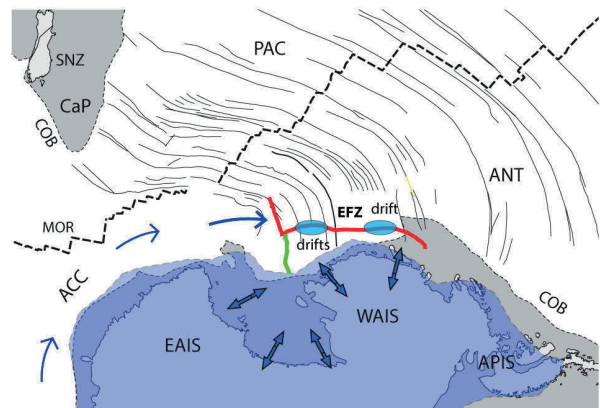
15.5 Ma



Transitional regime units: AS-4, AS-5, AS-6

D. PLIOC. - PLEIST.

4.8 Ma



Full glacial regime units: AS-7, AS-8, AS-9, AS-10

**Fig. 8-12.** Model showing the changes in plate-tectonic motion, pre-glacial to glacial sediment deposition, ice sheet development and ocean circulation in the greater Amundsen Sea region since the end Cretaceous. The corresponding sediment deposition for each regime, is illustrated in the AS-RS transect diagram below. Plate reconstruction adapted from Wobbe et al. (2012) and GPlates (Boyden et al., 2011). Thick dashed black lines – mid-oceanic ridge (MOR), thick black lines – fracture zones, EFZ – Endeavour fracture zone, PAC – Pacific plate, ANT – Antarctic plate, BEL – Bellingshausen plate, COB – continent-ocean boundary. The AS-RS transect – thick red line, link with Tan0602\_06 seismic profile – thick green line. Observed sedimentary drifts and mounds are indicated by ovals, and the arrows depict the inferred sediment supply and ocean circulation. Red and blue polygons – schematic extent of the East Antarctic Ice sheet (EAIS), West Antarctic Ice sheet (WAIS) and Antarctic Peninsula Ice sheet (EAIS) expanded to the continental shelf edge during the Transitional and Full-glacial climate regimes. ChP – Challenger Plateau, ChR – Chatham Rise, CaP – Campbell Plateau, BT – Bounty Trough, NNZ – North Island of New Zealand, SNZ – South Island, AUS – Australia, WL – Wilkes Land, MBL – Mary Byrd Land, AP – Antarctic Peninsula.

#### 8.6.4 The uT-FG boundary process: permanent grounding

Seismic stratigraphy work in the Wilkes Land ice-distal basin identified WL-U5 as the boundary horizon at which the EAIS grounded on the shelf permanently, and the stage at which Antarctica developed the polar climate (Fig. 26 in Escutia et al., 2011). Comparing the type sections for the Amundsen Sea basin and the seismic line across the IODP Leg 318 Site U1356 (Fig. 8-2; Escutia et al., 2005, 2011; De Santis et al., 1995, 2003), the sequences are virtually identical in amplitude, geometry and seismic character, and as such, correlated to our interpreted transitional sequence unconformity AS-u6/uT-FG. The age of WL-U5 (early / mid-Miocene transition) is consistent with our estimated horizon age of 15.3 Ma for the basin flanks (upper black dashed line through points 1 to 3 and 9 to 12 in Fig. 8-10; Fig. 8-11; section 8.4.4).

In the seismic reflection shelf-slope-rise correlation between the TAN0602-06 line and DSDP Leg 28 Sites 270–272, via lines BGR80-003, -004 and 005 (Figs. 8-2 and 8-8; Table 8-3), the transitional sequence unconformity AS-u6/uT-FG links to RSU4. RSU4 has age of 15–16 Ma constrained by the DSDP boreholes ~300 km away from the AS-RS transect (Figs. 8-2, 8-10 and 8-11; Brancolini et al., 1995; De Santis et al., 1999; Brancolini and Leitchenkov, 2010). This age range is the same as our model age of 15.3 Ma on the basin flanks. The upper boundary of the transitional sequence (horizon AS-u6/uT-FG) follows a similar age trend than uPG-T. It appears older on the basin flanks at 15.3 Myr (points 1–3 in Fig. 8-10; Fig. 8-11) but younger in the middle (9 Myr, Late Miocene, points 5–7, Fig. 8-10), probably due to bottom water circulation and reworking of the Ross Sea gyre and/or AABW.

In the eastern Amundsen Sea 3D seismic reflection correlation, the transitional sequence AS-u6/uT-FG in line AWI-20100117 of the AS-RS transect, matches the base of Unit III in crossing line AWI-95054 (Figs. 8-2, 8-9, 8-11). The base of Unit III was assigned a hypothetical age of 14 Ma (Gohl et al., 1997; Nitsche et al., 1997, 2000; Uenzelmann-Neben and Gohl, 2012), which is very close to our model age for the same area. Although these ages are almost identical they should still be tested by drilling.

#### 8.6.5 The full glacial (FG) sequence

During the mid-Miocene and into the Pliocene–Pleistocene, the ACC developed fully, whilst bottom water formation and circulation intensified, and the elevated topography in Western Antarctica had evolved close to the present day (Fig. 8-12d; Table 8-1; Fig. 1-1). The WAIS remained grounded on the continental shelf, but underwent advance/retreat oscillations (blue polygon and arrows in Fig. 8-12d). This period sees the lowest sediment influx ( $0.76$  to  $0.88 \times 10^6$  km<sup>3</sup>; Table 8-4) but the highest sedimentation rate (1.5–3.6 cm/ky), interpreted to probably be due to the frequent advance/retreat cycles in the shelf. The reflections in this sequence are very closely spaced with complex internal geometry, which attests to the ice sheet activity and related depositional processes.



In the seismic horizon Ross Sea shelf-slope-rise correlation, AS-u7 links to RSU3, AS-u8 to RSU2 and AS-u9 to RSU1 (Fig. 8-11). Unit RSS-8 pinches out down slope in line TAN0602 (Fig. 8-8 and 8-11). Our model ages of 9-12 Myr, 4.8 Myr and 1.2–2 Myr for AS-u7, -8 and -9, respectively are in very good agreement with the DSDP drilling data and seismic stratigraphy of the eastern Ross Sea shelf (Fig. 8-10 and 8-11; De Santis et al., 1999; Brancolini et al., 1995; Brancolini and Leitchenkov, 2010).

In the eastern Amundsen Sea seismic horizon correlation (Fig. 8-9) AS-7 and AS-8 correlate with Unit III, while AS-9 and AS-10 correlate with Unit IV (Figs. 8-9 and 8-11; Nitsche et al., 1997, 2000; Uenzelmann-Neben and Gohl, 2012). However, our age model suggests an older age of 8 Ma as oppose to 4 Ma in Uenzelmann-Neben and Gohl (2012). The units are the thickest on the eastern basin flank (up to 889 m; Fig. 8-4; Appendix B-1), which might be due to the close proximity to the glacial stream outlet. Similar to the transitional units, this sequence also thins over the AS-2 PG drift and the anomalous basement topography. See section 8.6.6 for the discussion on why this might be the case.

A series of stacked drifts lie on AS-u9. They are 50–100 km wide and 200–300 m high, and occur in the central and western parts of the basin. These FG-drifts are usually confined to their respective seismic units and may fill up part, or all, of the unit thickness. The stoss side of all the drifts trend West and this geometry suggests an eastward flowing current (Stow et al., 2002; Shanmugam, 2006; Shanmugam and Camerlenghi, 2008), which is consistent with the post mid-Miocene (<15.5 Ma) bottom-current observations of Uenzelmann-Neben and Gohl (2012; Fig. 8-4d). The FG-drifts in AS-8 are estimated to be 9-7 Myr old (points 3 and 7, Fig. 8-4b and Fig. 8-10), those in AS-9 in the 8–4 Myr age range, and the ones in AS-10, younger than 4.3 Myr (point 3, Fig. 8-4b and Fig. 8-10). A stacked buried channel-levee system can be seen in all the units, just to the East of the large PG-drift (line km 1500 to 1600, Fig. 8-4, Appendix B-1).

### 8.6.6 Basement geometry

The acoustic basement can be divided into four distinct regions, from West to East:

Region 1 – The Eastern Ross Sea up to the Kohiko fracture zone (line km 0–650 in Fig. 8-4; Appendix B-1): This part shows a rugged and irregular topography, ascribed to the spreading rates decreasing to below 60 mm/Myr after the Paleocene (C22n) at the mid-oceanic-ridge (AWI-20100107 in Figs. 8-1, 8-2; Fig. 8-4a; Wobbe et al., 2012). It has been well researched that spreading rates below 60–70 mm/Myr can lead to an abrupt increase in basement roughness (Malinverno, 1991; Small and Sandwell, 1989).

Region 2 – From the Kohiko fracture zone to the Endeavour fracture zone (line km 650–1200 in Fig. 8-4; Appendix B-1): The basin geometry deepens towards the basin centre and exhibits typical block faulting, which could possibly be associated with fracture zones that have a lateral and vertical displacement (Wobbe et al., 2012; Kalberg and Gohl, 2013; Luyendyk et al., 2003; Davey and De Santis, 2006; Jordan et al., 2010).

Region 3 – From the Endeavour fracture zone up to the Proto-Antipodes fracture zone (line km 1200–1650 in Fig. 8-4; Appendix B-1): The basement topography is much smoother and regular in this part. No faults were visible in the seismic image and the slope angle of this part is  $\sim 1$  degree (Fig. 8-5). This smoother basement could be due spreading rates for this region being more than  $60\text{--}70 \text{ mm Myr}^{-1}$  (Wobbe et al., 2012).

Region 4 – From the East of the Proto-Antipodes fracture zone to the eastern Amundsen Sea flank (line km 1650–2000 in in Fig. 8-4; Appendix B-1): Rugged basement topography but with an overall horizontal trend. The ruggedness is due to the transect crossing the Marie Byrd seamounts (MBS, line AWI-20100117 in Figs. 8-1, 8-2) and that we may have a mix of stretched continental crust with interleaved volcanic segments (Wobbe et al., 2012; Gohl et al., 2013).

Since regions 1, 2 and 4 are accounted for, both in basement roughness and the seismic characteristics, we centre our discussion on exploring the probable cause of the changing reflection angles and the abrupt thinning of most the seismic units in region 3. Fig. 8-5 illustrates an enlarged segment of region 3, showing the all the internal reflections and unit boundaries. Units AS-2 and AS-3 are mostly parallel to the general basin geometry and basement slope trend. Above AS-u3, the reflections become increasingly angular and reach their largest internal angles up to AS-u6. Above AS-u6, the reflections change to progressively more horizontal and parallel (line drawing in Fig. 8-5b). Additionally, unit thicknesses decrease markedly (section 8.5.3).

We speculate that this change in horizon angles may be attributed to tectonic uplift. For instance: reflections up to AS-u2 that are all parallel to the basement were either present before the uplift, or the rate of uplift was similar to rate of deposition. Towards AS-u3, the angle changes gradually, which could indicate that uplift may have started, or accelerated, up to AS-u6. Near or after AS-u6 uplift may have stopped and the units above AS-u6 deposited in a parallel manner.

If we impose the model horizon ages (Fig. 8-11) on this theory, the uplift started before or near AS-u3/uPG-T, which is  $\sim 30$  Ma in our age model (point 7 and 8 in Fig. 8-10). Uplift continued with increasing tempo till AS-u6/uT-FG ( $\sim 13$  Ma) and thereafter ended or slowed down significantly.

Which tectonic events on the Pacific margin of West Antarctica can account for this signature? We postulate that this change in horizon dip angles may be related to either the Marie Byrd Land uplift that was presumably caused by a mantle plume (LeMasurier, 2008), or by processes related to the emplacement of the Marie Byrd Seamounts (65-56 Ma; Kipf et al., 2013) associated with a thermally driven uplift of the crust via magmatic underplating as a product of partial melting (Kipf et al., 2013; Kalberg and Gohl, 2013).

## 8.7 Conclusions

Collective interpretation of the AWI-2010 and Tan0602 multichannel seismic reflection data (~2937 line kilometres) and supporting existing lines (~1784 line kilometres) increased our understanding of the Cretaceous to present Amundsen Sea basin geometry, bottom current development and likely ice sheet development. Having placed the first seismic stratigraphic results for this basin in a conceptualised age model that is in broad agreement with the Ross Sea shelf DSDP Leg 28 Sites 270–272 and IODP Leg 318 Site U1356 off the Wilkes Land margin, we summarise the main conclusions and contributions:

1. A new seismic horizon stratigraphic nomenclature was developed and assigned to key marker horizons in a representative Amundsen Sea basin type section. The seismic units (AS-1 to AS-10) and unconformities (AS-u1 to AS-u9) were grouped into three 1<sup>st</sup> order sequences, related to the pre-glacial, transitional and full glacial climate regimes of Antarctica.
2. The pre-glacial sequence comprises AS-1 to AS-3 and associated boundary horizons (bsmnt to AS-u3/uPG-T) with an age range estimate of 79–34 Myr. All units were traced throughout the basin and some terminate against the Pahemo fracture zone (AS-1) and the Kohiko fracture zone (AS-2 and AS-3). AS-1 is the thickest, in a valley at the Endeavour fracture zone (1256 m), which is also the centre-point and deepest part of the overall known basin geometry. AS-3 is anomalously thick compared to all the units and contain a large ~300 km long and up to ~400 m high elongate levee drift on the eastern basin flank, estimated to be of Eocene age. A Paleogene to Eocene eastward flowing bottom current is inferred. The sediment thickness for the PG sequence ranges from 358–2203 m with a sedimentation rate of 0.6–2.1 cm/ky.
3. The transitional sequence (AS-4 to AS-6 and boundary horizons AS-u3/uPG-T to AS-u6/uT-FG) has a collective age range estimate of 34–15.5 Myr, and are present throughout the basin along the AS-RS transect and the Tan0602 survey. The units thin markedly to 274 m thick above the region of the AS-2 PG-drift on the eastern flank of the basin. The T-drifts, mounds or sediment waves are confined to the far western basin flank and perched on a basement high, but the geometry does not allow for a current direction interpretation. The amalgamated base terminates either on AS-u4, within AS-4, or directly on the basement. The tops penetrate up to four of the seismic units above (AS-5 to AS-8). The sediment thickness for the T sequence ranges from 274 to 1070 m and thins from West to East. The sedimentation rate is estimated at 1.0–2.5 cm/ky.
4. The full glacial sequence (AS-7 to AS-10 and boundary horizons AS-u6/uT-FG to sflr) of age range 15.5 to 0 Myr, are also present throughout all the seismic lines and assumed, throughout the basin. AS-8 and AS-9 thins to 45 m and 52 m thick above the AS-2 PG-drift location, but the thickness of AS-10 remains consistent (~150 m thick). The FG-drifts are typically 50–100 km wide and 200–300 m high. They are

- mainly concentrated on the western flank of the basin and stacked (up to 3 levels) above the Pahemo fracture zone. The stoss side of the FG-drifts pinch out to the West and thus an eastward flowing, mid-Miocene to Pliocene current is inferred. AS-8 is the only FG unit that has a drift body on the eastern basin flank. The sediment thickness for the FG sequence ranges from 374–889 m and thins towards the basin flanks. It has the highest sedimentation rate of 1.5–3.6 cm/ky.
5. The regional stratigraphic correlation with the Wilkes Land deep-sea horizons, the Ross Sea shelf data and the far eastern Amundsen Sea supports the age model. The estimated 34 Myr AS-u3/uPG-T unconformity correlates with WL-U3 (33.5 Ma) in Wilkes Land, RSS-5 on the Ross Sea shelf, and with the base of Unit II in the eastern Amundsen Sea. The sequence boundary AS-u6/uT-FG correlates with WL-U5 in Wilkes Land, RSS-4 on the Ross Sea shelf, and with the base of Unit III in the far eastern Amundsen Sea.
  6. The major deposition centres for the pre-glacial to glacial periods are located in the basin centre and in front of Ross Sea outlet. They seem to have remained consistent in location during the basin evolution.
  7. The transitional sequence indicates the Eocene onset of the glacially dominated environment of West Antarctica.
  8. From only looking at the seismic data, there is no apparent difference in the deep-sea sediment transport processes or a shift in deposition between the Amundsen Sea and Ross Sea. The seismic sections in the deep-sea basins show continuous sequences with consistent internal geometry. However, the data used is of limited extent and this conclusion may change if more drilling or seismic data become available.
  9. Regional variation in acoustic basement topography revealed rugged basin flanks. On the western flank it is attributed to spreading rate decreasing below 60-70 mm and on the eastern flank, ascribed to the intrusion of the Marie Byrd Seamounts and a zone of a mix of stretched continental crust. The parts to the West of the basin centre show fracture zones with vertical displacement. The smooth part in the eastern part of the transect, is attributed to a faster seafloor spreading rate ( $>60 \text{ mm Myr}^{-1}$ ) and the absence of fracture zones.
  10. The change in the layering of the internal reflections and thickness of the seismic units in the region of the large AS-2 PG-drift may be attributed to tectonic uplift, for example during the Marie Byrd Land uplift or during the emplacement of the Marie Byrd Land Seamounts.
  11. It is estimated that at least 4 km sediment was eroded off land and deposited in the deep-sea basin, this may be larger because sediment in the seismic sections were not decompacted during thickness calculations. The total sediment volume estimate for the deep sea Amundsen Sea – eastern Ross Sea basin is  $2.8 \text{ to } 3.3 \times 10^6 \text{ km}^3$ . The pre-glacial (up to 34 Ma Eocene/Oligocene), Transitional (34–15.5 Ma, Eocene to mid-Miocene) and full glacial ( $<15.5 \text{ Ma}$ ) climate regime sediment volumes are estimated



at: PG = 1.5 to 1.8 x 10<sup>6</sup> km<sup>3</sup>, T = 0.8 to 1.0 x 10<sup>6</sup> km<sup>3</sup> and FG = 0.8 to 0.9 x 10<sup>6</sup> km<sup>3</sup>.

Our interpretations and conclusions rest on the assumption that the variation in amplitude and internal geometry observed in the seismic images, represent changes in the depositional processes that can be related back to the tectonic and ocean-circulation changes in the pre-glacial, transitional and full glacial climates. The sediment velocities are fairly well restrained with sonobuoy and refraction data, although this could be improved upon. The largest uncertainties lie in the age model due to the absence of deep-sea drilling information as age-control. Despite this, we believe the framework to be the best estimate based on all available data, and places our results in a useful context for future drilling, further seismic acquisition, or palaeotopography and palaeobathymetry reconstruction of this margin. Supplementary data to this article can be found online at <http://dx.doi.org/10.1016/j.palaeo.2015.11.017>.

## 8.8 Acknowledgements

The authors are grateful for the support of the masters and crews of RV *Polarstern* during expedition ANT-XXVI/3 (2010) and of RV *Tangaroa* during expedition TAN0602 (2006). We extend our gratitude to the seismic teams on board of both vessels for successful data acquisition. The German component of this project was funded by the Priority Program 1158 'Antarctic Research' of the Deutsche Forschungsgemeinschaft (DFG) under project number GO 724/10-1 and by institutional funds for Work Package 3.2 of the AWI research program PACES. The Government of New Zealand funded the 2006 data acquisition by RV *Tangaroa*. This project contributes to the Circum-Antarctic Stratigraphy and Palaeobathymetry (CASP) project, a Scientific Committee on Antarctic Research – Past Antarctic Ice Sheet Dynamics (SCAR-PAIS) working group. Navigation and SEG Y data for the Ross Sea shelf lines were obtained with thanks from the Antarctic Seismic Data Library System (SDLS; <http://sdl.s.ogs.trieste.it>).

## 8.9 References

- Arndt, J.E. et al., 2013. The International Bathymetric Chart of the Southern Ocean (IBCSO) - digital bathymetric model. doi:10.1594/PANGAEA.805734, In Supplement to: Arndt, J.E., Schenke, H.W., Jakobsson, M., Nitsche, F.-O., Buys, G., Goleby, B., Rebesco, M., Bohoyo, F., Hong, J.K., Black, J., Greku, R.K., Udintsev, G.B., Barrios, F., Reynoso-Peralta, W., Taisei, M., Wigley, R., 2013. The International Bathymetric Chart of the Southern Ocean Version 1.0 - A new bathymetric compilation covering circum-Antarctic waters. *Geophysical Research Letters*, 40(9), 1-7, doi:10.1002/grl.50413 doi:10.1594/PANGAEA.805734?format=html
- Anderson, J.B., 1999. *Antarctic Marine Geology*. Cambridge University Press, Cambridge, 289 pp.
- Anderson, J.B. (Ed.), 2006. *SHALDRIL II Cruise Report*, 369 pp. <http://shaldril.rice.edu/>
- Anderson, J.B., Bartek, L.R., 1992. Cenozoic glacial history of the Ross Sea revealed by intermediate resolution seismic reflection data combined with drill site information. In: Kennett, J.P., Warnke, D.A. (Eds.), *The*

- Antarctic Paleoenvironment: A Perspective on Global Change, Part One. Antarctic Research Series, 56. American Geophysical Union, Washington, DC, 231–263.
- ANTOSTRAT, 1995. Seismic Stratigraphic Atlas of the Ross Sea, in *Geology and Seismic Stratigraphy of the Antarctic Margin*, (Eds.) A. K. Cooper, Barker, P. F., Brancolini, G., 68 pp., 22 plates, American Geophysical Union, Washington, D.C.
- Bamber, J.L., Riva, R.E.M., Vermeersen, B.L.A. & LeBrocq, A.M., 2009. Reassessment of the potential sea-level rise from a collapse of the West Antarctic Ice Sheet, *Science* 324, 901–903, doi:10.1126/science.1169335.
- Barker, P.F., 2001. Scotia Sea regional tectonic evolution: implications for mantle flow and palaeocirculation. *Earth-Science Reviews* 55, 1–39.
- Barker, P.F., Dalziel, I.W.D., Storey, B.C., 1991. Tectonic development of the Scotia Arc region. In: Tingey, R.J. (Ed.), *Geology of Antarctica*. Oxford University Press, Oxford, 215–248.
- Barker, P.F., Camerlenghi, A., Acton G.D., Ramsay, A.T.S. et al., 2002. Proceedings of the ODP, Scientific Results 178, 1–40 (Online) [bhttp://www-odp.tamu.edu/publications/178\\_SRN](http://www-odp.tamu.edu/publications/178_SRN) and [http://www-odp.tamu.edu/publications/178\\_SR/178TOC.HTM](http://www-odp.tamu.edu/publications/178_SR/178TOC.HTM).
- Berner, R.A., Kothavala, Z., 2001. GEOCARB III: A revised model of atmospheric CO<sub>2</sub> over Phanerozoic time. *American Journal of Science* 304, 397–437.
- Bijl, P.K., Bendle, J.A.P., Bohaty, S.M., Pross, J., Schouten, S., Tauxe, L., Stickle, C.E., McKay, R.M., Röhl, U., Olney, M., Sluijs, A., Escutia, C., Brinkhuis, H., and Expedition 318 Scientists, 2013. Eocene cooling linked to early flow across the Tasmanian Gateway. *PNAS* 110, (24), 9645–9650. doi:10.1073/pnas.1220872110.
- Brancolini, G. and Leitchenkov, G., 2010. Ross Sea. 118–128. In: Cooper, A.K., Brancolini, G., Escutia, C., Kristoffersen, Y., Larer, R., Leitchenkov, G., O'Brien, P., Jokat, W., 2009. Chapter 5 - Cenozoic Climate History from Seismic Reflection and Drilling Studies on the Antarctic Continental Margin. In: Florindo, F., Siegert, M. (Eds.). *Developments in Earth and Environmental Sciences 8, Antarctic Climate Evolution*. The Netherlands: Elsevier, 115–228. ISBN: 978-0-444-52847-6.
- Brancolini, G., Cooper, A.K., Coren, F., 1995. Seismic Facies and Glacial History in the Western Ross Sea (Antarctica), Antarctic Research Series. American Geophysical Union, Washington, DC, 68, 209–234.
- Cande, S.C., Stock, J. M., Müller, R. D. & Ishihara, T., 2000. Cenozoic motion between East and West Antarctica. *Nature* 404, 145–150. doi:10.1038/35004501.
- Davey, F. J. and De Santis, L., 2006. A Multi-Phase Rifting Model for the Victoria Land Basin, Western Ross Sea. *Antarctica*, 303–308. doi: 10.1007/3-540-32934-X\_38.
- De Santis, L., Anderson, J.B., Brancolini, G. & Zayatz, I., 1995. Seismic record of late Oligocene through Miocene glaciation on the Central Eastern continental shelf of Ross Sea. In: *Geology and Seismic Stratigraphy of the Antarctic Margin*. Cooper, A.K., Barker, P.F. & Brancolini, G. (Eds.), Antarctic Research Series 68, 235–260, American Geophysical Union, Washington, D.C.
- De Santis, L., Prato, S., Brancolini, G., Lovo, M., Torelli, L., 1999. The Eastern Ross Sea continental shelf during the Cenozoic: implications for the West Antarctic ice sheet development. *Global and Planetary Change* 23, 173–196. PII: s0921-8181(99)00056-9.
- De Santis, L., Brancolini, G., Donda, F., 2003. Seismo-stratigraphic analysis of the Wilkes Land continental margin (East Antarctica): influence of glacially driven processes on the Cenozoic deposition. *Deep Sea Research Part II: Topical Studies in Oceanography* 50, 8-9, 1563–1594, doi:10.1016/S0967-0645(03)00079-1.
- Dowdeswell, J.A., O'Cofaigh, C., Pudsey, C.J., 2004. Continental slope morphology and sedimentary processes at the mouth of an Antarctic palaeo-ice stream. *Marine Geology* 204, 203–214.

- Dowdeswell, J.A., Cofaigh, C.Ó. & Anderson, J.B., 2006. Morphology and sedimentary processes on the continental slope off Pine Island Bay, Amundsen Sea, West Antarctica. *Geological Society of America Bulletin* 118, 606–619.
- Eagles, G., Jokat, W., 2014. Tectonic reconstructions for paleobathymetry in Drake Passage. *Tectonophysics*, 611, 28–50. doi:10.1016/j.tecto.2013.11.021.
- Eagles, G., Gohl, K., Larter, R.D., 2004. Life of the Bellingshausen plate, *Geophysical Research Letters* 31, L07603, doi:10.1029/2003GL019127.
- Escutia, C., De Santis, L., Donda, F., Dunbar, R.B., Cooper, A.K., Brancoli, G., Eittreimd, S.L., 2005. Cenozoic ice sheet history from East Antarctic Wilkes Land continental margin sediments. *Global and Planetary Change* 45, 1-3, 51–81 doi:10.1016/j.gloplacha.2004.09.010.
- Escutia, C., Brinkhuis, H., Klaus, A., and the Expedition 318 Scientists, 2011. Proceedings IODP, 318: Tokyo (Integrated Ocean Drilling Program Management International, Inc.), 101pp. doi:10.2204/iodp.proc.318.2011 and [http://publications.iodp.org/proceedings/318/104/104\\_.htm](http://publications.iodp.org/proceedings/318/104/104_.htm).
- Fritsch, J., 1980. Fahrtbericht Über Geophysikalische Messungen im Ross-Meer/Antarktis während der Monate Januar/Februar 1980. Archiv-Nr. 86058, Tagebuch-Nr. 10980/80, 7 Anlagen. Bundesanstalt für Geowissenschaften und Rohstoffe Hannover, Deutschland.
- Gradstein, F.M., Ogg, J.G., Smith, A.G. (Eds.), 2004. *A Geologic Time Scale 2004*. Cambridge University Press, Cambridge, 610 pp.
- Gohl, K., 2007. The Expedition ANTARKTIS-XXIII/4 of the Research Vessel “Polarstern” in 2006. *Berichte zur Polar- und Meeresforschung (Reports on Polar and Marine Research)* 557, 166 pp., <http://epic.awi.de/26756/>.
- Gohl, K., 2010. The expedition of the research vessel “Polarstern” to the Amundsen Sea, Antarctica, in 2010 (ANTXXVI/3). *Berichte zur Polar- und Meeresforschung / Reports on Polar and Marine Research*, 617 pp. <http://epic.awi.de/29635/>.
- Gohl, K., Nitsche, F., Vanneste, K., Miller, H., Fechner, N., Oszko, L., Hübscher, C., Weigelt, E., Lambrecht, A., 1997. Tectonic and sedimentary architecture of the Bellingshausen and Amundsen Sea Basins, SE Pacific, by seismic profiling. In: *The Antarctic Region: Geological Evolution and Processes*, by Ricci, C.A. (Ed.), p. 719-723, Terra Antarctica Publication, Siena.
- Gohl, K., Denk, A., Eagles, G., Wobbe, F., 2013a. Deciphering tectonic phases of the Amundsen Sea Embayment shelf, West Antarctica, from a magnetic anomaly grid. *Tectonophysics*, 585, 113–123. doi.org/10.1016/j.tecto.2012.06.036.
- Gohl, K., Uenzelmann-Neben, G., Larter, R.D., Hillenbrand, C.-D., Hochmuth, K., Kalberg, T., Weigelt, E., Davy, B., Kuhn, G., Nitsche, F.O., 2013b. Seismic stratigraphic record of the Amundsen Sea Embayment shelf from pre-glacial to recent times: Evidence for a dynamic West Antarctic Ice Sheet. *Marine Geology* 344, 115–131. doi:10.1016/j.margeo.2013.06.011
- Haq, B.U., and Schutter, S.R., 2008. A chronology of Paleozoic sea-level changes. *Science* 322, 5898, 64–68, doi:10.1126/science.1161648.
- Haq, B.U., Hardenbol, J., and Vail, P.R., 1987. Chronology of fluctuating sea levels since the Triassic (250 million years ago to present). *Science* 235, 1156–1167.
- Hayes, D.E., L.A. Frakes, and Shipboard\_Scientific\_Party, 1975. A geophysical study of the Ross Sea, Antarctica Sites 270, 271, 272 In: *Initial Reports of the Deep Sea Drilling Project, Leg 28*, Hayes, D.E., and Frakes, L.A. (Eds.), 211–334, 887–907, U.S. Government Printing Office, Washington, D.C.
- Hayes, D.E., Zhang, C., Weissel, R.A., 2009. Modeling Paleobathymetry in the Southern Ocean. *EOS, Transactions of the American Geophysical Union* 90 (19), 165–172.

- Haywood, A.M., Smellie, J.L., Ashworth, A.C., Cantrill, D.J., Florindo, F., Hambrey, M.J., Hill, D., Hillenbrand, C.-D., Hunter, S.J., Larter, R.D., Lear, C.H., Passchier, S., van de Wal, R., 2009. Chapter 10 - Middle Miocene to Pliocene History of Antarctica and the Southern Ocean. In: Florindo, F., Siebert, M. (Eds.). *Developments in Earth and Environmental Sciences 8, Antarctic Climate Evolution*. The Netherlands: Elsevier, 401–463. ISBN: 978-0-444-52847-6.
- Huber, M., H. Brinkhuis, C. E. Stickley, K. Döös, A. Sluijs, J. Warnaar, S. A. Schellenberg, and G. L. Williams (2004), Eocene circulation of the Southern Ocean: Was Antarctica kept warm by subtropical waters? *Paleoceanography* 19, PA4026, doi:10.1029/2004PA001014.
- Hinz, K. and Block, M., 1985. Results of geophysical investigations in the Weddell Sea and in the Ross Sea. *Proceedings of the 11th World Petrologic Congress, London 1983 (Vol. 2, Geology Exploration Reserves)*. New York: John Wiley and Sons.
- Iwai, M., Acton, G., Lazarus, D., Osterman, L.E., Williams, T., 2002. Magnetobiochronologic Synthesis of ODP Leg 178 Rise Sediments from the Pacific Sector of the Southern Ocean: Sites 1095, 1096, and 1101. In: Barker, P.F., Camerlenghi, A., Acton, G.D., Ramsay, A.T.S. (Eds.), *Proceedings of the Ocean Drilling Program, Scientific Results 178*. Ocean Drilling Program, College Station.
- Jordan T.A., Ferraccioli, F., Vaughan, D.G., Holt, J.W., Corr H., Blankenship, D.D., Diehl, T.M., 2010. Aerogravity evidence for major crustal thinning under the Pine Island Glacier region (West Antarctica). *GSA Bulletin* 122, 5-6, 714–726. doi: 10.1130/B26417.1.
- Kalberg, T. and Gohl, K., 2013. The crustal structure and tectonic development of the continental margin of the Amundsen Sea Embayment, West Antarctica: Implications from geophysical data. *Geophysical Journal International*, submitted.
- Kipf, A., Hauff, F., Werner, R., Gohl, K., van den Bogaard, P., Hoernle, K., Maicher, D., Klügel, A., 2013. Seamounts off the West Antarctic margin: A case of non-hotspot intraplate volcanism. *Gondwana Research*. doi:10.1016/j.gr.2013.06.013.
- Klages, J.P., Kuhn, G., Hillenbrand, C.-D., Graham, A.G.C., Smith, J.A., Larter, R.D., Gohl, K., 2013. First geomorphological record and glacial history of an inter-ice stream ridge on the West Antarctic continental shelf. *Quaternary Science Reviews* 61, 47–61, doi:10.1016/j.quascirev.2012.11.007.
- LaBrecque, J.L., Cande, S., Bell, R., Raymond, C., Brozena, J., Keller, M., Parra, J.C., Yáñez, G., 1986. Aerogeophysical survey yields new data in the Weddell Sea. *Antarctic Journal Review* 21, 69–71.
- Larter, R.D., Cunningham, A.P., Barker, P.F., Gohl, K., Nitsche, F.O., 2002. Tectonic evolution of the Pacific margin of Antarctica 1. Late Cretaceous tectonic reconstructions. *Journal of Geophysical Research* 107, B12, 2345. doi: 10.1029/2000JB000052.
- Lawver, L.A. and Gahagan, L., 2003. Evolution of Cenozoic Seaways in the circum-Antarctic region. *Palaeogeography, Palaeoclimatology, Palaeoecology* 198, 11–37, [http://dx.doi.org/10.1016/S0031-0182\(03\)00392-4](http://dx.doi.org/10.1016/S0031-0182(03)00392-4).
- Lear, C.H., Bailey, T.R., Pearson, P.N., Coxall, H.K., Rosenthal, Y., 2008. Cooling and ice growth across the Eocene–Oligocene transition. *Geology* 36, 251–254. <http://dx.doi.org/10.1130/G24584A.1>.
- Le Brocq, A.M., Payne, A.J., Vieli, A., 2010. An improved Antarctic dataset for high resolution numerical ice sheet models (ALBMAP v1). *Earth System Science Data Discussions* 3, 195–230. <http://dx.doi.org/10.5194/essdd-3-195-2010>, [www.earth-systsci-data-discuss.net/3/195/2010/](http://www.earth-systsci-data-discuss.net/3/195/2010/).
- Leitchenkov, G.L., Guseva, Y.B., Gandyukhin, V.V., 2007a. Cenozoic environmental changes along the East Antarctic continental margin inferred from regional seismic stratigraphy. In: Cooper, A.K. & Raymond, C.R. (Eds.), *Antarctica: A Keystone in a Changing World - Online Proceedings of the 10th ISAES: USGS Open-File Report 2007-1047 Short Research Paper 005*. <http://dx.doi.org/10.3133/of2007-1047.srp005>.



- Leitchenkov, G.L., V.V. Gandyukhin, and Y.B. Guseva, 2007b. Crustal structure and evolution of the Mawson Sea, western Wilkes Land margin, East Antarctica, in *Antarctica: A Keystone in a Changing World – Online Proceedings of the 10th ISAES*, Cooper, A.K., & Raymond, C.R., et al. (Eds.), USGS Open-File Report 2007-1047, Short Research Paper 028, 4 pp.; doi:10.3133/of2007-1047.srp028.
- Leitchenkov, G., Guseva, J., Gandyukhin, V., Grikurov, G., Kristoffersen, Y., Sand, M., Golynsky, A., Aleshkova, N., 2008. Crustal structure and tectonic provinces of the Riiser Larsen Sea area (East Antarctica): results of Geophysical studies. *Marine Geophysical Research* 29, 135–158. <http://dx.doi.org/10.1007/s11011-008-9051-z>.
- LeMasurier, W.E., 2008. Neogene extension and basin deepening in the West Antarctic rift inferred from comparisons with the East African rift and other analogs. *Geology* 36, 247–250, doi:10.1130/G24363A.
- Lindeque, A., Martin, Y.M., Gohl, K., Maldonado, M., 2013. Deep-sea pre-glacial to glacial sedimentation in the Weddell Sea and southern Scotia Sea from a cross-basin seismic transect. *Marine Geology* 336, 61–83. <http://dx.doi.org/10.1016/j.margeo.2012.11.004>.
- Lindow, J., Spiegel, C., Johnson, J., Lisker, F., Gohl, K., 2011, Constraining the latest stage exhumation of Marie Byrd and Ellsworth Land, West Antarctica, 11<sup>th</sup> International Symposium on Antarctic Earth Science; Edinburgh, Scotland.
- Livermore, R., Nankivell, A., Eagles, G., Morris, P., 2005. Paleogene opening of Drake Passage. *Earth and Planetary Science Letters* 236, 459–470. <http://dx.doi.org/10.1016/j.epsl.2005.03.027>.
- Lowe, A.L. and Anderson, J.B., 2002. Reconstruction of the West Antarctic Ice Sheet in Pine Island Bay during the last glacial maximum and its subsequent retreat history. *Quaternary Science Research* 21, 1879–1897.
- Luyendyk, B., Wilson, D. S., Siddoway, C. S., 2003. Eastern margin of the Ross Sea Rift in western Marie Byrd Land, Antarctic: Crustal structure and tectonic development. *Geochemistry Geophysics Geosystems*, 4, doi:10.1029/2002GC000462.
- Lythe, M. B., Vaughan, G.D., and the BEDMAP Consortium. (2001), BEDMAP: A new ice thickness and subglacial topographic model of Antarctica. *Journal of Geophysical Research* 106, 11,335–11,351, doi:10.1029/2000JB900449.
- Maldonado, A., Bohoyo, F., Galindo-Zaldívar, J., Hernández-Molina, F.J., Jabaloy, A., Lobo, F.J., Rodríguez-Fernández, J., Suriñach, E., Vázquez, J. T., 2006. Ocean basins near the Scotia-Antarctic plate boundary: Influence of tectonics and paleoceanography on the Cenozoic deposits. *Marine Geophysical Research* 27, 83-107, doi:10.1007/s11001-006-9003-4.
- Malinverno, A., 1991. Inverse square-root dependence of mid-ocean-ridge flank roughness on spreading rate. *Nature* 352, 6330, 58–60. doi: 10.1038/352058a0.
- Miller, H., Henriot, J.P., Kaul, N., Moons, A., 1990. A fine-scale stratigraphy of the eastern margin of the Weddell Sea. In: Bleil, U., Thiede, J. (Eds.), *Geological History of the Polar Oceans: Arctic Versus Antarctic*. Kluwer Academic Publishers, 131–161.
- Miller, K.G., Wright, J.D., Katz, M.E., Browning, J.V., Cramer, B.S., Wade, B.S., Mizintseva, S.F., 2008. A view of Antarctic ice-sheet evolution from sea-level and deep-sea isotope changes during the Late Cretaceous-Cenozoic. In: Cooper, A.K., Barrett, P.J., Stagg, H., Storey, B., Stump, E., Wise, W., the 10th ISAES editorial team (Eds.), *Proceedings of the 10th International Symposium on Antarctic Earth Sciences. Antarctica: A Keystone in a Changing World*. The National Academies Press, Washington, DC. <http://dx.doi.org/10.3133/of2007-1047.kp06>.
- Müller, R.D., Gohl, K., Cande, S.C., Goncharov, A., Golynsky, A.V., 2007. Eocene to Miocene geometry of the West Antarctic rift system. *Australian Journal of Earth Sciences* 54, 1033–1045, doi:10.1080/08120090701615691.

- Nitsche, F.O., Gohl, K., Vanneste, K., Miller, H., 1997. Seismic expression of glacially deposited sequences in the Bellingshausen and Amundsen Seas, West Antarctica. In: Barker, P.F. & Cooper, A.K. (Eds.) *Geology and Seismic Stratigraphy of the Antarctic Margin 2*. Antarctic Research Series 71, 95–108, American Geophysical Union, Washington, D.C.
- Nitsche, F.O., Cunningham, A.P., Larter, R.D., Gohl, K., 2000. Geometry and development of glacial continental margin depositional systems in the Bellingshausen Sea, *Marine Geology* 162, 2–4, 277–302.
- Oszko, L., 1997. Tectonic structures and glaciomarine sedimentation in the South-Eastern Weddell Sea from seismic reflection data. *Berichte zur Polarforschung (Reports on Polar Research)*, 222. Alfred Wegener Institut für Polar und Meeresforschung, Bremerhaven, Germany. PhD thesis, University of Bremen. hdl:10013/epic.12931.
- Pagani, M., Zachos, J., Freeman, K.H., Tipple, B., Bohaty, S., 2005. Marked decline in atmospheric carbon dioxide concentrations during the Paleogene. *Science* 309, 5734, 600–603. <http://dx.doi.org/10.1126/science.1110063>.
- Pollard, D., DeConto, R.M., 2009. Modelling West Antarctic ice sheet growth and collapse through the past five million years. *Nature* 458, 320–323. <http://dx.doi.org/10.1038/nature07809>.
- Rogenhagen, J., Jokat, W., Hinz, K., Kristoffersen, Y., 2004. Improved seismic stratigraphy of the Mesozoic Weddell Sea. *Marine Geophysical Researches* 25, 265–282, doi:10.1007/s11001-005-1335-y.
- Scheuer, C., Gohl, K., Eagles, G., 2006. Gridded isopach maps from the South Pacific and their use in interpreting the sedimentation history of the West Antarctic continental margin. *Geochemistry Geophysics Geosystems* 7, Q11015. <http://dx.doi.org/10.1029/2006GC001315>.
- Shanmugam, G., 2006. Deep-water processes and facies models. *Handbook of petroleum exploration and production*, 5. Elsevier, Amsterdam. 476 pp.
- Shanmugam, G. and Camerlenghi, M.R.a.A., 2008. Chapter 5 Deep-water bottom currents and their deposits. In: Rebesco, M. & Camerlenghi, A. (Eds.) *Contourites, Developments in Sedimentology* 60, Elsevier, Oxford, Great Britain. 59–81. doi:10.1016/S0070-4571(08)00205-7.
- Small, C. and D. T. Sandwell, 1989. An abrupt change in ridge axis gravity with spreading rate. *Journal of Geophysical Research - Solid Earth* 94, B12, 17383–17392. doi: 10.1029/JB094iB12p17383.
- Smith, R.T. and Anderson, J.B., 2010. Ice-sheet evolution in James Ross basin, Weddell Sea margin of the Antarctic Peninsula: the seismic stratigraphic record. *Geological Society of America Bulletin* 122, 5/6, 830–842. <http://dx.doi.org/10.1130/B26486.1>.
- Stow, D.A.V., Faugères, J.-C., Howe, J.A., Pudsey, C.J., Viana, A.R., 2002. Bottom currents, contourites and deep-sea sediment drifts: current state-of-the-art. In: Stow, D.A.V., Pudsey, C.J., Howe, J.A., Faugeres, J.-C., Viana, A.R. (Eds.), *Deep-water contourite systems: Modern drifts and ancient series*. Memoir. Geological Society of London, London, 7–20.
- Tripati, A.K., Roberts, C.D., Eagle, R.A., 2009. Coupling of CO<sub>2</sub> and ice sheet stability over major climate transitions of the last 20 million years. *Science* 326, 1394–1397. <http://dx.doi.org/10.1016/j.gca.2011.01.018>.
- Tripati, A.K., Roberts, C.D., Eagle, R.A., Li, G., 2011. A 20 million year record of planktic foraminiferal B/Ca ratios: systematics and uncertainties in pCO<sub>2</sub> reconstructions. *Geochimica et Cosmochimica Acta* 75, 10, 2582–2610. <http://dx.doi.org/10.1016/j.gca.2011.01.018>.
- Tucholke, B.E., Edgar, N.T., Boyce, R.E., 1976. Physical properties of sediments and correlations with acoustic stratigraphy: Leg 35, Deep Sea Drilling Project. In: Hollister, C.D., Craddock, C. (Eds.), *Initial Reports*. Deep Sea Drilling Project, Washington, D.C., 229–249.

- Uenzelmann-Neben, G., 2006. Depositional patterns at Drift 7, Antarctic Peninsula: Along-slope versus down-slope sediment transport as indicators for oceanic currents and climatic conditions, *Marine Geology* 233 1–4, 49–62. <http://dx.doi.org/10.1016/j.margeo.2006.08.008>.
- Uenzelmann-Neben, G. and Gohl, K., 2012. Amundsen Sea sediment drifts: Archives of modifications in oceanographic and climatic conditions. *Marine Geology* 299–302, 51–62, doi:10.1016/j.margeo.2011.12.007/.
- Wannesson, J., Perlas, M., Pettitperrin, B., Perret, M., Segoufin, J., 1985. A geophysical transect of the Adelie margin, East Antarctica. *Marine Petrology and Geology*, 2, 192–201. doi: 10.1016/0264-8172(85)90009-1.
- Weigelt, E., Gohl, K., Uenzelmann-Neben, G., Larter, R.D., 2009. Late Cenozoic ice sheet cyclicity in the western Amundsen Sea Embayment - Evidence from seismic records. *Global and Planetary Change* 69, 162–169.
- Wilson, D.S., Jamieson, S.S.R., Barrett, P.J., Leitchenkov, G., Gohl, K., Larter, R.D., 2012. Antarctic topography at the Eocene–Oligocene boundary. *Palaeogeography Palaeoclimatology Palaeoecology*, 335–336, 24–34. <http://dx.doi.org/10.1016/j.palaeo.2011.05.028>.
- Wilson, D.S., Pollard, D., DeConto, R.M., Jamieson, S.S.R., Luyendyk, B.P., 2013. Initiation of the West Antarctic Ice Sheet and estimates of total Antarctic ice volume in the earliest Oligocene. *Geophysical Research Letters*, 40, 4305–4309. <http://dx.doi.org/10.1002/grl.50797>.
- Wobbe, F., Gohl, K., Chambord, A., Sutherland, R., 2012. Structure and breakup history of the rifted margin of West Antarctica in relation to Cretaceous separation from Zealandia and Bellingshausen plate motion. *Geochemistry Geophysics Geosystems* 13, 4 Q04W12, <http://dx.doi.org/10.1029/2011GC003742>.
- Zachos, J., Pagani, M., Sloan, L., Thomas, E., Billups, K., 2001. Trends, rhythms, and aberrations in global climate 65 Ma to present. *Science* 292, 686–693.

## ONLINE SUPPLEMENTS

### **1.1 Supplement S1**

Compilation of palaeoproxy curves (*see Fig. 1-1 in Ch. 1*).

### **1.2 Supplement S2**

Tan0602 Sonobuoy data acquisition, processing and velocity model (*see section 5.4 in Ch. 5, Fig. 5-5 and Table 5-1*).

### **1.3 Supplement S3**

Amundsen Sea – Ross Sea (AS-RS) transect (*A0 plot and fold-out of Fig. 8-4 in this chapter, see Appendix B-1 and back pocket*).

### **1.4 Supplement S4**

Velocity model: interval velocities derived from stacking velocities (*see Appendix B-2*).

### **1.5 Supplement S5**

Velocity model: refraction data, 1D model from AWI-20060200 (*see section 5.3 in Ch. 5 and Figs. 5-1 to 5-4*).

# Chapter 9

## THIRD PAPER

### ANOMALOUS SOUTH PACIFIC LITHOSPHERE AND TOTAL SEDIMENT THICKNESS

Wobbe, F., Lindeque, A., Gohl, K., 2014. Anomalous South Pacific lithosphere dynamics derived from new sediment thickness estimates off the West Antarctic margin. *Global and Planetary Change*, 123 (A), 139–149, doi: 10.1016/j.gloplacha.2014.09.006

#### Highlights:

- First total sediment thickness grid for the Pacific margin of West Antarctica.
  - Residual basement topography show asymmetric trend over Pacific-Antarctic ridge.
  - Maximum sediment thickness ~4 km.
  - Initial sediment volumes for the Bellingshausen, Amundsen and Ross Sea basins.
- 

## 9.1 Abstract

Paleotopographic models of the West Antarctic margin, which are essential for robust simulations of paleoclimate scenarios, lack information on sediment thickness and geodynamic conditions, resulting in large uncertainties. A first total sediment thickness grid spanning the Ross Sea – Amundsen Sea – Bellingshausen Sea basins is presented and is based on all the available seismic reflection, borehole, and gravity modeling data offshore West Antarctica. This new grid was combined with NGDC's global 5 arc minute grid of ocean sediment thickness (Whittaker et al. 2013) and extends the NGDC grid further to the south. Sediment thickness along the West Antarctic margin tends to be 3–4 km, thicker than previously assumed. The sediment volume in the Bellingshausen, Amundsen, and Ross Sea basins amount to 4.15, 3.66, and 2.26 million cubic kilometers respectively. The residual basement topography of the South Pacific has been revised and the new data show an asymmetric trend over the Pacific-Antarctic Ridge. Values are anomalously high south of the spreading ridge and in the Ross Sea area, where the topography seems to be affected by persistent mantle processes. In contrast, the basement topography offshore Marie Byrd Land cannot be attributed to dynamic topography, but rather to crustal thickening due to intraplate volcanism. Present-day dynamic topography models disagree with the presented revised basement topography of the South Pacific, rendering paleotopographic reconstructions with such a limited dataset still fairly uncertain.

**Keywords:** sediment isopach map; sediment thickness grid; sediment volume; residual basement depth; dynamic topography; paleotopography.



## 9.2 Introduction

The accurate reconstruction of paleotopography is a main prerequisite for robust simulations of paleoclimate scenarios. Current paleotopographic models contain large uncertainties due to absent or sparse sediment thickness data and constraints on geodynamic conditions. Since the Southern Ocean plays an important role in global climate processes, we assess the sedimentary and geodynamic conditions of the Southern Pacific to ascertain these essential factors for modern paleotopographic reconstructions.

We present an improved sediment thickness grid for the West Antarctic margin, which is now based on all the available seismic reflection, borehole, and gravity modeling data. This new grid spans the Antarctic Peninsula, Bellingshausen Sea, Amundsen Sea and Ross Sea, and links to Whittaker et al.'s (2013) data off Victoria Land. In the first part of this publication, we compare our results to previous work and discuss possible implications for paleotopography and paleoclimate reconstructions of Antarctica.

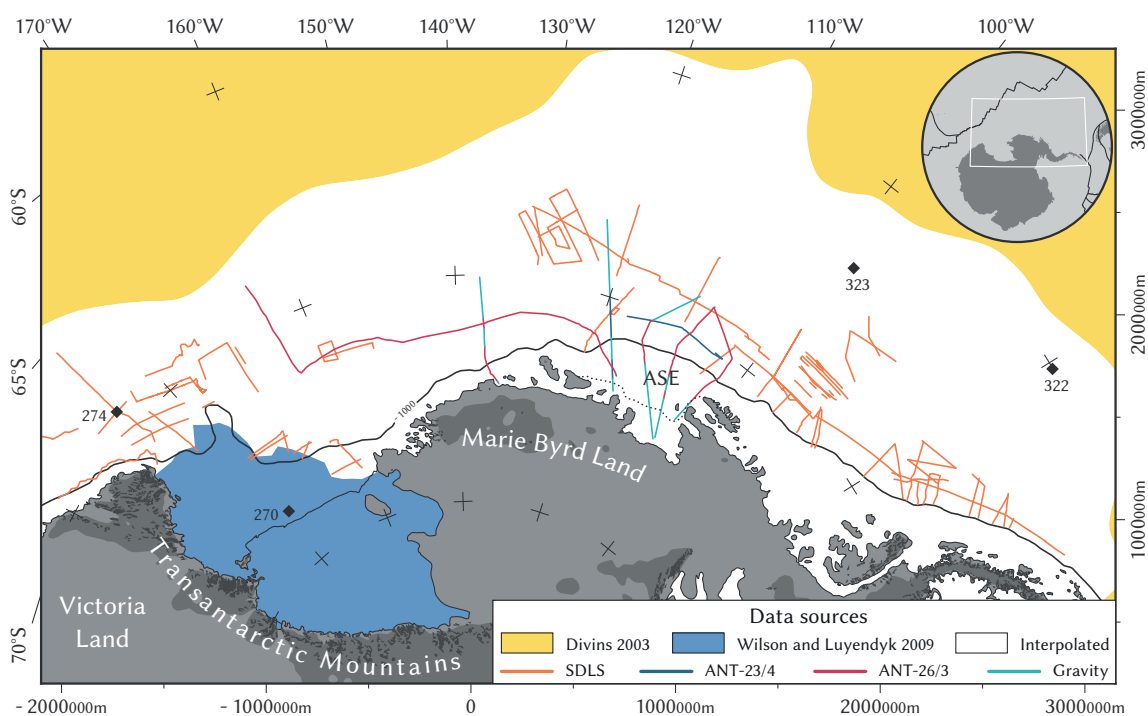


**Fig. 9-1.** Data sources used for compiling total sediment thickness and estimating sediment volumes. Areas based on gridded external data sources filled with solid colors (Divins 2003; Wilson and Luyendyk 2009). Data collected on transects are mostly multichannel seismic-reflection data available from the Antarctic Seismic Data Library System (SDLS, Wardell et al. 2007) and recent publications (ANT-23/4 and ANT-26/3: Scheuer et al. 2006a; Lindeque and Gohl 2010; Uenzelmann-Neben and Gohl 2012; Wobbe et al. 2012; Gohl et al. 2013; Kalberg and Gohl 2013). Some sediment thickness estimates in the Amundsen Sea sector are based on gravity models (Wobbe et al. 2012). Dotted line outlines limit of sedimentary cover on inner Amundsen Sea Embayment (ASE) shelf (Gohl et al. 2013). Polar stereographic projection with central meridian of 138° W and latitude of true scale at 71° S referenced to WGS84.

In a second part, we analyze and re-evaluate the Late Cretaceous to present lithosphere dynamics of the South Pacific after the final breakup of Gondwana. The rifted continental margins of New Zealand and West Antarctica experienced different tectonic histories: As New Zealand drifted away from Antarctica it was subjected to excess tectonic subsidence of 500–900 m, with a maximum during the interval 70–40 Myr (Spasojevic et al. 2010; Sutherland et al. 2010). The conjugate Marie Byrd Land margin, by contrast, was deformed by movement of the Bellingshausen plate relative to Antarctica (Wobbe et al. 2012), affected by intraplate volcanism (Kipf et al. 2014), and covered by large amounts of glacial sediments (e.g., Rebesco et al. 1997; Scheuer et al. 2006a).

The West Antarctic margin and its adjacent seafloor is currently more than 1000 m shallower than the conjugate New Zealand margin. It has been suggested that mantle upwelling following the Gondwana subduction cessation could have caused this anomalously high topography (e.g., Storey et al. 1999; Sieminski et al. 2003; Winberry and Anandakrishnan 2004; Finn et al. 2005; Spasojevic et al. 2010; Sutherland et al. 2010).

In order to test this hypothesis with new data, we determined the sediment corrected basement topography for the South Pacific and compared it to: (i) an empirical sediment corrected depth model from the North Pacific (Crosby et al. 2006), (ii) various dynamic topography models (e.g., Ricard et al. 1993; Steinberger 2007; Conrad and Husson 2009; Spasojevic and Gurnis 2012; Flament et al. 2013), and (iii) a current mantle shear wave velocity model (Schaeffer and Lebedev 2013). The differences between the dynamic topography models are discussed and the implications for reconstructing the South Pacific paleobathymetry and -topography are highlighted.

### 9.3 Sediment thickness grids of the West Antarctic margin

We derived new 5 km and 5 arc minute resolution sediment thickness grids from seismic reflection and refraction data, from gravity models, and from data of selected drill sites on the West Antarctic margin of the Pacific (Ross Sea – Amundsen Sea – Bellingshausen Sea – Antarctic Peninsula).

#### 9.3.1 Sediment thickness calculation

Total sediment thickness estimates of the continental margin and the deep ocean floor are largely based on multichannel seismic reflection surveys (Fig. 9-1). We used the two-way travel times (TWT) between the seafloor and the acoustic basement reflections along seismic reflection transects available from the Antarctic Seismic Data Library System (SDLS, Wardell et al. 2007; Table in Appendix C-1), and along recently acquired and processed seismic profiles (e.g., ANT-18/5a, ANT-23/4, and ANT-26/3: Scheuer et al. 2006a, b; Lindeque

and Gohl 2010; Uenzelmann-Neben and Gohl 2012; Wobbe et al. 2012; Gohl et al. 2013; Kalberg and Gohl 2013).

The TWT values,  $2T$  in s, were converted to depth,  $Z$  in km, using Carlson et al.'s (1986) empirical relation  $Z = 3.03 \ln(1 + 0.52T)$ . This method has been applied to seismic data acquired along the Antarctic Peninsula in past work (Rebesco et al. 1997; Scheuer et al. 2006a, b). Carlson et al.'s (1986) TWT-depth relationship is calibrated for sediments up to 1.4 km thick ( $\sim 1.4$  s TWT) only and the sediment thickness is considerably overestimated for TWTs larger than 2.8 s. This affects  $<5$  % of the data points, mainly located on the continental rise-slope transition. Due to the lack of area-wide seismic velocity models or downhole velocity measurements at drilling sites, we have to assume the acoustic velocity of sediments thicker than 2.8 s TWT.

P-wave velocities of 5–6 km thick sediments on the continental rise in polar regions typically range from 1800 to 4000 m/s (e.g., West Greenland, Chian et al. 1995; Suckro et al. 2012) or even 4200 m/s (e.g., East Greenland, Voss and Jokat 2007). On the Amundsen Sea continental rise, sediment layer interval velocities from a P-wave refraction model (Lindeque and Gohl 2010; Kalberg and Gohl 2013) and from stacking velocities (Gohl et al. 2007; Uenzelmann-Neben and Gohl 2012; Gohl et al. 2013) range from 1600 to 4200 m/s. We determined the best fitting average acoustic velocity of sediments thicker than 2.8 s TWT to be 2818 m/s and converted all TWT values greater than 2.8 s to depth using this velocity.

The seismic data coverage of the Amundsen Sea Embayment shelf (Gohl et al. 2013) is better than the profiles used for this publication imply (Fig. 9-1). However, only few seismic lines reveal the top of basement. We used gravity modeling to constrain basement depth. The limit of the sedimentary cover approaching the inner shelf is well documented (e.g., Gohl et al. 2013).

### 9.3.2 Data merging and gridding

In order to extend the data coverage of the mapped basement horizons from multichannel seismic data (Fig. 9-1) to the Ross Sea region, we incorporated sediment thickness above the RSU6 unconformity (e.g., Cooper et al. 1991). Sediments below the RSU6 unconformity were excluded, because they predate crustal extension in the Ross Sea (Cooper et al. 1991; De Santis et al. 1995; Wilson and Luyendyk 2009). Wilson and Luyendyk (2009), whose data we included as well, estimated sediment thickness under the Ross Ice Shelf by extrapolating thickness trends in the Ross Sea from gravity anomalies.

Four Deep Sea Drilling Project (DSDP) boreholes in the area of interest reach the basement and their borehole depth measurements complement the sediment thickness data from the Ross Sea (sites 270 and 274, Hayes et al. 1975) and fill in the gaps of the most distal areas along the Antarctic Peninsula (sites 322 and 323, Hollister et al. 1976).

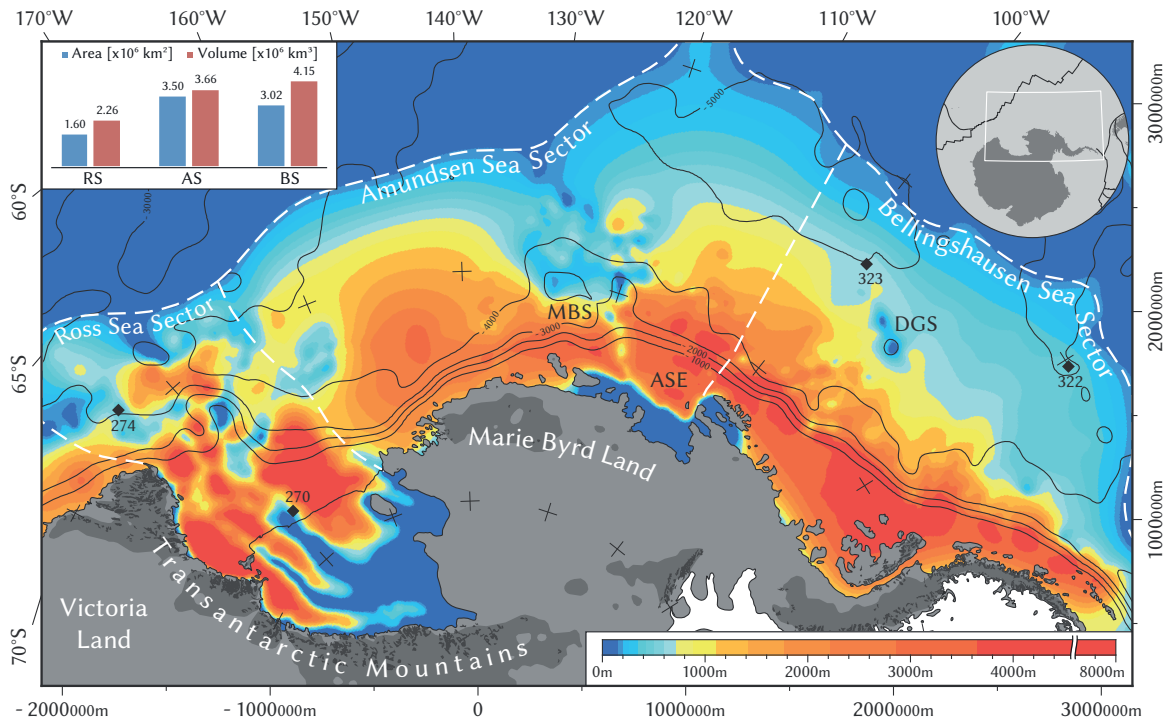


**Fig. 9-2.** The new total sediment thickness map of the Pacific margin of West Antarctica. Isopachs are color coded, contour lines indicate water depth in meter. White dashed lines delineate sediment catchment areas for the Ross Sea (RS), Amundsen Sea (AS) and Bellingshausen Sea (BS) basins. Compacted sediment volume estimates for these regions are illustrated in the top left corner. Black diamonds indicate locations of DSDP sites taken into account. Darker gray shading inland shows topography above 500 m. Rock outcrops from SCAR Antarctic Digital Database. DGS - De Gerlache Seamounts, MBS - Marie Byrd Seamounts. Polar stereographic projection with central meridian of 138° W and latitude of true scale at 71° S referenced to WGS84.

Data from other DSDP, Ocean Drilling Project (ODP), and Antarctic Drilling (ANDRILL) drill sites along the West Antarctic margin were discarded because these boreholes do not yield the acoustic basement. Some sediment thickness estimates in the Amundsen Sea sector are based on a P-wave refraction model (Lindeque and Gohl 2010; Kalberg and Gohl 2013) and gravity models (Wobbe et al. 2012). We allocated values from the original ocean sediment thickness grid of the National Geophysical Data Center (NGDC, Divins 2003) to areas further north and distant from the constrained data sources. These areas are roughly defined by the 100 m sediment isopach in the NGDC sediment thickness grid.

The compiled sediment thickness point-based data were pruned by calculating 10 by 10 km block medians to remove short wavelengths and to avoid spatial aliasing during gridding. The dataset was gridded using Smith and Wessel's (1990) continuous curvature splines algorithm, with a tension factor of 0.2 to suppress local maxima and minima. Although data along the coastline were tapered to zero, we had to introduce about 150 further estimates of total sediment thickness to maintain a sensible appearance of the grid in areas remote from constrained sediment thickness. This is mostly the case, where the acoustic basement could



not be identified on seismic profiles crossing the continental shelf. Our estimates are either plausible assumptions based on local geomorphology or inferred from the nearest constrained value.

A second-order Butterworth low-pass filter with a cut off wavelength of 100 km removed short-range variations from the grid. We chose the Butterworth filter because it has no ripple in the pass band at the expense of a relatively wide roll-off (Oppenheim and Schaffer 2009). The final grid was further resampled by bicubic interpolation to 5 km resolution.

This new total sediment thickness grid result is available in Antarctic Polar Stereographic Projection with a latitude of true scale at 71°S, referenced to WGS84 (Fig. 9-2). The new regional southern Pacific total sediment thickness grid was combined with the recently updated global sediment thickness grid of NGDC (Divins 2003; Whittaker et al. 2013) to create an updated 5 by 5 minute global grid of ocean sediment thickness. The blending of the datasets was done by interpolating a 40 km buffer between the global, and our smaller regional grid, using continuous curvature splines with a tension factor of 0.2.

### 9.3.3 Comparison to previous work and uncertainties

The presented total sediment thickness grid (Fig. 9-2) covers an area of more than 8 million square kilometers and reveals major differences when compared to the sediment thickness compilation of Divins (2003). Divins' original (2003) NGDC global sediment thickness grid has recently been updated for the Australian – Antarctic region (Whittaker et al. 2013), as it became apparent that sediment thickness along the continental margins has been underestimated by more than 2000 m. The current NGDC grid, which excludes areas south of 70°S, largely underestimates sediment thickness off the Antarctic Peninsula and off Marie Byrd Land whilst slightly overestimating total sediment thickness around the De Gerlache Seamounts and the Marie Byrd Seamounts.

Sediments in West Antarctic waters are approximately 4–4.8 km thick around the continental slope (approximately 1000 m contour in Fig. 9-2), which is about 3 km thicker than Divins' (2003) NGDC compilation indicates. Sediments reach a maximum thickness of 6–8 km in glacial troughs on the Ross Sea shelf but taper off to less than 2 km further north. Total sediment thickness is estimated as larger than 4 km off the Antarctic Peninsula but less than 2–2.5 km off the coast of Marie Byrd Land and Victoria Land (west of DSDP site 274), and is maintained farther west (cf. Whittaker et al. 2013). Data from several proprietary seismic profiles (R/V *Tangaroa*, TAN0207 survey for the New Zealand UNCLOS program) off Chatham Rise indicate that Divins' (2003) sediment thickness estimates of West Antarctica's conjugate margin are accurate and do not compromise our residual basement depth calculation south of New Zealand in Section 1.3.

The mean West Antarctic sediment thickness varies slightly. It is largest in the Ross Sea and Bellingshausen Sea sectors (1.5 and 1.4 km), consistent with the very large flux associated with glacial sediment transport, and decreases to about 1.1 km in the Amundsen

Sea sector. The Ross Sea and Bellingshausen Sea basins also have the highest volume per deposition area ratio of about 1.4 km, which is 30% larger than that of the Amundsen Sea sector. The total sediment volume amounts to 10.1 million cubic kilometers of which approximately 80% is equally distributed between the Amundsen and Bellingshausen Sea sectors, and the remaining 20% is spread across the Ross Sea sector.

Neglecting any margin parallel sediment transport, our calculations indicate that most of the terrigenous sediment influx from the West Antarctic originates from the smallest source area of the Antarctic Peninsula (15% of all area draining into the South Pacific). To illustrate this, we determined the hypothetical minimum height of a sediment pile that would cover West Antarctica if all sediments were returned to their source areas by applying Wilson et al.'s (2012) estimates for in situ sediment density (1.95–2.1 g/cm<sup>3</sup>) and source rock density (2.6 g/cm<sup>3</sup>).

DSDP and ODP boreholes around Antarctica yield a maximum pelagic fraction of 15%, which is not restored to the continent in this calculation. The terrigenous sediment source areas, draining into our three West Antarctic sectors, were determined from Zwally et al.'s (2012) present-day drainage system divides within the grounding line and west of the Transantarctic Mountains. Assuming these drainage system divides and their areas did not change with time, our calculations predict that sediments from the Ross Sea sector would pile up to a thickness of 2.5 km (or 561 m if source areas of East Antarctica are considered as well). Sediments from the Amundsen Sea sector would accumulate to a thickness of 3.9 km, and those from the Bellingshausen Sea sector would reach a height of 13 km.

The Ross Sea deposition area is about one third larger than that considered by Wilson and Luyendyk (2009). Even though, the volume estimate for the Ross Sea as previously proposed by Wilson and Luyendyk (2009) only is 10% smaller than the one we calculated, because the distal deposition areas contain much less sediment than the ones in the central and western Ross Sea.

Although Scheuer et al.'s (2006a) sediment thickness grid of the Bellingshausen Sea and eastern Amundsen Sea shows east–west directed low frequency oscillation artefacts and occasionally large local minima and maxima, it compares reasonably well to our results in that the total sediment volume deviates by about 3%. This similarity can be attributed to the common database constraining the sediment thickness along seismic profiles, whereas the deviation is likely caused by a varied degree of data pruning and low-pass filtering.

The accuracy of the presented total sediment thickness grid varies proportionally to the distribution and abundance of seismic data offshore West Antarctica (Fig. 9-1). To a lesser degree, the sediment thickness data is affected by the TWT to depth conversion uncertainties rooted in the lack of seismic velocity models and drilling sites with key constraining down-hole velocity data. The Ross Sea area is exceptionally well surveyed with a densely distributed seismic profile network and two basement yielding DSDP sites provide good calibration.

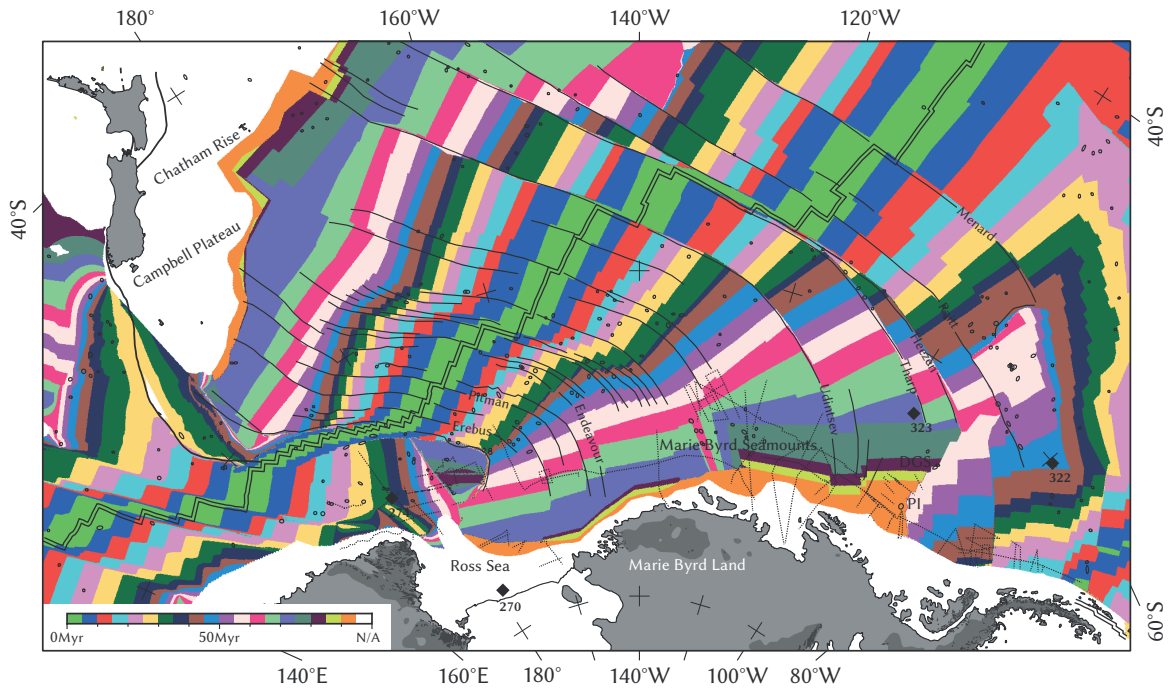


**Fig. 9-3.** Age of the oceanic lithosphere (Wobbe et al. 2012) overlain with locations of seamounts (black dots, Global Seamount Database, Kim and Wessel 2011), fracture zones (black lines), and seismic and gravity profiles (dotted lines). DGS - De Gerlache Seamounts, PI - Peter Island. Lambert conformal conic projection with central meridian 160° W and standard parallels 75° S and 69° S referenced to WGS84.

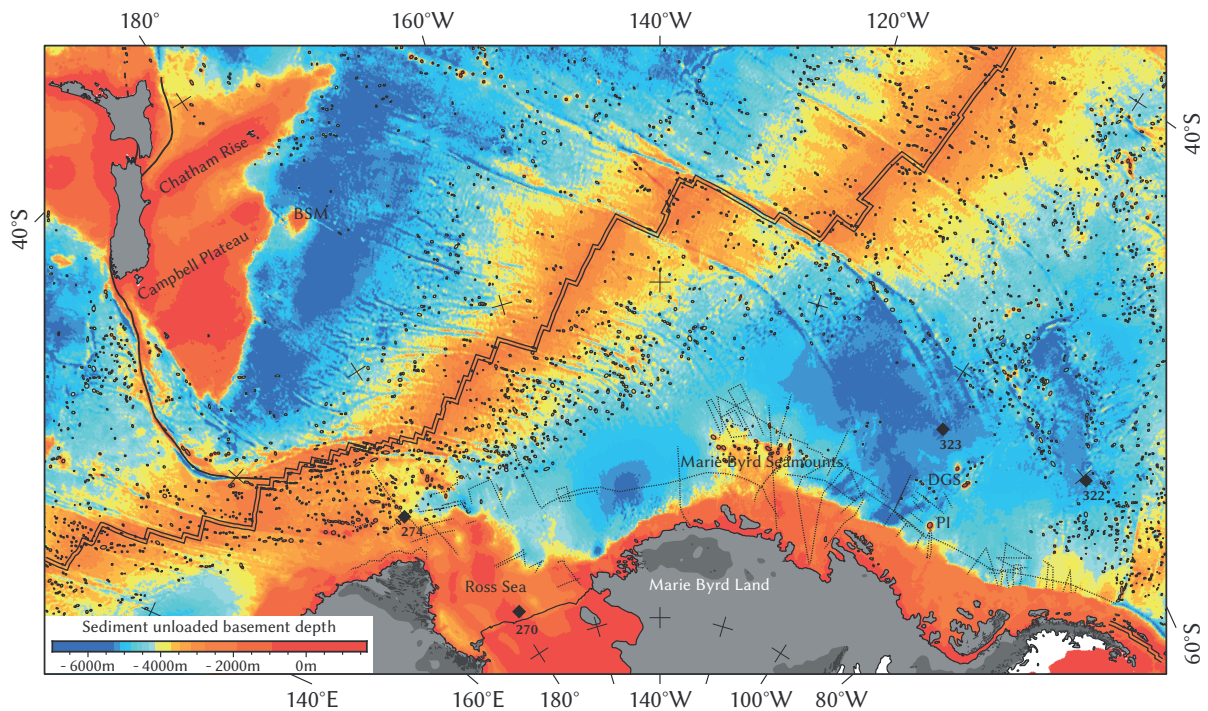


**Fig. 9-4.** Sediment unloaded basement depth determined by applying the correction from Sykes (1996) using the sediment thickness from Fig. 9-2. Overlain with locations of seamounts (black dots, Global Seamount Database, Kim and Wessel 2011). Abbreviations same as Fig. 9-3 and BSM - Bollons Seamount. Lambert conformal conic projection with central meridian 160° W and standard parallels 75° S and 69° S.

The continental rise and slope within all sectors except the westernmost and deeper Amundsen Sea are well mapped. In other places, where total sediment thickness is less constrained due to the absence of seismic reflection and borehole data, the thickness was interpolated over several hundred to thousand kilometers.

Fortunately, most of these less constrained areas fall into the abyssal plains north of 70°S in the western Amundsen Sea sector, and north of 65°S in the eastern Amundsen Sea and Bellingshausen Sea sectors, where DSDP sites 322 and 323 hardly reported any sediment cover. Sediment thickness on the shelves of the western Amundsen Sea could not be constrained by data but were based on observations from the central and eastern Amundsen Sea shelves.

#### 9.4 Age of the oceanic lithosphere and basement depth

In Figs. 9-3 to 9-5 we present the derived set of digital grids that represent the South Pacific ocean floor ages, sediment-corrected basement depth, and oceanic residual basement depth. Collectively these provide an opportunity to study lithosphere dynamics of the West Antarctic margin. The residual basement depth (Fig. 9-5) is the difference between the sediment unloaded basement depth (Fig. 9-4) and the predicted basement depth. The latter was derived from converting the crustal age (Fig. 9-3, Wobbe et al. 2012) to basement depth by using Crosby et al.'s (2006) North Pacific depth–age relationship,  $d = -2821 - 315\sqrt{t}$ .

We decided to apply Crosby et al.'s (2006) model for converting age to depth because it is based on sediment-corrected basement depths from the Pacific, and because it is unbiased by igneous crustal thickening. Therefore, it is considered suitable for detecting anomalies in the basement depth caused by, e.g., hotspot swells, plateaus, and seamounts. It should be noted however, that the difference between this chosen model and models proposed by other authors such as Stein and Stein's (1992) GDH1 depth–age relationship are marginal, and in the context of the scale of this study considered negligible for studying large-scale basement depth anomalies (see Müller et al. 2008).

In brief, the differences between GDH1 and Crosby et al.'s (2006) depth–age relationship range from -32 to 360 m for ages less than or equal to 90 Myr. The mean difference is 87 m and the median difference equals 55 m during this time interval. Both models are remarkably similar for ages younger than 80 Myr, which encompasses more than 96% of the area of interest (Fig. 9-3). Subsequently, GDH1 follows a shallower trend than Crosby et al.'s (2006) depth–age relationship.

Sediment loading was estimated from our total sediment thickness grid (Fig. 9-2), using the relationship between sediment thickness and isostatic correction from Sykes (1996). We calculated the sediment unloaded basement depth by subtracting the isostatic effect using the water depths of the International Bathymetric Chart of the Southern Ocean (IBCSO, Arndt et al. 2013).



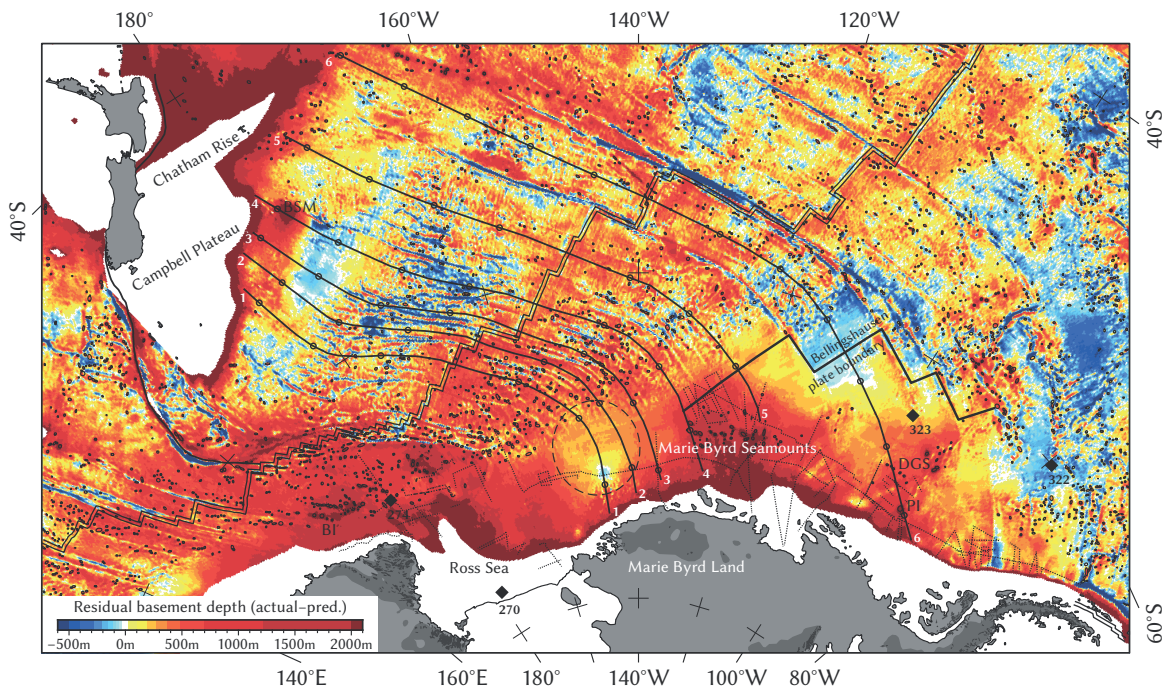


**Fig. 9-5.** Residual basement depth of the oceanic crust determined by calculating the difference between sediment unloaded basement depth (Fig. 9-4) and predicted basement depth from applying Crosby et al.'s (2006) North Pacific depth-age relationship to the age distribution from Fig. 9-3. Profiles 1–6 along flow lines shown in Figs. 9-6, 9-7, and 9-10. Small circles along profiles placed 500 km apart. Dashed circle delineates Endeavour Anomaly. Abbreviations same as in previous figures and BI - Balleny Islands hotspot/Charcot Ridge. Lambert conformal conic projection with central meridian 160° W and standard parallels 75° S and 69° S.

#### 9.4.1 Residual basement depth anomalies

The residual basement depth of the South Pacific (Fig. 9-5) is largely positive, with a few exceptions along the Udintsev, Hazen and Tharp fracture zones (labelled in Fig. 9-3) southeast of the Campbell Plateau, and northwest of the Antarctic Peninsula. The magnitude of the residual basement depth and its irregular surface tend to correlate with hotspot tracks, and with the size and abundance of seamounts. The residual basement depth is generally higher in proximity to Antarctica. This is reflected in the values of the mean residual basement depth of the Antarctic and Pacific plate, being 486 and 203 m respectively. The depth variation is best expressed by the root mean square, 706 and 389 m respectively.

Fig. 9-6 illustrates the unloaded basement depth and the predicted basement depth on selected profiles that are parallel to flow lines crossing the Pacific-Antarctic Ridge. The profiles, which were selected carefully to avoid undulations near fracture zones, confirm that the unloaded basement depth of the Antarctic plate is considerably higher than that of the Pacific plate. Due to the excessive sediment cover offshore West Antarctica, seafloor topography is more than 1000 m shallower compared to the conjugate New Zealand margin (Fig. 9-6). This is reflected by the isostatic correction for sediment thickness, which varies

from 100 to 500 m south of the Campbell Plateau and Chatham Rise but then reaches 800–1500 m and, occasionally, more than 2000 m in the Ross Sea and Amundsen Sea.

Despite the large difference in seafloor topography between the two conjugate margins, the unloaded basement depth, and hence the residual basement depth, usually differ by less than 250 m (Fig. 9-7). Exceptions are the Ross Sea and Marie Byrd Seamount area, where the residual basement depth exceeds 2000 m, and the Balleny Islands hotspot area south of the Pacific-Antarctic Ridge. Fig. 9-7 demonstrates that the residual basement depth usually oscillates between 0 and 500 m, and that a maximum depth is located 2000–2700 km southeast from the Pacific-Antarctic Ridge in an area with a significantly higher seamount density (Global Seamount Database, Kim and Wessel 2011, Fig. 9-5). Another distinctive feature within a circular area north of Marie Byrd Land is defined by an anomalously low residual basement depth, with values 500 m below the surrounding region. We name this the Endeavour Anomaly.

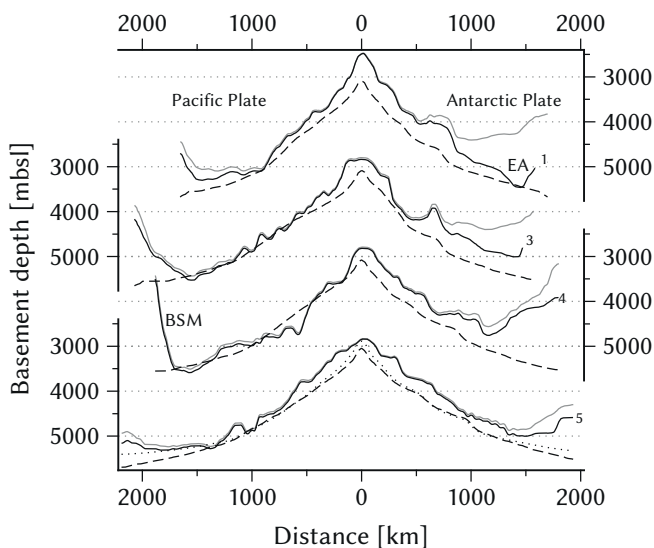


**Fig. 9-6.** IBCSO/GEBCO\_08 bathymetry (gray line), sediment unloaded basement depth (solid line), and predicted basement depth (dashed, Crosby et al. 2006) along profiles 1, 3, 4, and 5 across the Pacific-Antarctic Ridge (Fig. 9-5). Predicted basement depth from Stein and Stein's (1992) depth–age relationship (dotted line, profile 5). Abbreviations same as in previous figures and EA is Endeavour Anomaly.

#### 9.4.2 Residual basement depth vs. seafloor roughness

The residual Models explaining the morphology of mid-ocean ridge systems suggest that basement roughness depends on seafloor spreading rate and that abrupt roughness intensification develops below a full spreading rate threshold of 60–70 mm Myr<sup>-1</sup> (Small and Sandwell 1989; Malinverno 1991). This effect is readily, visible in the roughness map in Fig. 9-8, where morphologically flat basement close to New Zealand and its conjugate margin of West Antarctica, formed along an initially fast spreading Pacific-Antarctic Ridge (>60 mm Myr<sup>-1</sup>, Wobbe et al. 2012). Other parts of the ocean floor with large slope variability were formed less than 55 Myr ago when full-spreading velocities dropped below 60 mm Myr<sup>-1</sup> (Wobbe et al. 2012).

In the South Pacific, increased roughness is additionally caused by confined geological features including oceanic troughs, ridges, fracture zones, and seamounts. Cenozoic magmatism has been attributed to increased heat flow from the mantle (e.g., LeMasurier

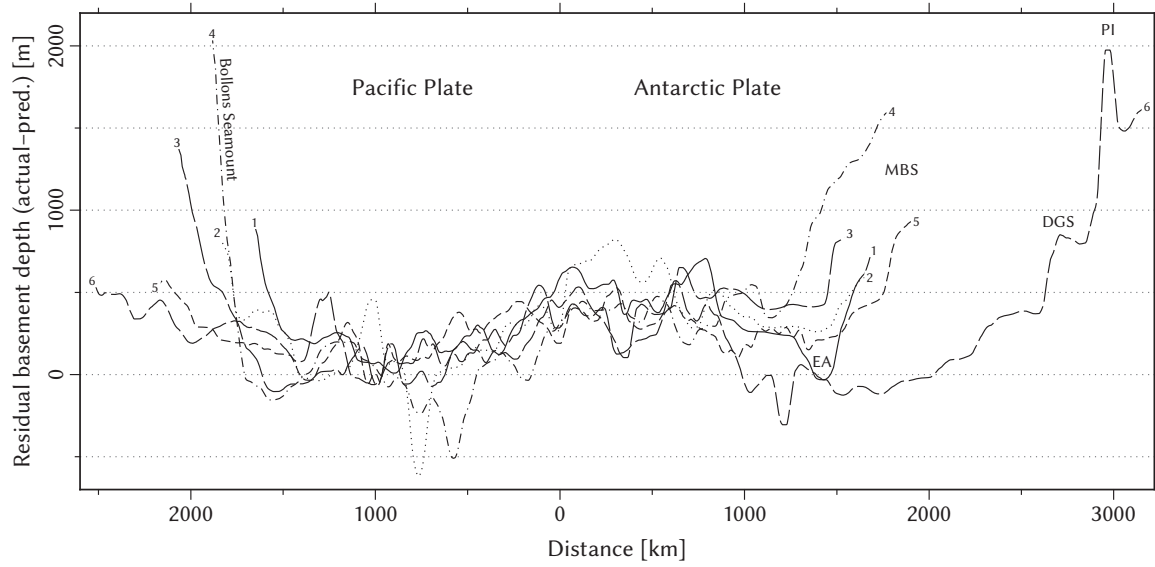


**Fig. 9-7.** Residual basement depth vs. distance from Pacific-Antarctic Ridge along profiles from Fig. 9-5. Abbreviations same as in previous figures.

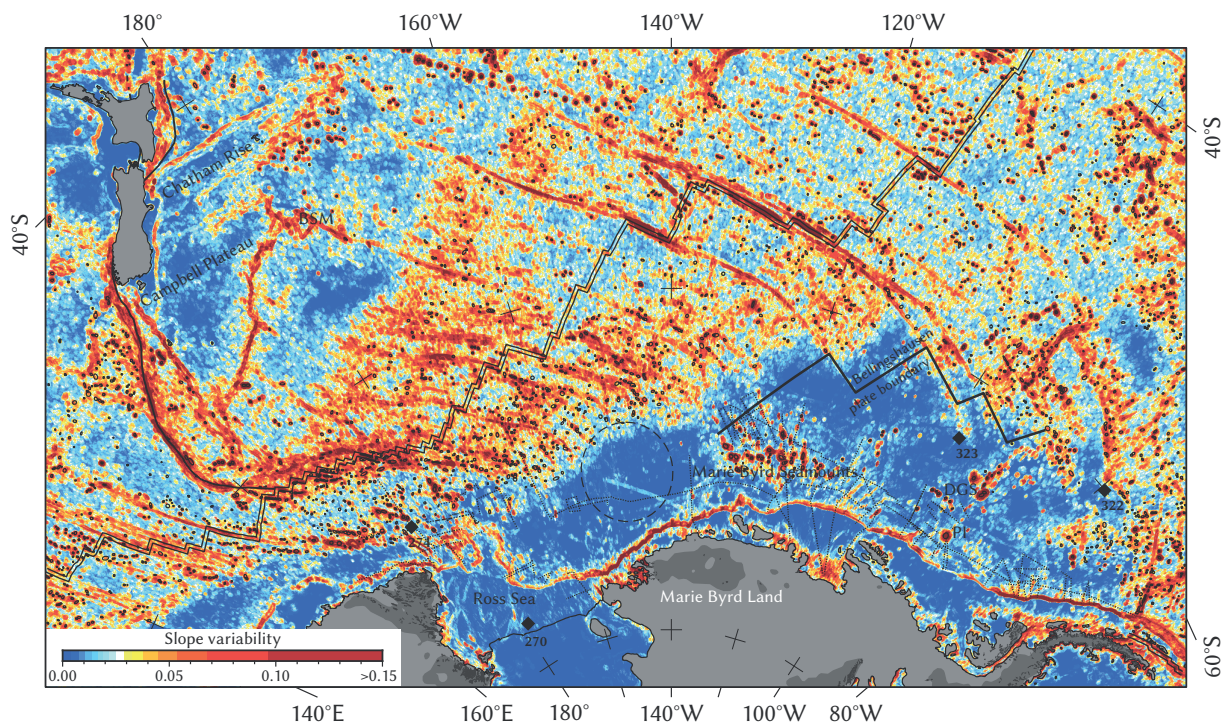


**Fig. 9-8.** Seafloor roughness computed by calculating the slope variability,  $S_v = S_{max} - S_{min}$ , over a 10' x 10' roving window.



1990; Rocchi et al. 2002; Finn et al. 2005; Kipf et al. 2014). While seamounts such as the Balleny Islands, Marie Byrd Seamounts, De Gerlache Seamounts, and Peter I Island are limited morphological surface expressions of these magmatic centers, oceanic crust may respond to the underlying heat source with thermal uplift. Consequently, residual basement depth and seafloor roughness of the Antarctic plate often correlate (Figs. 9-5 and 9-8). However, the area between Campbell Plateau and Pacific-Antarctic Ridge, for example, shows an opposing trend. Hence, seafloor roughness alone cannot be used to explain the residual basement depth distribution.

#### 9.4.3 Residual basement depth vs. Shear wave velocity

Schaeffer and Lebedev (2013) recently published a global tomographic shear wave velocity model of the upper mantle, which extends to a depth of 660 km, thereby improving the resolution of previous Southern Hemisphere models. Fig. 9-9 displays the shear wave velocity anomaly of the uppermost mantle in four slices at different depths.

As expected, low shear wave velocities, which indicate increased heat flow in the mantle, coincide well with magmatic centers of Marie Byrd Land, Balleny Islands, and the Ross Sea area. In contrast, the Marie Byrd Seamounts, the De Gerlache Seamounts, and Peter I Island are underlain by mantle with anomalously high shear wave velocities that by implication may mean lower heat flow in the mantle.

In these magmatic provinces off West Antarctica, the heat does not stem from the mantle directly below, as is the case in underplating, but may be provided by an upper mantle convective flow from warm mantle beneath the continental lithosphere of Marie Byrd Land (continental-insulation flow, Kipf et al. 2014, and references therein).

The distribution of seamounts that did not evolve from continental-insulation flow (e.g., Balleny Islands) matches the low shear wave velocity anomaly remarkably well. Similarly, the residual basement depth (Fig. 9-5) matches the shear wave velocity anomaly too. Noticeably, the shear wave velocity anomaly minimum below the mid-ocean ridges shifts asymmetrically in all depth slices. Particularly south of 60°S, the shear wave velocity anomaly is located 500 km south of the Pacific-Antarctic Ridge, where it also coincides with the maximum of the residual basement depth (Figs. 9-7 and 9-10).

The amplitude of the shear wave velocity anomaly in the study area decreases with depth and deviates less than 1% from zero at depths greater than 400 km. Distinct trends over the region or local extreme are absent. Well resolved shear wave velocity anomalies in this depth with an amplitude of less than 1% would require seismic velocity uncertainties better than 50 m/s.



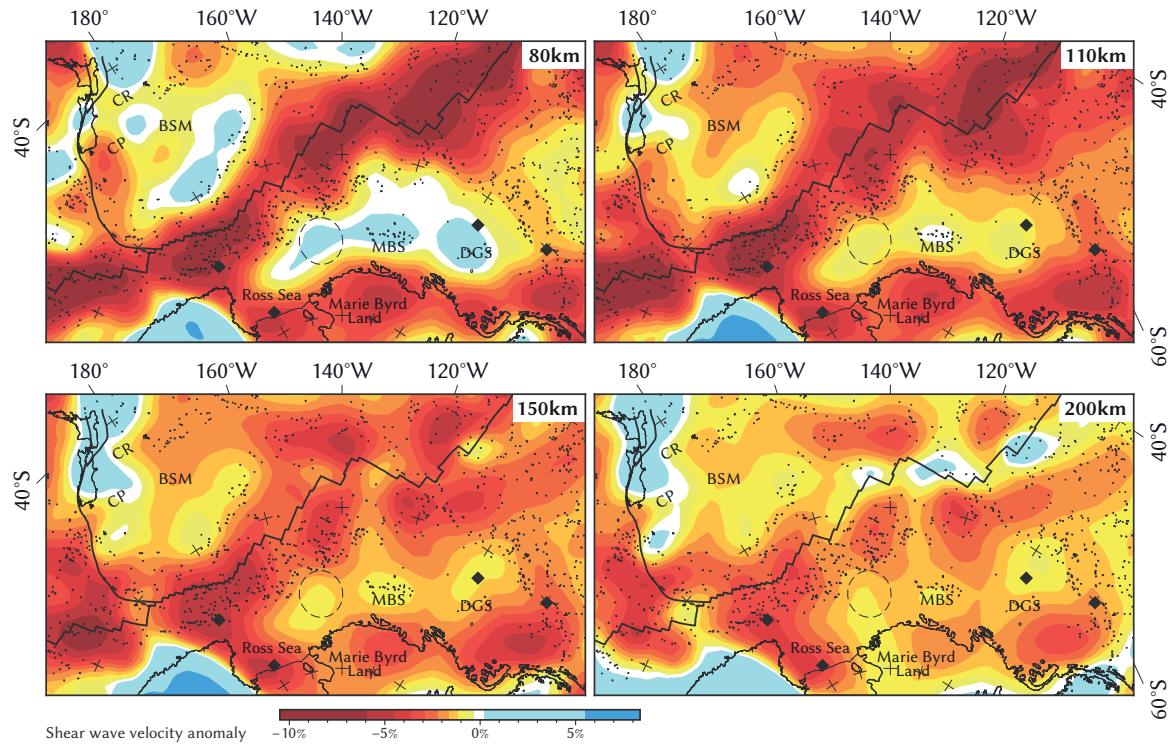


**Fig. 9-9.** Shear wave velocity anomalies (SL2013sv model, Schaeffer and Lebedev 2013) of the upper mantle at 80, 110, 150, and 200 km depth with reference velocities of 4.38, 4.38, 4.39, and 4.45 km/s.

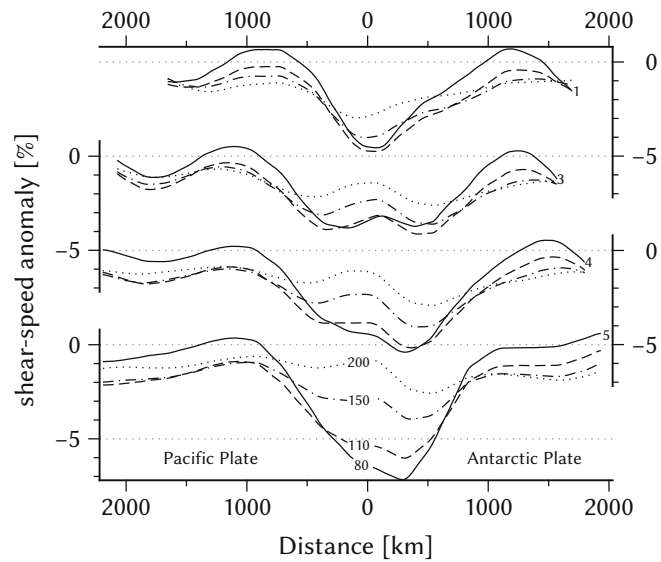


**Fig. 9-10.** Shear wave velocity anomalies of the upper mantle at 80, 110, 150, and 200 km depth vs. distance from Pacific-Antarctic Ridge along profiles 1, 3, 4, and 5 from Fig. 9-5.

## 9.5 Discussion

Improved paleoclimate and paleo-ice sheet models are subject to known limitations of current sediment volume approximations. With more robust sediment estimates, future reconstructions of paleotopography will improve our understanding of Antarctica's glaciation history. For instance, Wilson et al. (2013) estimated, based on the denudation history, that the total Antarctic ice volume since the Eocene–Oligocene transition was more than 1.4 times greater than previously assumed. This study and a recent work from Whittaker et al. (2013) both indicate that sediment thickness along the Antarctic margin has largely been underestimated. The landmass reduction of Antarctica due to erosion, therefore, has probably been larger than predicted (Wilson et al. 2012), and even larger ice sheet volumes may have covered Antarctica in the early times of glaciation. Of course, additional identifications of the volume and distribution of the pre-glacial to glacial components in the offshore sedimentary records are required in order to reconstruct the past topography for periods associated with large changes in climate proxies, such as the Eocene–Oligocene transition. However, the construction of pre-glacial to glacial sediment thickness grids is beyond the scope of this publication.

The previous section shows that there is a connection between residual basement depth and shear wave velocity on the one hand and magmatic processes on the other. Residual basement depth should also resemble the present-day dynamic topography predicted from mantle flow models. Present global studies of dynamic topography (e.g., Ricard et al. 1993; Steinberger 2007; Conrad and Husson 2009; Spasojevic and Gurnis 2012; Flament et al. 2013) are limited to a lateral resolution of about 3000–5000 km. There are regional mismatches at scales below 10 000 km and even inverse correlations, especially in the Pacific realm (Flament et al. 2013). None of the five above mentioned dynamic topography models (Fig. C-1 in Appendix C) resolve local residual basement anomalies in the South Pacific. Although absolute amplitudes vary as much as 1500 m, all models propose a topographic high beneath the Pacific Plate, north of 60°S/150°W, which is in contrast with the residual basement depth (Fig. 9-5) and the shear wave anomaly (Fig. 9-9). Depending on the chosen model, dynamic topography beneath the Antarctic Plate and West Antarctica varies between 500 m and 1000 m, and the magnitude beneath New Zealand is usually consistent with that beneath Marie Byrd Land.

Mantle upwelling following the Gondwana subduction cessation has been suggested, but its extent beneath the West Antarctic margin remains unclear (e.g., Storey et al. 1999; Sieminski et al. 2003; Winberry and Anandkrishnan 2004; Finn et al. 2005). We believe that present-day residual basement depth, mantle shear wave velocity anomaly (Schaeffer and Lebedev 2013), and Kipf et al.'s (2013) continental-insulation flow model confine upper mantle convective flow solely to an area located beneath Marie Byrd Land and the Ross Sea. Spasojevic et al. (2010) and Sutherland et al. (2010) constructed models of Late Cretaceous to Cenozoic mantle flow, attributed to low density material above the Gondwana slab

graveyard beneath Antarctica, to predict dynamic topography. Their models, which are based on present-day bathymetry, explain the high topography of the Ross Sea and Marie Byrd Land region as well as anomalous post-rift Campbell Plateau subsidence. Our findings complement Sutherland et al.'s (2010) dynamic topography model, and our total sediment thickness estimates confine areas of anomalous basement elevation more precisely. For example, Sutherland et al. (2010) attributed excess topography (0.5–2.0 km) offshore Marie Byrd Land and in the Ross Sea region to dynamic topography. Our results confirm this for the Ross Sea as well as the Balleny Islands hotspot area.

However, the residual basement depth of Marie Byrd Land does not exceed that south of Campbell Plateau by more than 250 m (Fig. 9-7). East of the Ross Sea area, anomalously high basement topography is associated with magmatic processes driven by continental-insulation flow only (Marie Byrd Seamounts, De Gerlache Seamounts, Peter I Island, e.g., Kipf et al. 2014). Oceanic crust elsewhere in that region seems unaffected by mantle processes (e.g., Endeavour Anomaly). Sutherland et al.'s (2010) present day dynamic topography model coincides with our residual basement depth maximum in the Ross Sea, but their proposed topography high beneath the Pacific Plate north of the Pacific-Antarctic Ridge lacks an equal counterpart anomaly in the residual basement depth.

A peculiar feature of the residual basement anomaly is its asymmetry over the Pacific-Antarctic Ridge, with a maximum south of the spreading center, exactly where Campbell Plateau passed through and, according to Wobbe et al.'s (2012) revised South Pacific plate motion model mouldering 70–40 Myr. This time interval also marks the peak subsidence of the Campbell Plateau as it moved away from Antarctica to its present-day position (Sutherland et al. 2010). Although residual basement depth represents only a snapshot of dynamic topography, which occurs over tens of millions of years (Flament et al. 2013), the anomalous basement elevation south of the Pacific-Antarctic Ridge seems to be caused by processes persisting since the Cretaceous separation of New Zealand from Antarctica. It should be kept in mind, though, that until more robust dynamic topography models become available, predictions of the South Pacific paleotopography remain highly speculative.

## 9.6 Conclusions

Seismic data, recently acquired along the West Antarctic margin, suggests that Divins' (2003) minimum sediment thickness estimates along the West Antarctic margin are much too low. We present a first total sediment thickness grid spanning the Ross Sea – Amundsen Sea – Bellingshausen Sea basins based on available seismic reflection, borehole, and gravity modeling data in West Antarctica (Fig. 9-2). Our sediment thickness and volume estimates are consistent with previous analyses that indicate larger sediment amounts on Antarctica's margin than previously assumed (e.g., Rebesco et al. 1997; Scheuer et al. 2006a; Whittaker et al. 2013). We therefore extended Divins' (2003) original NGDC grid further south by

merging our new data with data from Scheuer et al. (2006a), Wilson and Luyendyk (2009), and Whittaker et al. (2013) into an updated 5 by 5 minute global grid of total ocean sediment thickness. The sediment thickness estimation involved interpolation over areas without data constraints, but fortunately most of the less constrained areas fall into the abyssal plains where sediment cover is usually sparse. Due to a wider, better constrained dataset, the presented sediment volume estimates of West Antarctica are considered to be fairly accurate. The sediment volume is the largest in the Bellingshausen Sea basin, with 4.15 million cubic kilometers, although its sediment source area is the smallest (15% of all area draining into the South Pacific). Contrary, the Ross Sea basin, into which sediments are supplied from a much larger area (43%), contains just 2.26 million cubic kilometers of sediment. The Amundsen Sea basin, into which 42% of the present-day West Antarctic landmass on the Pacific side drain, is estimated to contain 3.66 million cubic kilometers of sediment.

We determined the sediment corrected basement topography for the South Pacific from our total sediment thickness model (Fig. 9-4). In addition, we obtained the residual basement depth of the oceanic crust (Fig. 9-5) by subtracting the sediment corrected basement depth from the theoretical basement depth, using a current South Pacific crustal age model (Wobbe et al. 2012) and Crosby et al.'s (2006) North Pacific depth–age relationship. The mean residual basement depths of the Antarctic and Pacific plate differ by about 300 m. The Antarctic Plate has a residual basement depth of nearly 500 m, but the excessive sediment cover offshore West Antarctica leads to seafloor depths in excess of 1000 m shallower than those of the conjugate New Zealand margin. No direct relationship between seafloor roughness (Fig. 9-8) and residual basement depth or overlying sediment accumulation has been observed. Ocean floor with large slope variability rather formed from 55 Myr ago until present, when full-spreading velocities dropped below 60 mm Myr<sup>-1</sup>.

Dynamic topography models (e.g., Ricard et al. 1993; Steinberger 2007; Conrad and Husson 2009; Spasojevic and Gurnis 2012; Flament et al. 2013) of the South Pacific are inconsistent with our local residual basement anomalies or even reversely correlate, and it remains unclear why. The pattern of residual basement depth, however, matches the distribution of seamounts and the shear wave velocity anomaly of the upper mantle (Fig. 9-9). Collectively these observations suggest that mantle dynamics play a role and that the resolution of dynamic topography models still lack the precision to pinpoint present-day small-scale residual basement anomalies. Our findings support Sutherland et al.'s (2010) model of Late Cretaceous to Cenozoic persistent mantle not beneath West Antarctica following the Gondwana subduction cessation, but show that basement elevation, estimated from seafloor topography only, has been overestimated off Marie Byrd Land. We believe the Marie Byrd Land margin is only affected by magmatic processes in the context of continental-insulation flow (Kipf et al. 2014, e.g., Marie Byrd Seamounts, De Gerlache Seamounts, Peter I Island). This seems to be supported by the observation that oceanic crust farther away from these magmatic centers is elevated less than 250 m higher than oceanic crust from the conjugate New Zealand margin. The Ross Sea as well as the Balleny Islands



hotspot area, and a region south of the Pacific-Antarctic Ridge, however, have been subject to mantle processes that lead to anomalously high basement elevations of more than 1500 m. A persistent basement high south of the ridge would explain the rapid subsidence of the Campbell Plateau during 740 Myr en-route to its present day position. Until more accurate dynamic topography models, that can explain the present-day anomalous basement depth both at the Pacific-Antarctic Ridge and along the continental margins, become available, predictions of the South Pacific paleotopography remain speculative.

## 9.7 Acknowledgements

This project has been funded by the Earth System Sciences Research School (ESSReS), a graduate school of the Helmholtz Association of German Research Centres (HGF) at the Alfred Wegener Institute (AWI), and through the Priority Program 1158 'Antarctic Research' of the Deutsche Forschungsgemeinschaft under project number GO 724/10-1. We thank Doug Wilson and Carsten Scheuer, with whom we had helpful discussions and for sharing their results, and Nicolas Flament for data exchange. Special thanks go to the New Zealand UNCLOS project for granting insight into seismic data to Chatham Rise. All of the figures in this publication were created using GMT (Generic Mapping Tools, Version 5, by Wessel et al. 2013).

## 9.8 References

- Arndt, J. E., H. W. Schenke, M. Jakobsson, F. O. Nitsche, G. Buys, B. Goleby, M. Rebesco, F. Bohoyo, J. Hong, J. Black, R. Greku, G. Udintsev, F. Barrios, W. Reynoso-Peralta, M. Taisei, and R. Wigley, 2013. The International Bathymetric Chart of the Southern Ocean (IBCSO) Version 1.0 - A new bathymetric compilation covering circum-Antarctic waters. *Geophys. Res. Lett.* doi:10.1002/grl.50413.
- Carlson, R. L., A. F. Gangi, and K. R. Snow, 1986. Empirical Rejection Travel Time Versus Depth and Velocity Versus Depth Functions for The Deep-Sea Sediment Column. *J. Geophys. Res.*, 91(B8), 8249–8266. doi:10.1029/JB091iB08p08249.
- Chian, D., K. E. Loudon, and I. Reid, 1995. Crustal structure of the Labrador Sea conjugate margin and implications for the formation of nonvolcanic continental margins. *J. Geophys. Res.-Sol. Ea.*, 100(B12), 24239–24253. doi:10.1029/95JB02162.
- Conrad, C. P. and L. Husson, 2009. Influence of dynamic topography on sea level and its rate of change. *Lithosphere*, 1(2), 110-120. doi: 10.1130/L32.1.
- Cooper, A. K., F. J. Davey, and K. Hinz, 1991. Crustal extension and origin of sedimentary basins beneath the Ross Sea and Ross Ice Shelf. In M. R. A. Thomson, J. A. Crame, and J. W. Thomson, editors, *Geological Evolution of Antarctica, Cambridge World and Regional Geology*, pp. 285–291. Cambridge University Press, Cambridge. ISBN 978-0521372664.
- Crosby, A. G., D. McKenzie, and J. G. Sclater, 2006. The relationship between depth, age and gravity in the oceans. *Geophys. J. Int.*, 166(2), 553–573. doi:10.1111/j.1365-246X.2006.03015.x.
- De Santis, L., J. B. Anderson, G. Brancolini, and I. Zayatz, 1995. Seismic Record of Late Oligocene Through Miocene Glaciation on the Central and Eastern Continental Shelf of the Ross Sea. In A. K. Cooper, P. F. Barker, and G. Brancolini, editors, *Geology and Seismic Stratigraphy of the Antarctic Margin*, volume 68 of *Antarct. Res. Ser.*, pp. 235–260. AGU, Washington, D.C. doi:10.1029/AR068p0235.

- Divins, D. L., 2003. Total Sediment Thickness of the World's Oceans & Marginal Seas. NOAA National Geophysical Data Center, Boulder, CO. Available from: <http://www.ngdc.noaa.gov/mgg/sedthick/>.
- Finn, C. A., R. D. Müller, and K. S. Panter, 2005. A Cenozoic diffuse alkaline magmatic province (DAMP) in the southwest Pacific without rift or plume origin. *Geochem. Geophys. Geosyst.*, 6(2). doi:10.1029/2004GC000723.
- Flament, N., M. Gurnis, and R. D. Müller, 2013. A review of observations and models of dynamic topography. *Lithosphere*, 5(2), 189–210. doi: 10.1130/L245.1.
- Gohl, K., D. Teterin, G. G. Eagles, G. Netzeband, J. W. G. Grobys, N. Parsiegl, P. Schlüter, V. Leinweber, R. D. Larter, G. Uenzelmann-Neben, and G. B. Udintsev, 2007. Geophysical Survey Reveals Tectonic Structures in the Amundsen Sea Embayment, West Antarctica. In A. K. Cooper, C. R. Raymond, and the 10th ISAES Editorial Team, editors, *Antarctica: A Keystone in a Changing World*. Online Proceedings of the 10th International Symposium on Antarctic Earth Sciences, USGS Open-File Report 2007-1047, Short Research Paper 047. USGS. doi:10.3133/of2007-1047.srp047.
- Gohl, K., G. Uenzelmann-Neben, R. D. Larter, C.-D. Hillenbrand, K. Hochmuth, T. Kalberg, E. Weigelt, B. Davy, G. Kuhn, and F. O. Nitsche, 2013. Seismic stratigraphic record of the Amundsen Sea Embayment shelf from pre-glacial to recent times: Evidence for a dynamic West Antarctic ice sheet. *Mar. Geol.*, 344(0), 115–131. doi:10.1016/j.margeo.2013.06.011.
- Hayes, D. E., L. A. Frakes, P. J. Barrett, D. A. Burns, P.-H. Chen, A. B. Ford, A. G. Kaneps, E. M. Kemp, D. W. McCollum, D. J. W. Piper, R. E. Wall, and P. N. Webb, editors, 1975. Initial Reports of the Deep Sea Drilling Project, volume 28. U.S. Government Printing Office, Washington, D.C. doi:10.2973/dsdp.proc.28.1975.
- Hollister, C. D., C. Craddock, Y. A. Bogdanov, N. T. Edgar, J. M. Gieskes, B. U. Haq, J. R. Lawrence, F. Roegl, H.-J. Schrader, B. E. Tucholke, W. R. Vennum, F. M. Weaver, V. N. Zhivago, and P. Worstell, editors, 1976. Initial Reports of the Deep Sea Drilling Project, volume 35. U.S. Government Printing Office. doi:10.2973/dsdp.proc.35.1976.
- Kalberg, T. and K. Gohl, 2013. The crustal structure and tectonic development of the continental margin of the Amundsen Sea Embayment margin, West Antarctica: Implications from geophysical data. *Geophys. J. Int.*, submitted.
- Kim, S.-S. and P. Wessel, 2011. New global seamount census from altimetry-derived gravity data. *Geophys. J. Int.*, 186(2), 615–631. doi: 10.1111/j.1365-246X.2011.05076.x.
- Kipf, A., F. Hauff, R. Werner, K. Gohl, P. van den Bogaard, K. Hoernle, and A. Maicher, D. and Klügel, A. 2014. Seamounts of the West Antarctic margin of the Pacific: A case of non-hotspot intraplate volcanism. *Gondwana Res.* doi:10.1016/j.gr.2013.06.013.
- LeMasurier, W. E., 1990. Late Cenozoic volcanism on the Antarctic Plate: An overview. In W. E. LeMasurier, J. W. Thomson, P. Baker, P. Kyle, P. Rowley, J. Smellie, and W. Verwoerd, editors, *Volcanoes of the Antarctic Plate and Southern Oceans*, volume 48 of *Antarct. Res. Ser.*, 1–17. AGU, Washington, D.C. ISBN 978-0-87590-172-5. doi:10.1029/AR048p0001.
- Lindeque, A. and K. Gohl, 2010. Western Antarctic palaeostratigraphy: implications for palaeobathymetry and palaeoclimate modelling. Poster presentation at IPY Oslo Science Conference, Oslo, 8–12 June 2010. Available from: [http://elsevier.conference-services.net/resources/247/1976/pdf/Oslo2010\\_0377.pdf](http://elsevier.conference-services.net/resources/247/1976/pdf/Oslo2010_0377.pdf).
- Malinverno, A., 1991. Inverse square-root dependence of mid-ocean-ridge flank roughness on spreading rate. *Nature*, 352(6330), 58–60. doi: 10.1038/352058a0.
- Müller, R. D., M. Sdrolias, C. Gaina, and W. R. Roest, 2008. Age, spreading rates, and spreading asymmetry of the world's ocean crust. *Geochem. Geophys. Geosyst.*, 9, Q04006. doi:10.1029/2007GC001743.
- Oppenheim, A. V. and R. W. Schafer, 2009. *Discrete-Time Signal Processing*. Prentice Hall Signal Processing. Prentice Hall, 3 edition. ISBN 978-0-13-198842-2.
- Rebesco, M., R. D. Larter, P. F. Barker, A. Camerlenghi, and L. E. Vanneste, 1997. The History of Sedimentation on the Continental Rise West of the Antarctic Peninsula. In P. F. Barker and A. K.

- Cooper, editors, *Geology and Seismic Stratigraphy of the Antarctic Margin*, 2, volume 71 of *Antarct. Res. Ser.*, 29–49. AGU, Washington, D.C. doi:10.1029/AR071p0029.
- Ricard, Y., M. Richards, C. Lithgow-Bertelloni, and Y. Le Stunf, 1993. A geodynamic model of mantle density heterogeneity. *J. Geophys. Res.-Sol. Ea.*, 98(B12), 21895–21909. doi:10.1029/93JB02216.
- Rocchi, S., P. Armienti, M. D'Orazio, S. Tonarini, J. R. Wijbrans, and G. Di Vincenzo, 2002. Cenozoic magmatism in the western Ross Embayment: Role of mantle plume versus plate dynamics in the development of the West Antarctic Rift System. *J. Geophys. Res.-Sol. Ea.*, 107(B9). doi:10.1029/2001JB000515.
- Schaeffer, A. J. and S. Lebedev, 2013. Global shear-speed structure of the upper mantle and transition zone. *Geophys. J. Int.* doi:10.1093/gji/ggt095.
- Scheuer, C., K. Gohl, and G. Eagles, 2006a. Gridded isopach maps from the South Pacific and their use in interpreting the sedimentation history of the West Antarctic continental margin. *Geochem. Geophys. Geosyst.*, 7(11), Q11015. doi:10.1029/2006GC001315.
- Scheuer, C., K. Gohl, R. D. Larter, M. Rebesco, and G. Udintsev, 2006b. Variability in Cenozoic sedimentation along the continental rise of the Bellingshausen Sea, West Antarctica. *Mar. Geol.*, 227(3–4), 279–298. doi:10.1016/j.margeo.2005.12.007.
- Sieminski, A., E. Debayle, and J.-J. LÈvÈrque, 2003. Seismic evidence for deep low-velocity anomalies in the transition zone beneath West Antarctica. *Earth Planet. Sci. Lett.*, 216(4), 645–661. doi:10.1016/S0012-821X(03)00518-1.
- Small, C. and D. T. Sandwell, 1989. An abrupt change in ridge axis gravity with spreading rate. *J. Geophys. Res.-Sol. Ea.*, 94(B12), 17383–17392. doi: 10.1029/JB094iB12p17383.
- Smith, W. H. F. and P. Wessel, 1990. Gridding with continuous curvature splines in tension. *Geophysics*, 55, 293–305.
- Spasojevic, S. and M. Gurnis, 2012. Sea level and vertical motion of continents from dynamic earth models since the Late Cretaceous. *AAPG Bulletin*, 96(11), 2037–2064. doi:10.1306/03261211121.
- Spasojevic, S., M. Gurnis, and R. Sutherland, 2010. Inferring mantle properties with an evolving dynamic model of the Antarctica – New Zealand region from the Late Cretaceous. *J. Geophys. Res.-Sol. Ea.*, 115(B5). doi:10.1029/2009JB006612.
- Stein, C. A. and S. Stein, 1992. A model for the global variation in oceanic depth and heat flow with lithospheric age. *Nature*, 359(6391), 123–129. doi:10.1038/359123a0.
- Steinberger, B., 2007. Effects of latent heat release at phase boundaries on flow in the Earth's mantle, phase boundary topography and dynamic topography at the Earth's surface. *Phys. Earth Planet. Inter.*, 164(1–2), 2–20. doi:10.1016/j.pepi.2007.04.021.
- Storey, B. C., P. T. Leat, S. D. Weaver, R. J. Pankhurst, J. D. Bradshaw, and S. Kelley, 1999. Mantle plumes and Antarctica – New Zealand rifting: evidence from mid-Cretaceous mafic dykes. *J. Geol. Soc. London*, 156(4), 659–671. doi:10.1144/gsjgs.156.4.0659.
- Suckro, S. K., K. Gohl, T. Funck, I. Heyde, A. Ehrhardt, B. Schreckenberger, J. Gerlings, V. Damm, and W. Jokat, 2012. The crustal structure of southern Baffin Bay: implications from a seismic refraction experiment. *Geophys. J. Int.*, 190(1), 37–58. doi:10.1111/j.1365-246X.2012.05477.
- Sutherland, R., S. Spasojevic, and M. Gurnis, 2010. Mantle upwelling after Gondwana subduction death explains anomalous topography and subsidence histories of eastern New Zealand and West Antarctica. *Geology*, 38(2), 155–158. doi:10.1130/G30613.1.
- Sykes, T. J. S., 1996. A correction for sediment load upon the ocean floor: Uniform versus varying sediment density estimations/implications for isostatic correction. *Mar. Geol.*, 133(1–2), 35–49. doi:10.1016/0025-3227(96)00016-3.

- Uenzelmann-Neben, G. and K. Gohl, 2012. Amundsen Sea sediment drifts: Archives of modifications in oceanographic and climatic conditions. *Mar. Geol.*, 299–302(0), 51–62. doi:10.1016/j.margeo.2011.12.007.
- Voss, M. and W. Jokat, 2007. Continent-ocean transition and voluminous magmatic underplating derived from P-wave velocity modelling of the East Greenland continental margin. *Geophys. J. Int.*, 170(2), 580–604. doi:10.1111/j.1365-246X.2007.03438.x.
- Wardell, N., J. R. Childs, and A. K. Cooper, 2007. Advances through Collaboration: Sharing Seismic Reflection Data via the Antarctic Seismic Data Library System for Cooperative Research (SDLS). In A. K. Cooper, C. R. Raymond, and the 10th ISAES Editorial Team, editors, *Antarctica: A Keystone in a Changing World – Online Proceedings of the 10th International Symposium on Antarctic Earth Sciences*, USGS Open-File Report 2007-1047, Short Research Paper 001. USGS. doi:10.3133/of2007-1047.srp001.
- Wessel, P., W. H. F. Smith, R. Scharroo, J. Luis, and F. Wobbe, 2013. Generic Mapping Tools: Improved Version Released. *EOS Trans. AGU*, 94(45), 409–410. doi:10.1002/2013EO450001.
- Whittaker, J., A. Goncharov, S. Williams, R. D. Müller, and G. Leitchenkov, 2013. Global sediment thickness dataset updated for the Australian Antarctic Southern Ocean. *Geochem. Geophys. Geosyst.* doi:10.1002/ggge.20181.
- Wilson, D. S. and B. P. Luyendyk, 2009. West Antarctic paleotopography estimated at the Eocene–Oligocene climate transition. *Geophys. Res. Lett.*, 36(16), L16302. doi:10.1029/2009GL039297.
- Wilson, D. S., S. S. R. Jamieson, P. J. Barrett, G. Leitchenkov, K. Gohl, and R. D. Larter, 2012. Antarctic topography at the Eocene–Oligocene boundary. *Palaeogeogr. Palaeoclimatol. Palaeoecol.*, 335–336(0), 24–34. *Cenozoic Evolution of Antarctic Climates, Oceans and Ice Sheets*. doi:10.1016/j.palaeo.2011.05.028.
- Wilson, D. S., D. Pollard, R. M. DeConto, S. S. Jamieson, and B. P. Luyendyk, 2013. Initiation of the West Antarctic Ice Sheet and estimates of total Antarctic ice volume in the earliest Oligocene. *Geophys. Res. Lett.*, 40(16), 4305–4309. doi:10.1002/grl.50797.
- Winberry, J. P. and S. Anandakrishnan, 2004. Crustal structure of the West Antarctic rift system and Marie Byrd Land hotspot. *Geology*, 32(11), 977–980. doi:10.1130/G20768.1.
- Wobbe, F., K. Gohl, A. Chambord, and R. Sutherland, 2012. Structure and breakup history of the rifted margin of West Antarctica in relation to Cretaceous separation from Zealandia and Bellingshausen plate motion. *Geochem. Geophys. Geosyst.*, 13(4), Q04W12. doi:10.1029/2011GC003742.
- Zwally, H. J., M. B. Giovinetto, M. A. Beckley, and J. L. Saba, 2012. Antarctic and Greenland Drainage Systems, GSFC Cryospheric Sciences Laboratory [online]. Available from: [http://icesat4.gsfc.nasa.gov/cryo\\_data/ant\\_grn\\_drainage\\_systems.php](http://icesat4.gsfc.nasa.gov/cryo_data/ant_grn_drainage_systems.php).



ONLINE SUPPLEMENTS

Appendix C-1

Fig. C-1. Present-day dynamic topography models of the South Pacific (Ricard et al. 1993; Steinberger 2007; Conrad and Husson 2009; Spasojevic and Gurnis 2012; Flament et al. 2013).

Appendix C-2

Table C-1. Source-ID (values of source identification grid) vs. data origin of data used for compiling sediment thickness, including DSDP boreholes (1–4), data from the Antarctic Seismic Data Library System (SDLS, Wardell et al. 2007, 5–93, 161–207), recently acquired and processed seismic data (99–140), and data from previous work (e.g., Scheuer et al. 2006a, b; Wilson and Luyendyk 2009; Uenzelmann-Neben and Gohl 2012; Wobbe et al. 2012; Gohl et al. 2013; Kalberg and Gohl 2013; Whittaker et al. 2013).

# Chapter 10

## FOURTH PAPER

### PRE-GLACIAL TO GLACIAL SEDIMENT THICKNESS GRIDS FOR THE PACIFIC MARGIN OF WEST ANTARCTICA

Lindeque, A., Wobbe, F., Gohl, K., 2014.  
Pre-glacial to glacial sediment thickness grids for the Pacific margin of West Antarctica.  
Manuscript prepared for G-cubed as a Technical brief.  
Currently with co-authors for comment.

#### Highlights:

- First total, pre-glacial and glacial sediment thickness grids for the Amundsen Sea.
- First pre-glacial to glacial grids for the Pacific margin off West Antarctica.
- Total sediment thickness up to 4 km, 1.5 km thereof comprising the full glacial sequence.

---

## 10.1 Abstract

Circum-Antarctic sediment thickness grids are needed to understand the first arrivals of the ice sheets on the shelf and to reconstruct the past topography for periods such as the Eocene/Oligocene and mid-Miocene. We identified seismic sequences representing the pre-glacial [pre-ice sheet], transitional [first arrival of the ice sheets on the shelf] and full glacial [permanent grounding of the ice sheets on the shelf] processes in newly acquired and pre-existing multichannel seismic reflection data on the Pacific margin of West Antarctica. Supporting age and velocity information was drawn from all available borehole, refraction and sonobuoy velocity data. Horizons in the Ross Sea, eastern Amundsen Sea, Bellingshausen Sea and Antarctic Peninsula were used as published, and interpreted horizons in the central Amundsen Sea basin and eastern Ross Sea basin expanded, to correlate the seismic stratigraphy. We present a revised total sediment thickness grid that improves the NGDC grid, and derive the first pre-glacial, transitional and full glacial sequence grids. The pre-glacial sediment processes grid depicts 1.3–4 km thick depocenters, relatively evenly distributed along the margin. The depocenters change markedly after Eocene/Oligocene transitions when the ice sheets arrive on the shelf, and shift towards the eastern Ross Sea basin, the central Amundsen Sea and the Antarctic Peninsula. The full glacial sequence indicates new depocenters formation in front of the Amundsen Sea Embayment and a localized eastward shift in the Bellingshausen Sea / Antarctic Peninsula basins. Using present-day drainage and source area divides, hypothetical estimates indicate that a sediment pile of

~2.7 km thick (volume of  $\sim 6 \times 10^6 \text{ km}^3$ ) should be placed back onto land if sediment thickness is to be considered in the E/O 34 Ma paleotopography reconstruction. Whereas a sediment pile of approximately ~3.6 km thick and  $\sim 8 \times 10^6 \text{ km}^3$  in volume would need to be considered for the 15.5 Ma mid-Miocene paleotopography reconstruction. From the Cretaceous to the present day topography, an estimated ~4.6 km of sediment ( $\sim 10.2 \times 10^6 \text{ km}^3$ ) was eroded off the Pacific margin of West Antarctica.

**Keywords:** isopach grid; sediment thickness; Ross Sea; Amundsen Sea; Bellingshausen Sea; ice sheet.

**AGU Index terms:**

Paleoceanography: glacial; Tectonophysics: sedimentary basin processes; Marine geology and geophysics: Marine sediments: processes and transport; Marine geology and geophysics: Marine seismics; Marine geology and geophysics: Seafloor morphology, geology, and geophysics

## 10.2 Introduction

The pre-glacial to glacial sequences in the sedimentary record provide an impression of the first arrival of the ice sheets on the shelf at the Eocene/Oligocene [E/O, e.g. Escutia et al., 2011; Wilson et al., 2013; Lindeque et al., 2014], here referred to as the transitional sequence, and the subsequent permanent grounding of the Antarctic ice sheets on the continental shelf in the mid-Miocene [ANTOSTRAT, 1995; Brancolini et al., 1995; De Santis et al., 1999; Rebesco et al., 1997; De Santis et al., 2003; Wilson and Luyendyk 2009; Brancolini and Leitchenkov, 2010; Escutia et al., 2011; Uenzelmann-Neben and Gohl, 2012], here referred to as the full glacial sequence.

By mapping the seismic boundary horizons of these sequences, regions of high sediment deposition, referred to as depocenters, can be identified. They point to alluvial and glacial drainage outlets from the continent. Shifts for particular time periods can reveal changes in sediment transport and bottom current development that could be associated with changes in climate, erosion or tectonic reorganization. These insights, in combination with quantifying the sediment distribution, thickness and volume for each sequence, are necessary to constrain paleotopography reconstructions in ice-sheet models [Wilson et al., 2013].

Of current interest is the Eocene/Oligocene topography reconstruction that provides a boundary condition for estimating the controversial ice volume used for modeling the past and near future growth/demise of the Antarctic ice sheets [DeConto and Pollard, 2003; Wilson and Luyendyk, 2009; Wilson et al., 2012, 2013].

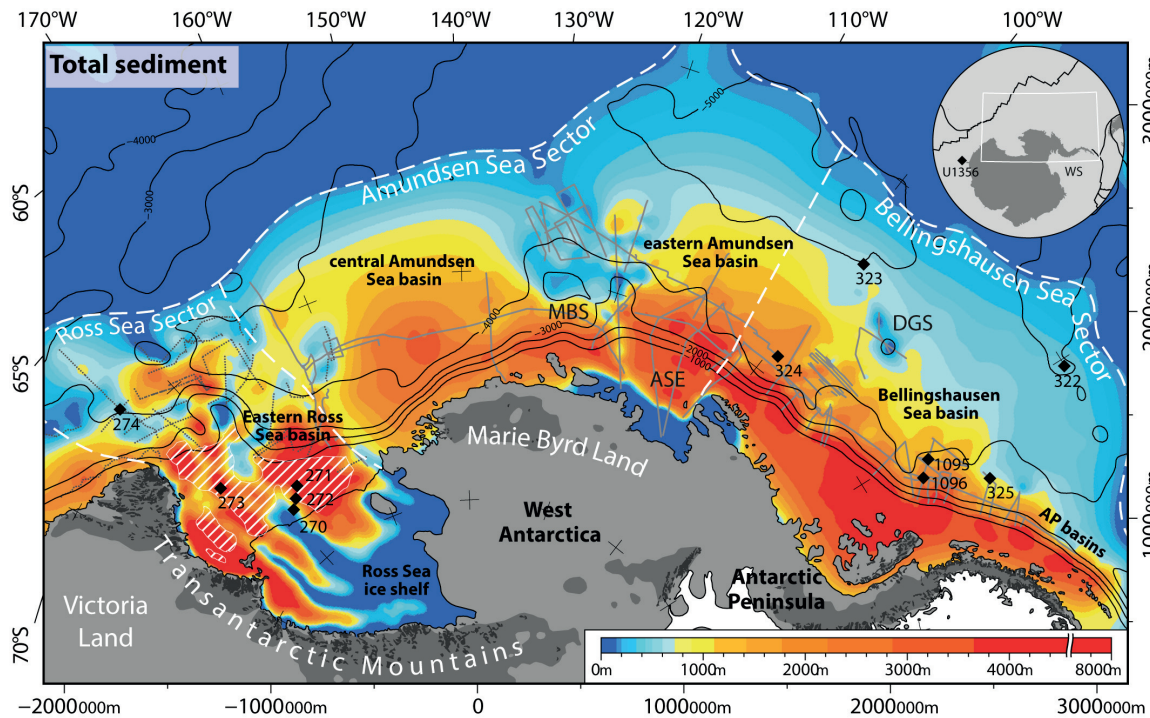


**Fig. 10-1.** Total sediment thickness map of the Pacific margin of West Antarctica, modified after Wobbe et al., [2014]. Catchment areas for the Ross Sea, central Amundsen Sea, Bellingshausen Sea and Antarctic Peninsula basins are demarcated in white dashed lines. Gray lines – published multichannel seismic reflection data used for the seismic horizon stratigraphy correlation and construction of subsequent grids [Figs. 10-3 to 10-5; TH86, Yamaguchi et al., 1988; IT-92, IT-95, Rebesco et al., 1997; ANT-11/3, Nitsche et al., 1997, 2000; De Santis et al., 1999, 2003; BAS-92, Petrov98, Scheuer et al., 2006; Uenzelmann-Neben, 2006; ANT-11/3, ANT-23/4, Uenzelmann-Neben and Gohl, 2012; ANT-26/3, Gohl et al., 2013; ANT-26/3, TAN0602, Lindeque et al., 2013, 2014]. Dotted lines – data analysis pending. Black diamonds – DSDP and ODP boreholes used for sediment thickness and age control. The location of the IODP Leg 318 Site U1356 is shown in the inset. White hashed polygon – Data coverage of ANTOSTRAT 1995, Brancolini and Leitchenkov, 2010. Dark grey polygons – present-day topography above 500 m. WS – Weddell Sea. Polar stereographic projection referenced to WGS84 with true scale latitude at 71°S and central meridian at 138°W.

To constrain these models better, circum-Antarctic sediment grids are required for the E/O topography reconstruction. However, current grids do not link up due to multichannel seismic data not being publically available, or the data does not exist, or the E/O horizon was not mapped. Whittaker et al., [2013] published an improved total sediment thickness grid of the southeastern Indian Ocean between Australia and East Antarctica.

The E/O transition sequence was identified in the Weddell Sea [Fig. 10-1 inset] along a deep sea transect [Lindeque et al., 2013] and work is ongoing to create the Weddell Sea grids. The Ross Sea shelf [Fig. 10-1] has a high coverage of seismic data, and Wilson and Luyendyk [2009] incorporated the sediment thickness of units above the E/O unconformity, RSU6 [ANTOSTRAT, 1995] to publish an initial 34 Ma E/O topography of West Antarctica.

However, the Ross Sea sediment grids stood in isolation from early isopach grids of the Bellingshausen Sea [Scheuer et al., 2006] due to a lack of seismic and borehole data needed to correlate the E/O unconformity across the Amundsen Sea [Fig. 10-1]. In addition, the



Bellingshausen Sea grids identified only the sediments in the full glacial period from mid-Miocene (~10 Ma), but the E/O sequence boundary remained unidentified. New seismic data acquired in the previously unexplored western and central Amundsen Sea [Gohl, 2010; Lindeque et al., 2014] allow us to correlate a basin-wide identification of the E/O sequence boundary [uPG-T in Lindeque et al., 2014] and seismic stratigraphy and to generate pre-glacial, transitional and full glacial isopach grids along the entire Pacific margin of West Antarctica.

### 10.3 Database and Methods

We largely improve on the total sediment thickness grid for the Pacific margin of West Antarctica [Fig. 10-1; Wobbe et al., 2014] by identifying top of basement in recently acquired multichannel seismic data in the eastern Ross Sea (TAN0602 survey) and western to central Amundsen Sea [Lindeque et al., 2014]. From this base dataset, we construct new basin-wide pre-glacial, transitional and full glacial sediment thickness grids of 5 km cell size, using the identified E/O and mid-Miocene unconformities for the new seismic data in the Amundsen Sea basin [Lindeque et al., 2014], as starting points to correlate the other seismic reflection stratigraphy studies Ross Sea, Amundsen Sea and Bellingshausen Sea basins to [seismic lines in Fig. 10-1; Yamaguchi et al., 1988; ANTOSTRAT, 1995; Brancolini et al., 1995; Nitsche et al., 1997, 2000; Rebesco et al., 1997; De Santis et al., 1999; De Santis et al., 2003; Scheuer et al., 2006; Uenzelmann-Neben, 2006; Wilson and Luyendyk 2009; Brancolini and Leitchenkov, 2010; Escutia et al., 2011; Uenzelmann-Neben and Gohl, 2012 and references to the seismic surveys on this margins therein].

#### 10.3.1 Stratigraphic correlation

The margin-wide seismic horizon correlation is summarized in Fig. 10-2. Supporting age control from boreholes [Fig. 10-1] is drawn from: IODP Leg 318 Site U1356 [Escutia et al., 2011] in Wilkes Land; selected Ross Sea boreholes [Fig. 10-1; DSDP Leg 28 Sites 270–274, Hayes and Frakes, 1975]; DSDP Leg 35 Sites 322–324 in the Bellingshausen Sea [Hollister et al., 1976; Tucholke et al., 1976], and ODP Leg 178 Sites 1095 and 1096 off the central Antarctic Peninsula [Rebesco et al., 1997; Barker et al., 2002; Uenzelmann-Neben, 2006].

The Ross Sea shelf and slope seismic stratigraphy are used as published [column 2 in Fig. 10-2]. Lindeque et al. [2014] correlated the Wilkes Land seismic interpretations [column 1 in Fig. 10-2] to the acquired data in the central Amundsen Sea basin [column 3 in Fig. 10-2]. The Amundsen sea basin correlation was extended up slope, to link in the Ross Sea seismic stratigraphy, and also extended to the east to incorporate the eastern Amundsen Sea basin seismic stratigraphy [columns 4 and 5 in Fig. 10-2].

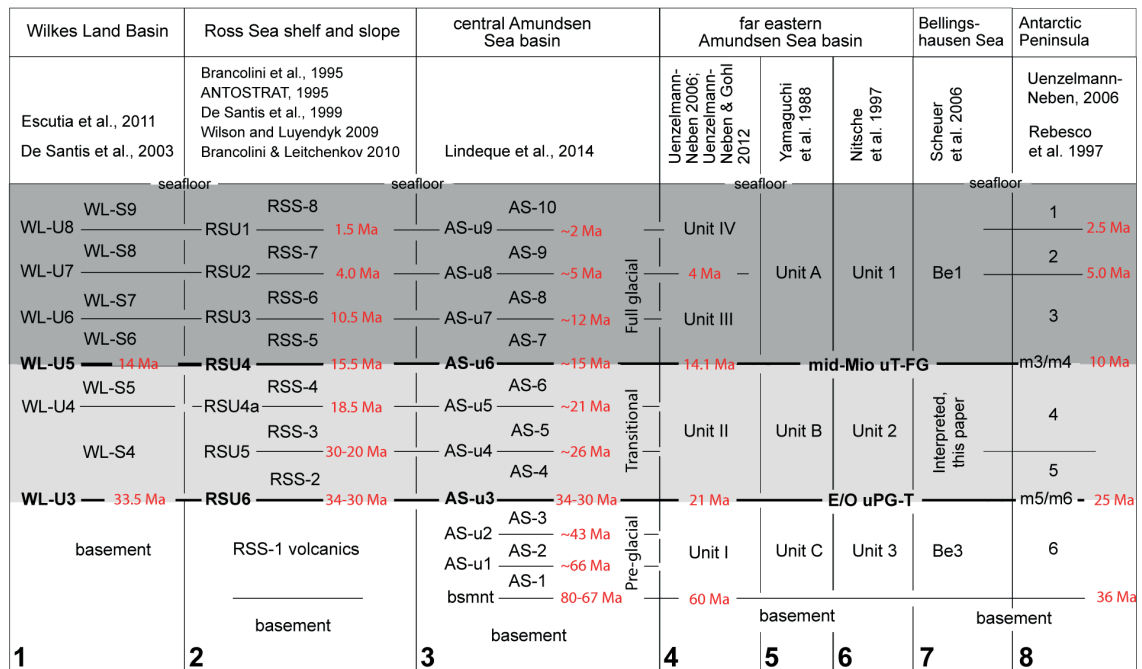


**Fig. 10-2.** Seismic stratigraphy correlation chart of several seismic interpretations on the Pacific margin of West Antarctica. Thick black lines – the Eocene/Oligocene uPG-T and the mid-Miocene uT-FG boundary horizons traced along the margin extent. Thin black lines – discontinuities or boundary horizons mapped in each study, see references at in the top row; red numbers – ages of the horizons taken as published, notice the lateral variation. Dark grey block – units assigned to the full glacial sequence, light grey block – the transitional sequence and lower white block, pre-glacial sequence

We expand on these correlations and map two key regional boundary seismic horizons, E/O uPG-T and mid-Miocene uT-FG, linking them to the horizon interpretations in the far eastern Amundsen Sea basin [Yamaguchi et al., 1988], Bellingshausen Sea [Scheuer et al., 2006] and Antarctic Peninsula [Rebesco et al., 1997] - listed in columns 5, 7 and 8 in Fig. 10-2. The Scheuer et al., [2006] and Rebesco et al., [1997] horizon picks were used as is. The only change is that the seismic lines in the isopach grids of Scheuer et al. [2006] did not identify the lower E/O transition and this was newly interpreted along the margin-parallel survey lines referred to in their paper.

The resulting correlated point data for the 34 Ma E/O transition horizon, **uPG-T**, which marks the start of the transitional sequence, is from west to east: WL-U3 → RSU6 → AS-u3 → base unit II and B → m5/m6. The resulting correlation for the mid-Miocene boundary horizon **uT-FG**, which marks the end of the transitional sequence, is from west to east: WL-U5 → RSU4 → AS-u6 → base unit III, B and I → m3/m4 [Fig. 10-2 and references therein].

### 10.3.2 Sediment thickness calculation

In addition to the total sediment thickness, sediment thickness grids are derived for three complementary parts:

[i] The pre-glacial [PG] sequence, representing the sediments deposited before the built-up of major ice sheets that extended to the coastal zone and the shelf. The sequence is estimated to be of Oligocene-Eocene age or older [Lindeque et al., 2013, 2014], and bounded by the acoustic basement below and the uPG-T horizon above [Fig. 10-2; section 2.1; Lindeque et al., 2013, 2014].

[ii] The transitional [T] sequence, which consists of Oligocene to middle Miocene sediments associated with the first arrival of the major ice sheets on the coasts and shelves. The sequence is bounded by the mid-Miocene uT-FG horizon above and uPG-T below [Fig. 10-2; section 2.1; Lindeque et al., 2013, 2014].

[iii] The full glacial sequence [FG], are sediments associated with pronounced advances of grounded ice across the shelves. This sequence is bounded by the mid-Miocene [uT-FG] unconformity below and seafloor above [Fig. 10-2; section 2.1; Lindeque et al., 2013, 2014].

For consistent comparison with the Scheuer et al., [2006] glacial grid and the previous total sediment thickness grid [Wobbe et al., 2014], we followed a similar approach as Wobbe et al. [2014] to derive the pre-glacial to glacial sediment thickness grids. We converted the two-way-travel times [TWT, T in s] for each boundary horizon to depth [km] using the empirical time-depth relation of Carlson et al., [1986]  $Z = 3.03 \ln(1 - 0.52T)$  for the sediments with a thickness of  $< 1.4$  s TWT ( $\sim 1.4$  km thick). For thicker sediments the sparse interval velocity measurements on the Pacific margin of West Antarctic were considered.

Sonobuoy data of the eastern Ross Sea rise recorded interval velocities from 1600 to 3900 m/s [TAN0602 survey and online supplement S2 in Lindeque et al., 2014]. These compare well with the interval velocities from the P-wave refraction model in the eastern Amundsen Sea, which ranges from 1600 to 4200 m/s [Gohl 2007; Lindeque and Gohl, 2010; Kalberg and Gohl, 2013; online supplement S5 in Lindeque et al., 2014]. Interval velocities derived from stacking velocities in the central Amundsen Sea basin, range from 1690 to 3760 m/s, over a maximum sediment thickness of 3.9 km [Table 3, online supplement S4 in Lindeque et al., 2014] and are consistent with the refraction and sonobuoy data. Sediments greater than 2.8 s TWT were converted to depth using the best fitting an average interval velocity of 2818 m/s.

### 10.3.3 Data merging and gridding

The sediment thickness grids are largely constrained by seismic data. In the eastern Amundsen Sea and Bellingshausen Sea, distal control points for the mid-Miocene/full glacial

unconformity uT-FG were filled in with borehole depth measurements from DSDP Leg 35 Sites 322, 323 [Hollister et al., 1976] and 324 [Tucholke et al., 1976], and ODP Leg 178 Sites 1095 and 1096 [Barker et al., 2002; Rebesco et al., 1997; Uenzelmann-Neben, 2006].

We use the same approach as in Wobbe et al., [2014] in order to maintain consistency for comparison, and for submission of the sediment thickness grids into the National Geophysical Data Center (NGDC). 10 x 10 km block medians were calculated to avoid spatial aliasing and the short-wavelength artifacts in the gridding process. Local minima and maxima were suppressed by applying a 0.2 tension factor to the continuous curvature splines gridding algorithm of Smith and Wessel [1990].

To avoid distortions and still maintain reasonable appearance of the PG, T, and FG grids, an additional 150 locations were selected and used for thickness estimates in areas devoid of seismic data. This was especially the case on the shelf, where these units have not been mapped or where seismic data is absent. A second-order Butterworth low-pass filter with a cut-off wavelength of 100 km was applied to remove short-range variations. The final grids were re-sampled by bicubic interpolation to 5 km resolution. The total sediment thickness grid [Fig. 10-1], pre-glacial sequence grid [Fig. 10-3], transitional sequence grid [Fig. 10-4] and full glacial sequence grid [Fig. 10-5] are presented in Antarctic Polar Stereographic Projection, true scale latitude at 71°S and referenced to WGS84.

These isopach grids should be seen as approximate time intervals in which certain sedimentation processes were dominant. The stratigraphic age model is however prone to large uncertainties due to lack of borehole age-control, which is demonstrated by lateral age variation in the sequence boundary horizons. For example: we assigned an age of around 34-30 Ma for the dominant uPG-T horizon in the Ross Sea and western Amundsen Sea rise, but younger ages (25-21 Ma) for the same horizon in the eastern Amundsen Sea and Bellingshausen Sea basins [Lindeque et al., 2014]. Thus the more generally accepted date for the onset of that process was selected as the main paleoclimate timeframe to place the grid result into.

An even larger uncertainty stems from the sparse data point distribution, which is directly limited by the availability of multichannel seismic reflection data. In places like the shelf and slope, where the pre-glacial to glacial units could not be identified, sediments are likely to be thicker than estimated. The T and FG sequences on the continental rise of the Ross Sea are currently underestimated, because these boundary horizons have not been picked in all the lines yet (dotted lines in Figs. 10-1 and 10-3 to 10-5) and this work is ongoing by others.

It can be assumed that the three sedimentary units consist mostly of terrigenous sediments with minor proportions of pelagic and hemi-pelagic components. The large seismic and borehole data distribution uncertainties overwrite the necessity to consider the estimated 15% pelagic component [DSDP and ODP boreholes; see section 2] and possible velocity time-depth conversion errors.



## 10.4 Results and discussion

We divided the West Antarctic margin into three main deposition sectors (Fig. 1) according to the terrigenous sediment source areas determined from the present-day ice drainage system divides (Zwally et al., 2012). These areas are shown in Fig. 10-1 and add up to about 8 million square kilometers. The Ross Sea Sector covers an area of  $1.59 \times 10^6$  km<sup>2</sup>, the Amundsen Sea Sector  $3.44 \times 10^6$  km<sup>2</sup> and the Bellingshausen Sea Sector  $3.01 \times 10^6$  km<sup>2</sup>. Table 10-1 summarizes the sediment volumes of the PG, T, and FG sequences in the three sectors.

Table 10-2 shows the hypothetical minimum height of a sediment pile that would cover West Antarctica if all sediments were returned to their source areas by applying Wilson et al.'s (2012) estimates for in-situ sediment density (1.95–2.1 g/cm<sup>3</sup>) and source rock density (2.6 g/cm<sup>3</sup>), and a maximum pelagic fraction of 15%, which was not subtracted from sediments restored to the continent in this calculation.

### 10.4.1 The pre-glacial sediment thickness grid

The pre-glacial sequence depicts depocenters that are relatively evenly distributed along the West Antarctic margin, ranging in maximum thickness from 1.3 km in the central Amundsen Sea basin, to >4 km in the Ross Sea and eastern Bellingshausen Sea basins [Fig. 10-3].

The thickest depocenters are in the eastern Ross Sea and eastern Amundsen Sea [Fig. 10-3]. From the margin-wide stratigraphic correlation [Fig. 10-2], the oldest sediments of this sequence were deposited on the oldest oceanic crust, which ranges from 84 Ma in the Amundsen Sea [C34 magnetic seafloor spreading anomaly, Wobbe et al., 2012] to less than 40 Ma west of the Antarctic Peninsula. The youngest limit of this sequence ranges between ~34 Ma in the western Amundsen Sea, the period when the ice sheets first arrived at the shelf [Escutia et al., 2011; Wilson et al., 2013], to 21 Ma in the eastern Amundsen Sea.

**Table 10-1.** Sediment volumes of PG, T, and FG sequences in Ross Sea (RS), Amundsen Sea (AS), and Bellingshausen Sea Sector (BS) in  $10^6$  km<sup>3</sup> and volume fraction in %.

	RS	AS	BS	All
FG	0.13 (5%)	1.00 (28%)	1.16 (28%)	2.29 (22%)
T	0.13 (5%)	0.83 (23%)	0.93 (22%)	1.90 (19%)
PG	2.24 (90%)	1.76 (49%)	2.06 (50%)	6.05 (59%)
Total	2.49	3.6	4.15	10.24

**Table 10-2.** Hypothetical sediment pile [km] reconstructed on source drainage areas [ $10^6$  km<sup>2</sup>] in West Antarctica (drainage areas defined by Zwally et al., 2012).

	RS	AS	BS	All
<b>FG</b>	0.13	1.07	3.55	1.03
<b>T</b>	0.14	0.89	2.85	0.85
<b>PG</b>	2.33	1.88	6.3	2.72
<b>Total</b>	2.6	3.84	12.7	4.61
<b>Drain. area</b>	0.61	0.6	0.21	1.42

The fairly even distribution of deposition is interpreted as sediment supply coming from most of the continental regions. This period has the highest sediment volume across all areas,  $6.05 \times 10^6 \text{ km}^3$  [59% of the total sediment volume; Table 10-1] and we estimated hypothetical sediment pile of 2.7 km was eroded [Table 10-2]. The reconstructed West Antarctic paleotopography at 34 Ma by Wilson and Luyendyk [2009] and Wilson et al., [2012] show a landmass of West Antarctica with a higher elevation than today and it is reasonable to assume that fast flowing, narrow river systems contributed to and a high erosion rate.

The even distribution could also partly be attributed to the gateway between Antarctica and Australia still being closed [Eagles et al., 2004; Wobbe et al., 2012], and ocean circulation being restricted to weaker localized currents such as a proto Ross Sea gyre [Huber et al., 2004], or, that eastward bottom water circulation that was only developed enough to form Paleocene to Eocene drift deposits within the depocenters through local reworking [Uenzelmann-Neben; 2006; Uenzelmann-Neben and Gohl, 2012; Lindeque et al., 2014]. Perhaps the sediment distribution remained relatively along the margin because these processes were not developed enough to transport large masses, or, the rate of sediment replenishment though along-slope and down-slope processes was similar to the erosion and transport rates.

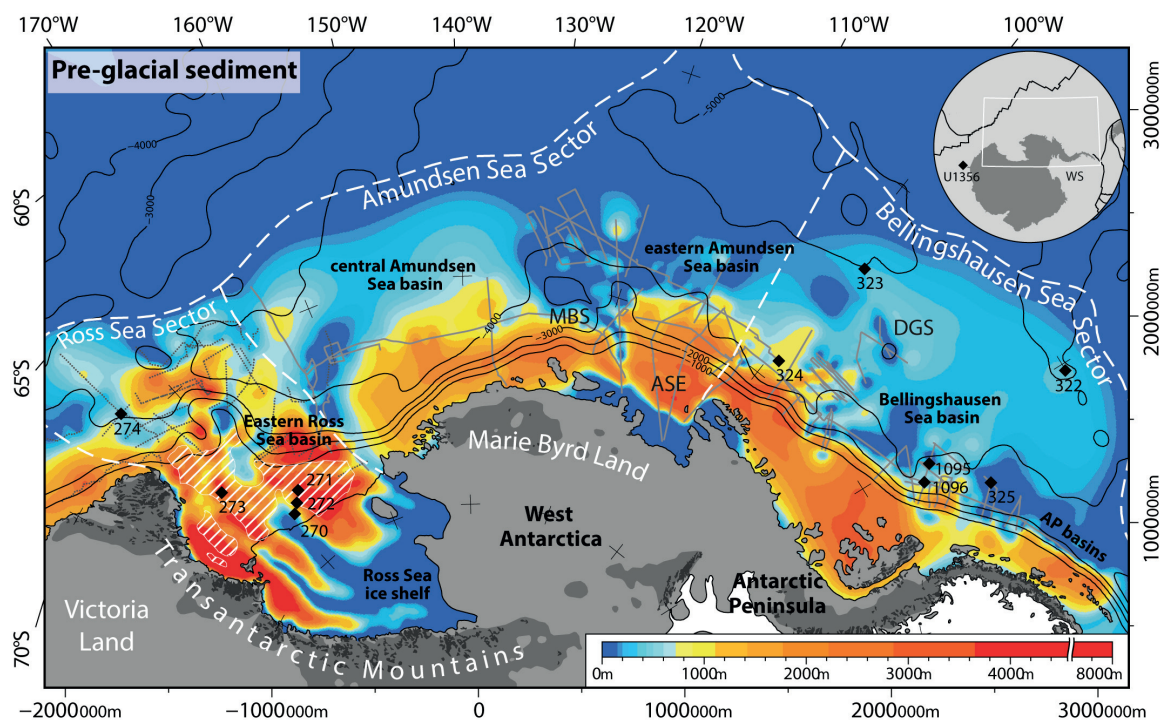


**Fig. 10-2.** The pre-glacial sediment thickness grid (> 34 Ma) including all units up to the Eocene–Oligocene, uPG-T boundary horizon [Fig. 10-2]. Annotations and map projection same as in Fig. 10-1.

### 10.4.2 The transitional sediment thickness grid

The up to 1.8 km thick transitional sequence shows a clear concentration of depocenters in the eastern Ross Sea basin, the central Amundsen Sea as well as the Bellingshausen Sea and the Antarctic Peninsula basins [Fig. 10-4]. Our stratigraphic correlation [Fig. 10-2] and consideration of available data on the margin, places an estimated maximum age range from 34 Ma to 15.5 Ma on this sequence. We relate this time interval to sedimentation processes affected by increasing continental ice sheets that expanded to the coasts and inner shelves [e.g., Anderson and Bartek, 1992; Lear et al., 2008; Miller et al., 2008; Escutia et al., 2011; Wilson et al., 2013] as Antarctica's climate became colder and more polar [Zachos et al., 2001; Berner and Kothavalla, 2001; Pagani et al., 2005; Haq and Schutter, 2008; Tripathi et al., 2009, 2011]. The gateways fully opened [Eagles et al., 2004; Livermore et al., 2005; Wobbe et al., 2012] and the Antarctic Circumpolar current, with associated bottom water formation started to develop [Barker et al., 1991; Lawver and Gahagan, 2003; Pollard and DeConto, 2009].

What may account for the marked shift in depocenters? We speculate that increased bottom ocean current circulation and higher current velocities may have enlarged the capacity to entrain and transport bigger volumes of sediment to the east [Uenzelmann-Neben and Gohl, 2012]. In addition to higher along-slope transport, there may have been changes inland and on the shelf. For instance, ice sheets that now cover the landmass may have altered the pre-glacial river drainage patterns as it advanced onto the shelf, and in so doing cut-off previous sediment supply paths to parts of the margin. Drainage could have been redirected to follow new pathways along lowered topography [Wilson et al., 2012, 2013], tectonic displacement zones such as faults, lineaments [Gohl et al., 2013] or rift zones such as the West Antarctic Rift System in the Ross Sea [Davey and De Santis, 2006; Müller et al., 2007; Wilson and Luyendyk, 2009].

Such processes would account for the concentration of glacial deposits in the eastern Ross Sea basin, central Amundsen Sea basin and Bellingshausen Sea [Fig. 10-3], as well as the decrease in sediment volume from  $6.1 \times 10^6 \text{ km}^3$  in the pre-glacial, to  $1.9 \times 10^6 \text{ km}^3$  the transitional climate regime [Table 10-1]. The elevated topography of the pre-glacial West Antarctic margin was reduced by a further 0.85 km [Table 10-2], which would have decreased the flow velocity and subsequent erosion and transport capacity of the drainage systems. This would have lead to a decrease in sediment supply to the shelf, slope and abyssal plains.

The sediment supply to the Bellingshausen Sea and Antarctic Peninsula basins remained high in comparison to the Ross Sea and Amundsen Sea areas [Table 10-1]. This is perhaps due to pre-glacial type river systems and down-slope sediment supply processes still dominating [Rebesco et al., 1997; Uenzelmann-Neben, 2006], because the Antarctic Peninsula ice sheet grounded later, early to late Miocene [Smith and Anderson 2010, 2011; Bohati et al., 2011; Lindeque et al., 2013].

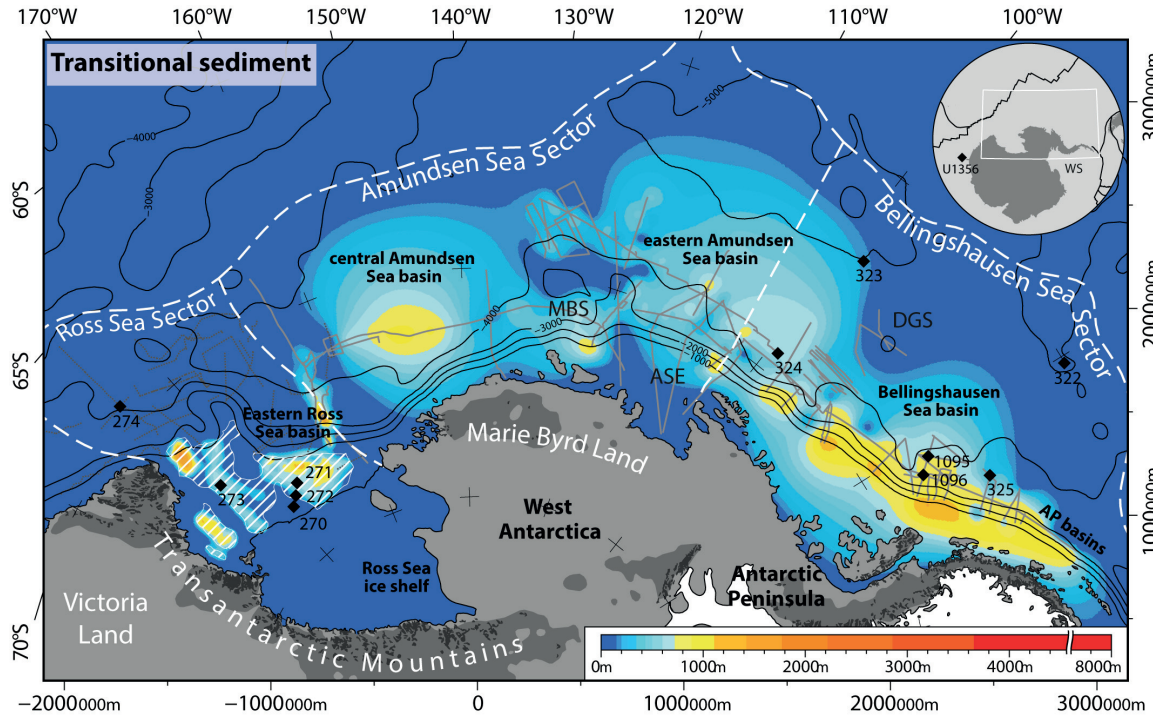


**Fig. 10-4.** The transitional sediment thickness grid (34–15.5 Ma) including all seismic units between the E/O uPG-T and the mid-Mio uT-FG boundary horizons [Fig. 10-2]. Annotations and map projection same as in Fig. 10-1.

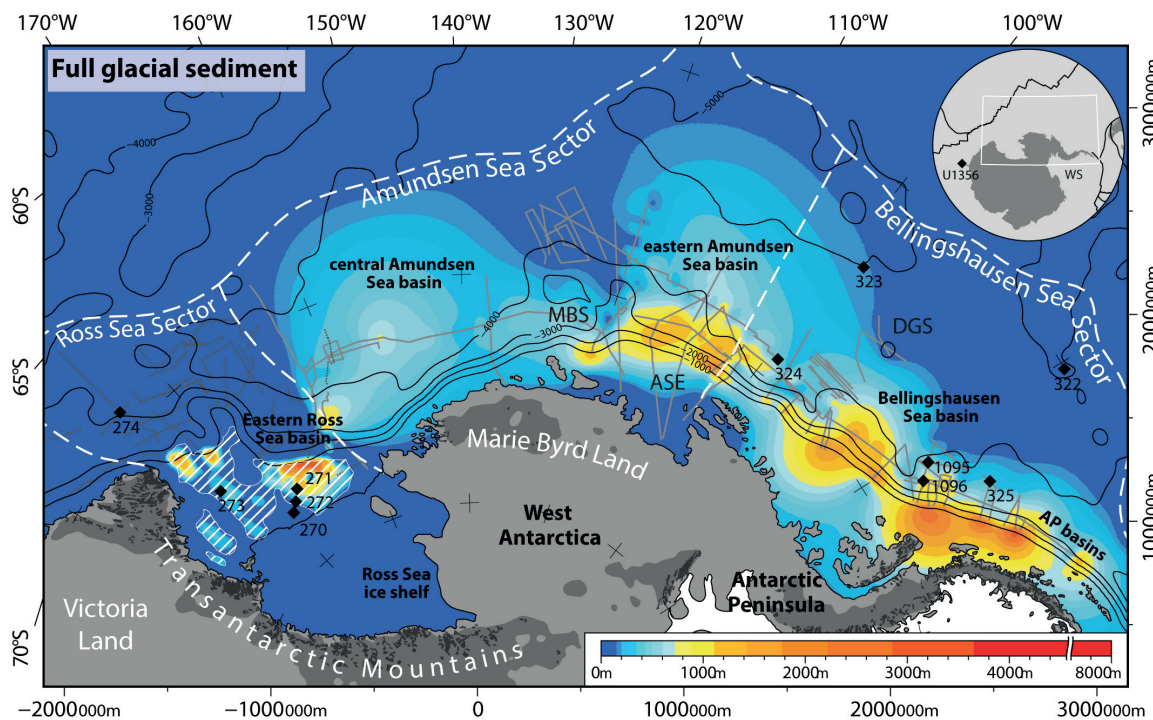


**Fig. 10-5.** The full glacial sediment thickness grid including all seismic units above the mid-Miocene (<15.5 Ma) uT-FG boundary horizons [Fig. 10-2]. Annotations and map projection same as in Fig. 10-1.



### 10.4.3 The full glacial sediment thickness grid

This sequence represents the mid-Miocene [15.5 Ma; Fig. 10-2] to present, where dominant sedimentary deposits are associated with ice sheets advancing across the shelves more frequently in glacial periods [e.g. Yamaguchi et al., 1988; Rebesco et al., 1997; Nitsche et al., 1997, 2000; De Santis et al., 1999, 2003; Scheuer et al., 2006; Uenzelmann-Neben, 2006; Brancolini and Leitchenkov, 2010; Smith and Anderson 2010, 2011; Uenzelmann-Neben and Gohl, 2012; Gohl et al., 2013; Lindeque et al., 2013, 2014].

Sediment supply increased from  $1.90$  to  $2.29 \times 10^6 \text{ km}^3$  [Table 10-1] compared to the transitional period. This could be explained by the grounded ice sheets advancing to the shelf edge more frequently, and in so doing, bulldozed sediment that the transitional stage ice sheets may have brought to the coast or inner shelf, down the slope and into the abyssal plain. The full glacial sequence indicates a second depocenter shift to the east [Fig. 10-4].

The central Amundsen Sea received less sediment input [-900 m maximum thickness, Table 10-1] and sediments were probably widely distributed by strong bottom water currents. A new depocenter of up to 2 km thickness formed north of the Amundsen Sea Embayment [Fig. 10-4]. Increased deposition in front of the Amundsen Sea Embayment may be ascribed to the development of ice streams that drain into the glacier systems [Bamber et al., 2009; Gohl et al., 2013]. Deposition in the Bellingshausen Sea and Antarctic Peninsula margin seem to have increased since the transitional period [maximum thickness ~2.5 km], probably in response to the growing Antarctic Peninsula Ice Sheet reaching the shelf and pushing the accumulated sediment from the pre-glacial to transitions periods down the slope [Uenzelmann-Neben, 2006] more frequently.

During this full glacial period, the landmass of Antarctica was reduced by a further 1 km [Table 10-2] to reach present-day topography [Le Brocq et al., 2010] and much of West Antarctica became inundated [Wilson et al., 2012, 2013]. This change would have terminated previous land based drainage systems and formed new glacial drainage systems that likely directed sediment supply towards the Amundsen Sea Embayment and eastern Ross Sea. Much of the Bellingshausen Sea and Antarctic Peninsula margin remained at high elevation and as such, sediment supply and erosional rates there would be higher, which could account for the increased deposition [Table 10-1].

## 10.5 Conclusions

Recently acquired multichannel seismic data in the central Amundsen Sea and eastern Ross Sea basin now allow the first cross-basin and margin-wide seismic horizon stratigraphy correlation for the Pacific margin of West Antarctica. From this correlation and additional borehole and velocity data, we present a revised total sediment thickness grid and the first sediment thickness grids for the pre-glacial (>34 Ma), transitional (34–15.5 Ma) and full glacial (< 15 Ma) sequences.

Our grids link the Ross Sea shelf grids with the localized grids in the Bellingshausen Sea and western margin of the Antarctic Peninsula along the estimated Eocene/Oligocene unconformity, here called uPG-T, and the mid-Miocene unconformity, uT-FG. Interpolation was needed in areas with no multichannel seismic data, mostly on the distal plains where sediments are scarce and in the underexplored regions. The total sediment thickness grid updates the global NGDC grid [Whitaker et al., 2013], whereas the other grids reveal the previously unknown Paleocene to present depocenters development for this margin.

The pre-glacial period shows a fairly equal distribution of deposits along the entire margin, but this changes after the first ice sheets arrived on the shelf (uPG-T unconformity). Many of the depocenters no longer received as much sediment, and sediment transport shifted towards congregating in the eastern Ross Sea, central Amundsen Sea basin and the eastern Bellingshausen Sea depocenters. After ice sheets advances became more frequent with grounding on the shelves beginning in the mid-Miocene (<15.5 Ma), as marked key horizon uT-FG, the central Amundsen Sea basin was no longer a main depocenter. A new depocenter developed north of the Amundsen Sea Embayment, from the ice streams and glacial drainage patterns along tectonic lineaments.

Based on present-day drainage and source area divides, hypothetical estimates indicate a pre-glacial (> 34 Ma) reduction of Pacific margin of West Antarctica's paleotopography of 2.7 km, translating to  $\sim 6 \times 10^6 \text{ km}^3$  of sediments being deposited offshore during this period. This indicates the amount of sediment that should be piled back onto land, if sediment thickness is to be considered in the Eocene–Oligocene paleotopography reconstruction. For the mid-Miocene paleotopography surface, the pre-glacial and transitional estimates are combined. Indications are that a sediment pile of approximately 3.6 km thick and  $\sim 8 \times 10^6 \text{ km}^3$  in volume, would need to be placed back onto. In total, from the Cretaceous to the present day topography,  $\sim 4.6 \text{ km}$  of sediment was eroded off land and deposited as a total volume of  $10.24 \times 10^6 \text{ km}^3$  on the Pacific margin of West Antarctica. These values are initial estimates and also the first values for this margin. Work is ongoing to improve them.

## 10.6 Acknowledgements

This project was funded by the Priority Program 1158 *Antarctic Research* of the *Deutsche Forschungsgemeinschaft* (DFG) under project number GO 724/10-1 and by institutional funds for Work Package 3.2 of the AWI Research Program PACES. This project contributes to the *Circum-Antarctic Stratigraphy and Palaeobathymetry* (CASP) project, a *Scientific Committee on Antarctic Research* (SCAR) a working group *Past Antarctic Ice Sheet Dynamics* (PAIS). Navigation and seismic data for lines other than those acquired by the *Alfred Wegener Institute, Helmholtz Centre for Polar and Marine Research* (AWI) the AWI-xx and *GNS New Zealand* (TAN0602 survey), were obtained with thanks from the *Antarctic Seismic Data Library System* (SDLS; <http://sdls.ogs.trieste.it>) All the grids were created using *Generic Mapping Tools* (GMT) Version 5 [Wessel et al. 2013].

## 10.7 References

- Anderson, J.B., Bartek, L.R., 1992. Cenozoic glacial history of the Ross Sea revealed by intermediate resolution seismic reflection data combined with drill site information. In: Kennett, J.P., Warnke, D.A. (Eds.), *The Antarctic Paleoenvironment: A Perspective on Global Change, Part One*. Antarctic Research Series, vol. 56. American Geophysical Union, Washington, DC, 231–263.
- ANTOSTRAT, 1995. Seismic Stratigraphic Atlas of the Ross Sea, in *Geology and Seismic Stratigraphy of the Antarctic Margin*, (Eds.) A. K. Cooper, Barker, P. F., Brancolini, G., 68pp., 22 plates, American Geophysical Union, Washington, D.C.
- Bamber, J.L., Riva, R.E.M., Vermeersen, B.L.A., LeBrocq, A.M., 2009. Reassessment of the potential sea-level rise from a collapse of the West Antarctic Ice Sheet, *Science*, 324, 901–903, doi:10.1126/science.1169335
- Barker, P.F., Dalziel, I.W.D., Storey, B.C., 1991. Tectonic development of the Scotia Arc region. In: Tingey, R.J. (Ed.), *Geology of Antarctica*. Oxford University Press, Oxford, 215–248.
- Barker, P.F., Camerlenghi, A., Acton G.D., Ramsay, A.T.S. et al., 2002. Proceedings of the ODP, Scientific Results, 178, 1–40 (Online) [http://www-odp.tamu.edu/publications/178\\_SRN](http://www-odp.tamu.edu/publications/178_SRN) and [http://www-odp.tamu.edu/publications/178\\_SR/178TOC.HTM](http://www-odp.tamu.edu/publications/178_SR/178TOC.HTM).
- Berner, R.A., Kothavala, Z., 2001. GEOCARB III: A revised model of atmospheric CO<sub>2</sub> over Phanerozoic time. *American Journal of Science* 304, 397–437.
- Bohaty, S.M., Kulhanek, D.K., Wise, S.W.Jr., Jemison, K., Warny, S., Sjunneskog, C., 2011. Age Assessment of Eocene-Pliocene Drill Cores Recovered During the SHALDRIL II Expedition, Antarctic Peninsula. In: Anderson, J.B., Wellner, J.S. (Eds.), *Tectonic, Climatic, and Cryospheric Evolution of the Antarctic Peninsula*. Special Publication 63, American Geophysical Union. 63–113. doi:10.1029/2010SP001049
- Brancolini, G., and Leitchenkov, G., 2010. Ross Sea. 118–128. In: Cooper, A.K., Brancolini, G., Escutia, C., Kristoffersen, Y., Larter, R., Leitchenkov, G., O'Brien, P., Jokat, W., 2009. Chapter 5 - Cenozoic Climate History from Seismic Reflection and Drilling Studies on the Antarctic Continental Margin. In: Florindo, F., Siegert, M. (Eds.). *Developments in Earth and Environmental Sciences 8, Antarctic Climate Evolution*. The Netherlands: Elsevier, 115–228. ISBN: 978-0-444-52847-6.
- Brancolini, G., Cooper, A. K., Coren, F., 1995. Seismic Facies and Glacial History in the Western Ross Sea (Antarctica), *Antarctic Research Series*. American Geophysical Union, Washington, DC, 68, 209–234.
- Carlson, R.L., Gangi, A.F., Snow, K.R., 1986. Empirical Reflection Travel Time Versus Depth and Velocity Versus Depth Functions for The Deep-Sea Sediment Column. *Journal of Geophysical Research*, 91(B8), 8249–8266. doi:10.1029/JB091iB08p08249.
- Davey, F. J., De Santis, L., 2006. A Multi-Phase Rifting Model for the Victoria Land Basin, Western Ross Sea. *Antarctica*. 303–308. doi: 10.1007/3-540-32934-X\_38
- DeConto, R. M., and Pollard, D., 2003. A coupled climate-ice sheet modeling approach to the Early Cenozoic history of the Antarctic ice sheet, *Palaeogeography Palaeoclimatology Palaeoecology*, 198, 39–52, doi:10.1016/S0031-0182(03)00393-6
- De Santis, L., Prato, S., Brancolini, G., Lovo, M. & Torelli, L., 1999. The Eastern Ross Sea continental shelf during the Cenozoic: implications for the West Antarctic Ice Sheet development. *Global and Planetary Change* 23, 173–196. PII: s0921-8181(99)00056-9.
- De Santis, L., Brancolini, G., Donda, F., 2003. Seismo-stratigraphic analysis of the Wilkes Land continental margin (East Antarctica): influence of glacially driven processes on the Cenozoic deposition. *Deep Sea*

- Research Part II: Topical Studies in Oceanography, 50, 8-9, 1563–1594, doi:10.1016/S0967-0645(03)00079-1
- Eagles, G., Gohl, K., Larter, R.D., 2004. Life of the Bellingshausen plate. *Geophysical Research Letters* 31, L07603, doi:10.1029/2003GL019127
- Escutia, C., Brinkhuis, H., Klaus, A., and the Expedition 318 Scientists, 2011. *Proceedings IODP*, 318: Tokyo (Integrated Ocean Drilling Program Management International, Inc.), 101pp, doi:10.2204/iodp.proc.318.2011. [http://publications.iodp.org/proceedings/318/104/104\\_.htm](http://publications.iodp.org/proceedings/318/104/104_.htm)
- Gohl, K., 2007. The Expedition ANTARKTIS-XXIII/4 of the Research Vessel “Polarstern” in 2006. *Berichte zur Polar- und Meeresforschung (Reports on Polar and Marine Research)* 557, 166 pp. <http://epic.awi.de/26756/>.
- Gohl, K., 2010. The expedition of the research vessel “Polarstern” to the Amundsen Sea, Antarctica, in 2010 (ANTXXVI/3). *Berichte zur Polar- und Meeresforschung / Reports on Polar and Marine Research*, 617. <http://epic.awi.de/29635/>
- Gohl, K., Uenzelmann-Neben, G., Larter, R.D., Hillenbrand, C.-D., Hochmuth, K., Kalberg, T., Weigelt, E., Davy, B., Kuhn, G., Nitsche, F.O., 2013. Seismic stratigraphic record of the Amundsen Sea Embayment shelf from pre-glacial to recent times: Evidence for a dynamic West Antarctic Ice Sheet. *Marine Geology*, 344, 115–131. doi:10.1016/j.margeo.2013.06.011
- Haq, B.U., and Schutter, S.R., 2008. A chronology of Paleozoic sea-level changes. *Science*, 322, 5898, 64–68, doi:10.1126/science.1161648
- Hayes, D.E., Frakes L.A., and Shipboard\_Scientific\_Party (1975), A geophysical study of the Ross Sea, Antarctica Sites 270, 271, 272 In: *Initial Reports of the Deep Sea Drilling Project, Leg 28*, Hayes, D.E., and Frakes, L.A. (Eds.) 211–334 and 887–907, U.S. Government Printing Office, Washington, D.C.
- Hollister, C. D., Craddock, C., Bogdanov, Y.A., Edgar, N.T., Gieskes, J.M. Haq, B.U., Lawrence, J.R., Roegl, F., Schrader, H.-J., Tucholke, B.E., Vennum, W.R., Weaver, F.M., Zhivago, V.N., Worstell, P. (Eds.), 1976. *Initial Reports of the Deep Sea Drilling Project 35*. U.S. Government Printing Office. doi:10.2973/dsdp.proc.35.1976.
- Huber, M., Brinkhuis, H., Stickley, C.E., Döös, K., Sluijs, A., Warnaar, J., Schellenberg, S.A., Williams G.L., 2004. Eocene circulation of the Southern Ocean: Was Antarctica kept warm by subtropical waters? *Paleoceanography* 19, PA4026, doi:10.1029/2004PA001014.
- Kalberg, T. and Gohl, K., 2013. The crustal structure and tectonic development of the continental margin of the Amundsen Sea Embayment, West Antarctica: Implications from geophysical data. *Geophysical Journal International*, submitted.
- Lawver, L.A., Gahagan, L., 2003. Evolution of Cenozoic Seaways in the circum-Antarctic region. *Palaeogeography, Palaeoclimatology, Palaeoecology* 198, 11–37. doi:10.1016/S0031-0182(03)00392-4
- Lear, C.H., Bailey, T.R., Pearson, P.N., Coxall, H.K., Rosenthal, Y., 2008. Cooling and ice growth across the Eocene–Oligocene transition. *Geology* 36, 251–254. doi:10.1130/G24584A.1
- Le Brocq, A.M., Payne, A.J., Vieli, A., 2010. An improved Antarctic dataset for high-resolution numerical ice sheet models (ALBMAP v1). *Earth System Science Data Discussions* 3, 195–230. doi:10.5194/essdd-3-195-2010 [www.earth-systsci-data-discuss.net/3/195/2010/](http://www.earth-systsci-data-discuss.net/3/195/2010/)
- Lindeque, A. and K. Gohl, 2010. Western Antarctic palaeostratigraphy: implications for palaeobathymetry and palaeoclimate modelling. Poster presentation at IPY Oslo Science Conference, Oslo, 8–12 June 2010. Available from: [http://elsevier.conference-services.net/resources/247/1976/pdf/Oslo2010\\_0377.pdf](http://elsevier.conference-services.net/resources/247/1976/pdf/Oslo2010_0377.pdf)



- Lindeque, A., Martin, Y.M., Gohl, K., Maldonado, M., 2013. Deep-sea pre-glacial to glacial sedimentation in the Weddell Sea and southern Scotia Sea from a cross-basin seismic transect. *Marine Geology* 336, 61–83. doi:10.1016/j.margeo.2012.11.004
- Lindeque, A., Gohl, K., Henrys, S., Wobbe, F., Davy B., 2014. Pre-glacial to glacial stratigraphy in the unexplored Amundsen Sea deep-sea basin: A first cross-regional correlation of deep-sea seismic reflection data. Manuscript prepared for *Palaeogeography, Palaeoclimatology, Palaeoecology* – see chapter 8.
- Livermore, R., Nankivell, A., Eagles, G., Morris, P., 2005. Paleogene opening of Drake Passage. *Earth and Planetary Science Letters* 236, 459–470.
- Miller, K.G., Wright, J.D., Katz, M.E., Browning, J.V., Cramer, B.S., Wade, B.S., Mizintseva, S.F., 2008. A view of Antarctic ice-sheet evolution from sea-level and deep-sea isotope changes during the Late Cretaceous-Cenozoic. In: Cooper, A.K., Barrett, P.J., Stagg, H., Storey, B., Stump, E., Wise, W., the 10th ISAES editorial team (Eds.), *Proceedings of the 10th International Symposium on Antarctic Earth Sciences. Antarctica: A Keystone in a Changing World*. The National Academies Press, Washington, DC. doi:10.3133/of2007-1047.kp06
- Müller, R.D., Gohl, K., Cande, S.C., Goncharov, A., Golynsky, A.V., 2007. Eocene to Miocene geometry of the West Antarctic rift system. *Australian Journal of Earth Sciences* 54, 1033–1045, doi:10.1080/08120090701615691.
- Nitsche, F.O., Gohl, K., Vanneste, K., Miller, H., 1997. Seismic expression of glacially deposited sequences in the Bellingshausen and Amundsen Seas, West Antarctica. In: *Geology and Seismic Stratigraphy of the Antarctic Margin 2*, Barker, P.F. and Cooper, A.K. (Eds.), *Antarctic Research Series* 71, 95–108, American Geophysical Union, Washington, D.C.
- Nitsche, F.O., Cunningham, A.P., Larter, R.D., Gohl, K., 2000. Geometry and development of glacial continental margin depositional systems in the Bellingshausen Sea, *Marine Geology* 162 (2–4), 277–302.
- Pagani, M., Zachos, J., Freeman, K.H., Tipple, B., Bohaty, S., 2005. Marked decline in atmospheric carbon dioxide concentrations during the Paleogene. *Science* 309 (5734), 600–603. doi:10.1126/science.1110063
- Pollard, D., DeConto, R.M., 2009. Modelling West Antarctic ice sheet growth and collapse through the past five million years. *Nature* 458, 320–323. doi:10.1038/nature07809
- Rebesco, M., Larter, R.D., Barker, P.F., Camerlenghi, A., Vanneste, L.E., 1997. The history of sedimentation on the continental rise west of the Antarctic Peninsula. In: Barker, P.F., Cooper, A.K. (Eds.), *Geology and seismic stratigraphy of the Antarctic margin, 2*. *Antarctic Research Series*, 71, 29–49. AGU.
- Scheuer, C., Gohl, K., Eagles, G., 2006. Gridded isopach maps from the South Pacific and their use in interpreting the sedimentation history of the West Antarctic continental margin. *Geochemistry Geophysics Geosystems (G-cubed)* 7, Q11015. doi:10.1029/2006GC001315.
- Smith, R.T., and Anderson, J.B., 2010. Ice-sheet evolution in James Ross basin, Weddell Sea margin of the Antarctic Peninsula: the seismic stratigraphic record. *Geological Society of America Bulletin* 122 (5/6), 830–842. doi:10.1130/B26486.1.
- Smith, R.T., and Anderson, J.B., 2011. Seismic Stratigraphy of the Joinville Plateau: Implications for Regional Climate Evolution. In: Anderson, J.B. and Wellner, J.S. (Eds.) *Tectonic, Climatic, and Cryospheric Evolution of the Antarctic Peninsula*. Geopress, American Geophysical Union, Washington DC, USA. 51–61. doi:10.1029/2010SP000980
- Smith, W. H. F. and P. Wessel, 1990. Gridding with continuous curvature splines in tension. *Geophysics* 55, 293–305.

- Tripati, A.K., Roberts, C.D., Eagle, R.A., 2009. Coupling of CO<sub>2</sub> and ice sheet stability over major climate transitions of the last 20 million years. *Science* 326, 1394–1397. doi:10.1016/j.gca.2011.01.018
- Tripati, A.K., Roberts, C.D., Eagle, R.A., Li, G., 2011. A 20 million year record of planktic foraminiferal B/Ca ratios: systematics and uncertainties in pCO<sub>2</sub> reconstructions. *Geochimica et Cosmochimica Acta* 75 (10), 2582–2610. doi:10.1016/j.gca.2011.01.018
- Tucholke, B.E., Edgar, N.T., Boyce, R.E., 1976. Physical properties of sediments and correlations with acoustic stratigraphy: Leg 35, Deep Sea Drilling Project. In: Hollister, C.D., Craddock, C. (Eds.), *Initial Reports. Deep Sea Drilling Project, Washington D.C.*, 229–249.
- Uenzelmann-Neben, G., 2006. Depositional patterns at Drift 7, Antarctic Peninsula: Along-slope versus down-slope sediment transport as indicators for oceanic currents and climatic conditions. *Marine Geology* 233 1–4, 49–62. doi.org/10.1016/j.margeo.2006.08.008
- Uenzelmann-Neben, G. and Gohl, K., 2012. Amundsen Sea sediment drifts: Archives of modifications in oceanographic and climatic conditions. *Marine Geology* 299-302, 51–62, doi:10.1016/j.margeo.2011.12.007/
- Whittaker, J., Goncharov, A., Williams, S., Müller, R.D., Leitchenkov, G., 2013. Global sediment thickness data set updated for the Australian-Antarctic Southern Ocean. *Geochemistry Geophysics Geosystems (G-cubed)* 14, 3297–3305, doi:10.1002/ggge.2018
- Wilson D.S. and Luyendyk, B., 2009. West Antarctic paleotopography estimated at the Eocene–Oligocene climate transition. *Geophysical Research Letters* 36, L16302, doi:10.1029/2009GL039297
- Wilson, D.S., Jamieson, S.S.R., Barrett, P.J., Leitchenkov, G., Gohl, K., Larter, R.D., 2012. Antarctic topography at the Eocene–Oligocene boundary. *Palaeogeography, Palaeoclimatology, Palaeoecology*, 335-336, 24–34. doi:10.1016/j.palaeo.2011.05.028
- Wilson, D. S., D. Pollard, R. M., S. S. R. Jamieson, and B. P. Luyendyk, 2013. Initiation of the West Antarctic Ice Sheet and estimates of total Antarctic ice volume in the earliest Oligocene. *Geophysical Research Letters* 40, 4305–4309. doi:10.1002/grl.50797.
- Wobbe, F., Gohl, K., Chambord, A., Sutherland, R., 2012. Structure and breakup history of the rifted margin of West Antarctica in relation to Cretaceous separation from Zealandia and Bellingshausen plate motion. *Geochemistry Geophysics Geosystems (G-cubed)* 13, 4, Q04W12. doi:10.1029/2011GC003742.
- Wobbe, F., Lindeque, A., Gohl, K., 2014. Anomalous South Pacific lithosphere dynamics derived from new sediment thickness estimates off the West Antarctic margin. *Global Planetary Change*, submitted.
- Yamaguchi, K., Tamura, Y., Mizukoshi, I., Tsuru, T., 1988. Preliminary report of geophysical and geological surveys in the Amundsen Sea, West Antarctica. *Proceedings NIPR Symposium on Antarctic Geoscience* 2, 55–67.
- Zachos, J., Pagani, M., Sloan, L., Thomas, E., Billups, K., 2001. Trends, rhythms, and aberrations in global climate 65 Ma to present. *Science* 292, 686–693.
- Zwally, H. J., Giovinetto, M.B., Beckley, M.A., Saba, J.L., 2012. Antarctic and Greenland Drainage Systems, GSFC Cryospheric Sciences Laboratory [online]. Available from: [http://icesat4.gsfc.nasa.gov/cryo\\_data/ant\\_grn\\_drainage\\_systems.php](http://icesat4.gsfc.nasa.gov/cryo_data/ant_grn_drainage_systems.php).



This work set out to explore some of the open questions on the evolution of the Pacific margin of West Antarctica, particularly regarding sediment processes indicating the first arrival of the ice sheets on the shelf – when a glacial environment started to dominate Antarctica. The ice sheet evolution, sediment transport processes and bottom current development in this margin is still poorly understood. This is mainly because the central Amundsen Sea basin is historically devoid of drilling and other geophysical, oceanographic and geological data. Whereas work to date in the Weddell Sea basin, was mainly focused on the slope or shelf and access to the deep-sea basin limited by sea ice. Through the analyses of unpublished and pre-existing multichannel seismic data in the Weddell Sea; pre-existing data in the Bellingshausen Sea, Antarctic Peninsula region, eastern Amundsen and Ross Seas; and newly acquired data in the central Amundsen Sea and eastern Ross Sea basins, we can begin to explore some of the initial answers to these questions. The key findings of this work is summarised in Figs. 11-1 and 11-2, and places some of the questions stated in Chapter 1, in context.

### **11.1 How does the seismic characteristics vary between the basins and what can it reveal about the past history of the margin development?**

Type sections in the Weddell Sea and Amundsen Sea basins display similar seismic characteristics in seismic reflection characteristics and internal facies geometry for the identified pre-glacial, transitional and full glacial sequences (compare the regional type sections in Fig. 11-1). These characteristics are also similar to those seen in deep-sea seismic profiles in the Bellingshausen Sea, Ross Sea and Wilkes Land basins, as well in type sections from other studies on the east Antarctic margin e.g. in the Riiser Larsen Sea, Cosmonaut Sea, Mawson Sea.

The striking similarities between these type sections implies that the Pacific margin of West Antarctica, and circum-Antarctic margin, had similar sediment transport processes dominating in more or less the same age range. By implication it is possible to trace the seismic reflection deemed most representative of this sediment process or sequence boundary around Antarctica. To this extent, new cross-basin seismic stratigraphic models have been mapped and proposed for both the Weddell Sea basin and the central Amundsen Sea basin. Selected horizons from the Amundsen Sea basin were successfully mapped further along the Pacific margin of West Antarctica, and enabled the identification of the pre-glacial, transitional and full glacial components of the historic margin development.



### 11.2 What variation is there in sediment thickness, volume and geometry within each basin, between basins, and between the pre-glacial to glacial units?

The sediment thickness in the Weddell Sea basin ranges from 1756–3136 m, which is slightly less than in the central Amundsen Sea basin 805–3090 m. The minimum sediment thickness in the Amundsen Sea basin occurs above a ~300 km long Eocene Pre-glacial drift (up to 680 m high) where most of the sediment units thin to 45–89 m thick. The progressively decreasing angles in the unconformities above this drift suggest syn- and post-depositional uplift for the eastern Amundsen Sea basin flank.

Total sediment volume in the central Amundsen Sea basin is estimated at  $3.6 \times 10^6$  km<sup>3</sup>, which is similar to the sediment volume in the Weddell Sea ( $3.3\text{--}3.9 \times 10^6$  km<sup>3</sup>), but less than in the Bellingshausen – Antarctic Peninsula basins ( $4.15 \times 10^6$  km<sup>3</sup>). The sediment volume in the Ross Sea is lower than expected ( $2.49 \times 10^6$  km<sup>3</sup>) but this is because not all the new seismic data has been incorporated yet. This work is on going.

In general, the sediment volume does not correlate to drainage area size. For example the Bellingshausen Sea drainage area is  $\sim 0.21 \times 10^6$  km<sup>2</sup>, which is a third of the Amundsen Sea's drainage area, but the sediment volume influx is larger ( $4.15 \times 10^6$  km<sup>3</sup>).

The Amundsen Sea basin geometry forms a classic 'saucer' shape whereas the Weddell Sea basin is more even. The magnetic seafloor spreading anomaly compilation done for the Weddell Sea basin indicates that the basement crust is much older (143–19 Ma) than the Amundsen Sea (80–63 Ma). It is also more rugged, which suggests the spreading rate in the Weddell basin was probably slower (compare grey basement polygons in Fig. 11-1).

In the Weddell Sea basin, the pre-glacial sequence is slightly thicker (~1130 m) than the full glacial sequence (1085 m) and the transitional unit is the thinnest (780 m). The pre-glacial sequence is also thickest in the Amundsen Sea basin (up to 2203 m), but the transitional sequence is thicker than the full glacial sequence (up to 1069 m and 889 m, respectively) (see diagrams in Fig. 11-1 for comparison).

### 11.3 Do the variations in sediment deposition geometry provide any clues about bottom current development?

Yes, a ~300 km long drift occurs on the eastern flank of the central Amundsen Sea basin, in the 55–34 Ma old pre-glacial AS-3 unit. This indicates an eastward bottom current activity in the Eocene or earlier. This new information and much earlier than the late Oligocene bottom current activity in the eastern Amundsen Sea basin, suggested in previous studies.

The pre-glacial sequence in the Weddell Sea forms a mound in the centre of the basin and together with the asymmetrical eroded flank geometry, allows the interpretation of a Cretaceous proto Weddell Gyre, which was not suggested in literature before.

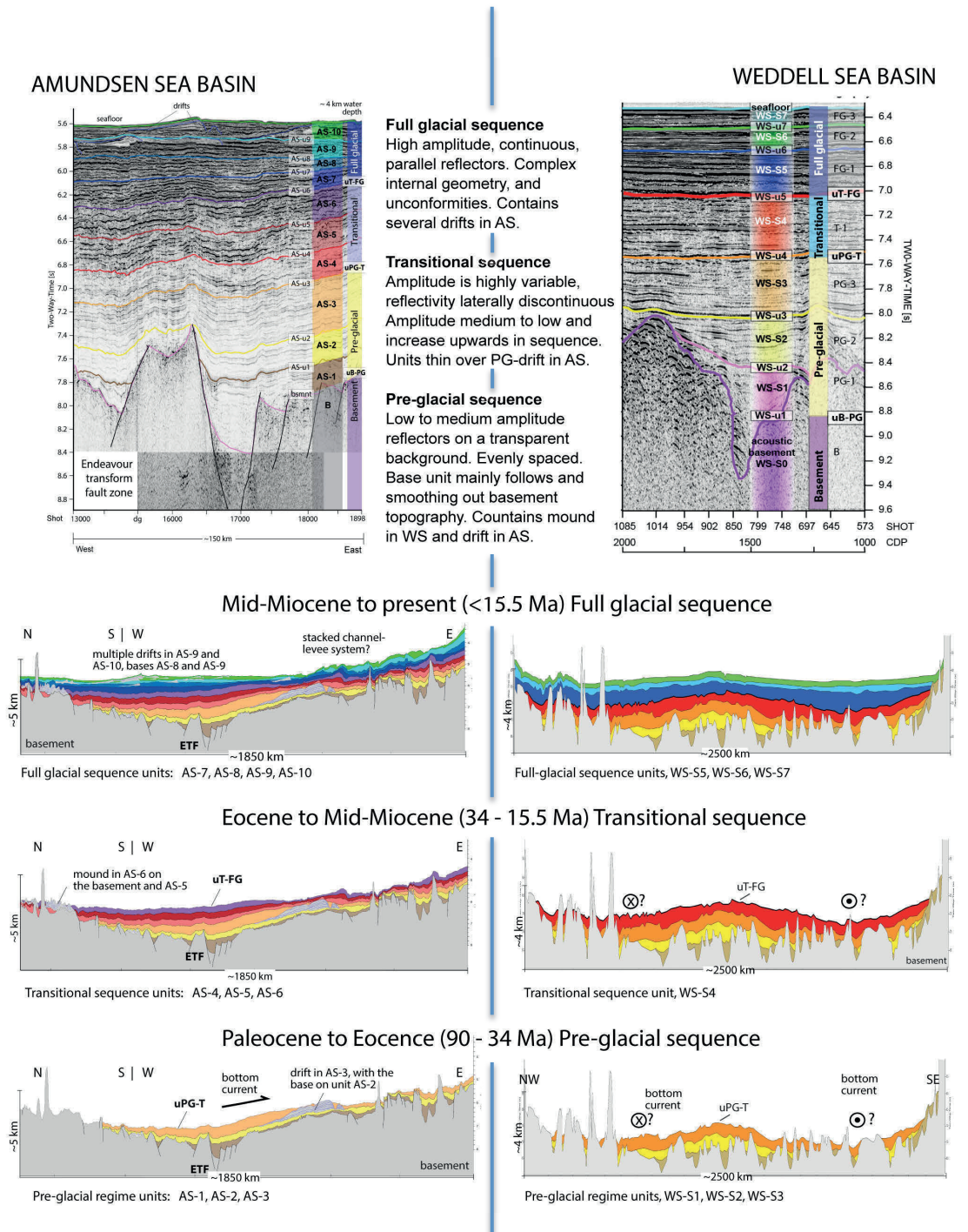


**Fig. 11-1.** Comparison of the central Amundsen Sea basin (Ch. 8) and the Weddell Sea basin (Ch. 7) in terms of seismic reflection characteristics identified in the type sections (top). The basin and margin wide seismic interpretation on each of the AS-RS transect and the WS-SS transect assigned each sequence to a probably time frame (see sequential deposition diagrams below the type sections). The horizons representing the pre-glacial, transitional and full glacial sequences are shown, from old to young. uPG-T represents the 34 Ma Eocene / Oligocene unconformity, in this study associated with the first arrival of the ice sheets on the shelf. uT-FG represents the 15.5 Ma mid-Miocene unconformity, associated here with the permanent grounding of the ice sheets on the shelf and several advance/retreat cycles to the outer shelf. The Amundsen Sea and Weddell Sea basin horizons are not directly linked yet, but the similarities are striking in the type section and unit divisions. ETF – Endeavour transform fault/fracture zone. Circle with black dot – ocean bottom current with flow direction out of the paper. Circle with cross – ocean bottom current with flow direction into the paper. Collectively these indicate a clockwise gyre current direction. Diagrams are based on the seismic data interpretation but vertically exaggerated.

### 11.4 Where are the major deposition centres for the pre-glacial to glacial periods? What processes may have caused their formation and did the centres move over time?

The pre-glacial depocenters are distributed along the Pacific margin of West Antarctica and are up to 4 km thick. A shift to the east occurs when the ice sheets expand and initially arrive on the shelf during the estimated Eocene/Oligocene period. We postulate that ice sheet advances may have changed drainage channel locations as it pushed sediment from inland onto the shelf. In addition, the ocean gateways opened and the Antarctic bottom water formation intensified, which could have contributed to increasing sediment transport to the east.

As the ice sheets grounded on the shelf for extended periods, and frequently advanced to the shelf edge from the mid-Miocene onwards, the eastward shift continued and a new depocentre formed north of the Amundsen Sea Embayment. This change is ascribed to glacial drainage following previous tectonic lineaments in the now exposed basement. Approximately  $\sim 4.6$  km ( $\sim 10.2 \times 10^6$  km<sup>3</sup>) of sediment was eroded off West Antarctica's topography since the Cretaceous.

### 11.5 Which part of the sediment record indicates the initial ice sheet advances onto the shelf at the beginning of the glacially dominated climate of West Antarctica? Can it be quantified?

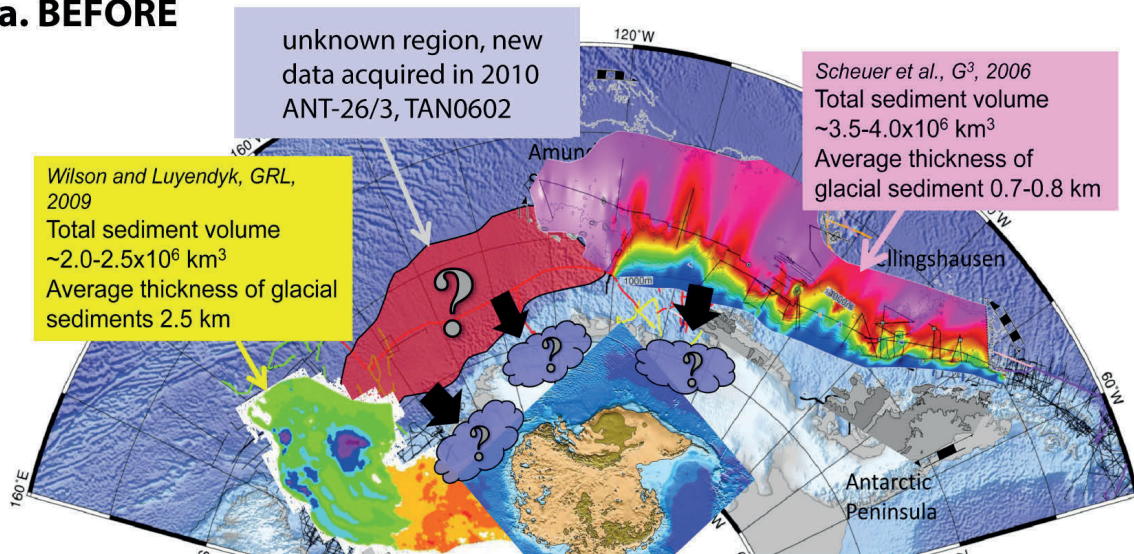
In comparing the seismic type sections around Antarctica to each other and combining it with borehole data, a visual correlation can be made based on the changes in seismic reflectivity and internal unit geometry. The boundary horizons of these key sequences were successfully mapped in the seismic data over long distances in the Amundsen Sea, Weddell Sea, and wider Pacific margin of West Antarctica.

The boundary horizon of the pre-glacial to transitional sequences, uPG-T, marks the first arrivals of the ice sheets on the shelf. The margin wide correlation incorporated seismic interpretation from all other studies on the Pacific margin of West Antarctica. This correlation is summarized from west to east as follows: Eocene/Oligocene boundary horizon **uPG-T** = WL-U3 → RSU6 → AS-u3 → base unit II and B → m5/m6. This unit was quantified as the pre-glacial sequence (see 11.2). The mid-Miocene boundary horizon **uT-FG** marks the end of the transitional sequence and correlates as: WL-U5 → RSU4 → AS-u6 → base unit III, B and I → m3/m4.

The constructed age model for the Weddell Sea suggests an Oligocene/Eocene West Antarctic ice sheet advance and an early Miocene APIS advance, which is earlier than what current models in literature suggest. The age model for the central Amundsen Sea basin indicates a West Antarctic Ice Sheet advance at the Eocene/Oligocene transition (34 Ma, uPG-T horizon in Fig. 11-1) on the basin flanks, and somewhat later on the margin south of the basin centre (assuming a direct drainage pattern).



**a. BEFORE**



**b. AFTER**

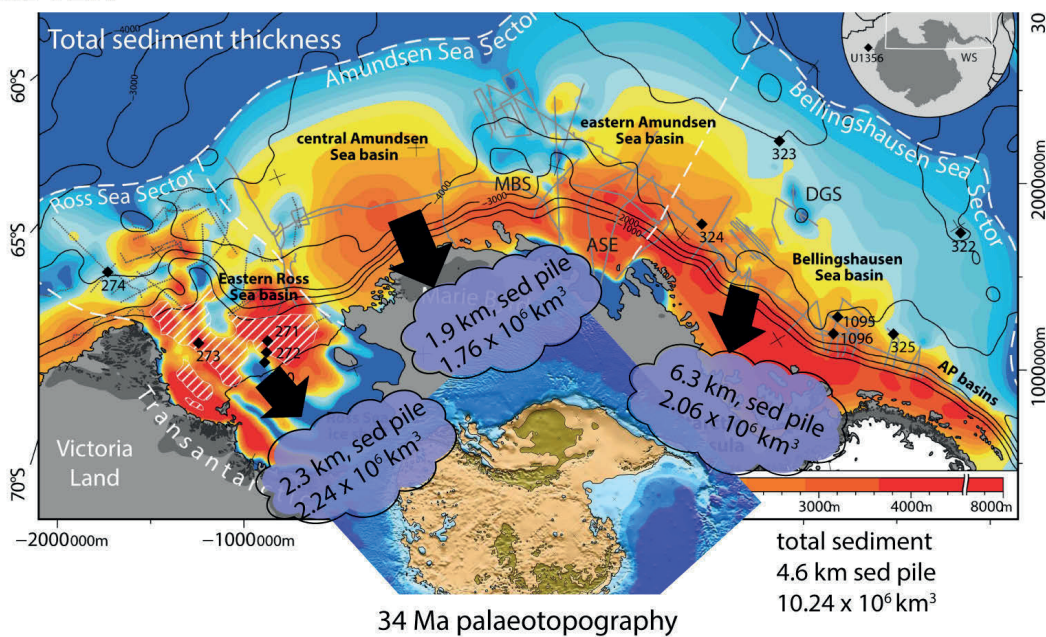


**Fig. 11-2.** Summary of information on the marine sediment record, off the Pacific margin of West Antarctica, before and after this work. (a) Sediment thickness grids on the Pacific margin off West Antarctica prior to the seismic data acquisition in 2010, Ant 26/3 and the TAN0602 seismic survey. Note the Amundsen Sea region being devoid of any seismic lines, other than the AS-RS transect acquired in 2010 (Ch. 4, 8 and 9). The sediment volumes, thicknesses and basin geometry for the Amundsen Sea were unknown (question mark in the red polygon). Due to this data gap it was not possible to complete the margin wide grid and estimate the amount of sediment to place back onto land for the palaeotopography reconstruction (question marks and clouds – size of the clouds representing the estimated sediment volume schematically, annotated on the inset from Wilson et al., 2012). (b) First total sediment thickness grid for the margin and initial quantification of sediment deposits. Sediment volume estimates for each basin is annotated together with the estimated hypothetical pile of sediment that would need to be placed back onto land for the 34 Ma palaeotopography reconstruction. Note how the new information from the Amundsen Sea basin closed the gap and although data is still sparse and work ongoing, it is an initial starting point. Black diamonds – Boreholes used, black lines – present-day bathymetry, Grey lines – multichannel seismic data used in this study. White hashed polygon – extent of the ANTOSTRAT (1995) interpretation.



### **11.6 If there is regional variation in acoustic basement topography, what does it reveal about the tectonic development of the Amundsen Sea basin?**

The western flank of the Amundsen Sea basin exhibits a rugged topography attributed to a spreading rate below 60-70 mm/Myr. The region between the Kohiko and Endeavour fracture zones show a block-faulted basement, indicating vertical as well as lateral displacement. A smooth basement topography from the Endeavour fracture zones to the Proto-Antipodes fracture zones is ascribed to a faster seafloor spreading rate, whereas the rugged basement topography on the eastern flank of the basin is accounted for by the AS–RS transect crossing a region of mixed oceanic and deformed continental crust.

### **11.7 How much sediment was eroded off land and deposited in the deep-sea basin in total, or at times of key climate change such as the Eocene/Oligocene boundary? Can it be quantified for palaeotopography and palaeobathymetry reconstructions?**

These results are illustrated in the context of the 34 Ma palaeotopography surface reconstruction and previous studies on the margin (see Fig. 11-2). Using the present day drainage divides, the hypothetical estimates indicate that 2.7 km ( $\sim 6 \times 10^6 \text{ km}^3$ ) of sediment should be piled back onto land if sediment thickness is to be considered in the Eocene/Oligocene palaeotopography reconstruction.

For the mid-Miocene palaeotopography reconstruction, a sediment pile of approximately 3.6 km thick ( $\sim 8 \times 10^6 \text{ km}^3$ ) would be needed to be placed back onto land. In total, from the Cretaceous to the present day topography,  $\sim 4.6$  km of sediment was eroded on land and deposited offshore on the Pacific margin of West Antarctica as a total volume of  $10.3 \times 10^6 \text{ km}^3$ .

### **11.8 Outlook**

Further work is in progress to expand the pre-glacial, transitional and full-glacial horizon correlations into the remaining seismic data of the Ross Sea (dashed lines in Fig. 11-2 b). This will increase the sparse data points for the sediment thickness grids and correct the anomalously low total sediment volume in front of the Ross Sea shelf. The sediment volume and hypothetical sediment pile estimates can be improved upon by incorporating the 34 Ma surface drainage areas, instead of present day drainage patterns.

In the Weddell Sea, work to create the pre-glacial to glacial grids is on going. Eventually we would be in a position to link the sediment thickness grids in the Riiser Larsen Sea, Cosmonaut Sea, Mawson Sea and Wilkes Land in as well, in order to construct the first circum-Antarctic sediment thickness grids – albeit with large uncertainties.

---

**References for Chapters 1 to 5**

- Amante, C., Eakins, B.W., 2009. ETOPO1 1 Arc-Minute Global Relief Model: Procedures, Data Sources and Analysis. NOAA Technical Memorandum NESDIS NGDC-24. (19 pp.)
- Allen, J.R.L., 1984. *Sedimentary Structures: Their character and Physical Basis*. 1, Elsevier, Amsterdam, Netherlands, 1235pp.
- Bamber, J.L., Riva, R.E.M., Vermeersen, B.L.A. and LeBrocq, A.M., 2009. Reassessment of the potential sea-level rise from a collapse of the West Antarctic Ice Sheet, *Science* 324, 901-903. doi:10.1126/science.1169335.
- Barker, P.F. Thomas, E., 2004. Origin, signature and palaeoclimatic influence of the Antarctic Circumpolar Current. *Earth-Science Reviews* 66, 1–2, 143–162. doi:10.1016/j.earscirev.2003.10.003.
- Barker, P.F., Diekmann, B., Escutia, C., 2007. Onset of Cenozoic Antarctic glaciation. *Deep Sea Research Part II: Topical Studies in Oceanography* 54, 2293–2307. doi:10.1016/j.dsr2.2007.07.027.
- Bart, P.J., Egan, D., Waarny, S.A., 2005. Direct constraints on Antarctic Peninsula ice sheet grounding events between 5.12 and 7.94 Ma. *Journal of Geophysical Research* 110, F04008. doi:10.1029/2004JF000254.
- Bell, R.E., Studinger, M., Shuman, C.A., Fahnestock, M.A., Joughin, I., 2007. Large subglacial lakes in East Antarctica at the onset of fast-flowing ice streams. *Nature* 445, 904–907.
- Berner, R.A., and Kothavala, Z., 2001. GEOCARB III: A revised model of atmospheric CO<sub>2</sub> over Phanerozoic time: *American Journal of Science* 301, 182–204.
- Bohoyo, F., 2004. Fragmentación continental y desarrollo de cuencas oceánicas en el sector meridional del Arco de Scotia, Antártida. Ph. D Thesis, University of Granada, Granada, 252 pp.
- Bohoyo, F., Galindo-Zaldívar, J., Maldonado, A., Schreider, A.A., Suriñach, E., 2002. Basin development subsequent to ridge-trench collision: the Jane Basin, Antarctica. *Marine Geophysical Research* 23, 413–421. doi:10.1023/B:MARI.0000018194.18098.0d.
- Cunningham, A.P., Larter, R.D., Barker, P.F., Gohl, K., Nitsche, F.O., 2002. Tectonic evolution of the Pacific margin of Antarctica 2. Structure of Late Cretaceous–early Tertiary plate boundaries in the Bellingshausen Sea from seismic reflection and gravity data. *Journal of Geophysical Research* 107 (B12), 2346. doi: 10.1029/2002JB001897.
- De Santis, L., Prato, S., Brancolini, G., Lovo, M., Torelli, L., 1999. The Eastern Ross Sea continental shelf during the Cenozoic: implications for the West Antarctic ice sheet development. *Global Planetary Change* 23, 173–196. doi:10.1016/S0921-8181(99)00056-9.
- De Santis, L., Brancolini, G., Donda, F., 2003. Seismo-stratigraphic analysis of the Wilkes Land continental margin (East Antarctica): influence of glacially driven processes on the Cenozoic deposition. *Deep Sea Research Part II: Topical Studies in Oceanography* 50, 8-9, 1563–1594. doi:10.1016/S0967-0645(03)00079-1.
- Domack, E., Ambala, D., Gilbert, R., Brachfeld, S., Camerlenghi, A., Rebesco, M., Canals, M., Urgeles, R., 2006. Subglacial morphology and glacial evolution of the Palmer deep outlet system, Antarctic Peninsula. *Geomorphology* 75, 125–142.

## 12. References

---

- Dowdeswell, J.A., Siegert, M., 1999. Ice-sheet numerical modeling and marine geophysical measurements of glacier-derived sedimentation on the Eurasian Arctic continental margins. *Geological Society of America (GSA) Bulletin* 111, 1080–1097.
- Dowdeswell, J.A., O'Cofaigh, C., Pudsey, C.J., 2004a. Continental slope morphology and sedimentary processes at the mouth of an Antarctic palaeo-ice stream. *Marine Geology* 204, 203–214.
- Dowdeswell, J.A., Ó Cofaigh, C., Pudsey, C.J., 2004b. Thickness and extent of the subglacial till layer beneath an Antarctic paleo-ice stream. *Geology* 32, 13–16.
- Escutia, C., De Santis, L., Donda, F., Dunbar, R.B., Cooper, A.K., Brancoli, G., Eitrem, S.L., 2005. Cenozoic ice sheet history from East Antarctic Wilkes Land continental margin sediments. *Global and Planetary Change* 45, 1-3, 51–81. doi:10.1016/j.gloplacha.2004.09.010.
- Escutia, C., Brinkhuis, H., Klaus, A., and the Expedition 318 Scientists (2011), *Proceedings IODP 318: Tokyo (Integrated Ocean Drilling Program Management International, Inc.)*, 101pp. doi:10.2204/iodp.proc.318.2011.
- Evans, J., Dowdeswell, J.A., Ó Cofaigh, C., Benham, T.J., Anderson, J.B., 2006. Extent and dynamics of the West Antarctic Ice Sheet on the outer continental shelf of Pine Island Bay during the last glaciation. *Marine Geology* 230, 53–72.
- Faugères, J.-C., Stow, D.A.V., 2008. Contourite drifts: nature, evolution and controls. In: M. Rebesco, A. Camerlenghi (Eds.), *Contourites, Developments in Sedimentology* 60, Elsevier, Amsterdam, 257–288.
- Gohl, K., 2010. The expedition of the research vessel “Polarstern” to the Amundsen Sea, Antarctica, in 2010 (ANT-XXVI/3). *Berichte zur Polar- und Meeresforschung / Reports on Polar and Marine Research*, 617. <http://epic.awi.de/29635/>
- Gordon, A.L., et al., 2009. Western Ross Sea continental slope gravity currents. *Deep Sea Research Part II: Topical Studies in Oceanography* 56 (13–14), 796–817.
- Graham, A.G.C., Later, R.D., Gohl, K., Hillenbrand, C.-D., Smith, J.A., Kuhn, G., 2009. Bedform signature of a West Antarctic ice stream reveals a multi-temporal record of flow and substrate control. *Quaternary Science Reviews* 28, 2774–2793. doi: 10.1016/j.quascirev.2009.07.003.
- Graham, A.G.C., Later, R.D., Gohl, K., Dowdeswell, J.A., Hillenbrand, C.-D., Smith, J.A., Evans, J., Kuhn, G., Deen, T., 2010. Flow and retreat of the Late Quaternary Pine Island-Thwaites palaeo-ice stream. West Antarctica. *Journal of Geophysical Research - Earth Surface* 115, F03025.
- Haq, B.U., Schutter, S.R., 2008. A chronology of Paleozoic sea-level changes. *Science* 322, 5898, 64–68. doi:10.1126/science.1161648.
- Haq, B.U., Hardenbol, J., and Vail, P.R., 1987. Chronology of fluctuating sea levels since the Triassic (250 million years ago to present). *Science* 235, 1156–1167.
- Hayes, D.E., LaBrecque, J.L., 1991. Sediment Isopachs: Circum-Antarctic to 30°S. In: *Marine Geological and Geophysical Atlas of the Circum-Antarctic to 30°S* (Ed.) D.E. Hayes, Antarctic Research Series 54. American Geophysical Union, Washington, D.C., 29–33.
- Hayes, D.E., Zhang, C., Weissel, R.A., 2009. Modeling Paleobathymetry in the Southern Ocean. *EOS, Transactions of the American Geophysical Union* 90, (19), 165–172.
- Hernández-Molina, F.J., Maldonado, A., Stow, D.A.V., 2008a. Chapter 18 Abyssal Plain Contourites. In: M. Rebesco, A. Camerlenghi (Eds.), *Developments in Sedimentology* 60, Elsevier, Amsterdam, 345, 347–378. doi: 10.1016/S0070-4571(08)10018-8.
- Hernández-Molina, F.J., Llave, E., Stow, D.A.V., 2008b. Chapter 19 Continental Slope Contourites. In: M. Rebesco, A. Camerlenghi (Eds.), *Developments in Sedimentology* 60, Elsevier, Amsterdam, 379–408. doi: 10.1016/S0070-4571(08)10019-X.
- Hoffman, P.F., 1999. The break-up of Rodinia, birth of Gondwana, true polar wander and the snowball Earth. *Journal of African Earth Sciences* 28, 1, 17–33. doi: 10.1016/S0899-5362(99)00018-4.

- Kalberg, T. and Gohl, K., 2013. The crustal structure and tectonic development of the continental margin of the Amundsen Sea Embayment, West Antarctica: Implications from geophysical data. *Geophysical Journal International*, submitted.
- Klages, J.P., Kuhn, G., Hillenbrand, C.-D., Graham, A.G.C., Smith, J.A., Larter, R.D., Gohl, K. 2013, First geomorphological record and glacial history of an inter-ice stream ridge on the West Antarctic continental shelf. *Quaternary Science Reviews* 61, 47–61. doi: 10.1016/j.quascirev.2012.11.007.
- Koenitz, D., White, N., McCave, I.N., Hobbs, R., 2008. Internal structure of a contourite drift generated by the Antarctic Circumpolar Current. *Geochemistry Geophysics Geosystems* 9, Q06012. doi: 10.1029/2007GC001799. ISSN: 1525-2027.
- König, M., Jokat, W., 2006. The Mesozoic breakup of the Weddell Sea. *Journal of Geophysical Research* 111 (B12102). doi: 10.1029/2005JB004035.
- Larter, R.D. and Barker, P.F., 1989. Seismic stratigraphy of the Antarctic Peninsula Pacific margin: a record of Pliocene-Pleistocene ice volume and paleoclimate. *Geology* 17, 731–734. doi:10.1130/0091-7613(1989)017b0731:SSOTAP>2.3.CO;2.
- Laske, G., Masters, G., 1997. A global digital map of sediment thickness. EOS, Transactions American Geophysical Union 78, (46), F483 (Fall Meeting Supplement).
- Le Brocq, A.M., Payne, A.J., Vieli, A., 2010. An improved Antarctic dataset for high resolution numerical ice sheet models (ALBMAP v1). *Earth System Science Data Discussions* 3, 195–230, www.earth-syst-sci-data-discuss.net/3/195/2010/. doi:10.5194/essdd-3-195-2010.
- Leitchenkov, G.L., Guseva, Y.B., Gandyukhin, V.V., 2007. Cenozoic environmental changes along the East Antarctic continental margin inferred from regional seismic stratigraphy. U.S. Geological Survey and U.S. National Academy, USGS OF-2007-1047, Short Research Paper 005. doi:10.3133/of2007-1047.srp005.
- Livermore, R., Nankivell, A., Eagles, G., Morris, P., 2005. Paleogene opening of Drake Passage. *Earth and Planetary Science Letters* 236, 459–470. doi: /10.1016/j.epsl.2005.03.027.
- Livingstone, J., Cofaigh, C.Ó., Stokes, C.R., Hillenbrand C.-D., Vieli, A., Jamieson, S.S.R., 2012. Antarctic palaeo-ice streams, *Earth-Science Reviews*. 111, (1–20), 90–128, doi:10.1016/j.earscirev.2011.10.003.
- Lythe, M. B., Vaughan, G.D., and the BEDMAP Consortium, 2001. BEDMAP: A new ice thickness and subglacial topographic model of Antarctica, *Journal of Geophysical Research* 106, 11,335–11,351. doi:10.1029/2000JB900449.
- Maldonado, A., Zitellini, N., Leitchenkov, G., Balanyá, J.C., Coren, F., Galindo-Zaldívar, J., Lodolo, E., Jabaloy, A., Zanolla, C., Rodríguez-Fernández, J., Vinnikovskaya, O., 1998. Small ocean basin development along the Scotia–Antarctica plate boundary and in the northern Weddell Sea. *Tectonophysics* 296, 371–402.
- Maldonado, A., Barnolas, A., Bohoyo, F., Galindo-Zaldívar, J., Hernández-Molina, J., Lobo, F., Rodríguez-Fernández, J., Somoza, L., Vázquez, J.T., 2003. Contourite deposits in the central Scotia Sea: the importance of the Antarctic Circumpolar Current and Weddell Gyre flows. *Palaeogeography, Palaeoclimatology, Palaeoecology* 198, 187–221. doi: 10.1016/S0031-0182(03)00401-2.
- Maldonado, A., Barnolas, A., Bohoyo, F., Escutia, C., Galindo-Zaldívar, J., Hernández-Molina, F.J., Jabaloy, A., Lobo, F.J., Nelson, C.H., Rodríguez-Fernández, J., Somoza, L., Vázquez, J.T., 2005. Miocene to recent contourite drifts development in the northern Weddell Sea (Antarctica). *Global Planet Change* 45, 99–129. doi:10.1016/j.gloplacha.2004.09.013.
- Maldonado, A., Bohoyo, F., Galindo-Zaldívar, J., Hernández-Molina, F.J., Jabaloy, A., Lobo, F.J., Rodríguez-Fernández, J., Suriñach, E., Vázquez, J. T., 2006a. Ocean basins near the Scotia–Antarctic plate boundary: Influence of tectonics and paleoceanography on the Cenozoic deposits. *Marine Geophysical Research* 27, 83–107. doi:10.1007/s11001-006-9003-4.
- Maldonado, A., Barnolas, A., Bohoyo, F., Escutia, C., Galindo-Zaldívar, J., Hernández-Molina, F.J., Jabaloy, A., Lobo, F.J., Nelson, C.H., Rodríguez-Fernández, J., Somoza, L., Suriñach, E., Vázquez, J. T.,



## 12. References

---

- 2006b. Seismic stratigraphy of Miocene to recent sedimentary deposits in the central Scotia Sea and Northern Weddell Sea: Influence of Bottom Flows (Antarctica). In: Fütterer, D.K., Damaske, D., Kleinschmidt, G., Miller, H., Tessensohn, F. (Eds.), *Antarctica: Contributions to global earth sciences*. Springer-Verlag, Berlin Heidelberg New York, 441–446.
- Michels, K.H., Rogenhagen, J., Kuhn, G., 2001. Recognition of contour-current influence in mixed contourite–turbidite sequences of the western Weddell Sea, Antarctica. *Marine Geophysical Research* 22, 465–485. doi:10.1023/A:1016303817273.
- Michels, K.H., Kuhn, G., Hillenbrand, C.-D., Diekmann, B., Fütterer, D.K., Grobe, H., Uenzelmann-Neben, G., 2002. The southern Weddell Sea: combined contourite–turbidite sedimentation at the southeastern margin of the Weddell Gyre. In: Stow, D.A.V., Pudsey, C., Howe, J.C., Faugères, J.-C., Viana, A.R. (Eds.), *Geological Society of London, Memoirs* 22, 305–323. doi: 10.1144/GSL.MEM.2002.022.01.32.
- Miller, H., Henriot, J.P., Kaul, N., Moons, A., 1990. A fine-scale stratigraphy of the eastern margin of the Weddell Sea. In: Bleil, U., Thiede, J. (Eds.), *Geological History of the Polar Oceans: Arctic Versus Antarctic*. Kluwer Academic Publishers, 131–161.
- Niedoroda, A.W., Reed, C.W., Hatchett, J.L., Das H.S., 2003. Developing engineering design criteria for mass gravity flows in deep ocean and continental slope environments. In: Locat, J. and Mienert, J. (Eds.), *Submarine Mass Movements and Their Consequences*. Kluwer Academic Press, Dordrecht, 85–94.
- Nielsen, T., Knutz, P.C., Kuipers, A., 2008. Seismic Expression of Contourite Depositional Systems. In: Rebesco, M. and Camerlenghi, A. (Eds.), *Contourites, Developments in Sedimentology* 60, Elsevier, Oxford, Great Britain. 301–321. doi:10.1016/S0070-4571(08)00216-1.
- Nitsche, F.O., Gohl, K., Vanneste, K., Miller, H., 1997. Seismic expression of glacially deposited sequences in the Bellingshausen and Amundsen Seas, West Antarctica. In: *Geology and Seismic Stratigraphy of the Antarctic Margin 2*, Barker, P.F. and Cooper, A.K. (Eds.), *Antarctic Research Series* 71, 95–108, American Geophysical Union, Washington, D.C.
- Nitsche, F.O., Cunningham, A.P., Larter, R.D., Gohl, K., 2000. Geometry and development of glacial continental margin depositional systems in the Bellingshausen Sea. *Marine Geology* 162, 277–302.
- Noormets, R., Dowdeswell, J.A., Larter, R.D., Ó Cofaigh, C., Evans, J., 2009. Morphology of the upper continental slope in the Bellingshausen and Amundsen Seas - implications for sedimentary processes at the shelf edge of West Antarctica. *Marine Geology* 258, (1–4), 100–114. doi:100-114. 10.1016/j.margeo.2008.11.011
- Ó Cofaigh, C., Taylor, J., Dowdeswell, J.A., Pudsey, C.J., 2003. Palaeo-ice streams, trough mouth fans and high-latitude continental slope sedimentation. *Boreas* 32, (1), 37–55.
- Ó Cofaigh, C., et al., 2004. Timing and significance of glacially influenced mass-wasting in the submarine channels of the Greenland Basin. *Marine Geology* 207, (1–4), 39–54.
- Ó Cofaigh, C., Larter, R.D., Dowdeswell, J.A., Hillenbrand, C.D., Pudsey, C.J., Evans, J., Morris, P., 2005. Flow of the West Antarctic Ice Sheet on the continental margin of the Bellingshausen Sea at the Last Glacial Maximum. *Journal of Geophysical Research* 110, B11103. doi:10.1029/2005JB003619.
- Orsi, A.H., Wiederwohl, C.L., 2009. A recount of Ross Sea waters. *Deep Sea Research Part II: Topical Studies in Oceanography* 56, (13–14), 778–795.
- Pagani, M., Zachos, J., Freeman, K.H., Tipple, B., Bohaty, S., 2005. Marked decline in atmospheric carbon dioxide concentrations during the Paleogene. *Science* 309, 5734, 600–603, doi:10.1126/science.1110063.
- Petit, J.R., Jouzel, J., Raynaud, D., Barkov, N.I., Barnola J.-M, Basile, I., Bender, M., Chappellaz, J., Davis, M., Delaygue, G., Delmotte, M., Kotlyakov, V.M., Legrand, M., Lipenkov, V.Y., Lorius, C., Pépin, L., Ritz, C., Saltzman, E., Stievenard, M., 1999. Climate and atmospheric history of the past 420, 000 years from the Vostok ice core, Antarctica. *Nature* 399, 429–436, doi:10.1038/20859.

- Pollard, D. and DeConto, R.M., 2009, Modelling West Antarctic ice sheet growth and collapse through the past five million years. *Nature* 458, 329–333, doi:10.1038/nature07809.
- Rahmstorf, S., 2006. Thermohaline ocean circulation. In: Elias, S.A. (Ed.), *Encyclopedia of Quaternary Sciences*. Elsevier, Amsterdam, Netherlands. 1–10. ISBN 0-444-52747-8.
- Rebesco, M., Pudsey, C.J., Canals, M., Camerlenghi, A., Barker, P.F., Estrada, F., Lucchi, R., Giorgetti, A., 2002. Sediment drift and deep-sea channel systems, Antarctic Peninsula Pacific Margin. In: Stow, D.A.V., Faugeres, J.-C., Howe, J., Pudsey, Viana, A. (Eds.), *Deep-Water Contourite Systems: Modern Drifts and Ancient Series, Seismic and Sedimentary Characteristics*. Geological Society of London Memoirs 22, 353–371.
- Rebesco, M., Camerlenghi, A., Volpi, V., Neagu, C., Accettella, D., Lindbergh, B., Cova, A., Zgur, F., the MAGICO party, 2007. Interaction of processes and importance of contourites: insights from the detailed morphology of sediment drift 7, Antarctica. In: Viana, A., Rebesco M. (Eds.), *Economic and Paleooceanographic Importance of Contourites*. Geological Society of London, Special Publication.
- Rogenhagen, J. and Jokat, W., 2000. The sedimentary structure in the western Weddell Sea, *Marine Geology* 168, 45–60. doi:10.1016/S0025-3227(00)00048-7.
- Rebesco, M. and Camerlenghi, A., 2008. Contourites. In: M. Rebesco, A. Camerlenghi (Eds.), *Developments in Sedimentology* 60, Elsevier, Amsterdam. 688pp, ISBN-13: 978-0444529985.
- Rogenhagen, J., Jokat, W., Hinz, K., Kristoffersen, Y., 2004. Improved seismic stratigraphy of the Mesozoic Weddell Sea. *Marine Geophysical Researches* 25, 265–282, doi:10.1007/s11001-005-1335-y.
- Scheuer, C., Gohl, K., Larter, R.D., Rebesco, M., Udintsev, G., 2006a. Variability in Cenozoic sedimentation along the continental rise of the Bellingshausen Sea, West Antarctica. *Marine Geology* 277, 279–298. doi:10.1016/j.margeo.2005.12.007.
- Scheuer, C., Gohl, K., Eagles, G., 2006b. Gridded isopach maps from the South Pacific and their use in interpreting the sedimentation history of the West Antarctic continental margin. *Geochemistry, Geophysics, Geosystems* 7,11, doi:10.1029/2006GC001315.
- Shanmugam, G., 2000. 50 years of the turbidite paradigm (1950s–1990): deep-water processes and facies models – a critical perspective. *Marine Petroleum Geology* 17, 285–342.
- Shanmugam, G., 2008. Deep-water bottom currents and their deposits. In: Rebesco, M. and Camerlenghi, A. (Eds.), *Contourites, Developments in Sedimentology* 60, Elsevier, Oxford, United Kingdom. 59–81. doi:10.1016/S0070-4571(08)00205-7.
- Siegenthahaler, U., Stocker, T.F., Monnin, E., Lüthi, D., Schwander, J., Stauffer, B., Raynaud, D., Barnola, J.-M., Fischer, H., Masson-Delmotte, V., Jouzel, J., 2005. Stable carbon cycle–climate relationship during the Late Pleistocene. *Science* 310, 1313–1317.
- Smith, R.T., Anderson, J.B., 2011. Seismic Stratigraphy of the Joinville Plateau: Implications for Regional Climate Evolution. In: Anderson, J.B. and Wellner, J.S. (Eds.), *Tectonic, Climatic, and Cryospheric Evolution of the Antarctic Peninsula*. Geopress, American Geophysical Union, Washington DC, USA. 51–61. doi:10.1029/2010SP000980. Peninsula. Geopress, American Geophysical Union, Washington DC, USA, 218pp. doi:10.1029/SP063.
- Smith, W.H.F., Sandwell, D.T., 1997. Global seafloor topography from satellite altimetry and ship depth soundings. *Science* 277, 1957–1962.
- Stickley, C.E., Brinkhuis, H., Schellenberg, S.A., Sluijs, A., Röhl, U., Fuller, M., Grauert, M., Huber, M., Warnaar, J., Williams, G.L., 2004. Timing and nature of the deepening of the Tasmanian Gateway, *Paleoceanography*, 19, PA4027. doi:10.1029/2004PA001022.
- Stow, D.A.V., Hunter, S., Wilkinson, D., Hernández-Molina, 2008. The Nature of Contourite Deposition. In: Rebesco, M. and Camerlenghi, A. (Eds.), *Contourites, Developments in Sedimentology* 60, Elsevier, Oxford, United Kingdom. 143–155. doi:10.1016/S0070-4571(08)00209-4.

## 12. References

---

- Tripati, A.K., Roberts, C.D., Eagle, R.A., 2009. Coupling of CO<sub>2</sub> and ice sheet stability over major climate transitions of the last 20 million years. *Science* 326, 1394–1397. doi:10.1016/j.gca.2011.01.018.
- Tripati, A.K., Roberts, C.D., Eagle, R.A., Li, G., 2011. A 20 million year record of planktic foraminiferal B/Ca ratios: Systematics and uncertainties in  $p\text{CO}_2$  reconstructions. *Geochimica et Cosmochimica Acta* 75, 10, 2582–2610. doi:10.1016/j.gca.2011.01.018.
- Uenzelmann-Neben, G., Gohl, K., 2012. Amundsen Sea sediment drifts: Archives of modifications in oceanographic and climatic conditions. *Marine Geology* 299-302, 51–62, doi:10.1016/j.margeo.2011.12.007/.
- Van Aken, H.M., 2007. The Oceanic Thermohaline circulation. An Introduction. Atmospheric and Oceanographic Sciences Library 39. Springer, New York. 326 pp. doi: 10.1007/978-0-387-48039-8.
- Veizer, J., Godderis, Y., François, L.M., 2000. Evidence for decoupling of atmospheric CO<sub>2</sub> and global climate during the Phanerozoic eon. *Nature* 408, 698–701.
- Warny., S and Askin., R., 2011. Last Remnants of Cenozoic Vegetation and Organic-Walled Phytoplankton in the Antarctic Peninsula's Icehouse World. In: Anderson, J.B. and Wellner, J.S (Eds.), Tectonic, Climatic and Cryospheric Evolution of the Antarctic Peninsula. Special Publication 63, American Geophysical Union. 167–210. Doi:10.1029/2010SP000996.
- Wardell, N., Childs, J. R., Cooper, A. K., 2007. Advances through collaboration: Sharing seismic reflection data via the Antarctic Seismic Data Library System for Cooperative Research (SDLS) In: Antarctica: A keystone in a Changing World – Online Proceedings of the 10th ISAES. Cooper, A. K., Raymond, C. R. (Eds.), USGS Open-File Report 2007-1047, Short Research Paper 001, 4p, doi:10.3133/of2007-1047.srp001 <http://snap.ogs.trieste.it/SDLS>.
- Weigelt, E., Gohl, K., Uenzelmann-Neben, G., Larter, R.D., 2009. Late Cenozoic ice sheet cyclicity in the western Amundsen Sea Embayment — Evidence from seismic records, *Global and Planetary Change* 69, 3, 162–169. doi: 10.1016/j.gloplacha.2009.07.004.
- Wellner, J.S., Heroy, D.C., Anderson, J.B., 2006. The death mask of the Antarctic ice sheet: comparison of glacial geomorphic features across the continental shelf. *Geomorphology* 75, 157–171.
- Wilson, D.S., Jamieson, S.S.R., Barrett, P.J., Leitchenkov, G., Gohl, K., Larter, R.D., 2012. Antarctic topography at the Eocene–Oligocene boundary. *Palaeogeography, Palaeoclimatology, Palaeoecology*. 335-336, 24–34. doi:10.1016/j.palaeo.2011.05.028.
- Wobbe, F., Gohl, K., Chambord, A., Sutherland, R., 2012. Structure and breakup history of the rifted margin of West Antarctica in relation to Cretaceous separation from Zealandia and Bellingshausen plate motion, *Geochemistry Geophysics Geosystems* 13, 4 Q04W12, doi:10.1029/2011GC003742.
- Wynn, R.B. and Stow, D.A.V., 2002. Classification and characterisation of deep-water sediment waves. *Marine Geology* 192, 7–22.
- Yilmaz, O., 2001. Seismic Data Analysis Volume I & II, Investigations in Geophysics No. 10, Society Of Exploration Geophysicists, 2027pp. ISBN-13: 978-1560800941.
- Zachos, J., Pagani, M., Sloan, L., Thomas, E., Billups, K., 2001. Trends, rhythms, and aberrations in global climate 65 Ma to present. *Science* 292, 686–693.

## 13 ACKNOWLEDGEMENTS

---

I express my sincerest thanks to several people who walked this journey with me:

To Prof. Dr. Heinrich Miller for being the first examiner on this project and to Prof. Dr. Cornelia Spiegel for being the second examiner of this thesis, and for her support during the ANT-26/3 expedition to the Amundsen Sea, Antarctica. Our Antarctic Island hopping time and flying over Pine Island Bay to collect rock samples will most likely stay with me for the rest of my life. Thank you for a great experience.

A special note of thanks to Prof. Heinrich Miller and Dr. Stefan Hain for their encouragement during the preparation of my presentation for the international AWI mid-term evaluation in 2012.

Thank you to the ANT-XXVI/3 expedition leader and PhD supervisor, Dr. Karsten Gohl for discussions as I was working through the data and developing ideas.

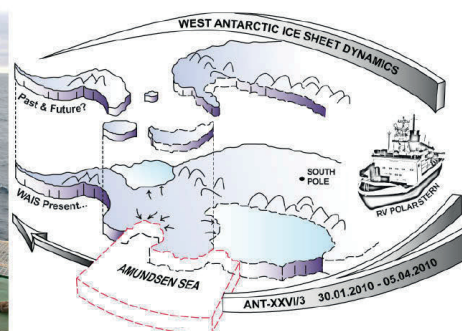
My gratitude goes to the ship and helicopter crews of the RV Polarstern for their assistance in collecting the seismic reflection and other data. In particular thank you to: Norbert Kaul, Bryan Davies, Tina Henning, Burkhard Clasen, Jürgen Gossler and Klaus Hammrich, for laughs, support and insightful conversations during the expedition; and to Igor Hering for many an after-the-graveyard-shift conversations on the Bridge.

Jens Grützner is thanked for fruitful discussions that greatly improved the manuscript of the Weddell Sea paper. Thank you to Christine Läderach for her friendship and support during our PhD's and for proof reading the Weddell Sea manuscripts and first chapters of the thesis.

Special extra thanks to my dear friend and colleague Florian Wobbe for his unwavering support, brilliant assistance in GMT, Mac, and for creating the polar stereographic projection in DUG Insight. Warm thank yous to Estella Weigelt and Coen Hofstede for your support and friendship during my time at AWI.

A big thank you to my dearest old friend Catherine Gray Bremer, for her long distance support from Cape Town and Australia. Indeed, true friends bridge the distance, no matter what. Thank you to all my beloved friends in the "Schwarzesbremen" clan for being my Bremen-home. I will never forget you...

This research was funded by the "Deutsche Forschungs Gemeinschaft" grant GO724/10-1. The Association for Polar Early Career Scientists (APECS) is thanked for financial travel support to the 2010 International Polar Year conference in Oslo, Norway. The "Deutsche Gesellschaft für Polarforschung e.V." is thanked for travel support to the 11<sup>th</sup> International Symposium on Antarctic Earth Sciences, held in Edinburgh, Scotland, July 2011.



Geophysics team of the ANT-26/3 Antarctic expedition on RV *Polarstern*, 2010; Expedition Logo that I designed.





# 14 CURRICULUM VITAE

## PERSONAL INFORMATION

---

Birth names in full	<b>Ansa Phoenix Titania Sapphire Garnet Snow Lindeque</b>
Date and place of Birth	18.06.1973, South Africa
Hometown and Nationality	Cape Town, South African, currently living in London, UK
Languages	English, German, Afrikaans
Email	ansa.lindeque@icloud.com

## WORK EXPERIENCE

---

- |                   |  |
|-------------------|--|
| 11/2012 – to date | <b>Senior Geophysicist – Geological Products &amp; Services - TGS</b><br>1 The Crescent, Surbiton, Surrey, KT6 4BN, United Kingdom. <ul style="list-style-type: none"><li>▪ Project leader on proprietary and multi-client geophysical data analysis and interpretation projects.</li></ul>  |
| 11/2008 – 10/2012 | <b>Associate Research Scientist</b> , Geophysics Section, Alfred Wegener Institut für Polar- und Meeresforschung, Bremerhaven, Germany <ul style="list-style-type: none"><li>▪ Acquisition, processing and interpretation of seismic reflection data in the Amundsen Sea, Antarctica</li><li>▪ Correlation of seismic reflection data with borehole information and seafloor spreading magnetic anomaly data to construct seismic stratigraphic and age models on the West Antarctic margin</li></ul>  |
| 08/2007 – 10/2008 | <b>Senior Geoscientist</b> , Land Geology and Geophysics, Council for Geoscience Western Cape, Cape Town, South Africa <ul style="list-style-type: none"><li>▪ Geological interpretation of the deep crust structure from land-based seismic reflection data</li><li>▪ Combination of these results with other geophysical data (Tomographic, Magnetotelluric, Teleseismic, Borehole information and Aeromagnetic) to investigate the Beattie Magnetic Anomaly and the tectonic evolution of the southern African continental margin</li></ul> |
| 05/2006 – 07/2007 | <b>Associate Research Scientist</b> , Geophysics section, GeoForschungsZentrum Potsdam, Germany <ul style="list-style-type: none"><li>▪ Processing und geological interpretation of land-based seismic reflection data within the German – South African “Inkaba yeAfrica” Cooperation initiative.</li></ul>   |
| 04/2005 – 04/2006 | <b>Senior Geoscientist</b> , Land Geology and Geophysics, Council for Geoscience Western Cape, Cape Town, South Africa <ul style="list-style-type: none"><li>▪ Logistical planning, acquisition, processing and interpretation of the land-based “Inkaba yeAfrica” Seismic Reflection field experiment</li></ul>   |

- Planning and supervision of drilling boreholes need for controlled sources
  
- 02/2003 – 04/2005      **Senior Geoscientist** in marine geology and geophysics, Council for Geoscience Western Cape, Cape Town, South Africa
  - Evaluating geophysical data (Bathymetry, Gravity, Magnetic and Seismic reflection) for the South African United Nations Law of the Sea, Article 76 (UNCLOS 76) Extended Continental Shelf Claims Assessment
  - Project leader for the Evaluation of the feasibility of UNCLOS76 Claims for African coastal states based on public-domain data (Bathymetry, remote sensing satellite images and sediment thickness)
  
- 01/2001 – 07/2002      **Exploration Geologist** at Middlebult Coalmine, owned by Sasol Pty. Ltd., located in Secunda, Mpumalanga Province, South Africa
  - Geological and financial planning of the exploration drilling programme
  - Correlating geophysical data (Aeromagnetic, Gravity and Seismic) with horizontal-, vertical und inclined Borehole data from core and geophysical logs
  - Developing 2D and 3D structural models to predict the location and orientation of dolerite dykes
  
- 02/1994 – 12/1996      **Junior Architect**, at OAC Architects in Pretoria, Gauteng Province, South Africa
  - Project monitoring from initial consultations on design concept through the drawing up of construction plans and supervision of the building until hand over to the client
  - Model building and drawing construction plans for Industrial and office buildings as well as private residences

## RESEARCH EXPEDITIONS

---

- 01/2010 – 04/2010      ANT-XXVI/3 on the RV Polarstern, from Wellington, New Zealand to the Amundsen Sea, Antarctica and ending in Punta Arenas, Chile.  
Assigned work included:  
Acquisition and quality control of seismic reflection data, wide-angle refraction data, gravity- and aeromagnetic data

## QUALIFICATIONS

---

- 04/2006 – 07/2008      Masters degree in Geophysics and Geology (*summa cum laude*) University of Cape Town, South Africa, Department of Geology and affiliated with the Africa Earth Observatory Network
  - South African Masters-system: 2 years full-time research and dissertation
  - **Topic:** "The Agulhas-Karoo Geoscience Transect: Deep seismic reflection profile across the Southern Karoo Basin, South Africa."
  
- 05/2006 – 06/2007      International research exchange year at the GeoForschungsZentrum Potsdam, Germany

	Acquisition and processing of land-based seismic reflection data Field work in setting up and magnetotelluric experiment
02/2000 – 12/2000	Bachelor of Science Honours degree in Geology (B.Sc.Hons.) University of Cape Town, South Africa, Department of Geology South African system: 1-year module lectures and 4-month dissertation <b>Topic:</b> “Metamorphism and Geochemistry of a Supracrustal Sequence in the Namaqua Metamorphic Complex.”
02/1997 – 12/1999	Bachelors of Science degree (B.Sc.) in Geology, Ocean- and Atmospheric Science. University of Cape Town, South Africa, Department of Geology.
02/1993 – 12/1995	National Diploma in Architecture (N.Dip.Arch.) Pretoria Technicon “Fachhochschule”, South Africa
02/1992 – 07/1996	Bachelors of Architecture (B.Arch) University of Pretoria, South Africa, Department of Construction

## AWARDS, SCHOLARSHIPS

---

2008 – 2012	“Deutsche Forschungsgemeinschaft”, DFG Germany
2006 – 2008	Scholarship from the Council for Geoscience, South Africa
2006 – 2007	“Inkaba yeAfrica” International exchange scholarship
1997 – 2000	Sasol full bursary
1998	Academic award, University of Cape Town, South Africa
1997	Nomination for the Dwayne M. Memorial scholarship
1997	Academic award, University of Cape Town, South Africa
1993	Academic award for best overall student in Architecture, Pretoria Technicon, South Africa

## SELECTED PUBLICATIONS

---

### INTERNATIONAL JOURNALS:

- 2015 **Lindeque, A.**, Gohl, K., Henrys, S., Wobbe, F., Davy, B., 2015. Seismic stratigraphy along the Amundsen Sea to Ross Sea continental rise: A cross-regional record of pre-glacial to glacial processes of the West Antarctic margin, *Palaeogeography, Palaeoclimatology, Palaeoecology*, 443, 183–202, published online before print doi:10.1016/j.palaeo.2015.11.017
- 2014 Wobbe, F., **Lindeque, A.**, Gohl, K., 2014. Anomalous South Pacific lithosphere dynamics derived from new total sediment thickness estimates off the West Antarctic margin. *Global and Planetary Change*, 123 (A), 139–149, doi:10.1016/j.gloplacha.2014.09.006.
- 2013 **Lindeque, A.**, Martos, Y.M., Gohl, K., Maldonado, A., 2013. Deep sea pre-glacial to glacial components in the Weddell Sea Basin and southwestern Scotia Sea from a cross-basin seismic transect. *Marine Geology* 336, 61–83, doi:10.1016/j.margeo.2012.11.004.
- 2011 **Lindeque, A.**, de Wit, M., Ryberg, T., Weber, M. and Chevallier, L., 2011. Deep crustal profile across the southern Karoo Basin and Beattie Magnetic Anomaly, South Africa: an integrated interpretation with tectonic implications. *South African Journal of Geology*, volume 114.3-4 Inkaba yeAfrica special volume, 265-292, doi:10.2113/gssajg.114.3-4.265.
- 2007 **Lindeque, A.**, Ryberg, T., Stankiewicz, J., Weber, M.H., de Wit, M.J., 2007. Deep Crustal Seismic Reflection Experiment Across the Southern Karoo Basin, South Africa. *South African Journal of Geology*, 110, 419-438.
- Bräuer, B., Ryberg, T., **Lindeque, A.**, 2007. Shallow seismic velocity structure along the Prince Albert Slingsfontein profile. *South African Journal of Geology*, 110, 439-448.



- Stankiewicz, J., Ryberg, T., Schulze, A., **Lindeque, A.**, Weber, M.H. and De Wit, M.J., 2007. Initial Results from Wide-Angle Seismic Refraction Lines in the Southern Cape. South African Journal of Geology, 110, 407-418
- 2006 **Lindeque, A.**, 2006. Inkaba yeAfrica, Report on the 4<sup>th</sup> Workshop held in Potsdam, Germany from 1-3 June 2006. GeoBulletin, 8-10.

#### PRESENTATIONS AT INTERNATIONAL CONFERENCES:

- 2012 **Lindeque, A.**, Gohl, K., Martos, Y. and Uenzelmann-Neben, G., 2012. The pre-glacial to glacial development of Antarctica: Footprints in deep-sea sediments, 72. Jahrestagung der Deutschen Geophysikalischen Gesellschaft, Hamburg, Germany, 5-8 March 2012. hdl:10013/epic.38790.
- 2011 **Lindeque, A.**, Gohl, K., Uenzelmann-Neben, G., Davy, D., 2011. The first Ross Sea – Amundsen Sea transect: A stratigraphic correlation of deep sea seismic reflection data along the Pacific margin of West Antarctica. 11th International Symposium on Antarctic Earth Sciences, 10-15 July 2011. University of Edinburgh, Scotland.
- 2010 **Lindeque, A** and Gohl, K., 2010. Deep sea seismic stratigraphy of the Amundsen Sea and Ross Sea, West Antarctica: Preliminary results of the first linking record, 24. Internationale Polartagung der DGP, Obergurgl, Austria, 6-10 Sept. 2010. hdl:10013/epic.35893.

#### POSTERS AT INTERNATIONAL CONFERENCES:

- 2011 **Lindeque, A.**, Martos, Y.M., Gohl, K., 2011. The Weddell Sea – Scotia Sea Transect: A stratigraphic correlation of deep sea seismic reflection data along the Atlantic margin of West Antarctica. Poster. 11th International Symposium on Antarctic Earth Sciences, 10-15 July 2011. University of Edinburgh, Scotland.
- 2010 **Lindeque, A.** and Gohl, K., 2010. Western Antarctic palaeostratigraphy: implications for palaeobathymetry and palaeoclimate modeling. International Polar Year, Oslo Science Conference, 8-12 June 2010, Oslo, Norway. hdl:10013/epic.37154.
- 2009 **Lindeque, A.** and Gohl, K., 2009. Stratigraphy of the Pacific margin of West Antarctica: A contribution to the CASP project. First Antarctic Climate Evolution Symposium, Granada, Spain. Sept 2009, hdl:10013/epic.33023
- 2007 **Lindeque, A.**, Ryberg, T., Weber, M.H., de Wit, M.J., 2007. A Near Vertical Seismic Reflection Profile Across the Beattie Magnetic Anomaly, South Africa. Poster. DGG, Deutscher Geophysikalische Gesellschaft 67.Jahrestagung, GD263, Aachen, Germany.
- Lindeque, A.**, Ryberg, T., Weber, M.H., de Wit, M.J., 2007. A Near Vertical Seismic Reflection Profile Across the Beattie Magnetic Anomaly, South Africa. Poster. EGU Vienna, Geophysical Research Abstracts, 9, 08497.
- 2006 **Lindeque, A.**, Ryberg, T., Weber, M.H., de Wit, M.J., 2006. Understanding the Beattie Magnetic Anomaly, Karoo Basin and Deep Crustal Tectonics of Southernmost Africa: Near Vertical Seismic Reflection Data of the Inkaba ye Africa Onshore-Offshore Agulhas-Karoo Geoscience Transect. Poster. American Geophysical Union Fall Assembly Abstracts, T31C-0476.

Appendix A  
Weddell Sea and Scotia Sea

---

A-1. Fold out plot of the WS–SS transect









## Appendix B

### Amundsen Sea and Ross Sea

---

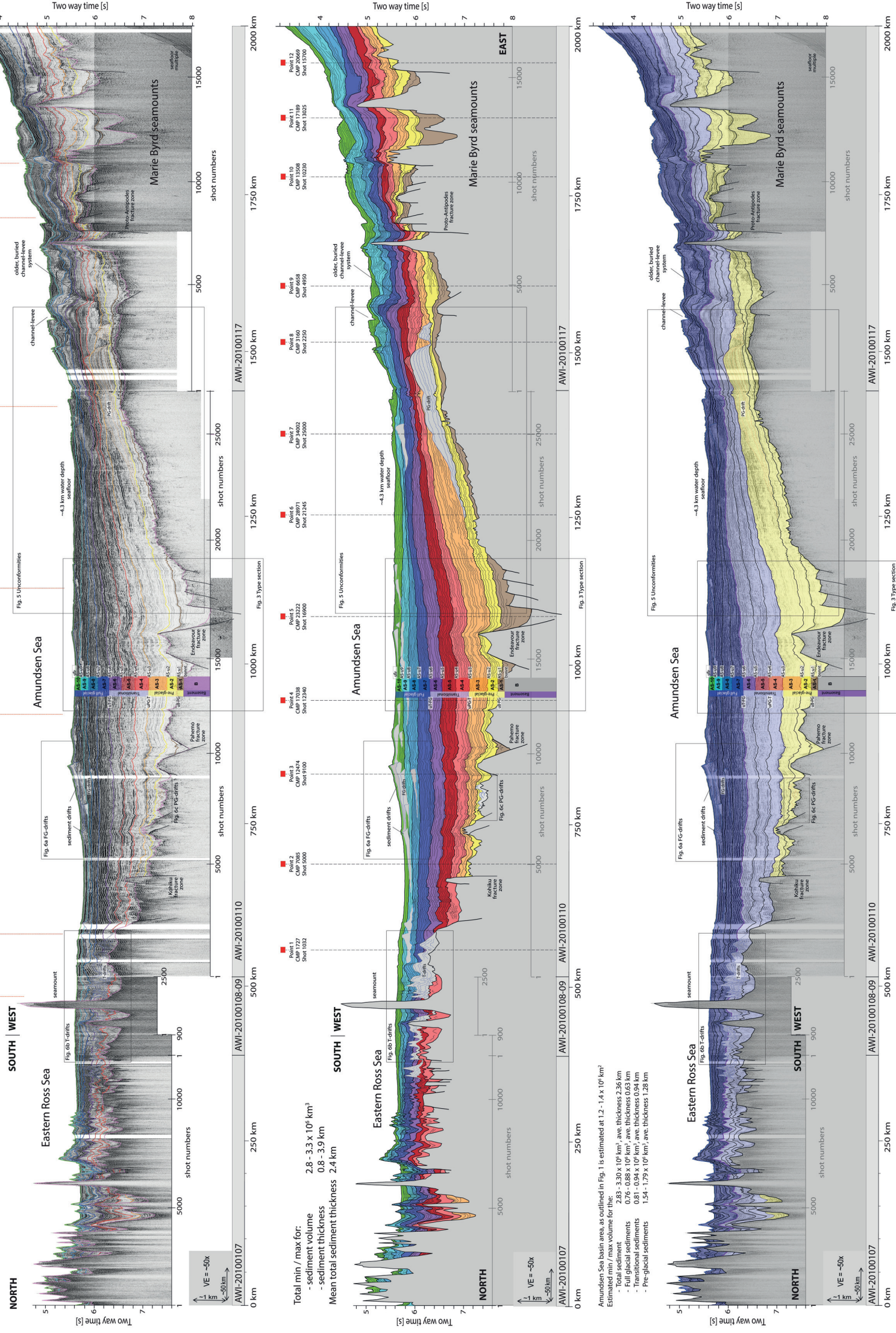
B-1. A0 fold-out plot of the AS–RS transect

B-2. Velocity model from seismic reflection data



# Amundsen Sea - Ross Sea Transect

Online supplement to Lindeque, et al., 2015







#POINT	CDP	LONSHOT	LATSHOT	SHOT	LINE_ID	SUMMARY		sediment thickness (m)		Velocity range (m/s)	
						Group	UNITS	min	max	min	max
1	1727	-160.3096	-72.321899	1032	AWI-20100110						
2	7085	-156.4375	-72.166298	5000	AWI-20100110						
3	12747	-152.34039	-72.255302	9100	AWI-20100110						
4	17038	-149.3943	-72.529099	12340	AWI-20100110						
5	23222	-144.8902	-72.579498	16900	AWI-20100110						
6	28971	-140.6447	-72.4422	21245	AWI-20100110						
7	34002	-137.0519	-72.183098	25000	AWI-20100110						
8	3160	-133.86571	-71.822998	2250	AWI-20100117						
9	6658	-131.5419	-71.548599	4950	AWI-20100117						
10	13508	-126.7833	-71.398903	10230	AWI-20100117						
11	17189	-124.2239	-71.4664	13025	AWI-20100117						
12	20669	-121.843	-71.597504	15700	AWI-20100117						
						AS-10		52.5	201.6	1690	1920
						AS-9	Full glacial	52.5	220.5	1750	2130
						AS-8		45.3	178.9	1876	2237
						AS-7		65.4	367.4	2043	2300
						AS-6	Transitional	47.5	393.2	2131	2357
						AS-5		89.8	419.5	2257	2432
						AS-4		173.1	359.8	2351	2674
						AS-3	Pre-glacial	108.7	679.9	2550	2917
						AS-2		67.5	519.0	3118	3245
						AS-1		133.5	1256.3	3574	3760
<b>point, cdp, shot</b>	<b>unit</b>	<b>time</b>	<b>vel</b>	<b>depth</b>	<b>thickness</b>	<b>point, cdp, shot</b>	<b>unit</b>	<b>time</b>	<b>vel</b>	<b>depth</b>	<b>thickness</b>
<b>1, 1727, 1032</b>	<b>sfir</b>	5690	1475	4196.4	4196.4	<b>7, 34002, 25000</b>	<b>sfir</b>	5534	1475	4081.3	4081.3
	AS-u9	5770	1850	4270.4	74.0		AS-u9	5608	1758	4146.4	65.0
	AS-u8	5898	1938	4394.4	124.0		AS-u8	5768	1909	4299.1	152.7
	AS-u7	6014	2040	4512.7	118.3		AS-u7	5793	1938	4323.3	24.2
	AS-u6	6211	2180	4727.5	214.7		AS-u6	6020	2085	4560.0	236.6
	AS-u5	6455	2246	5001.5	274.0		AS-u5	6064	2160	4607.5	47.5
	AS-u4	6455	2395	5001.5	0.0		AS-u4	6139	2395	4697.3	89.8
	AS-u3	6455	2546	5001.5	0.0		AS-u3	6275	2546	4870.4	173.1
	AS-u2	6455	2824	5001.5	0.0		AS-u2	6665	2824	5421.1	550.7
	AS-u1	6455	3138	5001.5	0.0		AS-u1	6761	3138	5571.7	150.6
	bsmnt	6455	3650	5001.5	0.0		bsmnt	6832	3760	5705.2	133.5
				9000.0	3998.5					9000.0	3294.8
											mbsl
<b>point, cdp, shot</b>	<b>unit</b>	<b>time</b>	<b>vel</b>	<b>depth</b>	<b>thickness</b>	<b>point, cdp, shot</b>	<b>unit</b>	<b>time</b>	<b>vel</b>	<b>depth</b>	<b>thickness</b>
<b>2, 7085, 5000</b>	<b>sfir</b>	5804	1475	4280.5	4280.5	<b>8, 3160, 2250</b>	<b>sfir</b>	5200	1475	3835.0	3835.0
	AS-u9	5899	1874	4369.5	89.0		AS-u9	5287	1758	3911.5	76.5
	AS-u8	5969	1970	4438.4	68.9		AS-u8	5394	1909	4013.6	102.1
	AS-u7	6084	2087	4558.4	120.0		AS-u7	5519	1938	4134.7	121.1
	AS-u6	6286	2119	4772.4	214.0		AS-u6	5621	2085	4241.1	106.3
	AS-u5	6510	2288	5028.7	256.3		AS-u5	5690	2179	4316.2	75.2
	AS-u4	6765	2407	5335.6	306.9		AS-u4	5842	2395	4498.3	182.0
	AS-u3	6935	2674	5562.9	227.3		AS-u3	6034	2546	4742.7	244.4
	AS-u2	7024	2917	5692.7	129.8		AS-u2	6301	2824	5119.7	377.0
	AS-u1	7166	3220	5921.3	228.6		AS-u1	6344	3138	5187.1	67.5
	bsmnt	7166	3750	5921.3	0.0		bsmnt	6429	3680	5343.5	156.4
				9000.0	3078.7					9000.0	3656.5
											mbsl
<b>point, cdp, shot</b>	<b>unit</b>	<b>time</b>	<b>vel</b>	<b>depth</b>	<b>thickness</b>	<b>point, cdp, shot</b>	<b>unit</b>	<b>time</b>	<b>vel</b>	<b>depth</b>	<b>thickness</b>
<b>3, 12747, 9100</b>	<b>sfir</b>	5564	1475	4103.5	4103.5	<b>9, 6658, 4950</b>	<b>sfir</b>	5090	1483	3774.2	3774.2
	AS-u9	5774	1920	4305.1	201.6		AS-u9	5235	1695	3897.1	122.9
	AS-u8	5943	2015	4475.3	170.3		AS-u8	5367	1770	4013.9	116.8
	AS-u7	6081	2169	4625.0	149.7		AS-u7	5555	1903	4192.8	178.9
	AS-u6	6407	2254	4992.4	367.4		AS-u6	5619	2043	4258.2	65.4
	AS-u5	6631	2297	5249.6	257.3		AS-u5	5811	2186	4468.1	209.9
	AS-u4	6858	2421	5524.4	274.8		AS-u4	5943	2331	4621.9	153.8
	AS-u3	7112	2589	5853.2	328.8		AS-u3	6041	2351	4737.1	115.2
	AS-u2	7322	2758	6142.8	289.6		AS-u2	6201	2550	4941.1	204.0
	AS-u1	7552	3220	6513.1	370.3		AS-u1	6483	3118	5380.7	439.6
	bsmnt	7552	3750	6513.1	0.0		bsmnt	6673	3750	5737.0	356.3
				9000.0	2486.9					9000.0	3263.0
											mbsl
<b>point, cdp, shot</b>	<b>unconformity</b>	<b>time</b>	<b>vel</b>	<b>depth</b>	<b>thickness</b>	<b>point, cdp, shot</b>	<b>unit</b>	<b>time</b>	<b>vel</b>	<b>depth</b>	<b>thickness</b>
<b>4, 17038, 12340</b>	<b>sfir</b>	5611	1475	4138.1	4138.1	<b>10, 13508, 10230</b>	<b>sfir</b>	4552	1450	3300.2	3300.2
	AS-u9	5821	1906	4338.2	200.1		AS-u9	4689	1690	3416.0	115.8
	AS-u8	5935	2130	4459.7	121.4		AS-u8	4885	1764	3588.8	172.9
	AS-u7	6091	2237	4634.1	174.5		AS-u7	5060	1876	3753.0	164.2
	AS-u6	6274	2300	4844.6	210.5		AS-u6	5229	2064	3927.4	174.4
	AS-u5	6520	2357	5134.5	289.9		AS-u5	5344	2177	4052.6	125.2
	AS-u4	6865	2432	5554.0	419.5		AS-u4	5472	2330	4201.7	149.1
	AS-u3	7149	2534	5913.8	359.8		AS-u3	5581	2379	4331.3	129.7
	AS-u2	7420	2611	6267.6	353.8		AS-u2	5666	2558	4440.1	108.7
	AS-u1	7749	3155	6786.6	519.0		AS-u1	5751	3245	4578.0	137.9
	bsmnt	7749	3750	6786.6	0.0		bsmnt	5907	3750	4870.5	292.5
				9000.0	2213.4					9000.0	4129.5
											mbsl
<b>point, cdp, shot</b>	<b>unit</b>	<b>time</b>	<b>vel</b>	<b>depth</b>	<b>thickness</b>	<b>point, cdp, shot</b>	<b>unit</b>	<b>time</b>	<b>vel</b>	<b>depth</b>	<b>thickness</b>
<b>5, 23222, 16900</b>	<b>sfir</b>	5583	1466	4092.3	4092.3	<b>11, 17189, 13025</b>	<b>sfir</b>	4512	1450	3271.2	3271.2
	AS-u9	5731	1886	4231.9	139.6		AS-u9	4574	1695	3323.7	52.5
	AS-u8	5892	2089	4400.1	168.2		AS-u8	4800	1884	3536.6	212.9
	AS-u7	6009	2154	4526.1	126.0		AS-u7	4800	1991	3536.6	0.0
	AS-u6	6232	2258	4777.8	251.8		AS-u6	4904	2163	3649.1	112.5
	AS-u5	6519	2301	5108.0	330.2		AS-u5	5261	2203	4042.3	393.2
	AS-u4	6765	2391	5402.1	294.1		AS-u4	5399	2335	4203.5	161.1
	AS-u3	7083	2495	5798.8	396.7		AS-u3	5697	2416	4563.4	360.0
	AS-u2	7598	2573	6461.4	662.5		AS-u2	5873	2626	4794.5	231.1
	AS-u1	7775	3209	6745.4	284.0		AS-u1	6095	3126	5141.5	347.0
	bsmnt	8478	3574	8001.6	1256.3		bsmnt	6725	3455	6229.8	1088.3
				9000.0	998.4					9000.0	2770.2
											mbsl
<b>point, cdp, shot</b>	<b>unit</b>	<b>time</b>	<b>vel</b>	<b>depth</b>	<b>thickness</b>	<b>point, cdp, shot</b>	<b>unit</b>	<b>time</b>	<b>vel</b>	<b>depth</b>	<b>thickness</b>
<b>6, 28971, 21245</b>	<b>sfir</b>	5582	1465	4088.8	4088.8	<b>12, 20669, 15700</b>	<b>sfir</b>	4086	1450	2962.4	2962.4
	AS-u9	5752	1768	4239.1	150.3		AS-u9	4172	1700	3035.5	73.1
	AS-u8	5806	1946	4291.6	52.5		AS-u8	4424	1750	3256.0	220.5
	AS-u7	5851	2014	4337.0	45.3		AS-u7	4560	1850	3381.8	125.8
	AS-u6	5976	2008	4462.5	125.5		AS-u6	4699	1989	3520.0	138.2
	AS-u5	6200	2131	4701.1	238.7		AS-u5	4924	2130	3759.6	239.6
	AS-u4	6394	2257	4920.1	218.9		AS-u4	5131	2260	3993.5	233.9
	AS-u3	6532	2360	5082.9	162.8		AS-u3	5300	2357	4192.7	199.2
	AS-u2	7052	2615	5762.8	679.9		AS-u2	5506	2578	4458.2	265.5
	AS-u1	7177	3230	5964.7	201.9		AS-u1	5506	3130	4458.2	0.0









## Appendix C

### South Pacific Lithosphere dynamics

---

C-1. Present-day dynamic topography models

C-2. List of seismic reflection profiles used for grids



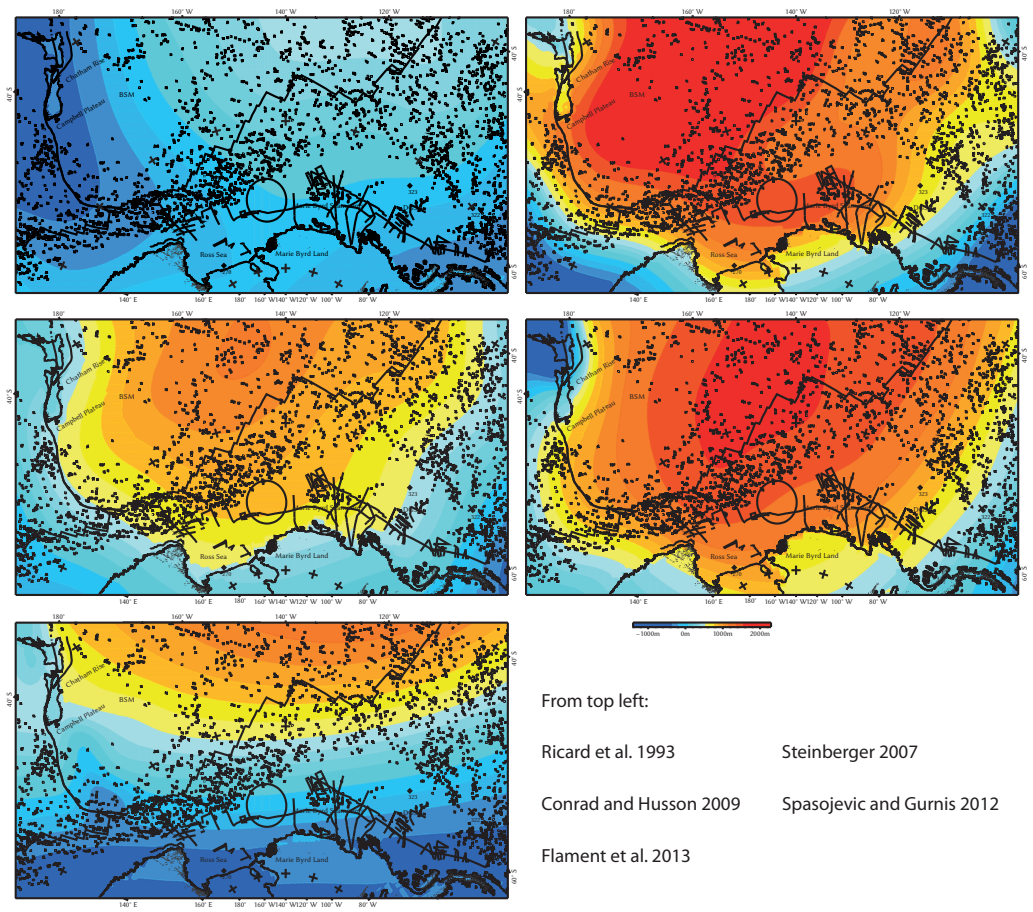


Figure A.1. Present-day dynamic topography models of the South Pacific (Ricard et al. 1993; Steinberger 2007; Conrad and Husson 2009; Spasojevic and Gurnis 2012; Flament et al. 2013).





**Table C-1.** Source-ID (values of source identification grid) vs. data origin of data used for compiling sediment thickness, including DSDP boreholes (1-4), data from the Antarctic Seismic Data Library System (SDLS, Wardell et al. 2007, 5-93, 161-207), recently acquired and processed seismic data (99-140), and data from previous work (e.g., Scheuer et al. 2006a, b; Wilson and Luyendyk 2009; Uenzelmann-Neben and Gohl 2012; Wobbe et al. 2012; Gohl et al. 2013; Kalberg and Gohl 2013; Whittaker et al. 2013).

SID	Source	SID	Source	SID	Source
0	interpolated	32	AWI-94052	64	IT92A113
1	DSDP-28-270	33	AWI-94053	65	IT92A114
2	DSDP-28-274	34	AWI-94054-A	66	IT92A114A
3	DSDP-35-322	35	AWI-94054-B	67	IT92A115
4	DSDP-35-323	36	AWI-94054-C	68	IT92A124
5	AWI-010001	37	AWI-95200	69	IT97235
6	AWI-20060022	38	AWI-95201	70	IT97236
7	AWI-20060023	39	AWI-95210	71	PET-98401c
8	AWI-94002-A	40	BAS-92322	72	PET-98402a
9	AWI-94002-B	41	BAS-92323	73	PET-98403a
10	AWI-94002-C	42	BAS-92324	74	PET-98404
11	AWI-94002-D	43	BAS-92325	75	PET-98405b
12	AWI-94003-A	44	BAS-92327	76	PET-98405c
13	AWI-94003-B	45	BAS-92328	77	PET-98407
14	AWI-94003-C	46	BAS-92329	78	PET-98408
15	AWI-94030-A	47	BAS-92330	79	PET-98409
16	AWI-94030-B	48	I95130	80	TH86002A
17	AWI-94030-C	49	I95130A	81	TH86002B
18	AWI-94030-D	50	I95130B	82	TH86003A
19	AWI-94030-E	51	I95135	83	TH86003B
20	AWI-94040-A	52	I95135A	84	TH86003C
21	AWI-94040-B	53	I95136	85	TH86003D
22	AWI-94041-A	54	I95137	86	TH86003E
23	AWI-94041-B	55	I95138A	87	TH86003F
24	AWI-94041-C	56	IT89A45B	88	TH86004A
25	AWI-94042-A	57	IT89A48	89	TH86004B
26	AWI-94042-B	58	IT89A49	90	TH86004C
27	AWI-94042-C	59	IT92A106	91	TH86006
28	AWI-94043-A	60	IT92A107	92	TH86008
29	AWI-94043-B	61	IT92A108	93	TH86009
30	AWI-94050	62	IT92A109	95, 96	<i>Scheuer et al. (2006a)</i>
31	AWI-94051	63	IT92A110	<b>97</b>	<b>assigned (this work)</b>
99	AWI-20060200	164	IT89AR36B	186	NBP9602-07H
107	AWI-20100107	165	NBP9601L010A	187	NBP9602-07I
108	AWI-20100108	166	NBP9601L010B	188	NBP9602-08A
109	AWI-20100109	167	NBP9601L010C	189	NBP9602-08B
110	AWI-20100110	168	NBP9601L082A	190	NBP9702-01A
111	AWI-20100111	169	NBP9601L082B	191	NBP9702-01C
112	AWI-20100112	170	NBP9601L08B	192	NBP9702-01D
113	AWI-20100113	171	NBP9602-01A	193	NBP9702-01E
117	AWI-20100117	172	NBP9602-01B	194	NBP9702-02C
118	AWI-20100118	173	NBP9602-04	195	NBP9702-05A
119	AWI-20100119	174	NBP9602-05A	196	NBP9702-05B
126	AWI-20100126	175	NBP9602-05B	197	NBP9702-05C
129	AWI-20100129	176	NBP9602-06A	198	NBP9702-06A
130	AWI-20100130	177	NBP9602-06C	199	NBP9702-06B
131	AWI-20100131	178	NBP9602-06D	200	SEV87-02B
132	AWI-20100132	179	NBP9602-07A	201	SEV87-07
139	AWI-20100139	180	NBP9602-07B	202	SEV87-11
140	AWI-20100140	181	NBP9602-07C	203	TH82-12
151	Wobbe et al. (2012)	182	NBP9602-07D	204	TH82-13
161	ATC82B-208	183	NBP9602-07E	205	TH82-14
162	BGR80-100	184	NBP9602-07F	206	TH82-16
163	IT89A37	185	NBP9602-07G	207	TH82-17
251	Ross Sea, Wilson and Luyendyk (2009)				
252	Ross Sea, Cooper et al. (1991)				
253	Divins (2003)/Whittaker et al. (2013)				